

Robbin Bastiaansen
robbin.bastiaansen@gmail.com

Pattern Formation in Animal Populations

The effect of a density dependent movement speed
on the making of a mussel bed

Master Thesis
July 2015

Thesis Advisor:
dr. V. Rottschäfer



Mathematisch Instituut, Universiteit Leiden

Abstract

In this master thesis we study patterns in animal populations that arise due to a density dependent movement speed v of one of the involved species. This new description of the movement leads to a Cahn Hilliard equation describing the evolution of the concentration of the animal specie in question. Our main interest is a modification of the generally used standard predator-prey reaction-diffusion type of description of the evolution of two interacting species, where the standard diffusive movement of one of the species is replaced with this fast Cahn-Hilliard like movement. This leads to a fourth order slow-fast partial differential equation, which forms the system that will be the main object of study in this thesis:

$$\begin{aligned}\frac{\partial m}{\partial t} &= d_m \nabla \left(v \left[v + m \frac{\partial v}{\partial m} \right] \nabla m + v m \frac{\partial v}{\partial a} \nabla a - \kappa \nabla \Delta m \right) + \varepsilon H(m, a) \\ \frac{\partial a}{\partial t} &= \varepsilon d_a \Delta a + \varepsilon G(m, a)\end{aligned}$$

In this thesis we first present an in-depth literature study of the general Cahn Hilliard system focusing on the evolution - both short and long term - of solutions starting from an uniform state. Subsequently we will analyze the full population model, with the Cahn-Hilliard like movement, on an one-dimensional spatial domain via a weakly non-linear stability analysis, leading to a (real) Ginzburg-Landau equation as amplitude equation for variations from steady states of the model. All our findings will be applied to a system describing the interaction between mussels and algae. This analytic approach, supplemented by numerical simulations on the one-dimensional model, is then used to explain the occurrence and behaviour of patterns in mussel beds.

Contents

Introduction	6
1 Ecological Set-Up	11
1.1 Explanation of the model	12
1.1.1 Reaction-Diffusion Equations	12
1.1.2 Density-dependent movement speed	13
1.1.3 Interaction terms for the Mussel-Algea system	15
1.1.4 Choices for the density dependent movement speed	18
1.2 A Reaction-Diffusion model for mussels	23
1.2.1 Uniform Steady States	24
1.2.2 Linear Stability of the Uniform Stationary States	24
1.2.3 Weakly Non-Linear Stability Analysis	29
2 $\varepsilon = 0$ - A study of the Cahn-Hilliard Equation	31
2.1 Cahn Hilliard Equation: general behaviour	32
2.1.1 Steady states	34
2.1.2 Global minimizer of the energy	38
2.1.3 Linear stability of uniform steady state	40
2.1.4 Stability of all stationary solutions	42
2.1.5 Bifurcation diagram for the quadratic speed $v = v_q$	44
2.1.6 Bifurcation diagram for mussel system with $v = v_p$	49
2.2 Long time behaviour - Ostwald Ripening	51
2.2.1 General Description of Ostwald Ripening	52
2.2.2 Ostwald Ripening with mussels	55
2.3 Simulations	58
2.3.1 The start - short-time behaviour	59
2.3.2 The end - long-time behaviour	59
2.4 Summary	63
3 $\varepsilon \neq 0$ - The Full Population Model	64
3.1 Linear Stability of the uniform steady states	65
3.1.1 On using the trace and the determinant to determine eigenvalues	67
3.1.2 The determinant and the trace of our matrix $M(\vec{k})$	69
3.1.3 On the form of $\det M(\vec{k})$	71
3.1.4 On the form of $\text{Tr } M(\vec{k})$	74
3.1.5 Stability Analysis of the uniform stationary point	75

3.2	Approximations, assuming $\delta, \theta > 0$ and $\mathcal{O}(\varepsilon)$	76
3.2.1	Approximations of bifurcation plane	77
3.2.2	Approximations of eigenvaluecurves	80
3.3	Modulation Equation when $\{\det \mathcal{M} = 0\}$ is crossed.	88
3.3.1	The matrix \mathcal{M}_c	89
3.3.2	Perturbations	90
3.3.3	The full perturbation	92
3.3.4	Rewriting the equations	93
3.3.5	Weakly non linear stability analysis	96
3.4	Analytic study of the Mussel's system	101
3.4.1	Uniform Steady States and their stability	103
3.4.2	Bifurcation Lines	106
3.4.3	Modulation Equation	109
3.5	Simulations	110
3.5.1	Short time behaviour	111
3.5.2	Long time behaviour	111
3.5.3	Other initial conditions	112
Conclusion & Outlook		118
Acknowledgments		121
Appendix A Modulation Equation for Reaction-Diffusion system		122
Appendix B Approximations for bifurcation planes		129
B.1	Approximation of bifurcation lines	129
B.2	Bifurcation lines in the (η, γ) -plane	136
B.3	Approximation of Eigenvalue curves	137
Appendix C Study of the Real Ginzburg-Landau Equation		151
C.1	Reformulation in polar coordinates	152
C.2	Phase planes	154
C.3	Stationary solutions of the Ginzburg-Landau equation	156
C.3.1	Uniform solutions $\rho(\xi) = \rho_*$	156
C.3.2	Periodic solutions	157
C.3.3	Homoclinic connections	157
C.4	The situation when $\Omega = 0$	158
C.5	Stability of the stationary solutions	159
C.5.1	Uniform states	160
C.5.2	Periodic solutions of the form $A(\xi) = a(\theta)e^{i\theta\xi}$	160
C.5.3	Periodic solutions of the form $A(\xi) = \rho(\xi)$	161
C.5.4	The other stationary solutions	162
Bibliography		163

Introduction

Finding Jesus in a pizza, seeing a face on Mars's surface, computing the golden ratio with cauliflowers or going all-in on black after a red streak in roulette. Patterns - humans tend to see them everywhere. Though some of these observed ‘patterns’ arise by mere coincidences, nature *does* have many real patterns. With the aid of science we have already successfully explained patterns in (solar) eclipses, the creation of offspring and fractals - amongst many others.

A special kind of patterns are the so-called self-organised patterns. These patterns arise purely out of local interactions between components of the system, without external stimuli. Examples of these kind of patterns include the stripes of zebras, the facet eye of a fruit fly and vegetation patterns (see Figure 1).

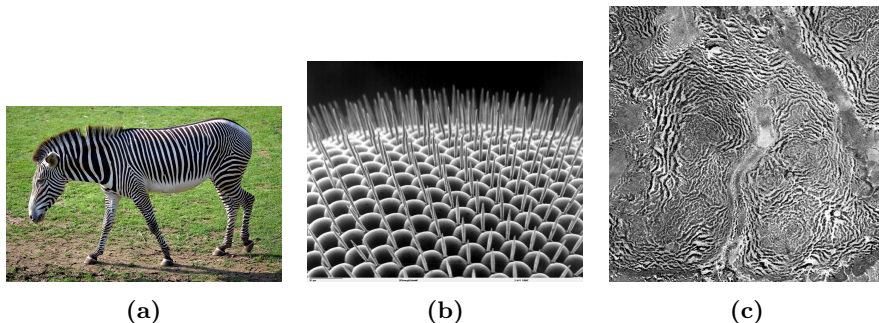


Figure 1 – Examples of self-organized patterns in nature. (a) The stripes of a zebra. Photo by André Karwath under the Creative Commons Attribution License, (b) a scanning electron microscope image of the eye of a fruit fly, by Dartmouth Electron Microscope Facility and (c) the vegetation patterns in a Tiger Bush, courtesy of the U.S. Geological survey.

Studying this self-organisation is important. In ecological systems, a good understanding of the patterns can point us to early warning signals to prevent catastrophic shifts in our ecosystem - for instance to prevent desertification. In biological systems, it can lead to better ways to repair coincidental defects in early embryos. And in chemical engineering, this understanding can give clues how to increase the desired output, while minimizing the unwanted, often polluting, side products.

The first breakthrough in this line of research was by Alan Turing. In his 1952 paper [1] he described how activator-inhibitor mechanisms in reaction-diffusion

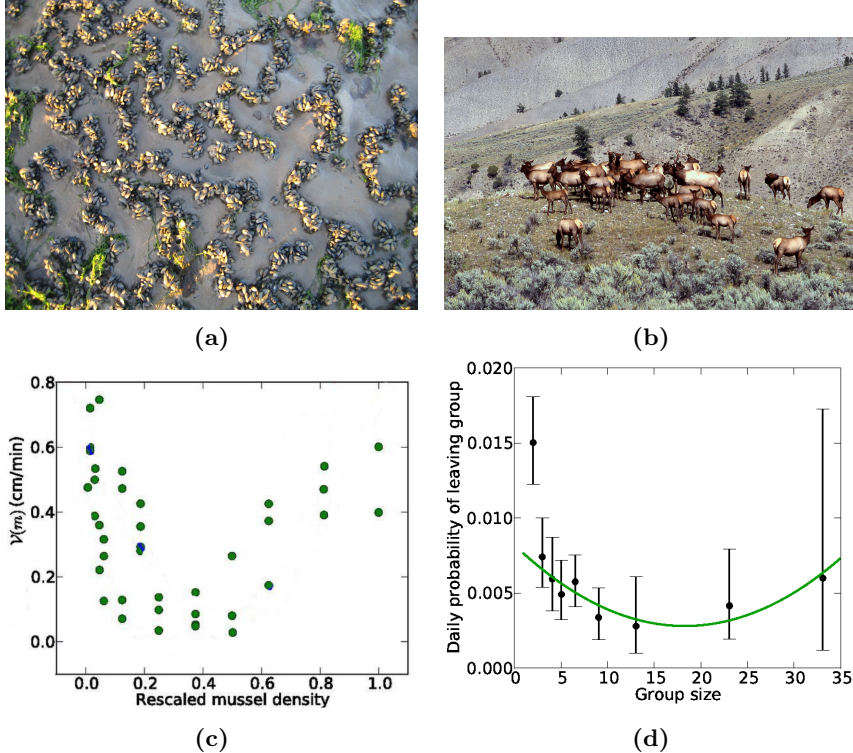


Figure 2 – Density depend movement as observed in populations of mussels (a,c) and elks (b,d). In (a) and (b) the patterns, that are observed in nature, are shown for both mussels (a) and elk herds (b). The black circles denote the data points, while the green line in (d) is a quadratic fit. In both figures (c) and (d) we can see that there is a global minimum in the movement speed at some intermediate density of the animals. (conform [7, 6])

equations can lead to spatial patterns via a bifurcation of a homogeneous state (nowadays called a Turing bifurcation). This insight was so powerful that it explained a vast variety of phenomena, ranging from animal markings [2] to desertification [3] to patterns in chemical reactions [4].

This Turing mechanism is not the only way self-organisation presents itself. It can also occur via a density dependent movement, where the speed of a specie is determined by the local density of the specie. This sort of movement is seen in many animal populations, such as mussels [5, 6], elk herds [7], bacteria and snails [8]. In Figure 2 examples of these density dependent movements are shown, for both mussels and elk herds.

It is theorized that this specific density dependent movement, with a non-zero speed minimizing density, is the result from a balancing of two conflicting desires of an individual. On one hand it is beneficial to be near others, as this diminishes ones chances of being eaten by a predator. For some species this can be a biological effect - mussels, for example, have the tendency to literally stick to each other - though it's also a probabilistic effect - as an individual prey is less likely to be eaten when there is an abundance of them. On the other hand

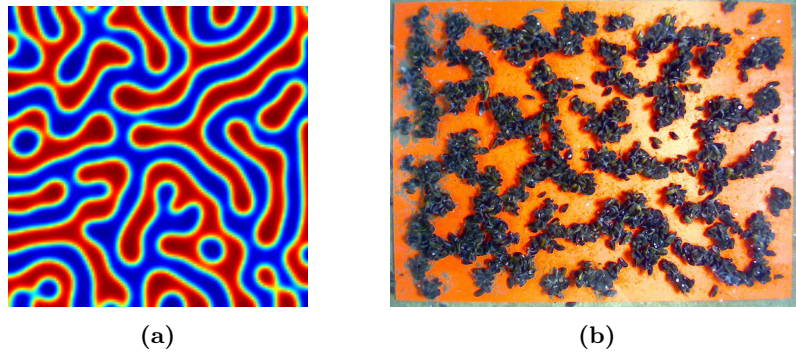


Figure 3 – Typical patterns observed in (a) the Cahn-Hilliard equation (b) mussel beds. The latter image is made in an lab experiment (see [5]).

sticking together has a negative effect as well, because the available food must be shared with many, possibly leading to hunger or death.

In 2013 Liu et al [5] showed that the density dependent movement speed of mussels can be incorporated in a single-species evolution model as a Cahn-Hilliard equation,

$$\frac{\partial m}{\partial t} = d_m \nabla \left(v(m) \left[v + m \frac{\partial v}{\partial m} \right] \nabla m - \kappa \nabla (\Delta m) \right), \quad (1)$$

where d_m and κ are constants, m is the density of the mussels and $v(m)$ is the movement speed of the mussels at density m . It does not matter whether this density is in mass per volume or units per volume.

The Cahn-Hilliard equation is a well-studied equation in solid state physics. This equation was introduced by Cahn and Hilliard in 1958-1959 [9, 10, 11] to model the behaviour of a two-component liquid. The most basic and most often seen form of this Cahn-Hilliard equation is

$$\frac{\partial c}{\partial t} = D \Delta [c - c^3 - \gamma \Delta c], \quad (2)$$

where D is the diffusion constant, γ is some (often small) constant and c is the concentration of one of the components.

The ingenious idea of Cahn and Hilliard was to include both a double well-potential and a surface energy. Since the latter only has a secondary role in determining the energy of the system it was often neglected altogether in earlier descriptions of these systems. However, only by the inclusion of these terms it is possible to find the patterns that were observed in real materials. These patterns - as turned out - were also very similar to some of the patterns observed in mussel beds [5]. In Figure 3 we have shown patterns resulting from the Cahn-Hilliard equation and patterns observed in mussels [5].

Though visually the patterns of mussels and the Cahn-Hilliard equation look similar, this does not necessarily mean that we can accurately model mussels with this equation. To strengthen this belief, we can inspect more advanced behaviour of the Cahn-Hilliard equation. In 1961 Lifschitz and Slyozov [12]

showed that the typical wavelength of the patterns created by the Cahn-Hilliard equation follows a power law: $L(t) \propto t^{1/3}$. This same power law is also initially found in mussel beds (see Figure 4 and [5]), strengthening our belief in the Cahn-Hilliard equation as description for the movement of mussels.

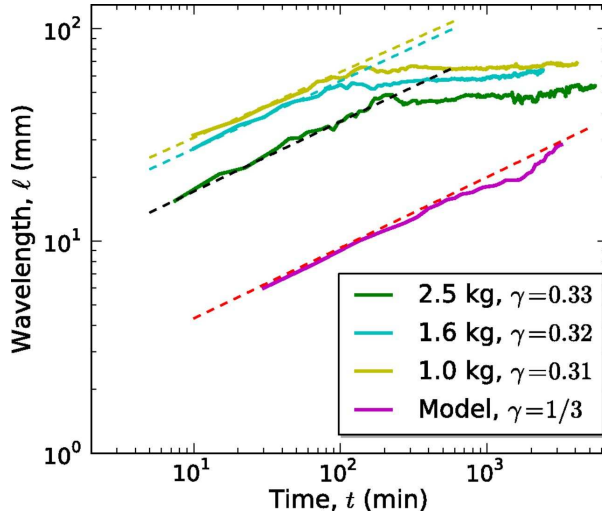


Figure 4 – Correlation between the typical wavelength of patterns for mussels, in experimental set-up (blue and green lines) and in a numerical simulation (purple). The dashed lines are linear fits over the initial behaviour (i.e. before a wavelength is ‘selected’). For the numerical simulation the theorized power law is used instead. In these plots we can clearly see that there is some sort of wavelength selection in the experiments after some hours.

Over longer time periods this Lifschitz-Slyozov power law is no longer obeyed - it seems like the mussels select a wavelength. Hence this means that the Cahn-Hilliard equation no longer accurately describes the behaviour of mussels. In experiments this was observed already after several hours so the mortality and reproduction of mussels does not play a role. Moreover, the experiments were conducted without any food supply (algae) so that there isn’t any interaction with other species as well. Hence this ‘wavelength selection’ must be explained *without* any of these effects that generally lead to patterns.

The aim of this master’s research is twofold: on one hand we want to understand the occurrence of this wavelength selection; on the other hand we want to understand the long-time effect of the density-dependent movement speed on populations in nature - where there *are* interactions with other species and mortality and birth play a role. The general equation that will be our model throughout this thesis is

$$\frac{\partial m}{\partial t} = d_m \nabla \left(v \left(v + m \frac{\partial v}{\partial m} \right) \nabla m + v m \frac{\partial v}{\partial a} \nabla a - \kappa \nabla \Delta m \right) + \varepsilon H(m, a) \quad (3a)$$

$$\frac{\partial a}{\partial t} = \varepsilon d_a \Delta a + \varepsilon G(m, a). \quad (3b)$$

Here m denotes the concentration of the predator (mussels) and a of the prey (algae). Moreover $H, G : \mathbb{R}^2 \rightarrow \mathbb{R}$ are so-called interaction terms that model the interactions between the species, d_m and d_a are diffusion constants and κ is a small parameter. Finally $0 < \varepsilon \ll 1$ is a small parameter, which is added to emphasize that interactions between species and the diffusion of the second specie is small compared to the Cahn-Hilliard like behaviour of the predators (e.g. the mussels).

In this model we can think of the movement speed of mussels, v , as a function not only of the mussels density but of the algae's density as well; i.e. $v : \mathbb{R}^2 \rightarrow \mathbb{R}$ $(m, a) \mapsto v(m, a)$. This is a more general form of the previously described density dependent movement speed and allows us to study situation in which movement speed is decreased in case of an abundance of food, which is found in experiments [6].

Although we will constantly talk about mussels and algae, we emphasize that this model is suitable for many other predator-prey and animal-food systems as well - as long as either the predator or the prey has a density dependent movement speed. The general analysis of this thesis is therefore applicable to these models as well, though the analysis on the specific mussel-algae system, with corresponding interactions terms, is not and should be adapted for each new population system.

This thesis is divided into three major chapters. In Chapter 1 we explain the model in-depth and we set-up the specific situation of a mussel-algae system. We also describe two possible forms for the density dependent movement speed in this chapter. Then in Chapter 2 we study the Cahn-Hilliard equation (i.e. equation (3) with $\varepsilon = 0$) and give a possible explanation for the wavelength selection. Finally Chapter 3 deals with the full model, when $\varepsilon \neq 0$. Here we apply a linear stability analysis and a weakly non-linear stability analysis to get a grip on the possible patterns that can occur. Both Chapter 2 and Chapter 3 also feature simulations of the population model for a system of mussels, that give a good insight in the behaviour of these systems.

Chapter 1

Ecological Set-Up

Mathematics has been very successful in explaining a vast variety of phenomena, from ecological ones to medical and economical effects. Applied mathematics is very powerful and useful. Though before we can exploit all the machinery it has to offer, we need to capture the essences of the phenomena we want to study in a mathematical model. Ideally this model is as simple as it can be, though it should still include all essential subtleties of the system we are interested in. As this is a very important - if not the most important - task in a study in applied mathematics, this first chapter deals with the modeling aspect of pattern formation in animal populations.

This chapter starts in section 1.1 by building up the model, starting from an often used reaction-diffusion equation. We describe everything in generalities, though we also include concrete possibilities for the specific mussel-algae system that we want to understand. Specifically, we discuss how we can model the density dependent movement speed in section 1.1.4. This all results in the following equation describing our model that we study in the following chapters:

$$\begin{aligned}\frac{\partial m}{\partial t} &= d_m \nabla \left(v \left(v + m \frac{\partial v}{\partial m} \right) \nabla m + v m \frac{\partial v}{\partial a} \nabla a - \kappa \nabla \Delta m \right) + \varepsilon H(m, a) \\ \frac{\partial a}{\partial t} &= \varepsilon d_a \Delta a + \varepsilon G(m, a).\end{aligned}$$

Moreover, in the second part of this chapter, in section 1.2, we study a reaction-diffusion system, that describes the interaction between algae and mussels. We determine the kind of patterns that can already be explained by this model, of the form

$$\begin{aligned}\frac{\partial m}{\partial t} &= d_m \Delta m + H(m, a) \\ \frac{\partial a}{\partial t} &= d_a \Delta a + G(m, a).\end{aligned}$$

This description does not have the density-dependent movement speed. However it is still useful to study this system, so we know what kind of patterns can be explained with this description. Therefore we can ultimately get a good idea of the additional effects that adding a density-dependent movement has.

1.1 Explanation of the model

In this section we explain the general set-up of population models. We start by explaining a general reaction-diffusion equation and then later modify it to include a density-dependent movement speed. Throughout this section we denote one of the species with m (for mussel) and the other as a (for algae). The general description is however also applicable to other systems, for instance other predator-prey population models or chemical reactions.

1.1.1 Reaction-Diffusion Equations

Let's start by imagining that our mussels and algae don't move and inspect what happens at a particular point. We want to have a model that describes how the concentration of mussels and algae (at a specific point) change over time. Since there is interaction between mussels and algae, because mussels eat algae and because of mortality and birth, we do not expect this concentration to be constant. Hence we should try to model the rate of change of the concentration, taking the interactions into account. This can in general be done by the following ordinary differential equation:

$$\begin{aligned}\frac{\partial m}{\partial t} &= H(m, a) \\ \frac{\partial a}{\partial t} &= G(m, a)\end{aligned}$$

The functions $H, G : \mathbb{R}^2 \rightarrow \mathbb{R}$ are the so-called interactions terms. These terms describe the behaviour that is observed in the system (mortality, births, eating and so on). They dependent heavily on the specific system we want to inspect - the functions H and G probably will change a lot when we try to study any other population model. In section 1.1.3 we will describe a possible form of these interaction terms for our mussel-algae system.

In reality our no-movement assumption is nonsense of course. Hence a good model should also include this spatial movement. The easiest and most used way to incorporate this into our equations is to model it as diffusion. In this description we need to find the amount of concentration that flows in each direction, i.e. the flux of the concentration of mussel and algae. This flux, denoted as \vec{J} , can be computed using Fick's law of diffusion that states that the flux is proportional to the diffusion, i.e.

$$\vec{J} = -D\nabla m.$$

Here D is the diffusion constant of the specific specie¹.

The amount of mussels that now move out due to diffusion is then equal to minus the gradient of the flux (i.e. $\frac{\partial m}{\partial t} = -\nabla \cdot \vec{J}$ - this is the continuity equation; see for example [13]). The interactions terms that we have derived before of course

¹We should note that D is not really a constant - it can for instance depend on the temperature. For our study we assume that D is a constant and we ignore these fluctuations in D in our study.

still play the same role. Hence a model that combines this diffusion and the interactions between species can be written as

$$\begin{aligned}\frac{\partial m}{\partial t} &= d_m \Delta m + H(m, a) \\ \frac{\partial a}{\partial t} &= d_a \Delta a + G(m, a).\end{aligned}$$

Here $d_m > 0$ is the diffusion constant for mussels and $d_a > 0$ that for algae.

The model that we have now is not yet complete. It needs to be accompanied by initial conditions and boundary conditions. For population models it is most natural to assume that there is no concentration flowing out through the boundaries². Hence we normally will apply so-called zero-flux or Neumann boundary conditions at the boundaries. Hence the complete model can be captured in the following set of equations:

$$\frac{\partial m}{\partial t}(x, t) = d_m \Delta m(x, t) + H(m(x, t), a(x, t)) \quad \text{when } x \in \Omega, \quad (1.1a)$$

$$\frac{\partial m}{\partial t}(x, t) = d_a \Delta a(x, t) + G(m(x, t), a(x, t)) \quad \text{when } x \in \Omega, \quad (1.1b)$$

$$\nabla m(x, t) \cdot \hat{n}(x) = \nabla a(x, t) \cdot \hat{n}(x) = 0 \quad \text{when } x \in \partial\Omega, \quad (1.1c)$$

$$m(0, x) = m_0(x), a(0, x) = a_0(x) \quad (1.1d)$$

Here Ω denotes the region we want to model and $\partial\Omega$ its boundary. Moreover \hat{n} is the unit vector pointing outwards of the region³ Ω . For laboratory experiments we can think of the box in which the mussels lie as this region Ω . The functions m_0 and a_0 specify the initial configuration of the system. When we want to study the behaviour of the mussel-algae system in nature, the region we are inspecting is very large. Hence we can think of this region as infinitely large in all directions and forget about the boundary conditions.

The model that we have described in equation (1.1) is a reaction-diffusion equation. These are called this way, because of their initial usage in describing the behaviour of chemical reactions. The major assumption in this description is that of Fickian diffusion, which implicitly assumes that the movement speed does not depend on density.

1.1.2 Density-dependent movement speed

As was shown by Liu et al [5] the movement speed of mussels *does* depend on the density of the mussels. For population systems like these, with a density dependent movement, we cannot model this system accurately with a reaction-diffusion equation. Hence we must work to get a good description of the movement of the mussels, which we can use instead of the Fickian diffusion we have used before.

Now that the movement speed is not constant for all densities, we can assume that the mussels still perform a random walk, though with individual density

²It is also possible to assume that we have an unbounded domain

³This implicitly assumes some regularities on the domain Ω . We will not talk about these issues and just assume everything is smooth enough for our analysis.

dependent movement speeds $v(m, a)$. Moreover, we will also assume that the mussels change directions with a turning rate τ that does not depend on the density. The flux in this case is given by (see [14])

$$J_v = -\frac{v(m, a)}{2\tau} \nabla(v(m, a)m).$$

In this situation it is necessary to also include the effects of non-local long-range interactions to the flux of the mussels. To do this, we must inspect the first correction to the normal diffusion. It is shown in [15] that this first correction comes from the third spatial derivative. Hence the flux due to non-local effects is of the form

$$J_{nl} = \hat{\kappa} \nabla(\Delta m),$$

where $\hat{\kappa} > 0$ is some (positive) constant that generally is small, because it is only a correction to the normal diffusion.

The total flux in our model is just the sum of the two fluxes that we have derived. Hence this specific form of the flux gives rise to the following equation for the mussels (ignoring the interaction terms for now):

$$\begin{aligned} \frac{\partial m}{\partial t} &= -\nabla[J_v + J_{nl}] \\ &= \nabla \left[\frac{1}{2\tau} v(m, a) \nabla(v(m, a)m) - \hat{\kappa} \nabla(\Delta m) \right] \\ &= \nabla \left[\frac{1}{2\tau} v \left((v + m \frac{\partial v}{\partial m}) \nabla m + m \frac{\partial v}{\partial a} \nabla a \right) - \hat{\kappa} \nabla(\Delta m) \right] \end{aligned}$$

In the last step we have expanded the term $\nabla(vm)$ and we suppressed the explicit dependence of the speed on the density of mussels and algae for notational simplicity. We can simplify this expression even more when we define $d_m := \frac{1}{2\tau}$ and $\kappa = 2\tau\hat{\kappa}$. Hence we obtain

$$\frac{\partial m}{\partial t} = d_m \nabla \left[v \left(v + m \frac{\partial v}{\partial m} \right) \nabla m + v m \frac{\partial v}{\partial a} \nabla a - \kappa \nabla(\Delta m) \right].$$

When we don't include algae in our model, we can forget about the effect of the algae's density on the movement speed of the mussels. In this situation this description reduces to the special form of the Cahn-Hilliard equation:

$$\frac{\partial m}{\partial t} = d_m \nabla \left[v \left(v + m \frac{\partial v}{\partial m} \right) \nabla m - \kappa \nabla \Delta m \right]$$

We are however interested in the model that includes algae. Moreover, we are also interested in the long-term behaviour of the system and hence we also want to include the interaction terms. In principle we can just add the interaction terms like we did in the reaction-diffusion equation and obtain the following system:

$$\begin{aligned} \frac{\partial m}{\partial t} &= d_m \nabla \left[v \left(v + m \frac{\partial v}{\partial m} \right) \nabla m + v m \frac{\partial v}{\partial a} \nabla a - \kappa \nabla \Delta m \right] + H(m, a) \\ \frac{\partial a}{\partial t} &= d_a \Delta a + G(m, a) \end{aligned}$$

Doing this however ignores an important ecological fact: the movement of the mussels is much faster than that of the algae or their interactions. For instance one can easily imagine that the mortality rate of mussels is much slower than their movement. We want to incorporate this fact into the model and therefore we write the system as a fast-slow system as

$$\frac{\partial m}{\partial t} = d_m \nabla \left[v \left(v + m \frac{\partial v}{\partial m} \right) \nabla m + v m \frac{\partial v}{\partial a} \nabla a - \kappa \nabla \Delta m \right] + \varepsilon H(m, a) \quad (1.2a)$$

$$\frac{\partial a}{\partial t} = \varepsilon d_a \Delta a + \varepsilon G(m, a), \quad (1.2b)$$

where $0 < \varepsilon \ll 1$ is a very small constant, that emphasizes the slow terms. Moreover, $d_m, d_a, \kappa > 0$ are positive constants and κ is generally a small constant (but still larger than ε).

In this description of the model as a partial differential equation we again need to impose boundary conditions and initial conditions. Because of the addition of a fourth order spatial derivative in this model, we also need another set of boundary conditions as the previous set of no-flux boundary conditions was not sufficient. For the last set of boundary conditions we therefore will use the standard choice of boundary conditions for the Cahn-Hilliard equation on a bounded domain (see Chapter 2) and hence we have the following set of boundary conditions for this problem:

$$\begin{aligned} \nabla m \cdot \hat{n} &= 0 && \text{when } x \in \partial\Omega; \\ \nabla a \cdot \hat{n} &= 0 && \text{when } x \in \partial\Omega; \\ \nabla(\Delta m) \cdot \hat{n} &= 0 && \text{when } x \in \partial\Omega. \end{aligned}$$

With this we have made the model that will be the subject of our study throughout this thesis. In the next sections we will delve into the specific possibilities for the interactions terms H and G for the specific mussel-algae system and the possible forms of the density dependent movement speed that will serve as our base example in the rest of this study.

1.1.3 Interaction terms for the Mussel-Algea system

The general model that we have created in equation (1.2) is - logically - not very concrete. In this section we will inspect the most used forms of the interaction terms H and G . To really understand what these interaction terms mean, we must go back to the real situation and determine *how* we will model the system. The interaction terms that we derive in this section are also found in the literature [16, 17, 18].

For our system, with both mussels and algae, we immediately can understand that they both live in water. Algae can flow in water, though mussels can only be present at the bottom. Hence there will only be an interaction between algae and mussels in the lower layer of water, where mussels and algae coexist. To model this we will divide the water into two layers: the lower layer, of depth h , that we will actually describe with our model, and an upper layer (see Figure 1.1).

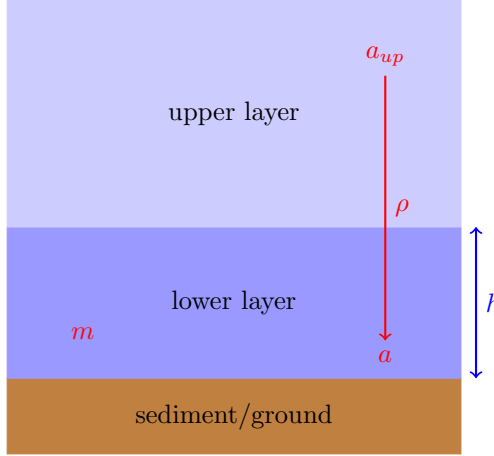


Figure 1.1 – Sketch of a side-view of the set-up for the model. The water is divided into two parts: one lower layer, which is actually modeled in the equations, of depth h and an upper layer, where there is assumed to be a constant concentration of algae a_{up} (and no mussels). The algae flow from the upper layer to the lower layer at a rate ρ .

It is assumed that there is a constant concentration of algae, a_{up} , in the upper layer. Because the upper layer is in contact with the lower layer it is possible for algae to flow from the upper layer to the lower layer. The amount of algae that flow in this way is proportional to the difference in concentration between both layers and to some rate ρ . Hence we see that the concentration of algae in the lower layer changes as $\rho(a_{up} - a)$. That is, the contribution of this effect, the renewal/birth of algae, to the interaction term G is G_b where G_b is defined as

$$G_b(m, a) = (a_{up} - a)\rho.$$

Besides this renewal of algae there is also a decrease in algae because they are being eaten by the mussels. This effect is generally seen as proportional to the product of the concentration of algae and that of mussels; when there are more predators more prey are eaten and when there are more prey to eat, more will be eaten. This term, representing algae being eaten, is also proportional to some constant c , the consumption constant, that describes how fast algae are being eaten. Moreover, because we have modeled the lower layer as a layer of depth h , the real consumption constant is only $\frac{c}{h}$ since mussels only live on the sediment. Therefore the contribution to the interaction term G due to eating is:

$$G_d(m, a) = -\frac{c}{h}ma$$

Since there are no other contributions to the interaction term G , we can now write down the full expression for G , representing the change in the density of algae as the following function:

$$G(m, a) = G_b(m, a) + G_d(m, a) = (a_{up} - a)\rho - \frac{c}{h}ma$$

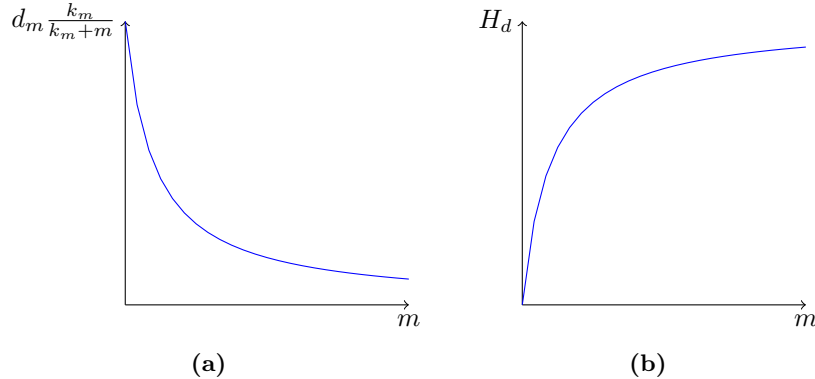


Figure 1.2 – Plots of the fraction $\hat{d}_m \frac{k_m}{k_m+m}$ (a) and the mortality contribution to the interaction terms (b).

The other interaction term, H , describes how the density of the mussels changes due to the interactions. The first interaction that one can think of is the eating of algae. Again this change is proportional to the product of densities ma and the consumption constant c . However there is also a conversion rate - since one mussel must eat many algae before it can and will reproduce. Hence we find the contribution of this effect to the interaction terms as

$$H_b(m, a) = ecma$$

On the other hand, mussels will die as well. The amount of mussels that die is proportional to the density of mussels and to some number, representing the fraction of mussels that will be eaten. Since - as we have argued in the introduction - mussels want to stick together as this gives them better chances to survive, we must include this effect in our model here. That means that the fraction of mussels that will be eaten must decrease when the concentration increases.

The common choice - and one of the easiest in computations⁴ - for this fraction is $\hat{d}_m \frac{k_m}{k_m+m}$. Here \hat{d}_m is the maximal fraction (achieved when $m = 0$) and k_m is the mussel density at which this fraction is only half of the maximal fraction. A plot of this particular fraction is given in Figure 1.2. The corresponding contribution to the interaction term is then

$$H_d(m, a) = \hat{d}_m \frac{k_m}{k_m + m} m.$$

A plot of this function is also given in Figure 1.2.

Hence at this moment we have all necessary information to formulate the complete interaction terms, H and G . We have found and explained now that they must

⁴One could also think of many other models for this fraction, for instance an exponential one: e^{-m} . This formulation has the same properties - it decreases when m increases. Since working with exponentials is generally more cumbersome, people generally tend to work around these.

have the following form:

$$H(m, a) = ecam - \hat{d}_m \frac{k_m}{k_m + m} m \quad (1.3a)$$

$$G(m, a) = (a_{up} - a)\rho - \frac{c}{h}am \quad (1.3b)$$

Finally, from the way we have defined these interaction terms, we should remember that all parameters in this description must be positive.

The interaction terms that we have derived in this section are applicable to both the reaction-diffusion system (see equation (1.1)) and the model that includes the density-dependent movement (see equation (1.2)). In Section 1.2, and later in Chapter 3 we will use these interaction terms to study the specific mussel-algae system.

1.1.4 Choices for the density dependent movement speed

The main focus point of our research comes from the addition of the density dependent movement speed in our model. The specific form of this movement speed is important, as this can influence the patterns that are predicted by the model. Therefore we will discuss the possible choices to define this movement speed, as function of the density of mussels and algae.

In the introduction we already saw the experimental data, that suggested the density dependent movement (this graph is repeated in Figure 1.3). As we have stated before the concentration of algae (i.e. food) is important as well [6]; if there is much food available, the mussel don't need to move that much to feed themselves, while they need to move much when food is sparse.

In this section we will discuss two ways to model the movement speed, that we will use later on in this thesis for simulations and analysis on the mussel-algae system.

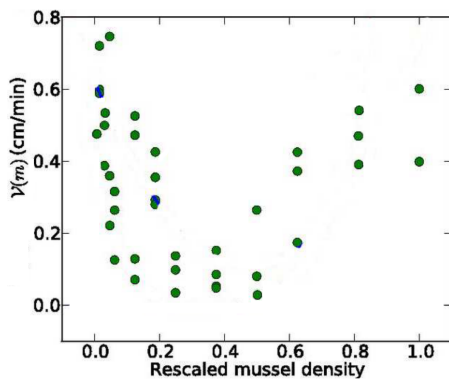


Figure 1.3 – Graph of the density dependent movement speed as observed in mussels, when there are no algae [6]. The green dots are the data points.

Possibility 1: Quadratic fit

Liu et al found - by empirical methods - that we can take the speed v of the mussels to depend on m in a quadratic way [5], as an approximation. So they use

$$v(m) = c_1 m^2 + c_2 m + c_3,$$

where c_1, c_2 and c_3 are constants such that $v(m) > 0$ for all possible $m \in \mathbb{R}$.

To incorporate the effect of the density of the algae, we need to figure out how they contribute to this speed. As a first rule of thumb we can follow our biological intuition: if there is much food available, the mussels don't need to move to feed themselves, whereas they need to move much when food is sparse. Hence we would expect that $v(m, a_1) > v(m, a_2)$ if and only if $a_1 < a_2$. Since we do not know the explicit relation, we will for now assume that this effect is linear in the algae concentration - as this is the simplest for our analysis. Hence we assume that

$$v(m, a) = c_1 m^2 + c_2 m + c_3 - d_1 a,$$

where $d_1 > 0$ is now an additional (positive) constant.

Since we want the speed to be always positive and since a higher concentration of algae leads to a lower speed, we would expect to run into trouble as $a \rightarrow \infty$. Luckily, there is an upper bound on the concentration of algae. In our model (and most others; see [17] and [16]) for the mussel-algae system, it is assumed that the concentration of algae can only be depleted in the lower section of the water (where mussels live) and that reproduction occurs elsewhere.

Hence the only way for the algae concentration to increase is by a transportation of algae from higher sections of water. This means that the concentration of algae in the lower section cannot exceed the concentration at higher sections. We will denote this concentration as a_{up} . So we know that $a \in [0, a_{up}]$. Thus we know that $v(m, a) \geq v(m, a_{up})$ for all $a \in [0, a_{up}]$. Hence in order to have a positive speed of the mussels for all possible concentrations, we just need

$$v(m, a_{up}) = c_1 m^2 + c_2 m + (c_3 - d_1 a_{up}) > 0$$

for all possible mussel concentrations m .

To investigate for what parameters values that happens, we rewrite this by completing the square as

$$v(m, a_{up}) = c_1 \left(m + \frac{c_2}{2c_1} \right)^2 - \frac{c_2^2}{4c_1} + c_3 - d_1 a_{up}$$

From this we know that $v(m, a_{up}) > 0$ if

$$\begin{aligned} c_1 &> 0 \\ c_2^2 &< 4c_1(c_3 - d_1 a_{up}). \end{aligned}$$

The second constraint can only be obeyed if $c_3 - d_1 a_{up} > 0$. So we also have this as a condition. Hence to summarize: the speed of the mussels - in this

description - is positive for all possible concentrations if and only if

$$c_1 > 0 \quad (1.4a)$$

$$c_3 > d_1 a_{up} \quad (1.4b)$$

$$c_2^2 < 4c_1(c_3 - d_1 a_{up}). \quad (1.4c)$$

To make life easier we can scale the densities m and a by defining $M := \sqrt{\frac{c_1}{c_2}}m$, $A := \frac{1}{a_{up}}a$ and the new parameters $\tilde{\beta} := \frac{c_2}{\sqrt{c_1 c_3}}$ and $\tilde{d} = \frac{d_1 a_{up}}{c_3}$. With this scaling it is possible to write the speed as

$$v(M, A) = c_3 \left(M^2 + \tilde{\beta}M + 1 - \tilde{d}A \right).$$

Since the constant c_3 now can be incorporated into the constants d_m and κ (see equation (1.2)), we can ignore this constant here and still have a good model (i.e. take $c_3 = 1$). Hence we will think of the ‘quadratic fit’ movement speed as the following function of M and a :

$$v_q(M, A) = M^2 + \tilde{\beta}M + 1 - \tilde{d}A$$

Because of the non-negativity of the speed we find the following condition on the parameters $\tilde{\beta}$ and \tilde{d} , which can be derived directly from the conditions in equation (1.4):

$$\tilde{\beta}^2 < 4(1 - \tilde{d})$$

The concentration of mussels, M , and the concentration of algae, A , must be non-negative, since a negative concentration is unphysical. Therefore we only need to make sure that the function v is positive for non-negative concentrations. Hence it is sufficient to put the following condition on the parameter $\tilde{\beta}$ to ensure positiveness of the mussel’s movement speed:

$$\tilde{\beta} > -2\sqrt{1 - \tilde{d}}$$

Possibility 2: A piecewise-linear function

Previously we modeled the speed of the mussels via a quadratic approach. This description is perhaps a bit too rough. From biological data [6] it seems that the influence of the algae density is small when the mussel density is small and big when the mussel density is high. This seems logical: sticking together decreases the probability that an individual will be eaten, regardless of the availability of food. The term $-da$ does not take this into account and hence the previous ‘quadratic’ description ignores this fact. Therefore we now want to model the speed in an other way, that takes this effect into account.

There is not enough experimental data to really see how we should define the density dependent speed, as a function of both the density of mussels and that of algae. Hence we must make a *guess* about the form. As suggested in the previous paragraph, it seems that the concentration of algae only starts to play a significant role when the density of mussels is high enough. We suspect that the more food the slower the mussels will move. To make our formulation as simple

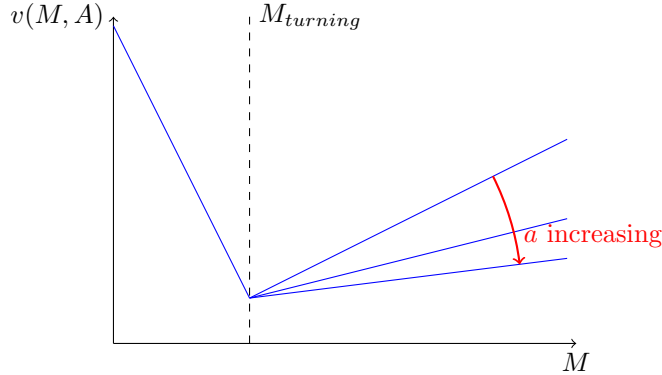


Figure 1.4 – Schematic illustration of the density-dependent speed $v(m, a)$, modeled as piecewise linear function. For low mussel densities the speed is assumed to not depend on the concentration of algae, whereas at higher densities more algae means slower mussels.

as it can be, we will assume that the speed $v(m, a)$ is piecewise linear, where the slope of the righter part, for higher mussel densities, depends on the algae concentration. In Figure 1.4 we have sketched the guessed density dependent speed.

This piecewise linear approach will give us a description of the following form:

$$v(M, A) = \begin{cases} v_1(M, A) & \text{when } M < M_{turning}; \\ v_2(M, A) & \text{when } M > M_{turning}. \end{cases}$$

Since the quadratic fit approach of last section gave a minimum that depends on the parameter $\tilde{\beta}$ it is logical to ensure that our piecewise-linear speed also has this dependence. To resemble this we will put the density, which is the turning point between low mussel densities and high densities (i.e. the dashed line in Figure 1.4), at $M_{turning} = \frac{\tilde{\beta}}{2}$.

At lower densities we want the speed to be linear (and decreasing). We will simply put⁵

$$v_1(M, A) = 1 - \tilde{\beta}M.$$

Here $\tilde{\beta} > 0$ because we want this line to decrease. Since we need the movement speed to be positive, we find the condition $\frac{2-\tilde{\beta}^2}{2} > 0$ on the parameter $\tilde{\beta}$.

For higher densities we want another linear function, of which the slope depends on the local algae density. We also need to make sure that v_1 and v_2 line up at the density $M_{turning}$. Hence we obtain the following form for v_2 :

$$v_2(M, A) = \frac{2 - \tilde{\beta}^2}{2} + \tilde{\gamma}(A) \left[M - \frac{\tilde{\beta}}{2} \right],$$

where $\tilde{\gamma}(A)$ is positive to ensure the positiveness of the movement speed.

⁵By a scaling, similar to the scaling before, we can transform the general formulation of a movement speed to this form.

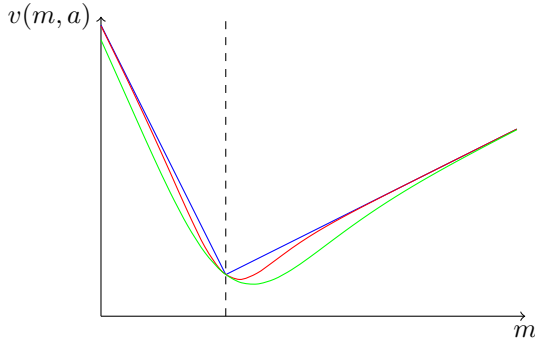


Figure 1.5 – Plots of the piecewise linear function (blue) and the infinitely smooth approximations, using $K = \frac{1}{2}$ (green) and $K = 1$ (red). As can be seen these smooth approximations resemble the piecewise linear function well. Increasing K even more will give even better (smooth) approximations.

Since we want the speed to be (infinitely) smooth - to be able to differentiate as necessary - we can use a mollification to define the speed, for example as

$$v(M, A) = v_1(M, A) + \frac{1 + \tanh(K[M - \tilde{\beta}/2])}{2}(v_2(M, A) - v_1(M, A))$$

where $K \in \mathbb{R}$ must be chosen large enough.

In the limit $K \rightarrow \infty$ we see that $v(M, A)$ will become

$$v_p(M, A) = \begin{cases} v_1(M, A) = 1 - \tilde{\beta}M & \text{if } M < \tilde{\beta}/2; \\ v_2(M, A) = \frac{1-\tilde{\beta}^2}{2} + \tilde{\gamma}(A)[M - \tilde{\beta}/2] & \text{if } M > \tilde{\beta}/2. \end{cases}$$

So if K is chosen large enough we can use the piecewise linear description as a very good approximation (see Figure 1.5). Therefore we will work with this piecewise-linear speed $v_p(M, A)$ in the analysis of this thesis.

The function $A \mapsto \tilde{\gamma}(A)$ gives the slope of the line v_2 . Since biological data suggests that a high density of algae corresponds to a low slope and vice-versa, we must choose γ such that it is a decreasing, positive function. The straightforward choice for this kind of function is $\gamma(A) := \gamma_0 e^{-\tilde{d}A}$ where \tilde{d} and $\gamma_0 > 0$ are (new) parameters.

Summary of the possible choices for the speed

In this section we described two possible ways to model the density dependent movement of the mussels, taking the effect of the algae's concentration into account. We have found a 'quadratic fit' approach with speed, which we will be calling v_q as

$$v_q(M, A) = M^2 + \tilde{\beta}M + 1 - \tilde{d}A.$$

Here $\tilde{d} > 0$ and $\tilde{\beta} > 2\sqrt{1 - \tilde{d}}$.

We have also found a piecewise linear approach, which we will denote by v_p . This piecewise linear function for the speed has the following form:

$$v(M, A) = \begin{cases} v_1(M, A) = 1 - \tilde{\beta}M & \text{if } M < \tilde{\beta}/2; \\ v_2(M, A) = \frac{1-\tilde{\beta}^2}{2} + \gamma_0 e^{-\tilde{d}A} [M - \tilde{\beta}/2] & \text{if } M > \tilde{\beta}/2, \end{cases} \quad (1.5)$$

where $0 < \tilde{\beta} < \sqrt{2}$, $\gamma_0 > 0$ and $\tilde{d} > 0$.

1.2 A Reaction-Diffusion model for mussels

In the previous sections we introduced the possible Cahn-Hilliard like, density dependent movement, description of the mussel-algae system. In this thesis we want to study the effect of the addition of the density-dependent movement speed to the model. Therefore it is necessary to first study the normally studied model, of reaction-diffusion type that we have described in equation (1.1). We will use the interaction terms that we have found in section 1.1.3 (see equation (1.3)).

The complete reaction-diffusion model for the mussel-algae system then reads

$$\begin{aligned} \frac{\partial m}{\partial t} &= d_m \Delta m + ecam - \hat{d}_m \frac{k_m}{k_m + m} m \\ \frac{\partial a}{\partial t} &= d_a \Delta a + (a_{up} - a)\rho - \frac{c}{h} am. \end{aligned}$$

Recall that all the parameters must be positive. In this section we study this system on a two-dimensional unbounded domain.

To reduce the amount of parameters that we need to consider, we can write the differential equation in a dimensionless way. Therefore we introduce the following scalings and new parameters:

$$\begin{aligned} \tau &= \hat{d}_m & r &= \frac{eca_{up}}{\hat{d}_m} \\ (x', y') &= \sqrt{\frac{ck_m}{d_a h}} & \tilde{\gamma} &= \frac{hd_m}{ck_m} \\ m &= k_m M & \tilde{\alpha} &= \frac{\rho h}{ck_m} \\ a &= a_{up} A & \tilde{\mu} &= \frac{d_m ck_m}{d_a h \hat{d}_m}. \end{aligned}$$

Under this scaling the partial differential equation transform into the system

$$\frac{\partial M}{\partial \tau} = \tilde{\mu} \Delta' M + r M A - \frac{M}{1 + M} \quad (1.6a)$$

$$\tilde{\gamma} \frac{\partial A}{\partial \tau} = \Delta' A + \tilde{\alpha}(1 - A) - M A. \quad (1.6b)$$

In the rest of the section we will drop the apostrophe and we will write τ as t for notational convenience. Also note that the parameters, $\tilde{\mu}, \tilde{\gamma}, \tilde{\alpha}$ and r are all (still) positive.

This remainder of this section will be devoted to the analysis of this scaled reaction-diffusion system. We will focus on the stability of the uniform stationary points, by applying standard linear stability analysis and later on also weakly non-linear stability analysis. We will roughly follow Cangelosi et al [17], though they used a Landau expansion to determine the patterns.

1.2.1 Uniform Steady States

Our first objective is to find the uniform steady states of the reaction-diffusion equation (1.6). To do so, we are interested in solution with $M(x, y, t) = M_e$ and $A(x, y, t) = A_e$. Hence we know that the time derivatives and the Laplacians will vanish. Hence to find the uniform stationary states (M_e, A_e) we must solve the algebraic system

$$\begin{aligned} 0 &= rM_e A_e - \frac{M_e}{1 + M_e} \\ 0 &= \tilde{\alpha}(1 - A_e) - M_e A_e \end{aligned}$$

To solve the first condition we must have either (A) $M_e = 0$ or (B) $M_e = \frac{1-rA_e}{rA_e}$. In case (A) we find the second condition reduces to $\tilde{\alpha}(1 - A_e) = 0$. This gives $A_e = 1$. In case (B) we find the second condition to be $A_e r(1 - \tilde{\alpha}) - (1 - \tilde{\alpha}r) = 0$, which gives $A_e = \frac{1-\tilde{\alpha}r}{r(1-\tilde{\alpha})}$. The first relation then gives the value for M_e as $M_e = \tilde{\alpha} \frac{r-1}{1-\tilde{\alpha}r}$.

So to summarize, we have found the following two (possible) uniform stationary states of equation (1.6):

- (i) $(M_e, A_e) = (0, 1)$;
- (ii) $(M_e, A_e) = \left(\tilde{\alpha} \frac{r-1}{1-\tilde{\alpha}r}, \frac{1-\tilde{\alpha}r}{r(1-\tilde{\alpha})}\right)$.

However the system must be physical and thus we must have $M_e \geq 0$ and $A_e \geq 0$ because negative densities do not occur in reality. The stationary state $(M_e, A_e) = (0, 1)$ is already physical, but the second one need not be. Specifically, this stationary state is only physical when $r - 1, 1 - \tilde{\alpha}r$ and $1 - \tilde{\alpha}$ all have the same sign. It is easy to verify that all these terms are positive when $\tilde{\alpha} < 1$ and $r \in (1, \frac{1}{\tilde{\alpha}})$. On the other hand all these terms are negative when $\tilde{\alpha} > 1$ and $r \in (\frac{1}{\tilde{\alpha}}, 1)$. In the next section we will discover that this non-trivial steady state is (always) unstable when $r < 1$, which does not lead to any interesting effects. Hence we will assume that we are dealing with the former case, in which all terms are positive.

1.2.2 Linear Stability of the Uniform Stationary States

The following step in our analysis is to figure out the linear stability of the uniform stationary states. In order to do this, we must first linearise the system of equation (1.6). The Laplacians and the time derivatives are already linear functionals. Hence we only need to linearise the interaction terms $H(M, A)$ and

$G(M, A)$ around the fixed points (M_e, A_e) . Note that the interaction terms are now the interaction terms in the rescaled system. Hence we have

$$H(M, A) = rMA - \frac{M}{1+M}$$

$$G(M, A) = \tilde{\alpha}(1-A) - MA.$$

We can now make a Taylor polynomial of these functions and hence find their linearisations around the uniform steady state (M_e, A_e) as

$$H(M, A) = H(M_e, A_e) + \left(rA_e - \frac{1}{(1+M_e)^2} \right) M + rM_e A + \dots$$

$$G(M, A) = G(M_e, A_e) - A_e M - (\tilde{\alpha} + M_e) A + \dots$$

We want to study the linear stability of these stationary states that we found. In order to do so we must investigate how the system reacts to small perturbations. So we set $(M, A) = (M_e + \delta\tilde{M}, A_e + \delta\tilde{A})$. Here $0 < \delta \ll 1$ is very small and \tilde{M}, \tilde{A} are functions of both the time and the spatial coordinates. Because of the way we have defined this, we know that $|M - M_e|$ is of order $\mathcal{O}(\delta)$ as is $|A - A_e|$. Hence we can forget about the higher order terms in the Taylor polynomial we derived before and hence acquire the linearisation of equation (1.6). Substitution of this Ansatz into the linearized, rescaled reaction-diffusion equation then gives us the following linear partial differential equation

$$\frac{\partial \tilde{M}}{\partial t} = \tilde{\mu}\Delta\tilde{M} + \left(rA_e - \frac{1}{(1+M_e)^2} \right) \tilde{M} + rM_e \tilde{A} \quad (1.7a)$$

$$\tilde{\gamma}\frac{\partial \tilde{A}}{\partial t} = \Delta\tilde{A} - A_e \tilde{M} - (\tilde{\alpha} + M_e) \tilde{A}. \quad (1.7b)$$

We will now assume that $(\tilde{M}, \tilde{A}) = e^{i\vec{k}\cdot\vec{x}+\omega(\vec{k})t}(\bar{M}, \bar{A})$ as a Fourier expansion. Here $\vec{x} = (x, y)$ and \bar{M} and \bar{A} are constants. In this expansion $\vec{k} = (k_x, k_y)$ is the wavelength (in two dimensions) of the perturbation. In the following we will determine the sign of real part of $\omega(\vec{k})$ for the possible wavelengths $\vec{k} \in \mathbb{R}^2$. When $\text{Re } \omega(\vec{k}) < 0$ we know that the wave with wavelength \vec{k} will shrink over time, whereas $\text{Re } \omega(\vec{k}) > 0$ implies that the wave will grow. For linear stability of the uniform stationary state, we need that $\text{Re } \omega(\vec{k}) < 0$ for all wavelengths \vec{k} as this implies that all small perturbations eventually will fade out and the system returns to the stationary state (M_e, A_e) .

Substitution of such general Fourier expansion in the system of equation (1.7) gives us the following system of (algebraic) equations:

$$\omega\bar{M} = \left[-\tilde{\mu}|\vec{k}|^2 + \left(rA_e - \frac{1}{(1+M_e)^2} \right) \right] \bar{M} + rM_e \bar{A}$$

$$\tilde{\gamma}\omega\bar{A} = -A_e \bar{M} + \left[-|\vec{k}|^2 - \tilde{\alpha} - M_e \right] \bar{A}$$

This description is equivalent to the following matrix equation:

$$0 = \begin{pmatrix} \omega(\vec{k}) + \tilde{\mu}|\vec{k}|^2 - \left(rA_e - \frac{1}{(1+M_e)^2} \right) & -rM_e \\ A_e & \tilde{\gamma}\omega(\vec{k}) + |\vec{k}|^2 + \tilde{\alpha} + M_e \end{pmatrix} \begin{pmatrix} \bar{M} \\ \bar{A} \end{pmatrix}$$

It is easiest now to inspect the two possible steady states one by one, as this simplifies the equations.

Linear stability of $(M_e, A_e) = (0, 1)$

When we inspect the uniform steady state $(M_e, A_e) = (0, 1)$ we find the following matrix equation:

$$0 = \begin{pmatrix} \omega(\vec{k}) + \tilde{\mu}|\vec{k}|^2 - r + 1 & 0 \\ 1 & \tilde{\gamma}\omega(\vec{k}) + |\vec{k}|^2 + \tilde{\alpha} \end{pmatrix} \begin{pmatrix} \bar{M} \\ \bar{A} \end{pmatrix} \quad (1.8)$$

Hence we obtain two values for ω : $\omega_1(\vec{k}) = r - 1 - \tilde{\mu}|\vec{k}|^2$ and $\tilde{\gamma}\omega_2(\vec{k}) = -\tilde{\alpha} - |\vec{k}|^2$. Clearly $\omega_2 < 0$ for all wavelengths $\vec{k} \in \mathbb{R}^2$. So this means that the uniform steady state $(0, 1)$ is stable if and only if $\omega_1(\vec{k}) < 0$ for all wavelengths \vec{k} . This happens when $r < 1$. On the other hand, when $r > 1$ we have $\omega_1 > 0$ and hence the state is unstable in this situation.

Linear stability of the non-trivial steady state

For the second, non-trivial, steady state $(M_e, A_e) = (\tilde{\alpha} \frac{r-1}{1-\tilde{\alpha}r}, \frac{1-\tilde{\alpha}r}{r(1-\tilde{\alpha})})$ we find the following matrix equation

$$0 = \begin{pmatrix} \omega(\vec{k}) + \tilde{\mu}|\vec{k}|^2 - \frac{M_e}{(1+M_e)^2} & -rM_e \\ A_e & \tilde{\gamma}\omega(\vec{k}) + |\vec{k}|^2 + \frac{\tilde{\alpha}}{A_e} \end{pmatrix} \begin{pmatrix} \bar{M} \\ \bar{A} \end{pmatrix} \quad (1.9)$$

Here we have used that $rA_e - \frac{1}{(1+M_e)^2} = \frac{M_e}{(1+M_e)^2}$ and $\tilde{\alpha} + M_e = \frac{\tilde{\alpha}}{A_e}$ which follow from a straight-forward computation. In order for this matrix equality to hold we find that $\omega(\vec{k})$ must satisfy the following dispersion relation:

$$0 = \left(\omega(\vec{k}) + \tilde{\mu}|\vec{k}|^2 - \frac{M_e}{(1+M_e)^2} \right) \left(\tilde{\gamma}\omega(\vec{k}) + |\vec{k}|^2 + \frac{\tilde{\alpha}}{A_e} \right) + rM_eA_e$$

This dispersion relation can be expanded to the following form (for notational clarity we have suppressed the notation of the argument \vec{k} of the exponent ω):

$$\begin{aligned} 0 = & \tilde{\gamma}\omega^2 + \omega \left((1 + \tilde{\gamma}\tilde{\mu})|\vec{k}|^2 + \tilde{\alpha}/A_e - \tilde{\gamma} \frac{M_e}{(1+M_e)^2} \right) \\ & + \tilde{\mu}|\vec{k}|^4 + |\vec{k}|^2 \left(\tilde{\mu}\tilde{\alpha}/A_e - \frac{M_e}{(1+M_e)^2} \right) + \frac{\tilde{\alpha}(r-1)(1-\tilde{\alpha}r)}{1-\tilde{\alpha}} \end{aligned} \quad (1.10)$$

We know the uniform steady state (m_e, a_e) is stable when the two solutions for ω of this dispersion relation both have negative real parts. Since $\tilde{\gamma} > 0$, we need the other coefficients to be positive as well in order for this to happen⁶. This must hold for all possible values of the wavelength \vec{k} . We inspect these two remaining coefficients one by one.

⁶A quadratic form $Ax^2 + Bx + C$ has roots $x_{1,2} = -\frac{B}{2A} \pm \frac{1}{2A}\sqrt{B^2 - 4AC}$. When $A > 0$, we need to have that $B > 0$ and $B^2 - 4AC < B^2$ in order to have two negative solutions. Hence we must have that $A, B, C > 0$ to guarantee two negative solutions.

The first coefficient is $(1 + \tilde{\gamma}\tilde{\mu})|\vec{k}|^2 - \tilde{\alpha}/A_e + \tilde{\gamma}\frac{M_e}{(1+M_e)^2}$. Since $(1 + \tilde{\gamma}\tilde{\mu}) > 0$ we know that this term is positive, for all possible wavelengths \vec{k} , if and only if

$$\tilde{\alpha}/A_e - \tilde{\gamma}\frac{M_e}{(1+M_e)^2} > 0. \quad (1.11)$$

According to Cangelosi et al [17] this condition is satisfied for the typical values of the parameters in our model. In the remainder we will just assume that this condition is obeyed.

For the last coefficient we must be careful. We first investigate the condition for $\vec{k} = 0$. Then the condition simply is

$$\frac{\tilde{\alpha}(r-1)(1-r\tilde{\alpha})}{1-\tilde{\alpha}} > 0. \quad (1.12)$$

In Section 1.2.1 we briefly mentioned that the non-trivial steady state is (always) unstable when $r < 1$. We can now verify this from this condition: in this situation we have $(r-1), (1-\tilde{\alpha}r), (1-\tilde{\alpha}) < 0$ and hence the condition is violated, meaning that the stationary state (M_e, A_e) is unstable for perturbation with wavelength $\vec{k} = 0$ and hence unstable in general. When $r > 1$ there is no problem and the stationary state is stable for perturbations with wavelength $\vec{k} = 0$.

This does not, however, mean that the uniform stationary state (when $r > 1$) is always stable. It can happen that this last coefficient is negative for some wavelength $\vec{k} \neq 0$. For stability this is not allowed and hence we find that the stationary state is stable when the following inequality holds for all wavelengths \vec{k} :

$$\tilde{\mu}|\vec{k}|^4 + |\vec{k}|^2 \left(\tilde{\mu}\tilde{\alpha}/A_e - \frac{M_e}{(1+M_e)^2} \right) + \frac{\tilde{\alpha}(r-1)(1-\tilde{\alpha}r)}{1-\tilde{\alpha}} > 0$$

We can also write this as a condition on the parameter $\tilde{\mu}$ as follows:

$$\begin{aligned} \tilde{\mu} &> \frac{\frac{M_e}{(1+M_e)^2}|\vec{k}|^2 - \frac{\tilde{\alpha}(r-1)(1-\tilde{\alpha}r)}{1-\tilde{\alpha}}}{|\vec{k}|^2(|\vec{k}|^2 + \tilde{\alpha}/A_e)} \\ &= \frac{M_e}{(1+M_e)^2} \frac{|\vec{k}|^2 - \frac{(1+M_e)^2\tilde{\alpha}(r-1)(1-\tilde{\alpha}r)}{M_e(1-\tilde{\alpha})}}{|\vec{k}|^2(|\vec{k}|^2 + \tilde{\alpha}/A_e)} \end{aligned}$$

Upon noticing that $\frac{(1+M_e)^2\tilde{\alpha}(r-1)(1-\tilde{\alpha}r)}{M_e(1-\tilde{\alpha})} = (1-\tilde{\alpha})$ we can write this condition more compactly as

$$\tilde{\mu} > \tilde{\mu}_c := \frac{M_e}{(1+M_e)^2} \frac{|\vec{k}|^2 - (1-\tilde{\alpha})}{|\vec{k}|^2(|\vec{k}|^2 + \tilde{\alpha}/A_e)}. \quad (1.13)$$

In Figure 1.6 the curve $\tilde{\mu}_c$ is shown as function of the squared (absolute value of the) wavelength. The function $\tilde{\mu}_c(\vec{k})$ clearly has a maximum. Because the condition on $\tilde{\mu}$ that $\tilde{\mu} > \tilde{\mu}_c(\vec{k})$ for all wavelengths \vec{k} , we can also reduce this to the condition $\tilde{\mu} > \tilde{\mu}_C := \max_{\vec{k} \in \mathbb{R}^2} \tilde{\mu}_c(\vec{k})$.

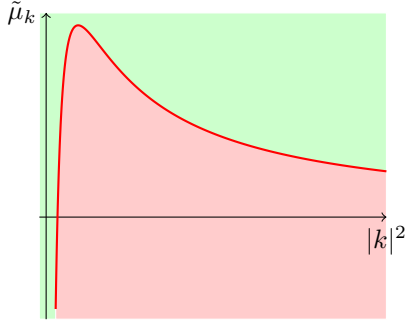


Figure 1.6 – Plot of the function $\tilde{\mu}_c = \frac{m_e}{(1+m_e)^2} \frac{|\vec{k}|^2 - (1-\tilde{\alpha})}{|\vec{k}|^2(|\vec{k}|^2 + \tilde{\alpha}/A_e)}$, where we have used the parameter values $A_e = 0.857$, $\alpha = 2/3$ and $M_e = 0.111$. The uniform stationary point (M_e, A_e) is stable for perturbations with wavelengths \vec{k} when $\tilde{\mu}u > \tilde{\mu}_c(\vec{k})$ and unstable when $\tilde{\mu} < \tilde{\mu}_c(\vec{k})$.

In our quest to find the maximal value $\tilde{\mu}_C$ we compute the derivative $\frac{\partial \tilde{\mu}_c}{\partial |\vec{k}|^2}(\vec{k})$ and set it to zero. Hence we find the following equation for the wavelengths \vec{k}_c that maximize $\tilde{\mu}(\vec{k})$:

$$0 = \frac{-|\vec{k}_c|^4 + 2(1-\tilde{\alpha})|\vec{k}_c|^2 + (1-\tilde{\alpha})\tilde{\alpha}/A_e}{|\vec{k}_c|^4 \left(|\vec{k}_c|^2 + \tilde{\alpha}/A_e \right)^2} \quad (1.14)$$

With use of the quadratic formula we can easily verify that the maximizers are given by

$$|\vec{k}_c|^2 = (1-\tilde{\alpha}) \left(1 \pm \sqrt{(1-\tilde{\alpha}r)^{-1}} \right).$$

Since we are only inspecting the situation in which we have $1 < r < \tilde{\alpha}^{-1}$ and $0 < \tilde{\alpha} < 1$ (see Section 1.2.1), we have $\sqrt{(1-\tilde{\alpha}r)^{-1}} > 1$. Hence we must ignore the solution with a negative sign, because the absolute wavelength cannot be negative. Hence the (true) maximizers \vec{k}_c must obey the equation

$$|\vec{k}_c|^2 = (1-\tilde{\alpha}) \left(1 + \sqrt{(1-\tilde{\alpha}r)^{-1}} \right).$$

Substitution of this maximizer in the equation for $\tilde{\mu}_c$ then gives the value of the maximum $\tilde{\mu}_C$. For this we obtain

$$\begin{aligned} \tilde{\mu}_C &= \frac{M_e}{(1+M_e)^2} \frac{|\vec{k}_c|^2 - (1-\tilde{\alpha})}{|\vec{k}_c|^2 \left(|\vec{k}_c|^2 + \tilde{\alpha}/A_e \right)} \\ &= \frac{M_e}{(1+M_e)^2} \frac{\sqrt{(1-\tilde{\alpha}r)^{-1}}}{(1 + \sqrt{(1-\tilde{\alpha}r)^{-1}})(1-\tilde{\alpha}) \left(1 + \sqrt{(1-\tilde{\alpha}r)^{-1}} + \tilde{\alpha}r/(1-\tilde{\alpha}r) \right)} \\ &= \frac{M_e}{(1+M_e)^2} \frac{1}{(1-\tilde{\alpha})(2 + 2\sqrt{1-\tilde{\alpha}r} + \tilde{\alpha}r/(1-\tilde{\alpha}r))} \\ &= \frac{M_e}{(1+M_e)^2} \frac{1}{2|\vec{k}_c|^2 + \frac{\tilde{\alpha}}{A_e}}. \end{aligned}$$

So we know that the uniform stationary point $(M_e, A_e) = \left(\tilde{\alpha} \frac{r-1}{1-\tilde{\alpha}r}, \frac{1}{r} \frac{1-\tilde{\alpha}r}{1-\tilde{\alpha}}\right)$ is (linearly) stable when $\tilde{\mu} > \tilde{\mu}_C = \frac{M_e}{(1+M_e)^2} \frac{1}{2|\vec{k}_c|^2 + \tilde{\alpha}/A_e}$. When $\tilde{\mu} < \tilde{\mu}_C$ this point is unstable for perturbations of some band of wavelengths around \vec{k}_c . When the parameters are chosen in such way that the stationary state (M_e, A_e) is linearly unstable, but $\tilde{\mu}$ is close to $\tilde{\mu}_C$ we expect to see patterns arise from this stationary state. In the next section we will use weakly non-linear stability analysis to study this option in-depth.

1.2.3 Weakly Non-Linear Stability Analysis

In the last section we have determined the linear stability of the non-trivial stationary state $(M_e, A_e) = \left(\tilde{\alpha} \frac{r-1}{1-\tilde{\alpha}r}, \frac{1}{r} \frac{1-\tilde{\alpha}r}{1-\tilde{\alpha}}\right)$. We have found that this state is linearly stable when $\tilde{\mu} > \tilde{\mu}_C$ and unstable when $\tilde{\mu} < \tilde{\mu}_C$. In this section we will determine what happens to the state (M_e, A_e) when $\tilde{\mu} - \tilde{\mu}_C < 0$ via means of a weakly non-linear stability analysis. We don't inspect the other steady state, $(0, 1)$, since there are no mussels in this steady state and therefore does not lead to patterns in the mussel concentration.

We let $\tilde{\mu} = \tilde{\mu}_C - \varepsilon^2 s$, where $s > 0$ and $0 < \varepsilon \ll 1$. This choice now ensures that $\tilde{\mu} < \tilde{\mu}_C$, but it is still close to the critical value of the parameter. Our linear stability analysis predicts that in this situation the stationary state (M_e, A_e) is unstable and that the wavelengths \vec{k}_c that obey $|\vec{k}_c|^2 = (1 - \tilde{\alpha}) \left(1 + \sqrt{(1 - \tilde{\alpha}r)^{-1}}\right)$ are the most unstable ones (i.e. $\omega(\vec{k}_c) \geq \omega(\vec{k})$ for all wavelengths \vec{k} when $\tilde{\mu} = \tilde{\mu}_C$). Hence the deviation from the stationary state will be dominated by this wavelength.

In the remainder of this section we will restrict ourself to one-dimensional spatial domains. This hugely simplifies the computations and still will give us some clue about the patterns that can arise. The critical wavelengths $k_c \in \mathbb{R}$ (there are now two of them) now satisfy

$$k_c^2 = (1 - \tilde{\alpha}) \left(1 + \sqrt{(1 - \tilde{\alpha}r)^{-1}}\right) \quad (1.15)$$

This critical wavelength dominates the perturbations of the stationary state (M_e, A_e) and we will use the Ansatz that the solution (M, A) of equation (1.6) - with $\tilde{\mu}$ as stipulated before - has the following form

$$\begin{pmatrix} M \\ A \end{pmatrix} = \begin{pmatrix} M_e \\ A_e \end{pmatrix} + \varepsilon \vec{v}_{11} A(\xi, \tau) e^{ik_c x} + c.c. + h.o.t. \quad (1.16)$$

Here k_c is the critical wavelength, \vec{v}_{11} is a vector pointing in the most unstable direction (i.e. the eigenvector corresponding to the eigenvalue $0 = \omega(k_c)$ when $\tilde{\mu} = \tilde{\mu}_c$). A is some complex-valued function of τ and ξ , which in turn are the slow space and time variables. The explicit form of τ and ξ in terms of the original space and time variables x and t is at this point still to be determined. Also, *c.c.* means that we also have complex conjugates and *h.o.t.* means that there are also higher order terms (both in the Fourier and in the Taylor series).

The derivation of the modulation equations is quite complicated and tedious. The complete computation can be found in Appendix A. These calculations

show that the relevant amplitude equation for this reaction-diffusion mussel-algae system is given (after some additional rescaling) by

$$A_\tau = -A - A_{\chi\chi} - h|A|^2 A.$$

where the sign of h is determined by the precise values of the original reaction-diffusion system. In Appendix C we study the real Ginzburg-Landau equation in detail. For now, we will just observe that this leads to patterns only when $h < 0$. Hence only for some specific combinations of parameters there will be patterns. These patterns will have the form

$$(M, A) = (M_e, A_e) + A(\varepsilon x, \varepsilon^2 t) e^{ik_c x} + c.c.$$

where A is the amplitude, which is a solution to the Ginzburg-Landau equation that we have derived in this section. When $h < 0$ this amplitude will have the form $A = \sqrt{\frac{1-q^2}{h}} e^{iqx}$ where $|q| < 1$. Hence the solution to the original partial differential equation will be of the form

$$(M, A) = (M_e, A_e) + A_0 e^{i(k_c + \varepsilon q)x} + c.c.$$

This means that a solution will resemble waves of the critical wavelength k_c , though they differ by a little amount. A sketch of a possibility is given in Figure 1.7. Hence we can conclude that the reaction-diffusion equation already gives rise to patterns. Thus the density-dependent movement speed of the mussels is not necessary to explain all sort of patterns that can arise in a mussel bed.

However, the patterns that arise due to the density-dependent movement speed of the mussel are created in a very short time and generally have a far lower wavelength, whereas the Turing patterns in the reaction-diffusion equation typically have larger wavelengths. When we look at real mussel beds, one can see that there essentially are patterns of different wavelengths. When you zoom out, you can observe patterns with a typical length in the order of tens of metres and when you zoom in, you can see patterns with a length of a few mussels. Therefore we expect that the first of these can be seen as Turing patterns, whereas the others arise due to the density-dependent movement speed. In Chapters 2 and 3 we study the behaviour of the system with a density-dependent movement speed and see if we can also observe these new patterns in our mathematical model.

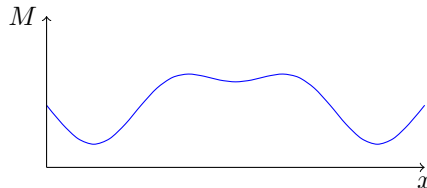


Figure 1.7 – Sketch of a possible wave that can occur as a pattern of a reaction-diffusion kind of equation with the Ginzburg-Landau equation as amplitude equation.

Chapter 2

$\varepsilon = 0$ - A study of the Cahn-Hilliard Equation

In Chapter 1 we have postulated a mussel-algae system that incorporates a Cahn-Hilliard structure on short timescales and a diffusion-interaction structure for large timescales. This model is given by the following set of equations:

$$\begin{aligned}\frac{\partial m}{\partial t} &= d_m \nabla \left(v \left[v + m \frac{\partial v}{\partial m} \right] \nabla m + v m \frac{\partial v}{\partial a} \nabla a - \kappa \nabla(\Delta m) \right) + \varepsilon H(m, a) \\ \frac{\partial a}{\partial t} &= \varepsilon [d_a \nabla a + G(m, a)]\end{aligned}$$

The ε in this description indicates that some terms only contribute on larger time scales. These terms represent phenomena like the mortality of the mussels and the diffusion of the algae. On shorter time scales these effects are not significant in the dynamics of the system. It is found that the behaviour of mussels, kept in a small box for several hours, can be described using the Cahn-Hilliard equation [5].

We can study this situation by setting $\varepsilon = 0$ in our model. Our proposed system of partial differential equations can thus be rewritten to:

$$\begin{aligned}\frac{\partial m}{\partial t} &= d_m \nabla \left(v \left[v + m \frac{\partial v}{\partial m} \right] \nabla m + v \frac{\partial v}{\partial a} \nabla a - \kappa \nabla(\Delta m) \right) \\ \frac{\partial a}{\partial t} &= 0\end{aligned}$$

This means that at short time scales we would expect the concentration of algae to be constant in time. Note that this concentration is not necessarily uniform in space per se. We will, however, assume that this concentration of algae *is* uniform in space during this chapter. With this additional assumption the description reduces to

$$\frac{\partial m}{\partial t} = d_m \nabla \left(v \left[v + m \frac{\partial v}{\partial m} \right] \nabla m - \kappa \nabla(\Delta m) \right). \quad (2.1)$$

This is precisely the description that is given in [5]. In the article the speed v of the mussels is taken to be $v(m) = m^2 + \tilde{\beta}m + 1$, whereas we work with $v(m) = m^2 + \tilde{\beta}m + 1 - da$ (or the piecewise linear definition, see section 1.1.4). Since we have assumed that a is uniform in space and we have found it to be constant in time, a simple rescaling $\bar{m} = \frac{m}{\sqrt{1-d_a}}$, $\bar{\beta} = \frac{\tilde{\beta}}{\sqrt{1-d_a}}$ gives that these descriptions are qualitatively similar in this situation where the concentration of algae is assumed to be uniform.

In this chapter we will start with a general study of the Cahn-Hilliard system. For this we will not use our specific form of equation (2.1), but we analyse the more general form

$$\frac{\partial m}{\partial t} = d_m \nabla(f(m) \nabla m - \kappa \nabla(\Delta m)). \quad (2.2)$$

In Section 2.1 we'll study the linear stability of the uniform solutions of this equation. Moreover, we'll see what kind of stationary solutions are possible in one dimension. We also give the description of the global minimizer of the associated energy as found by Carr et al. These considerations are given as a summary of the current knowledge of the Cahn-Hilliard equation (see [19], [20], [21] and [22]).

The last part of Section 2.1 is devoted to the specific mussel system as given in equation (2.1), on a bounded domain $[0, L] \subset \mathbb{R}$ with natural boundary conditions $m_x(0) = m_x(L) = 0$, $m_{xxx}(0), m_{xxx}(L) = 0$. In that, we consider both introduced descriptions for the density dependent movement speed $v(m)$ as introduced in Section (1.1.4) and describe the bifurcation diagrams illustrating the possible behaviour of the Cahn-Hilliard equation.

Then in Section 2.2 we inspect one interesting phenomena of the Cahn-Hilliard equation: Ostwald Ripening. This is a very slow process that qualitatively describes the dynamics of solutions of the Cahn-Hilliard Equation. It is this process that could explain the wavelength selection that is observed in experiments with mussels.

Finally in Section 2.3 we continue to study the Cahn-Hilliard equation for our mussel system, though this time via numerical methods. Here we present one-dimensional simulations for both possibilities of the density dependent movement speed. These simulations illustrate the analytically obtained knowledge of the previous sections and give a good illustration of what happens in the system.

2.1 Cahn Hilliard Equation: general behaviour

The Cahn-Hilliard equation is a special sort of a gradient system. In general such a gradient system can be expressed as

$$\frac{\partial m}{\partial t} = \nabla^2 \mu(m),$$

where m is a concentration (for example of mussels) and μ is a chemical potential, which is just a function of the concentration m . For the Cahn-Hilliard

description this chemical potential is the operator defined as

$$\mu(m) = F(m) - \kappa \nabla^2 m.$$

Here F is some known function of the concentration m . The Cahn-Hilliard equation in its standard form is formulated as

$$\frac{\partial m}{\partial t} = \nabla^2 [F(m) - \kappa \nabla^2 m]. \quad (2.3)$$

It is immediately clear that we can also write this Cahn-Hilliard equation in the form of equation (2.2) when we define $f(m) := \frac{dF}{dm}(m)$. Note that is also possible to include an additional constant, d_m , before the differential operator, as we have done in equation (2.2).

In this section we focus on the dynamics of the Cahn-Hilliard equation in a closed system. The domain of the system will be denoted by Ω . This domain Ω can in general be a subset of \mathbb{R}^n , though we will be particularly interested in the one and two dimensional cases.

The mathematical formulation of the system is not yet complete: we need to impose boundary conditions. Since we want to investigate a closed system, we need to choose these such that no matter escapes. Therefore we need to have mass conservation. This means that no concentration may flow in or out of the systems boundaries. Thus one boundary condition is

$$\nabla m \cdot n \equiv 0 \text{ on } \partial\Omega,$$

where n is a vector normal to the boundary.

This condition is however not sufficient to accommodate the wanted mass conservation. To see this we first observe that the total mass is $M := \int_{\Omega} m dx$. For mass conservation we need to find $\frac{dM}{dt} = 0$. With integration by parts¹ one finds

$$\begin{aligned} 0 = \frac{dM}{dt} &= \int_{\Omega} \frac{\partial m}{\partial t} dx = \int_{\partial\Omega} \nabla [F(m) - \kappa \nabla^2 m] \cdot n dx \\ &= \int_{\partial\Omega} f(m) \nabla m \cdot n dx - \int_{\partial\Omega} \kappa \nabla (\Delta m) \cdot n dx. \end{aligned}$$

Therefore we also need to have $\nabla \mu \cdot n \equiv 0$ on $\partial\Omega$. Or, equivalently, we can also reformulate this to the boundary condition

$$\nabla(\Delta m) \cdot n \equiv 0 \text{ on } \partial\Omega.$$

Since we have chosen our boundary conditions such that the mass is conserved, we also need to specify what this total mass is - that is the total mass is determined by the initial distribution as $M = \int_{\Omega} m_0 dx$ where m_0 is the initial configuration. With this additional constraint, which is normal for system with Neumann boundary conditions, it has been shown in [23] that it has (unique) solutions.

¹We are also implicitly assuming the domain Ω is constant in time.

Thus the Cahn-Hilliard system on a bounded domain Ω with natural boundary conditions can be formulated as

$$\frac{\partial m}{\partial t} = \nabla^2 [F(m) - \kappa \nabla^2 m] \quad \text{in } \Omega, \quad (2.4a)$$

$$\nabla m \cdot n \equiv 0 \quad \text{on } \partial\Omega, \quad (2.4b)$$

$$\nabla(\Delta m) \equiv 0 \cdot n \quad \text{on } \partial\Omega. \quad (2.4c)$$

$$M = \int_{\Omega} m \, dx = \int_{\Omega} m_0 \, dx. \quad (2.4d)$$

This equation is also often formulated as a variational problem. To do this, we can introduce the free energy of a point as

$$e_f := W(m) + \frac{\kappa}{2} |\nabla m|^2,$$

where W is some function such that $W' = F$. Now the (free) energy of the whole system is

$$E := \int_{\Omega} e_f \, dx.$$

The original partial differential equation can be written in this formulation as

$$\frac{\partial m}{\partial t} = \nabla^2 \frac{\delta e_f}{\delta m}.$$

Here $\frac{\delta e_f}{\delta m}$ is the functional derivative of e_f .

When we are looking for steady states, we can now choose which method we want to use. We can either try to solve the original partial differential equation or we can try to find extreme points of the energy functional. When these extreme points are minimizers we also (additionally) know that these are stable steady solutions of the Cahn-Hilliard equation, whereas they are unstable when they are maximizers of the energy functional. In this chapter we sometimes switch between those two approaches to make use of the advantages of both methods.

2.1.1 Steady states

Our first interest is in the steady states of the Cahn-Hilliard equation. For this we can set $\frac{\partial m}{\partial t} = 0$ in equation (2.4). Thus to find the steady state solutions we must solve

$$0 = \nabla^2 [F(m) - \kappa \nabla^2 m],$$

with the boundary conditions $\nabla m \cdot n \equiv 0, \nabla(\Delta m) \cdot n \equiv 0$ on $\partial\Omega$.

We will inspect the steady state solutions of this equation only in one dimension, where we assume that $\Omega = [0, L]$. Then by integrating twice we obtain the following implicit expression for those steady state solutions:

$$F(m) - \kappa m_{xx} = C + C_1 x,$$

where the subscripts x denote the derivative with respect to x . Moreover, C and C_1 are two constants whose values are yet undetermined. By differentiation of both sides of this expression we find that

$$C_1 = F'(m)m_x - \kappa m_{xxx}$$

Therefore we can apply the boundary conditions to find that $C_1 = 0$. Hence the correct expression for the steady state solutions is

$$F(m) - \kappa m_{xx} = C, \quad (2.5)$$

where C is still not determined. We also note that steady state solutions should satisfy the mass constraint $M = \int_0^L m(x)dx$. So our quest now is to find all possible constants C and functions $x \mapsto m(x)$ that satisfy the differential equation (2.5) and the mass constraint.

To do so we introduce $v := m_x$ and rewrite the differential equation into a system of ordinary differential equations as

$$\begin{cases} m_x &= v \\ v_x &= \frac{F(m)-C}{\kappa} \end{cases} \quad (2.6)$$

The steady states of this system can be easily be found as (m, v) where m satisfies $F(m) = C$ and $v = 0$. How many solutions there exist, depends on the form of the polynomial $F(m)$ and the value of the constant C .

For our mussel model it turns out - as we shall see later in this chapter - that there are two different forms possible for the polynomial $F(m)$:

- (i) $F(m)$ is a (fifth order) polynomial that is increasing.
- (ii) $F(m)$ is a (fifth order) polynomial that has two extreme values m_1 and m_2 . It is decreasing when $m \in (m_1, m_2)$ and increasing otherwise.

We will study both of these possibilities one by one in the next two subsections.

Phase Plane - for F monotonically increasing

When F is an increasing function we will always find only one solution to $F(m) = C$, regardless of the value of C . Thus we will find one steady state solution to the system (2.6). Its eigenvalues are $\lambda_{1,2} = \pm\sqrt{f(m)/\kappa}$, which indicates that this solution is a saddle. A sketch of a possible phase plane is given in Figure 2.1.

Steady state solutions to the Cahn-Hilliard equation are now those orbits of length L of the system in equation (2.6) that start on the line $\{v = 0\}$ and end on $\{v = 0\}$ and also satisfy the mass condition. From the phase plane in Figure 2.1 it is clear that the steady state is the only possible candidate. The mass condition then determines that the steady state solution to the Cahn-Hilliard equation must be $m(x, t) = M/L$ (and thus $C = F(M/L)$).

Thus the Cahn-Hilliard system has only one steady state solution when F is strictly increasing. This is the uniform steady state $m(x, t) = M/L$. So when we start with some initial distribution $m(x, 0) = m_0(x)$ we know for sure that eventually it will evolve to the uniform steady state M/L .

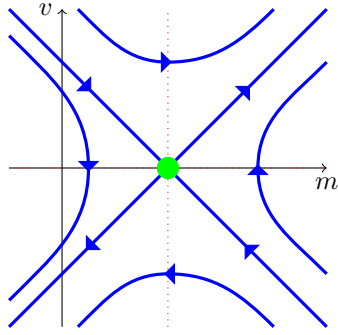


Figure 2.1 – Sketch of a possible phase plane when F is an increasing function. The red, dotted lines denote the nullclines, while the blue lines indicate some of the orbits. The steady state is given in green.

Phase Plane - F has two extreme points

The second form that is of our interest is the function F that has two extreme points m_1 and m_2 such that:

- F is increasing on $[0, m_1)$ and (m_2, ∞) ;
- F is decreasing on (m_1, m_2) .

A sketch of a possible function F is given in Figure 2.2. It is clear that the number of steady states of the system of equation (2.6) depends on the value of the constant C . Let C_{low} be the local minimum and C_{up} the local maximum of the function F . When $C < C_{low}$ or $C > C_{up}$ we clearly have only one solution. In these cases the steady states are saddles and the phase plane looks like it did before (see Figure 2.1).

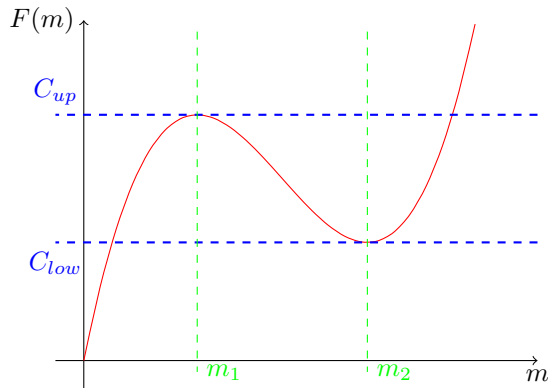


Figure 2.2 – Sketch of a function F that satisfies the assumptions that it has two extreme points, between which the function is decreasing. The dashed, blue lines indicate the upper and lower limits of the constant C such that $F(m) = C$ has three solutions.

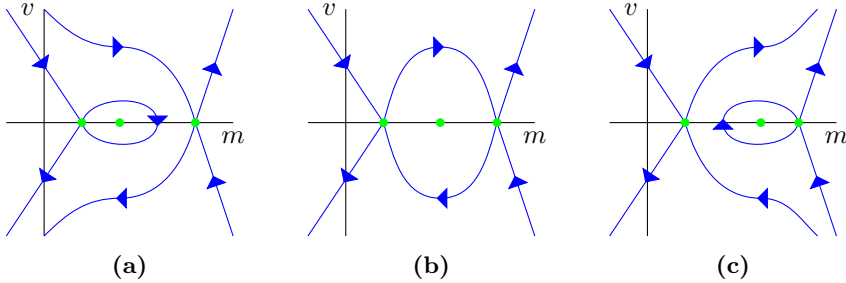


Figure 2.3 – Sketches of the three possible, qualitatively different, phase planes when $C \in (C_{low}, C_{up})$. In (a) we have a homoclinic orbit to the point $(m_a, 0)$, in (b) we have two heteroclinic orbits and in (iii) we have a homoclinic orbit connecting $(m_c, 0)$ to itself.

However, when we choose $C \in (C_{low}, C_{up})$ we have three solutions to the equation $F(m) = C$. We will denote these three solutions with $m_a < m_b < m_c$. Clearly $F'(m_a) = f(m_a) > 0$, $f(m_b) < 0$ and $f(m_c) > 0$. Therefore the steady states $(m_a, 0)$ and $(m_c, 0)$ are saddles and $(m_b, 0)$ is a center.

In order to be able to give a qualitative description of the dynamics of the system of equation (2.6) in these situations we need more information. We can acquire this by noting that this system is integrable and that we can define the Hamiltonian

$$H(m, v) = W(m) - Cm - \frac{\kappa}{2}v^2,$$

where $W(m) := \int^m F(m)dm$.

Since the value of the Hamiltonian is constant along solutions this already implicitly gives an expression for the steady states solutions of the Cahn-Hilliard equation. In [24] this relation is used to find explicit forms of the steady states in case F is a polynomial of fourth order. However in our situation F is of fifth order and this method won't work anymore.

However we can say something qualitatively about the phase plane. For this we must distinguish between the three situations (i) $H(m_a, 0) < H(m_c, 0)$, (ii) $H(m_a, 0) = H(m_c, 0)$ and (iii) $H(m_a, 0) > H(m_c, 0)$. In situation (i) there is a homoclinic orbit from $(m_a, 0)$ to itself, in situation (ii) there are two heteroclinic orbits connecting $(m_a, 0)$ and $(m_b, 0)$ and in situation (iii) there is a homoclinic orbit connecting $(m_b, 0)$ with itself. These three possibilities are sketched in Figure 2.3.

Situation (ii) with two heteroclinic orbits occurs when $H(m_a, 0) = H(m_c, 0)$. Thus that means that we need C such that $W(m_a) - W(m_c) = C(m_a - m_c)$. We denote this value by C_m . We will for now assume that C_m is uniquely determined in this matter, which is something we will see later in this chapter. When $C > C_m$ we have $H(m_a, 0) < H(m_c, 0)$ and when $C < C_m$ we have $H(m_a, 0) > H(m_c, 0)$.

In all of these possible situations we thus find heteroclinic or homoclinic orbits. Besides these solutions we find three stationary solutions (i.e. $(m_a, 0)$, $(m_b, 0)$

and $(m_c, 0)$). Finally there are also (infinitely) many periodic solutions, enclosed by the heteroclinic (or homoclinic) orbits.

However not all of these solutions are really steady state solutions of the Cahn-Hilliard equation because they not necessarily satisfy the imposed boundary conditions and the mass condition. These conditions are only met when an orbit starts at the line $\{v = 0\}$ when $x = 0$ and ends on the line $\{v = 0\}$ when $x = L$. Moreover such a solution should also satisfy the mass condition $M = \int_0^L m dx$.

Let's now define $m_e := M/L$ (i.e. a uniform state). Clearly this state is a steady state of the Cahn-Hilliard equation (we can choose $C = F(m_e)$). There are now two different scenarios²: (i) $F(m_e) \in (C_{low}, C_{up})$ or (ii) $F(m_e) \notin (C_{low}, C_{up})$.

In situation (ii) we find that *all* non-uniform solutions won't satisfy the mass condition. Let's assume $F(m_e) < C_{low}$ (the argument for $F(m_e) > C_{up}$ is similar). That means that periodic orbits can only exist for C values such that $m_e < m_a < m_b < m_c$. Since the periodic orbits and heteroclinic and homoclinic have $m(x) \geq m_a$ for all x we find that the mass of these orbits is too large. Therefore in this situation we will only find one steady state, being $m(x, t) = m_e$.

From our analysis thus far we can only say something about the possible steady states in situation (i): we have seen that there are four possible sort of steady state solutions:

1. The uniform steady state $m_e = M/L$;
2. A periodic orbit;
3. One (or more) homoclinic connection(s);
4. One (or more) heteroclinic connection(s);

For all of these solutions we need to have $C \in (C_{low}, C_{up})$ and we also of course need the mass constraint to be satisfied. In [19] it is shown that (only) solutions of the fourth kind (i.e. one heteroclinic connection) are the global minimizers of the related variational problem. In the next section we will reformulate the reasoning of that article. We should now emphasize that this fact alone does not mean that a solution always will tend to this heteroclinic connection necessarily, as the other solutions could in theory be local minimizers of the problem (and hence stable solutions as well).

2.1.2 Global minimizer of the energy

In the previous section we have studied the Cahn Hilliard equation using its differential form. We have already found a lot of information about the steady states of the system. In this section we now turn to the variational form and use that to determine the form of the global minimizer, following the reasoning by Carr et al [19].

²We could indeed also have $F(m_e) = C_{low}$ or $F(m_e) = C_{up}$ but we ignore these situations for now

At this point we recall the variational form of the Cahn Hilliard equation. In this form we are looking for a function m that minimizes the energy

$$E = \int_0^L \left(W(m) - \frac{\kappa}{2} |m_x|^2 \right) dx,$$

under the mass constraint

$$M = \int_0^L m dx$$

Finally we also need to make sure that the found minimizer m satisfies the boundary conditions $m_x(0) = m_x(L) = 0$ and $m_{xxx}(0) = m_{xxx}(L) = 0$. Since we are not interested to the precise functional setting, that is needed for many existence and uniqueness theorems, we won't give the precise functional analytic setting - the given description is sufficient for our understanding of the system.

At this point we also must observe that the constant κ is usually very small (compared to the size of the domain). Therefore it is logical to investigate the system in the extreme limit when $\kappa \rightarrow 0$. Setting $\kappa = 0$ in the energy description gives a variational problem: we need to find the appropriate function m that minimizes the energy $\int_0^L W(m) dx$ under the mass constraint $M = \int_0^L m dx$.

This setting - i.e. finding minimizers of a functional under a constraint - means that we need to introduce a Lagrange multiplier σ and find the appropriate function m and constant σ that minimizes the new functional

$$\tilde{E}(\sigma, m) = \int_0^L (W(m) - \sigma m) dx.$$

The minimizer of this functional \tilde{E} must satisfy the Euler-Lagrange equation,

$$F(m) = \sigma.$$

This means that minimizers must be constant when $\sigma \notin (C_{low}, C_{up})$ and that minimizers can jump between m_a, m_b and m_c when $\sigma \in (C_{low}, C_{up})$. However a function that jumps between various states can only be a good solution to our variational problem when it also satisfies the Weierstrass-Erdman corner condition at the jumps in m :

$$W(m) - \sigma m \text{ must be continuous across jumps in } m.$$

These two conditions give rise to two sort of solutions. We either find constant solutions $m(x) = m_e$ or piece-wise constant solutions with $m(x) \in \{m_a, m_c\}$ where $W(m_a) - W(m_c) = C_m(m_a - m_c)$, $C_m = F(m_a) = F(m_c)$. Note that C_m here is precisely the same constant as we had found in the previous section that gave rise to a heteroclinic connection³.

For the single-state solution it is clear that the mass constraint can only be satisfied when $m(x) = m_e = M/L$. The two-phase solution, on the other hand,

³The condition on C_m can also be written as $\int_{m_a}^{m_c} (F(m) - C_m) dm = 0$, where we have $m_a < m_b < m_c$ as solutions to $F(m) = C_m$. Thus this constant C_m must be chosen to be the Maxwell line, explaining the subscript m . We can also see from this that C_m is uniquely determined.

satisfies this constraint when $m_a S(m_a) + m_b S(m_b) = M$ where $S(m_a)$ and $S(m_b)$ are the measures of the space on which the solution m has the value m_a or m_b respectively. Thus from this analysis it is also clear that the two-phase solution can only exist when $F(M/L) \in (C_{low}, C_{up})$, which is in agreement with our findings in the previous section.

Note that - in the two phase solution - it is possible to have infinitely many jumps from state m_a to m_c . However, those infinitely many jumps can only exist in our limit case $\kappa \downarrow 0$, because there is no energy penalty for those interfaces. When we inspect $\kappa > 0$ we introduce such an energy penalty for interfaces. Therefore one expects to find a two-phase solution with only one interface to have the least possible energy for the system. That is, a solution of the form⁴

$$m_0(x) = \begin{cases} m_a & 0 \leq x < \frac{L(m_c-m_e)}{m_c-m_a}; \\ m_b & \frac{L(m_c-m_e)}{m_c-m_a} < x \leq L. \end{cases}$$

We note that, when $\kappa > 0$, the interfaces cannot be discontinuous (as otherwise taking the derivative does not make sense). So to be more precise, the two-phase solution, has $m(x) = m_a$ on one side and $m(x) = m_c$ on the other, with a transition from one state to the other. This transition from one state to the other must be a stationary solution to the Cahn-Hilliard equation. In the previous section we have found two heteroclinic orbits, connecting the states m_a and m_c . Therefore one of these orbits must describe the transition from m_a to m_c (and the other describes the transition from m_c to m_a in the mirrored solution). A sketch of this two-phase solution is given in Figure 2.4.

In [19] it is shown that a two-phase solution is - indeed - the global minimizer of the energy functional, associated to the Cahn-Hilliard equation in case $F(m_e) \in (C_{low}, C_{up})$ when κL^2 is small enough. That means that m_0 is the energetically favorable state and that m_0 also is a stable steady state solution to the Cahn-Hilliard (differential) equation. It does not, however, mean that all solutions will eventually tend to this steady-state solution m_0 as there could be other, local, minimizers.

2.1.3 Linear stability of uniform steady state

In the previous sections we found several possible stationary solutions to the Cahn-Hilliard equation. We have however not yet discussed their stability. Some of these steady state solutions will probably be unstable and others stable. In this section we briefly discuss the stability of the uniform steady states.

In general we can find the linear stability of a stationary solution by linearizing the differential equation around this solution. Thus, now, let's assume that \bar{m} is a stationary solution to (2.3). To find the desired linearization we now let $m(x, t) = \bar{m}(x) + v(x, t)$ where v is a small perturbation. Hence the linearized version is

$$\frac{\partial v}{\partial t} = [f(m)v - \kappa v_{xx}]_{xx}, \quad (2.7)$$

⁴or the associated mirrored solution $m_{0,mirrored}(x) = m_0(-x)$

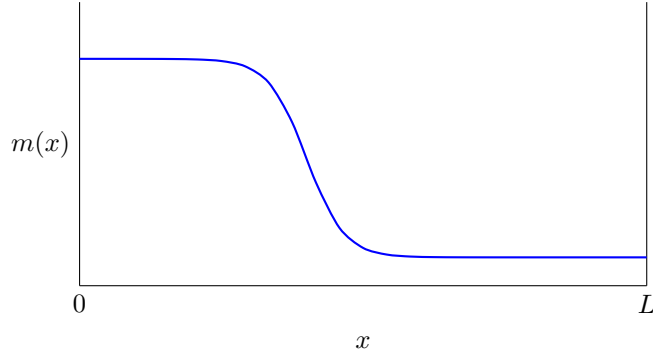


Figure 2.4 – Plot of a possible global minimizer of the Cahn-Hilliard problem. The location of the transition depends on the mass condition. The specific form of the transition (e.g. how fast the solution decreases) depends on the form of F and the value of κ .

where v should also satisfy the boundary conditions $v_x(0) = v_x(L) = 0$ and $v_{xxx}(0) = v_{xxx}(L) = 0$ and the mass conservation $0 = \int_0^L v \, dx$ to ensure that $M = \int_0^L m \, dx$ still holds.

We determine the linear stability by setting $v = e^{\omega t} \cos(kx)$, where we have used the cosine, to make sure that v can (possibly) satisfy the boundary conditions. We are interested in the linear stability of the uniform steady state solutions $m_e = M/L$. In this situation we can find the following dispersion relation

$$\omega(k) = -k^2 [f(m_e) + \kappa k^2]$$

The uniform steady state m_e is now linearly stable when $\omega < 0$ for all possible wavelengths k . We can easily see that $\omega < 0$ for all $k \in \mathbb{R}$ when $f(m_e) > 0$. When $f(m_e) < 0$ there is a wavelength $k_1 > 0$ such that $f(m_e) + \kappa k_1^2 = 0$ and therefore such that $\omega(k_1) = 0$. Now all wavelengths in the range $(-k_1, 0) \cup (0, k_1)$ correspond to $\omega > 0$ and thus the uniform stationary state is linearly unstable under perturbations with these wavelengths. The eigenvalue curve is given in Figure 2.5.

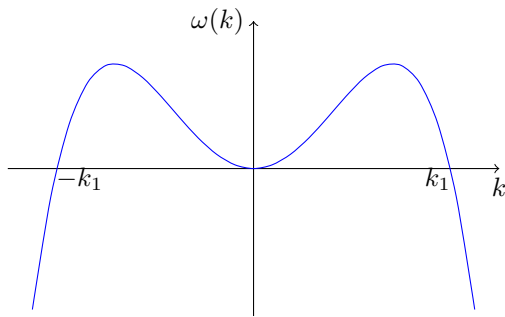


Figure 2.5 – Sketch of the eigenvalue curve when $f(m_e) < 0$. We see that there is a range of wavelengths for which the eigenvalue is positive.

So this reasoning seems to suggest that the uniform stationary state $m_e = M/L$ is linearly unstable when $f(m_e) < 0$. We are however working on a finite domain. Therefore the perturbation v needs to satisfy the boundary conditions. This puts some restrictions on the possible wavelengths k : we need to have $kL = n\pi$ where $n \in \mathbb{Z}$. So that means that the uniform stationary state m_e is only linearly unstable when $f(m_e) < 0$ and $k_1 > \pi/L$. When this last inequality does not hold, the domain is too small for the unstable waves to fit in and therefore the system maintains its stability.

Note that k_1 can be explicitly found as $k_1 = \sqrt{\frac{-f(m_e)}{\kappa}}$. Therefore we can also write the condition $k_1 > \pi/L$ as the following condition on the value of $f(m_e)$:

$$f(m_e) < -\frac{\kappa}{L^2}\pi^2$$

So from this it is clear that the stationary state $m_e = M/L$ is only linearly unstable when $f(m_e) < 0$ and $\frac{\kappa}{L^2}$ is small enough. That is, the domain has to be large enough, compared to the value of κ .

In the limit $\kappa/L^2 \downarrow 0$ the condition for linear instability becomes $f(m_e) < 0$. That means that F must be decreasing at m_e . In a previous section we worked with two sort of functions F : (i) a function F where F is strictly increasing and (ii) a function where F was increasing on $(0, m_1)$ and (m_2, ∞) and decreasing on (m_1, m_2) for some $m_1, m_2 \in (0, \infty)$. Therefore we now know that only in situation (ii) we will find that the uniform steady states m_e can be linearly unstable - and that happens precisely when $m_e \in (m_1, m_2)$. This region is often called the *spinodal region* in the literature.

2.1.4 Stability of all stationary solutions

In section 2.1.1 we have found four kind of stationary solutions:

- Uniform stationary states;
- Periodic orbits;
- A homoclinic connection;
- A heteroclinic connection.

In section 2.1.2 we have argued that the heteroclinic connection corresponds to the global minimizer of the associated energy. Therefore this stationary solution must be stable. Moreover, in section 2.1.3 we have determined the linear stability of the uniform stationary solutions and found out they are unstable when $f(m_e) < 0$ (and the domain is large enough).

However, we have not yet talked about the other stationary solutions - i.e. the periodic orbits or the homoclinic connections. In theory we could use the linearized differential form of equation (2.7) - this time linearized around the periodic orbit or homoclinic orbit. For this we need the exact, closed form of those orbits. Unfortunately this is too difficult in most cases, including our mussel model.

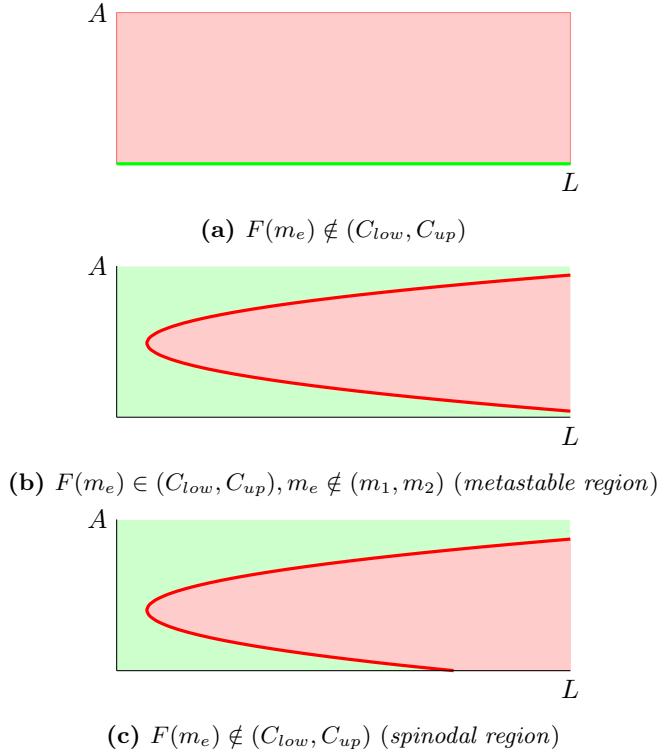


Figure 2.6 – Sketches of the conjectured bifurcation planes for the parameters L and $A = m_{max} - m_{min}$ in the three different regions. The green areas denote stable solutions, while the red regions indicate unstable solutions.

In section 2.1.1 we have found the existence of periodic orbits (and homoclinic orbits) when $C \in (C_{low}, C_{up})$. For these periodic orbits to be stationary solutions to the Cahn-Hilliard equation (with boundary conditions) they need to start at the line $\{v = 0\}$ and end on this line $\{v = 0\}$, while the length of the orbits must be L and the mass condition $M = \int_0^L m \, dx$ must be satisfied.

By inspection of the phase planes of Figure 2.3 we see that each periodic orbit crosses the line $\{v = 0\}$ twice during its orbit. We can now characterize the type of periodic solution to the Cahn-Hilliard equation by looking how many times this solution crosses the line $\{v = 0\}$ when $x \in (0, L)$. Let's define this amount of times as the amount of transitions. It turns out to be possible to always find a stationary solution to the Cahn-Hilliard equation, for any given amount of desired transitions (see [19]).

As of 2015 there is not yet a clear understanding of the stability of all possible solutions, including the periodic and homoclinic orbits. The most thorough study that we know of is done in [19] where it is proven that solutions with transitions in the open interval $(0, L)$ will not be minimizers of the associated energy of the Cahn-Hilliard system. Therefore these kind of solutions will be unstable.

When there are no transitions in $(0, L)$ no general information is available. However, it is generally believed (see for example [20]) that only a few of those solutions are stable. Here there is made a distinction between the following three regions: (i) $m_e \in (m_1, m_2)$, (ii) $m_e \in \{m \notin (m_1, m_2) : F(m) \in (C_{low}, C_{up})\}$ and (iii) $F(m_e) \notin (C_{low}, C_{up})$. Normally the results are given as a bifurcation diagram with the parameters L and $A := m_{max} - m_{min}$ (i.e. the difference between the highest and lowest concentration of the solution). A sketch of the *conjectured* bifurcation diagrams is given in Figure 2.6.

What happens when $F(m_e) \notin (C_{low}, C_{up})$ is now clear, as we have seen before: only the uniform stationary state $m_e = M/L$ is a stationary solution and it is stable. When $F(m_e) \in (C_{low}, C_{up})$ (but $m_e \notin (m_1, m_2)$) we are in the so-called metastable region. Here the uniform stationary state is still stable, regardless of the length of the domain, but there are also non-trivial stable solutions. We have also found that the global minimizer of the energy here is the two-phase solution with one interface.

Finally we can have $m_e \in (m_1, m_2)$. In this case the uniform stationary state $m_e = M/L$ is unstable, when the domain is big enough, and non-trivial solutions are preferred by the system, with A away from 0. We also found that the global minimizer is the two-phase solution with one interface in this situation as well.

2.1.5 Bifurcation diagram for the quadratic speed $v = v_q$

In the previous section we analysed the Cahn-Hilliard equation in a general way. From now on, we will abandon this general setting and try to apply our findings to the specific form of the Cahn-Hilliard equation that describes our mussels. In this setting the relevant equation is

$$\frac{\partial m}{\partial t} = \nabla[f(m)\nabla m - \kappa\nabla(\Delta m)],$$

where the function f is defined as

$$f(m) = v(v + m \frac{dv}{dm}).$$

Here v is the speed of the mussels. In section 1.1.4 we have described two ways to define the density dependent movement speed of the mussels. We have defined a quadratic fit approach as

$$v_q(m) = m^2 + \tilde{\beta}m + 1 + \tilde{d}a.$$

We also introduced a piecewise linear description as

$$v(m, a) = \begin{cases} v_1(m, a) = 1 - \tilde{\beta}m & \text{if } m < \tilde{\beta}/2; \\ v_2(m, a) = \frac{1-\tilde{\beta}^2}{2} + \gamma_0 e^{-\tilde{d}a} (m - \tilde{\beta}/2) & \text{if } m > \tilde{\beta}/2. \end{cases}$$

In this section we will inspect the system when we choose the quadratic fit approach for the density dependent movement speed of the mussels. In the next section we will then study the system when we have the piecewise linear description.

Quadratic fit: $v(m) = m^2 + \tilde{\beta}m + 1$ without algae

When we choose $v(m) = m^2 + \tilde{\beta}m + 1$ we find the function f to be

$$f(m) = (m^2 + \tilde{\beta}m + 1)(3m^2 + 2\tilde{\beta}m + 1).$$

The function F can also be found by integration of f . In this way we obtain the following possible form of F , which is defined up to a constant:

$$F(m) = \frac{3}{5}m^5 + \frac{5}{4}\tilde{\beta}m^4 + \frac{4+2\tilde{\beta}^2}{3}m^3 + \frac{3}{2}\tilde{\beta}m + m$$

Since the speed of the mussels must be positive, we need to have $v(m) > 0$ for all $m \in [0, \infty)$. Therefore we need to have $\tilde{\beta} > -2$. Hence we find that $f(m)$ can only be negative when $3m^2 + 2\tilde{\beta}m + 1$ is negative. From this we find the condition $\tilde{\beta} < -\frac{3m_e^2+1}{2m_e}$. Hence we obtain that the uniform stationary states $m_e = M/L$ are unstable when $\tilde{\beta} < -\frac{3m_e^2+1}{2m_e}$.

We can also find that the maximum value of the expression $-\frac{3m_e^2+1}{2m_e}$ is attained when $m_e = \frac{1}{3}\sqrt{3}$. Therefore there must be a bifurcation when $\tilde{\beta} = \beta_c = -\sqrt{3}$.

When $\tilde{\beta} > \beta_c$ we find $f(m) > 0$ for all $m \in (0, \infty)$. Therefore F is strictly increasing and therefore only the uniform steady states $m_e = M/L$ are stationary solutions for the problem.

When $\tilde{\beta} < \beta_c$ we can find concentrations m_1 and m_2 such that $f(m) < 0$ for $m \in (m_1, m_2)$ and $f(m) > 0$ for $m \in (0, m_1) \cup (m_2, \infty)$. Thus in this situation we will find a spinodal region and a metastable region as we have discussed in the previous sections. Since finding the constant C_m as a function of β is highly nontrivial and requires numerical approaches, we won't discuss this here and only acknowledge the existence of a curve that indicates the start of the metastable region.

In Figure 2.7 we sketched the bifurcation plane for the parameters $\tilde{\beta}$ and $m_e = M/L$. Here we made a distinction between the various regions and the possible stationary solutions.

Quadratic fit v_q with algae

In the previous section we inspected the Cahn-Hilliard equation in the mussel setting when the speed is defined as $v(m) = m^2 + \tilde{\beta}m + 1$. It is however logical that the speed also depends on the concentration of available algae, i.e. $v(m) = m^2 + \tilde{\beta}m + 1 - \tilde{d}a$.

We have already argued that the concentration of algae should be more or less constant on the fast time scales we are inspecting. Therefore we can introduce the new parameter $\beta' = \frac{\tilde{\beta}}{\sqrt{1-\tilde{d}a}}$ and the new variable $m' = \frac{m}{\sqrt{1-\tilde{d}a}}$. In this way the speed can be written as $v(m') = (1 - \tilde{d}a)(m'^2 + \beta'm' + 1)$, which means that we essentially are in the same situation as before. In particular is it possible to use the same bifurcation diagram as we derived in Figure 2.7 with

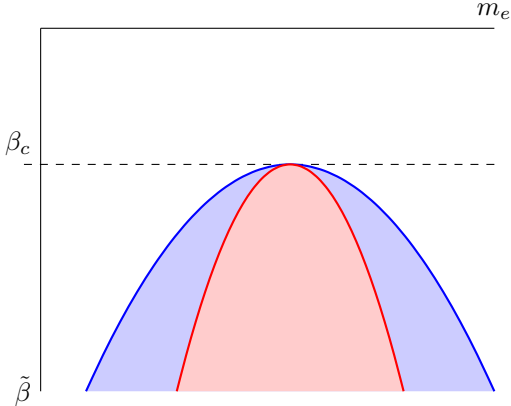


Figure 2.7 – Sketch of the bifurcation plane (β, m_e) . Here the red region denotes the spinodal region, in which the uniform steady states are unstable, the blue region denote the metastable region in which the uniform steady states are stable and the white region denotes the other region, in which the uniform steady states are the only stable stationary solutions. We see that only when $\beta < \beta_c = -\sqrt{3}$ we can find non-trivial stationary solutions. So one would expect to only see patterns when $\beta < \beta_c$.

our new parameters. For clarity we have given this bifurcation diagram again in Figure 2.8, with the new parameters. We should note that now the bifurcation value for β' is given by $\beta_c = -\sqrt{3}$. Therefore the bifurcation value for $\tilde{\beta}$ is now $\frac{-\sqrt{3}}{\sqrt{1-\tilde{d}a_e}}$.

Since the variables β' and m' now depend on the value of a_e and \tilde{d} this formulation is perhaps not the neatest formulation. Hence we also try another approach. In this approach we try to determine the linear stability of the uniform stationary state given by (m_e, a_e) . From the previous section we know that this state is linearly unstable when $\beta' < -\frac{3m_e'^2+1}{2m_e'}$. When we transform this back to the original parameters we obtain the condition

$$\beta < \beta_C(d) := -\frac{3m_e^2+1}{2m_e} + d \frac{a_e}{2m_e} \quad (2.8)$$

Since the speed v is assumed to be positive, it is not always possible to choose the parameter β small enough for this instability to set in. More precisely, for the speed of the mussels to be positive we need to have $\beta > -2\sqrt{1-\tilde{d}}$ (and $d < 1$).

Since $m_e > 0$ and $a_e \geq 0$ we know that the function $d \mapsto \beta_C(d)$ is non-decreasing in d . Therefore there are three forms that are possible for the bifurcation curve in the (β, d) -plane:

- (A) $\beta_C(0) > -2$, in which case the bifurcation line starts in the permissible region;
- (B) $\beta_C(0) < -2$ and $\frac{a_e}{2m_e}$ is large enough, so that the bifurcation line does not start in the permissible region, but $\beta_C(d)$ is for some range of values for d ;

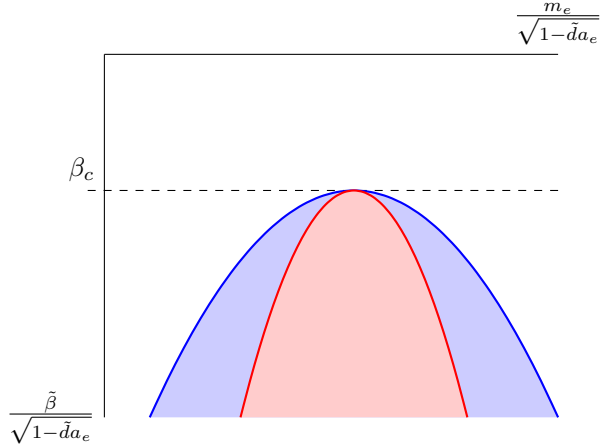


Figure 2.8 – Sketch of the bifurcation plane (β', m'_e) . Here the red region denotes the spinodal region, in which the uniform steady states are unstable, the blue region denote the metastable region in which the uniform steady states are stable and the white region denotes the other region, in which the uniform steady states are the only stable stationary solutions. We see that only when $\beta' < \beta_c$ we can find non-trivial stationary solutions. So one would expect to only see patterns when $\beta' < \beta_c$.

(C) $\beta_C(0) < -2$ and $\frac{a_e}{2m_e}$ is too small, so that the bifurcation line does not lie in the permissible region for any d .

In Figure 2.9 we sketched those three possible bifurcation planes for the parameters β and d , for a given specific uniform stationary state (m_e, a_e) . In the next paragraphs we will determine how we can distinguish between those cases, when the stationary state (m_e, a_e) is given.

Situation (A) occurs when $\beta_C(0) > -2$. That is, when $-2 < -\frac{3m_e^2+1}{2m_e}$. This is equivalent to the condition $3m_e^2 - 4m_e + 1 < 0$ and with the quadratic formula one immediately finds that $\beta_C(0) > -2$ if and only if $m_e \in (\frac{1}{3}, 1)$.

Logically, situations (B) and (C) can only occur if $m_e \notin (\frac{1}{3}, 1)$. In this case $\beta_C(0) < -2$. It remains to determine if there is a value for $d \in (0, 1)$ such that $\beta_C(d) > -2\sqrt{1-d}$. Whether this happens is determined by the size of the slope $\frac{a_e}{2m_e}$. There will be some threshold slope $C(m_e)$ which is the largest slope at which $\beta_C(d) < -2\sqrt{1-d}$ for all $d \in (0, 1)$. When $\frac{a_e}{2m_e} > C(m_e)$ we find ourselves in situation (B) and otherwise we are in situation (C). The remainder of this section will be devoted to finding an expression for the constant $C(m_e)$.

We are interested in the largest slope $C(m_e)$ such that we still have $\beta_C(d) < -2$ for all $d \in (0, 1)$. The resulting line $\left\{ -\frac{3m_e^2+1}{2m_e} + C(m_e)d : d \in \mathbb{R} \right\}$ will be a line tangent to the function $d \mapsto -2\sqrt{1-d}$. It is more convenient to find this constant $C(m_e)$ by reverse engineering. Instead of looking for all possible slopes to see which one is a tangent line, we will look at each tangent line and see which crosses the point $\left(0, -\frac{3m_e^2+1}{2m_e}\right)$.

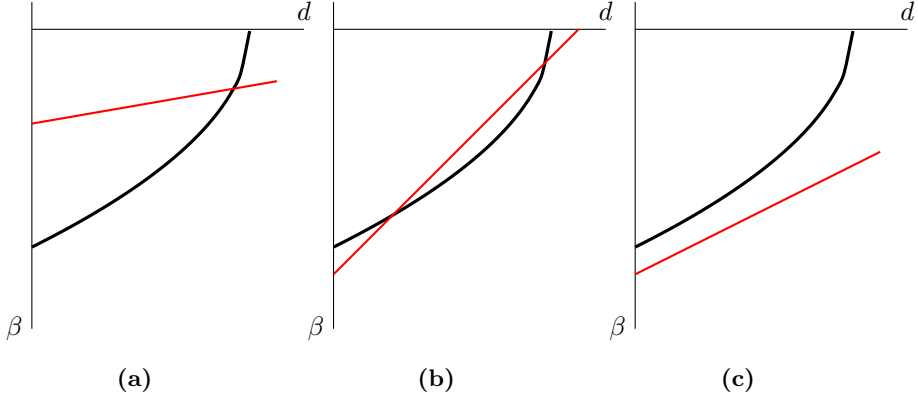


Figure 2.9 – Sketch of the three possible bifurcation planes (β, d) . The red line illustrates the bifurcation line, while the black line denotes the allowed values to ensure positiveness of the mussel's speed. In (a) we plotted the plane when $\beta_C(0) > -2$. In (b) we sketched the bifurcation line when $\beta_C(0) < -2$, but when there are values for d such that $\beta_C(d) > -2\sqrt{1-d}$. Finally in (c) we sketched the situation when $\beta_C(0) > -2\sqrt{1-d}$ for all $d \in (0, 1)$. So in (c) the stationary state is stable, while in (b) and (a) some of them can be unstable when the parameters β and d are chosen right. The region below the red line corresponds to the spinodal region that we found before.

So for this let $d^* \in (0, 1)$. The point $(d^*, -2\sqrt{1-d^*})$ is a point on the graph of the function $d \mapsto -2\sqrt{1-d}$, with the tangent line given by

$$l_{d^*}(d) = -2\sqrt{1-d^*} + \frac{d-d^*}{\sqrt{1-d^*}} = \frac{1}{\sqrt{1-d^*}}[d+d^*-2].$$

This line crosses the β -axis in the point $\left(0, \frac{d^*-2}{\sqrt{1-d^*}}\right)$. Now we are interested in the d^* -value for which this point coincide with the point $\left(0, -\frac{3m_e^2+1}{2m_e}\right)$. Then the derivative of the function $d \mapsto -2\sqrt{1-d}$ in the point d^* will be our desired slope $C(m_e)$. To find this particular value for d^* we solve the equality

$$\begin{aligned} \frac{d^*-2}{\sqrt{1-d^*}} &= \beta_C(0) \\ (d^*)^2 - 4d^* + 4 &= \beta_C(0)^2(1-d^*) \\ (d^*)^2 + d^*(\beta_C(0)^2 - 4) + (4 - \beta_C(0)^2) &= 0 \end{aligned}$$

The solutions are easily found with the quadratic formula to be

$$d_{1,2}^* = \frac{4 - \beta_C(0)^2}{2} \pm \frac{1}{2}|\beta_C(0)|\sqrt{\beta_C(0)^2 - 4}.$$

Since assumed that $\beta_C(0) < -2$ we know that both of these values are indeed well-defined. From this it is also clear that $d_2^* < 0$. Since we need to choose $d^* \in (0, 1)$ this value is irrelevant. So the only relevant solution is d_1^* . Note that $d_1^* \in (0, 1)$ for all values $\beta_C(0) \in (-2, -\infty)$ as the expression for d_1^* is increasing in $\beta_C(0)$ and $d_1^*(-2) = 0$ and $\lim_{\beta_C(0) \rightarrow -\infty} d_1^*(\beta_C(0)) = 1$.

Now the slope $C(m_e)$ that we were interested in is simply $\frac{1}{\sqrt{1-d_1^*}}$. Upon substitution of the value of d_1^* and $\beta_C(0) = -\frac{3m_e^2+1}{2m_e}$ we find that this slope can be expressed as

$$C(m_e) = \frac{1}{8m_e^2} \left(-(9m_e^2 + 1)(m_e^2 + 1) + (3m_e^2 + 1)\sqrt{(9m_e^2 + 1)(3m_e^2 + 1)} \right).$$

Thus we are finally able to make a distinction between situations (B) and (C): we are in situation (B) when $a_e > 2m_e C(m_e)$ and in situation (C) when we have $a_e \leq 2m_e C(m_e)$.

The metastable region

In Figure 2.7 we have seen that there is a spinodal region and a metastable region. In theory we should be able to apply the same procedure to the curve introducing the metastable region. However, we were not able to find an exact closed form of this line. Therefore the same approach cannot be performed here. Instead we try to explain what can happen by carefully examining the diagram in Figure 2.7.

If we fix the value m'_e we see that, upon decreasing β' , we come into the metastable region and then enter the spinodal region (unless $m'_e = \frac{\sqrt{3}}{3}$, in which case we immediately enter the spinodal region). Now if we fix the value of m_e and that of a_e we see that the value of m'_e is fixed and that $\beta = \sqrt{1 - da_e \beta'}$. Therefore when we keep decreasing β we still find ourselves first in the metastable region, before entering the spinodal region (unless, again $m'_e = \frac{\sqrt{3}}{3}$).

Therefore the curve that denotes the beginning of the metastable region, in the (d, β) -plane (i.e. keeping m_e and a_e fixed), must lie above the curve corresponding to the beginning of the spinodal region, and may only touch this line when $m'_e = \frac{\sqrt{3}}{3}$. Therefore the complete diagram in the (d, β) -plane can have many forms, of which we have sketched a few in Figure 2.10.

2.1.6 Bifurcation diagram for mussel system with $v = v_p$

In the previous section we studied the Cahn-Hilliard equation for our mussel system when we choose the quadratic fit approach $v = v_q$ for the density dependent movement. We have also introduced a piecewise linear description for this speed as

$$v(m, a) = \begin{cases} v_1(m, a) = 1 - \tilde{\beta}m & \text{if } m < \tilde{\beta}/2; \\ v_2(m, a) = \frac{2-\tilde{\beta}^2}{2} + \gamma_0 e^{-\tilde{d}a}(m - \tilde{\beta}/2) & \text{if } m > \tilde{\beta}/2. \end{cases}$$

In this section we will analyse the mussel system again, but now with this piecewise linear description for the density dependent movement speed. Recall that all the parameters in this description are positive and that we need to have $0 < \tilde{\beta} < \sqrt{2}$ and $\gamma_0 > 0$ to ensure positiveness of the movement speed.

By construction we know that $m \mapsto v(m; a)$ is increasing when $m > \tilde{\beta}/2$ and decreasing otherwise. Hence $f := v(v + m \frac{dv}{dm})$ is increasing for $m > \tilde{\beta}/2$ and

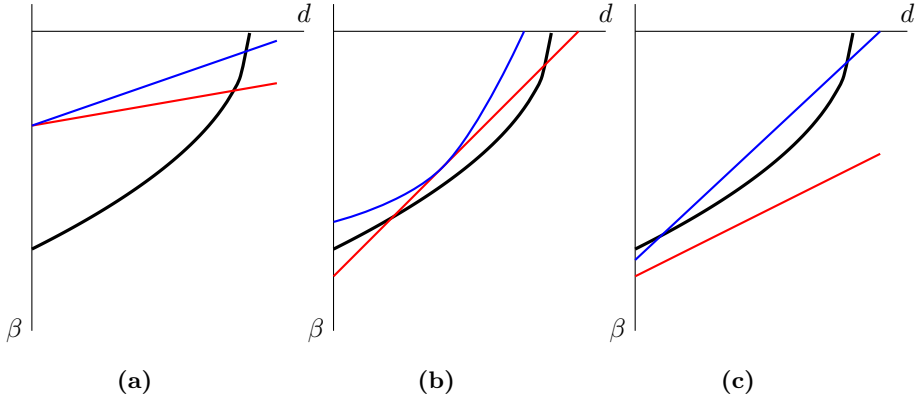


Figure 2.10 – Sketch of three possible complete bifurcation planes (β, d) . The spinodal region is the region between the red line, the metastable region lies below the red and blue line. Finally all allowed combinations of the parameters β and d lie above the black line. In (a) we have sketched a possible plane when $m_e = \sqrt{3}$, in (b) we have $m_e < \frac{1}{3}$ and $a_e > 2m_e C(m_e)$. Finally, in (c), we have $m_e > 1$ and $a_e < 2m_e C(m_e)$. Note that these are mere sketches of examples; there are even more, different planes possible.

might be decreasing for $m < \tilde{\beta}/2$. Since the uniform steady state $m(x, t) = m_e$ is unstable when $f(m_e) < 0$ we can conclude that only when $m_e < \tilde{\beta}/2$ this state possibly is unstable. More precisely, the state is unstable when $1 - 2\tilde{\beta}m_e < 0$, or equivalently when $m_e > \frac{1}{2\tilde{\beta}}$.

We are however also interested to see what form the function $m \mapsto F(m)$ has. Therefore we want to know for which values of $\tilde{\beta}$ the function $m \mapsto f(m)$ has two roots. Clearly the minimum value for $f(m)$ is attained close to $m = \tilde{\beta}/2$, but a bit to the left, so that $v(m, a) = v_1(m, a)$. Hence in this point the value $\lim_{m \uparrow \tilde{\beta}/2} f(m) = 1 - \tilde{\beta}$. Hence we see that a bifurcation occurs when $\tilde{\beta} = 1$.

When $\tilde{\beta} > 1$ we know that there is a value $m_1 = \frac{1}{2\tilde{\beta}} \in (0, \tilde{\beta}/2)$ such that $f(m_1) = 0$. Because the piecewise linear description assumes that there is a fast transition between v_1 and v_2 around the density $m = \tilde{\beta}/2$ and that this transition is continuous, we know from the intermediate value theorem that the other root, m_2 , will be close to $\tilde{\beta}/2$ and lie on this fast transition.

Hence we have again found a spinodal region (m_1, m_2) when $1 < \tilde{\beta}$. There is also again a metastable region for the same parameter values $\tilde{\beta} > 1$, though it is again too complicated to capture in closed form. It is however clear that the right-hand corner of this metastable region will lie on the fast transition as well and hence will be very close to m_2 . A sketch of the bifurcation diagram is given in Figure 2.11.

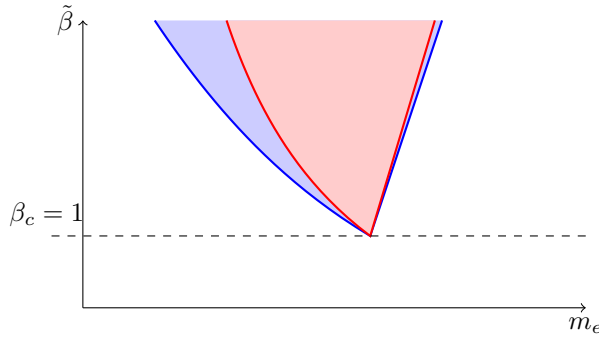


Figure 2.11 – Sketch of the bifurcation plane $(\tilde{\beta}, m_e)$ for the piecewise linear description $v = v_p$ of the movement speed of the mussels. Here the red region denotes the spinodal region, in which the uniform steady states are unstable; the blue region is the metastable region in which the uniform steady state is stable and the white region is the region in which the uniform steady states are the only (stable) stationary states. When $\tilde{\beta} > 1$ we see we can find non-trivial stationary solutions. So one would expect only to see patterns arising from the uniform steady state when $\tilde{\beta} > 1$.

2.2 Long time behaviour - Ostwald Ripening

In the first part of this chapter we have started our study of the Cahn-Hilliard equation. We have described the possible steady states of the equation and determined the stability of some of them. The steady states alone do not tell the whole story of a gradient system. We should also look at the dynamics that such a system possesses.

This second part of Chapter 2 is devoted to the long-time behaviour of solutions of the Cahn-Hilliard equation, starting from an uniform stationary state. In Section 2.1 we have already seen that these uniform steady states are stable when they don't lie in the spinodal region. These solution thus will always remain in their starting position - since they are stable. Hence we focus on those starting configurations that lie in the spinodal region - i.e. uniform states that are unstable.

These solution will quickly evolve from an uniform configuration to a patterned configuration. The wavelength of this pattern can be found using the linear stability analysis from Section 2.1.3: the most critical wavelength will be the dominant wavelength in these patterns. After this initial pattern has emerged the analysis of Section 2.1 is no longer applicable.

From simulations (we come to these in Section 2.3. Also see [25]) it is known that patterned solutions of the Cahn-Hilliard equation are not always stable. After a ‘long’ time the pattern suddenly changes to another pattern, with a smaller wavelength. This newly created pattern is also temporarily and again after a ‘long’ time will change to yet another pattern, with an even smaller wavelength. This sequence repeats itself until the system hits a steady state - presumably a global minimizer (see Section 2.1.2).

This process is called ‘Ostwald Ripening’ and it will be the subject of our study in this section. We start in Section 2.2.1 with a general qualitative description of this phenomenon. We also give a few examples of other system that also exhibit Ostwald Ripening, besides the Cahn-Hilliard equation. Then in Section 2.2.2 we explain how this Ostwald Ripening is related to the Cahn-Hilliard equation and finally how this phenomenon can explain the observed wavelength selection in Figure 4.

2.2.1 General Description of Ostwald Ripening

Imagine this: a few weeks ago you bought a big package filled with your favorite ice cream. That same evening you opened it. You ate some and it was delicious: exactly the right flavour and very soft. As the package was too big to eat at once, you decide to put the rest in the freezer so you can enjoy it again some time in the future. Two weeks later you decide to treat yourself once again with the delicious ice cream. Will it taste as good as before?

Sadly, the answer is no. Though the flavour is still good, the ice cream is not soft any more. In fact, the ice cream has become quite hard and it tastes more like normal, hard ice at some places. Something has changed in the structure of the ice cream over time. This process, responsible for this ice cream ruining, is Ostwald Ripening (see [26] for more science behind ice cream).

We have already said that Ostwald Ripening is also the process that dictates the long time behaviour of the Cahn-Hilliard equation. So what exactly is this phenomenon? Generally this name is given to the process that describes the change of inhomogeneous structures over long time periods. In this section we will inspect this Ostwald Ripening. To do so we will describe this phenomenon at smaller and smaller scales, using the ice cream example to go by.

The ice cream of our little story spoiled over the course of a few weeks. At the start of this period the ice cream was perfectly soft. The softness of ice cream is determined by the size of the ice crystals in the ice cream. When they are all small the ice is soft and when they are big the ice cream is hard. Since our ice cream lost its softness over time, that means that the ice crystals in the ice cream grew in size over time.

To explain why this happens we need to zoom in on our ice cream and look at some physics. We will look at the energy of the system (i.e. of our ice cream). It turns out that it is energetically favourable for ice crystals to stick together; a boundary between an ice crystal and something else gives an energy penalty (see [27] Chapter 3). Therefore the most energetically favourable configuration of the system is achieved when all ice crystals are clustered and the boundary between ice crystals and other material is minimal.

In Section 2.1.2 we saw that the global (energy) minimizer of the Cahn-Hilliard equation has the same properties. However this does not mean that the system in fact will attain this state when given enough time. After all, it is possible that there is a local minimum in the energy landscape. Hence the description thus far is not good enough to understand what is happening during Ostwald Ripening.

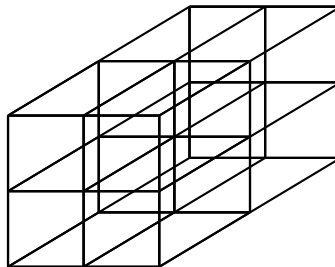


Figure 2.12 – Schematic illustration of an ice-crystal. The black lines denote the bonds between atoms, which are located at the intersections of the black lines. Clearly the ice atom in the interior of the crystal is in an energetically favourable place as it has 6 neighbours, whereas the other atoms, at the surface, have less bonds and thus are less stable.

Ice atoms want to stay together, because they bond with each other. When we look at an ice crystal it is clear that atoms in the interior are quite stable, as they are bonded to six neighbours (see Figure 2.12). Atoms on the surface of the crystal have less neighbours and hence are less stable. If we now have a fixed amount of ice atoms, it is clear that it is best to create ice crystals with larger volume to surface ratio. Therefore larger ice crystals are preferred.

This however still does not explain why the system is able to evolve from one state, with small ice crystals, to an other state, with larger ice crystals. For this we need to delve even deeper in the physics literature. The crystals in our ice cream are made from water (in ice form). However, the rest of the ice-cream is also made of water, though not in ice form. Hence our ice cream contains water in two phases: a liquid phase and a solid phase (ice). So we are essentially dealing with phase transitions.

In physics there is a concept called free energy, which indicates the amount of energy that is available for the system. Water in liquid phase has a specific free energy curve depending on the concentration of water. In the solid phase (i.e. the ice crystals) there is also a curve describing the free energy. However this curve depends on the size of the ice crystals⁵. It turns out that the free energy in this solid phase can be described as

$$G_s(R) - G_s(\infty) = \frac{C}{R},$$

where $G_s(\infty)$ is the free energy (that still depends on the concentration) of the solid phase when the curvature is infinite, R is the radius of the ice crystal and C is some constant.

In Figure 2.13 we have sketched these free energies for both the solid and the liquid phases. In the solid phase the atoms are closer together, explaining the higher densities for this phase. At the ice-water surface there is transition between the liquid and solid phases. During a phase transition the chemical potential must be constant (see e.g. [28] section 2.3). The chemical potential is the derivative of the free energy with respect to the concentration (see

⁵More precisely, on the curvature of the interface.

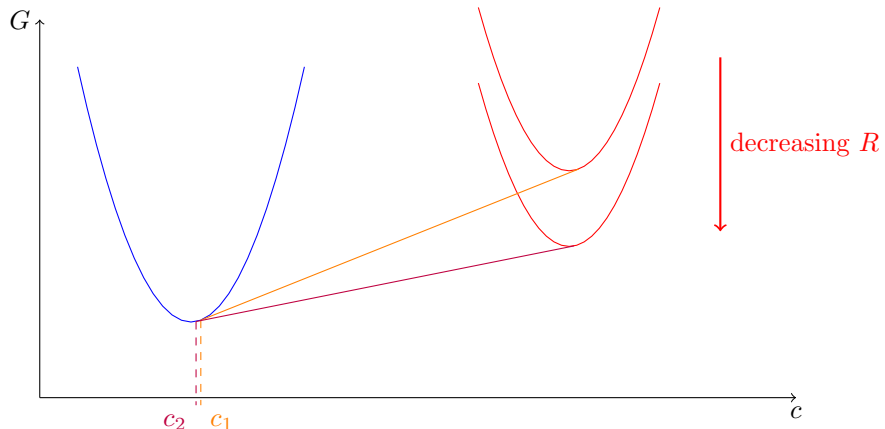


Figure 2.13 – Sketch of the free energy of water in liquid phase (blue) and in solid phase for two different crystal sizes (red). The orange and purple lines are the common tangent lines, needed to understand the phase transition between liquid and solid phase.

e.g. [29] Chapter 1). Hence we can construct a common tangent between the liquid phases free energy and that of the solid phase. In Figure 2.13 we have constructed this line for two sizes of ice crystals.

The concentration at which a tangent line touches the free energy of the liquid phase is the concentration of water (in liquid phase) at the ice-water interface, for ice crystals with that particular radius R . Since the free energy decreases for ice crystals with bigger sizes, we know that the concentration of water (in liquid phase) at the interface is smaller for larger ice crystals.

Now, let's look at an ice cream with two ice crystals, of sizes R_1 and $R_2 > R_1$. In Figure 2.14a we have sketched this situation. Because of the difference in size the concentration of water near the two interfaces is different as we have seen. In Figure 2.14b we have sketched the concentration along a line from the center of the left crystal to the center of the right crystal.

The concentration of water in the liquid phase will just decrease when going from the left interface to the right interface. Hence there will be a difference in the concentration in this phase, which will lead to diffusion of the water. Thus the water near the interface with the smaller crystal will move to the interface with the bigger crystal over time. This can only happen when the smaller crystal shrinks and the larger one grows.

There is a positive feedback loop in this process. A small crystal will shrink to an even smaller crystal, which will lead to even faster shrinking and so on. On the other hand, the larger crystals will grow to even bigger crystals and continue to grow faster, until all material from the smaller crystals is captured in the larger crystals. In the end this process will end with a configuration that has the smallest interface possible, for the given amount of atoms and the shape of the volume.

It is possible to derive an equation that describes the evolution of the mean size

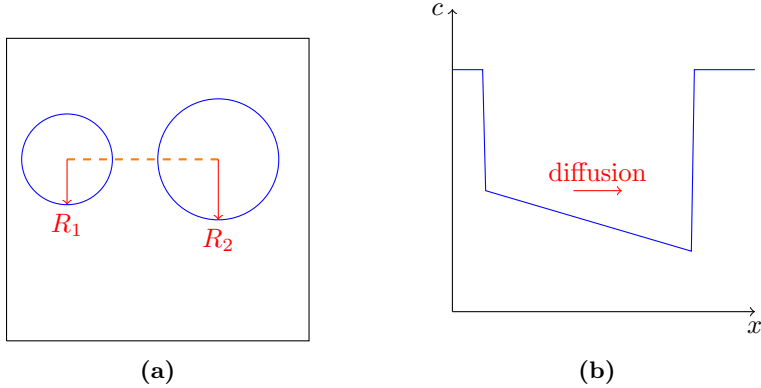


Figure 2.14 – Sketch of an ice cream with two ice crystals (a), one smaller one (left) and one bigger one (right). A side view of the concentration along the orange line is sketched in (b). Here the smaller crystal is on the left and the bigger on the right. Because of the gradient in the concentration, this configuration will lead to diffusion of water from the smaller crystal to the bigger crystal, causing the smaller to shrink and the larger to grow.

of the ice crystals:

$$\langle R(t) \rangle^3 - \langle R(0) \rangle^3 = \lambda t$$

Here $\langle R(t) \rangle$ is the *mean* radius of all the crystals in the system at time t and λ is some parameter that depends on material properties, like the interface energy. This law, sometimes referred to as the ‘*t-to-the-one-third*’ law, is the Lifschitz-Slyozov law (after the researchers Lifschitz and Slyozov who discovered this law in 1961 [12]). It has been verified in many experiments and simulations and it is also possible to derive it analytically in many other systems, for example in the Cahn-Hilliard equation.

2.2.2 Ostwald Ripening with mussels

In the previous section we gave a general description for Ostwald Ripening. For our situation we need to understand the long time behaviour of the Cahn-Hilliard equation. Historically the Cahn-Hilliard equation was introduced just to capture this effect of Ostwald Ripening (explaining the terminology in the Cahn-Hilliard equation - e.g. chemical potential and free energy), though a formal analytic verification of this phenomenon was not found immediately. However, nowadays we do know that the Cahn-Hilliard equation leads to Ostwald Ripening [30], though only for systems in dimensions 2 and larger.

Our analysis in section 2.1 is and our simulation in section 2.3 will be for the Cahn-Hilliard system in one spatial dimension. There will be no Ostwald Ripening in these systems, as the size of the interface does not depend on the size of the (mussel) clusters in a one-dimensional system. However, it is possible to study interactions between pulse solutions of the one-dimensional Cahn-Hilliard equation to determine the long time behaviour. Both from this analysis and through simulations it has been verified that the one-dimensional Cahn-Hilliard

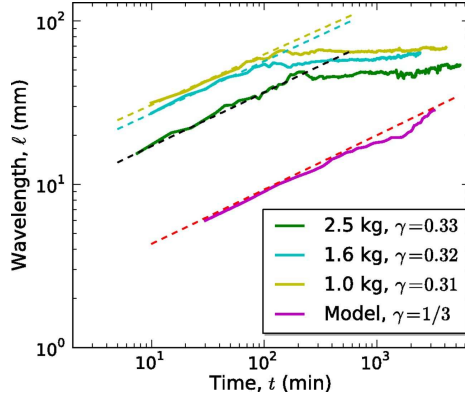


Figure 2.15 – Correlation between the typical wavelength of patterns for mussels, in experimental set-up (blue and green lines) and in a numerical simulation (purple). The dashed lines are linear fits over the initial behaviour (i.e. before a wavelength is ‘selected’). For the numerical simulation the theorized power law is used instead. In these plots we can clearly see that there is some sort of wavelength selection in the experiments after some hours. (Repeat of Figure 4)

equation, like the higher dimensional equations, has a long-term ripening effect preferring bigger clusters as well, similar to the Ostwald Ripening (see [30] and [25]).

For the analysis of patterns in animal populations, we don’t need to worry about this however, as animal populations never live in one-dimensional worlds, but rather in two-dimensional or three-dimensional ones. Hence the Cahn-Hilliard equation will lead to Ostwald Ripening for these populations. So in our standard example, of mussel populations, the mathematical theory predicts a ripening effect (as we already discussed in the introduction).

So from this perspective we should indeed expect that a tank filled with mussels will - when the average density is in the spinodal region - start to form a pattern. This pattern will then - as the Ostwald Ripening predicts - slowly evolve such that the typical wavelength of the patterns increases, until finally all mussels are clumped together, such that the interface is as small as possible.

However, in reality this is not what happens, as we have seen in the introduction (a repeat of the plot presented in the introduction is given in Figure 2.15). So the Ostwald Ripening in the Cahn-Hilliard equation is not observed in experiments with mussels over longer time periods. Of course this can mean that the (standard) Cahn-Hilliard description is not suited to understand the behaviour of mussels in a tank and that we need to add additional terms to the standard description or derive a completely other model. However, there is still something we can learn from the standard Ostwald Ripening phenomena as starting point.

In Section 2.2.1 we have seen what happens when we have two ice crystals of different sizes $R_1 < R_2$. We can directly translate this to two clumps of mussels of different sizes. However, what happens when the clumps of mussels are exactly as large? In that case the concentration at the interface (between

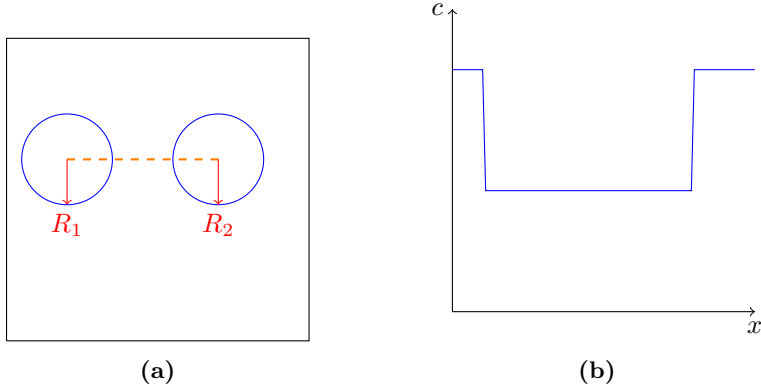


Figure 2.16 – Sketch of a configuration with two clumps of mussel of the same size (a) and a side view of the concentration along the orange line (b). Because the clumps are of the same size, there is no gradient in the concentration (in the low density state) and therefore this configuration will not evolve (i.e. it is a steady state).

a high and a low density ‘state’ of mussels) is exactly the same and there is no gradient in the system. Hence this system is (meta)stable⁶ and nothing will happen; the system will stay in this configuration (see Figure 2.16).

We can also look what happens when we have two clumps of mussels, with approximately the same size, e.g. $R_2 = R_1 + \varepsilon$ (with $0 < \varepsilon \ll 1$). In Figure 2.17 we have sketched this situation. Since the clumps are now of different size there is a gradient in the concentration and hence diffusion is expected. However, the difference in concentration is minimal and therefore diffusion is only marginal. That is, only a ‘small amount of mussels’ is expected to be transported from the smaller clump to the bigger clump.

For a theoretical model this is no problem; it does not matter for a simulation that the Cahn-Hilliard equation dictates that ‘one half of a mussel’ or ‘three twentieths of a mussel’ must be transported. In a real system this is not possible; only whole mussels can exist. Because of this, there will be no transportation of mussels from the somewhat smaller clump to the somewhat larger clump in reality, as the (through Ostwald Ripening) predicted amount of transportation is too small.

Hence the discrepancy between the predicted and observed behaviour of mussels (i.e. the wavelength selection observed in experiments) can stem from one (implicit) assumption of the Cahn-Hilliard equation. The Cahn-Hilliard equation is only applicable to systems where the concentration can be chosen continuously and fractional mass transportation is possible. As the experiments are conducted with ‘only’ a few hundred mussels at best, the concentration is by no means continuous. Therefore at some moment the Ostwald Ripening will stop, because the desired amount of transportation is too small.

⁶since a little perturbation will make one of the clumps bigger, so that we are back in the initial situation with different sized clumps

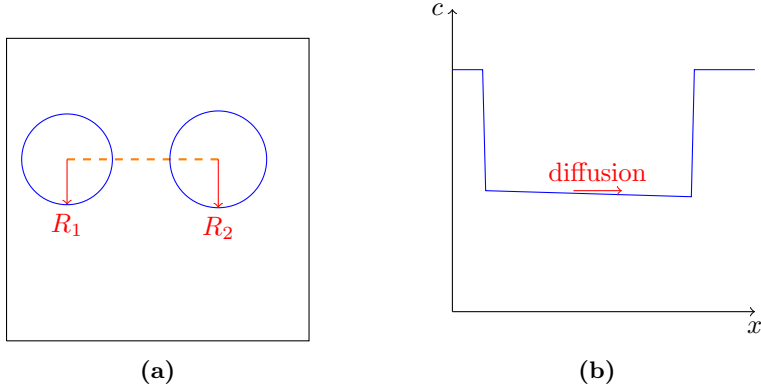


Figure 2.17 – Sketch of a configuration with two clumps of mussel of approximately the same size (a) and a side view of the concentration along the orange line (b). Because the clumps are approximately equally large there is a small gradient in the concentration of the mussels. Hence there will be diffusion in this system, but it will only transport a ‘small amount of mussels’.

2.3 Simulations

In Sections 2.1 and 2.2 we studied the Cahn-Hilliard equation analytically. In this section we turn our attention to simulations of this equation. More specifically we examine the one-dimensional Cahn-Hilliard equation for our test-case: a population of mussels.

In this section we will present simulations of the following equation

$$\frac{\partial m}{\partial t} = d_m \frac{\partial}{\partial x} \left(v \left[v + m \frac{\partial v}{\partial m} \right] \frac{\partial m}{\partial x} - \kappa \frac{\partial^3 m}{\partial x^3} \right), \quad (2.9)$$

along with the natural boundary conditions:

$$m_x(0) = m_x(L) = 0; \\ m_{xxx}(0) = m_{xxx}(L) = 0,$$

and initial condition

$$m(0, x) = m_e.$$

Here d_m and κ are positive constants and v is the density dependent speed. We will present simulations for both presented choices of this movement speed (see Section 1.1.4).

All simulations in this section start from an uniform steady state, as this is the most common approach in the study of pattern formation. Because we need to perturb the initial configuration a little bit, to prevent the simulations being stuck in an unstable steady state, we apply a non-symmetric perturbation⁷. The Fortran code used to perform these simulations was kindly provided by *Paul Zegeling* and uses finite-difference numerical methods on a moving grid. In this section we use these simulations to get a better intuition about the solutions of the Cahn-Hilliard equation.

⁷Would the perturbation be symmetric in $x = L/2$ then the solution will always have this symmetry, preventing us from seeing the ‘real’ evolution of the system.

2.3.1 The start - short-time behaviour

Our first aim is to understand the initial behaviour of solutions. In Section 2.1 we have found that a solution, starting from a uniform steady state, will only evolve to a configuration with patterns when this state m_e is located in the spinodal region. For this reason, all simulations in this section start from steady states in this region⁸.

In Figure 2.18 and Figure 2.19 we show the initial behaviour for respectively the ‘quadratic’ movement speed v_q as the ‘piecewise’ one v_p . In both plots we see patterns arising from the initial uniform configuration. From these figures it is clear that both choices for the speed indeed lead to patterns, as expected by our previous analysis. In fact, the patterns for both choices look very similar and there is no clear distinction possible.

2.3.2 The end - long-time behaviour

In Section 2.2 we discussed the long term behaviour of the Cahn-Hilliard equation from a physics viewpoint. Here we mentioned the ripening effect, that is enclosed in the equation. After an initial pattern has been chosen by the solution, it will stay close to this pattern for a long time, after which it suddenly will change to another pattern only to repeat this process until the solution reaches a minimizer, possibly the global minimizer, in which the amount of interfaces is minimized (i.e. one in a one-dimensional system).

In this section we will study this behaviour using numerical methods. In Figures 2.20 and 2.21 we show pattern plots of simulations for $v = v_q$ and $v = v_p$, respectively. In both figures one can clearly see that the initial pattern settles and then after a while some of the initial peaks suddenly disappear. So these figures indeed show the predicted ripening effect. Note that the initial peaks start to form near the center of the domain; this is merely an effect of the chosen perturbation, which is most prominent at the center of the domain.

In these simulation we again see no clear difference between the two possible descriptions for the density dependent movement speed. In fact in all our simulations we observed no qualitative difference between those two approaches. Therefore in the rest of this section we shall only present the plots for the ‘quadratic’ approach $v = v_q$.

Figures 2.20 and 2.21 show the ripening effect of the Cahn-Hilliard equation. Because the domains in these simulation were so big they however fail to show what happens when a peak disappears. Therefore we present a simulation for a smaller domain in Figure 2.22. In this plot we can clearly see that the disappearance of one peak leads to an increase in size of the central peak. So this indicates that there is indeed a transport of mass when a peak disappears, as was predicted in 2.2.

Finally, in Sections 2.1 and 2.2 we described a global minimizer of the system of equation (2.9). This global minimizer is the configuration which has the least possible number of transitions between the low and high density states (i.e.

⁸other choices would lead to boring behaviour: the solution just returns to the steady state.

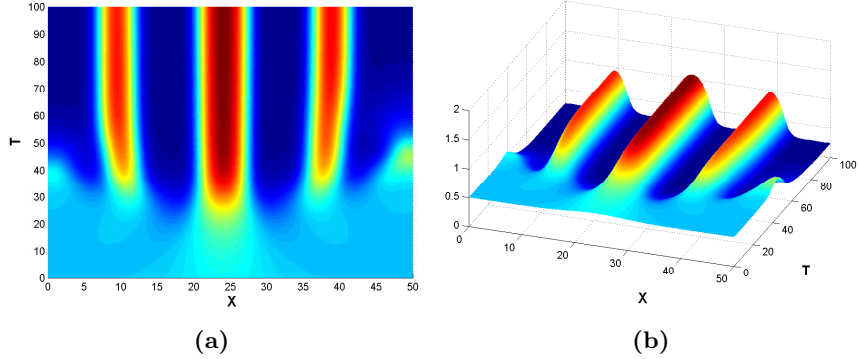


Figure 2.18 – Pattern plot of a simulation of initial behaviour of equation (2.9) with ‘quadratic’ speed $v = v_q = m^2 + \tilde{\beta}m + 1$ on a one-dimensional domain $[0, L]$. In (a) we see a pattern plot from the top and in (b) from the side. X denotes the spatial position and T the time. The z -axis in (b) denotes the concentration of the mussels. The colours denote the density of the mussels, m , on a scale from blue (low) to red (high). Parameter values: $L = 50$, $T = 100$, $m_e = 0.5$, $\kappa = 0.05$, $d_m = 20$, $\tilde{\beta} = -1.9$.

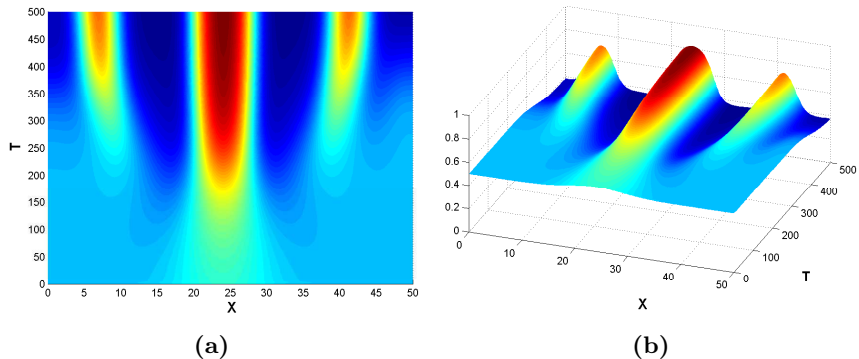


Figure 2.19 – Pattern plot of a simulation of initial behaviour of equation (2.9) with speed $v = v_p$ (see section 1.1.4) on a one-dimensional domain $[0, L]$. In (a) we see a pattern plot from the top and in (b) from the side. X denotes the spatial position and T the time. The z -axis in (b) denotes the concentration of the mussels. The colours denote the density of the mussels, m , on a scale from blue (low) to red (high). Parameter values: $L = 50$, $T = 500$, $m_e = 0.5$, $\kappa = 0.01$, $d_m = 20$, $\tilde{\beta} = 1.35$, $\gamma_0 = 1$, $d = 0$, $K = 1$

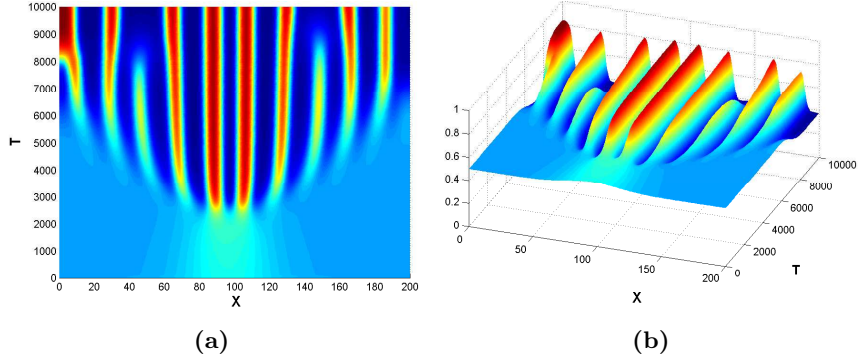


Figure 2.20 – Pattern plot of a simulation of long-time behaviour of equation (2.9) with ‘quadratic’ speed $v = v_q = m^2 + \tilde{\beta}m + 1$ on a one-dimensional domain $[0, L]$. In (a) we see a pattern plot from the top and in (b) from the side. X denotes the spatial position and T the time. The z -axis in (b) denotes the concentration of the mussels. The colours denote the density of the mussels, m , on a scale from blue (low) to red (high). Parameter values: $L = 200$, $T = 10000$, $m_e = 0.5$, $\kappa = 0.05$, $d_m = 3$, $\tilde{\beta} = -1.78$.

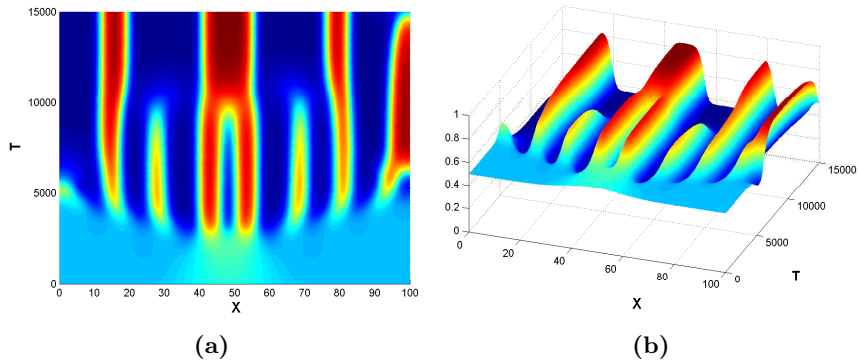


Figure 2.21 – Pattern plot of a simulation of the long-time behaviour of equation (2.9) with speed $v = v_p$ (see section 1.1.4) on a one-dimensional domain $[0, L]$. In (a) we see a pattern plot from the top and in (b) from the side. X denotes the spatial position and T the time. The z -axis in (b) denotes the concentration of the mussels. The colours denote the density of the mussels, m , on a scale from blue (low) to red (high). Parameter values: $L = 100$, $T = 10000$, $m_e = 0.5$, $\kappa = 0.01$, $d_m = 3$, $\tilde{\beta} = 1.35$, $\gamma_0 = 1$, $d = 0$, $K = 1$

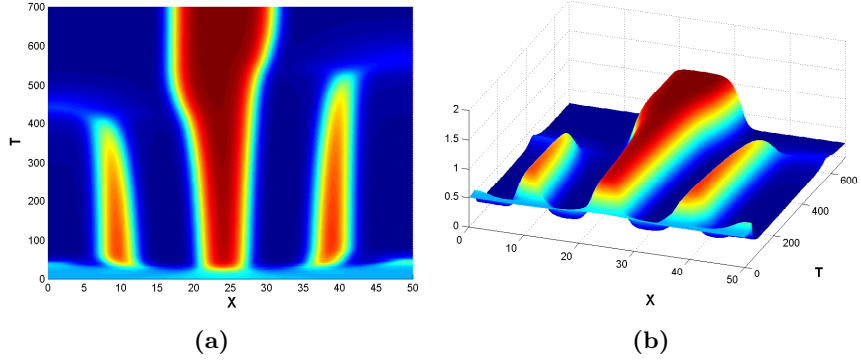


Figure 2.22 – Pattern plot of a simulation of long-time behaviour of equation (2.9) with ‘quadratic’ speed $v = v_q = m^2 + \tilde{\beta}m + 1$ on a one-dimensional domain $[0, L]$. In (a) we see a pattern plot from the top and in (b) from the side. X denotes the spatial position and T the time. The z -axis in (b) denotes the concentration of the mussels. The colours denote the density of the mussels, m , on a scale from blue (low) to red (high). Parameter values: $L = 50$, $T = 70$, $m_e = 0.5$, $\kappa = 0.05$, $d_m = 20$, $\tilde{\beta} = -1.9$. Note that this is the same set-up as used for the simulation of Figure 2.18 but with a longer simulation time.

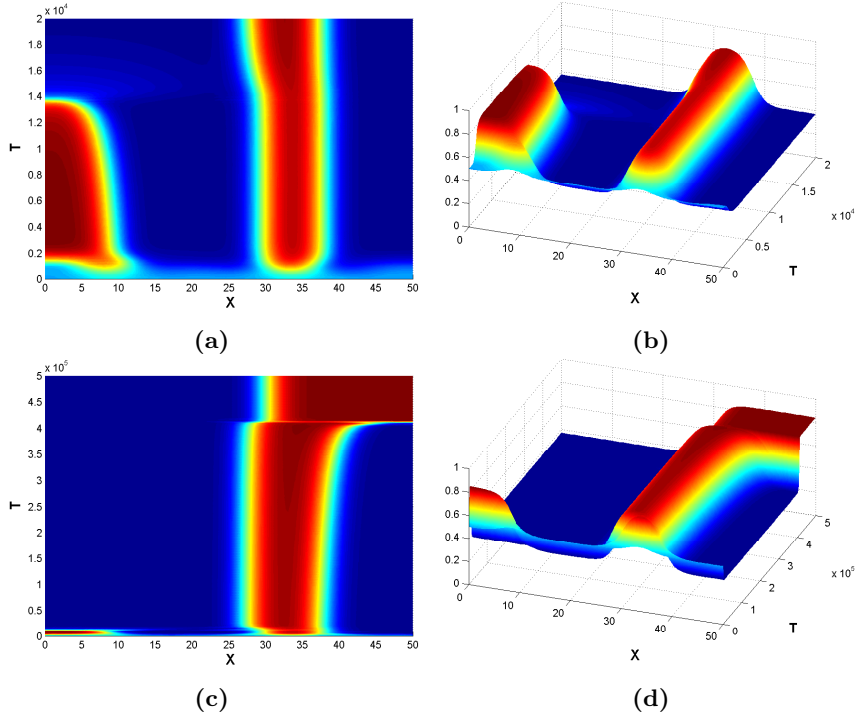


Figure 2.23 – Pattern plot of a simulation of (very) long-time behaviour of equation (2.9) with ‘quadratic’ speed $v = v_q = m^2 + \tilde{\beta}m + 1$ on a one-dimensional domain $[0, L]$. In (a) we see a pattern plot from the top and in (b) from the side. X denotes the spatial position and T the time. The z -axis in (b) denotes the concentration of the mussels. The colours denote the density of the mussels, m , on a scale from blue (low) to red (high). Parameter values: $L = 50$, $T = 5 \cdot 10^5$, $m_e = 0.5$, $\kappa = 0.05$, $d_m = 3$, $\tilde{\beta} = -1.78$.

interfaces). Since the ripening is a very slow and subtle phenomenon, it is quite difficult to observe it in a simulation, due to the amount of computation time that is sometimes needed. Besides, simulations sometimes tend to get stuck in metastable configurations, which also prevent an easy study of them.

Moreover, it is very difficult to predict what will happen to a pattern over time. In Figure 2.23 we show simulations in which the global minimizer is found. Here we see that after about $4.5 \cdot 10^5$ time steps this minimizer is found. However, when we look at the configuration at $2 \cdot 10^4$ steps there is no real way we could have predicted this behaviour, which in turn couldn't really be predicted by a view of the pattern at $t = 1 \cdot 10^4$.

So the simulations that we have presented in this section are in good agreement with the analysis we have done in the rest of this chapter. Moreover, we can conclude here that there is no real qualitative difference between solutions of equation (2.9) between the two choices for the movement speed, $v = v_q$ and $v = v_p$.

2.4 Summary

In this chapter we studied the general Cahn-Hilliard equation and applied this knowledge to a system describing the dynamics of a mussel population (in the absence of algae). When this system starts from an uniform steady state, $m(x, t) = m_e$, we have seen that patterns can form, but only when this steady state is located in the spinodal region, i.e. when $f(m_e) = v(m_e) \left[v(m_e) + m \frac{\partial v(m_e)}{\partial m} \right] < 0$. When this condition is satisfied we see that the system creates patterns, deviating from this steady state.

However, the initially created patterns are not stable, although they tend to persist for quite long time periods. When we wait long enough, we see that the system suddenly and rapidly changes its pattern, to a new configuration with a shorter typical wavelength. This process, called Ostwald Ripening, occurs because the Cahn-Hilliard system allows for infinitesimal mass transportation between peaks of the patterns.

In reality this is obviously not possible, as there can't be an exchange of a fraction of a mussel. Because this small transportation is the key ingredient of the observed ripening effect, this could explain why the ripening stops in experimental setups (see Figure 4). The assumed continuous modeling approach, as implicitly used by the use of the Cahn-Hilliard equation, seems too smooth to capture the behaviour of the mussels in the long run.

Chapter 3

$\varepsilon \neq 0$ - The Full Population Model

In Chapter 1 we created a general model that describes the interaction between a predator and a prey, when the speed of one of the two depends on the local density of the involved species. This model was captured in the following set of equations:

$$\frac{\partial m}{\partial t} = d_m \nabla \left(v \left(v + m \frac{\partial v}{\partial m} \right) \nabla m + v m \frac{\partial v}{\partial a} \nabla a - \kappa \nabla \Delta m \right) + \varepsilon H(m, a) \quad (3.1a)$$

$$\frac{\partial a}{\partial t} = \varepsilon d_a \Delta a + \varepsilon G(m, a) \quad (3.1b)$$

Chapter 2 dealt with the situation in which interactions between species are not relevant, i.e. when we take $\varepsilon = 0$. We discussed the behaviour of such a system on both short and long time scales and found patterns arising.

However, in the reality of nature, the interactions between species *are* important. So real statements about the effective ecology cannot be made with the simplification of setting $\varepsilon = 0$ and we need to inspect the full population model, when $\varepsilon \neq 0$. This chapter is devoted to the study of this general model.

We start by inspecting the general model, that is not adapted to the specific behaviour of mussels. In Section 3.1 we determine the uniform stationary points and their stability. Moreover, we also derive and discuss bifurcation lines, indicating a change in stability of these points.

Subsequently in Section 3.2 we approximate the general model of equation (3.1). For this we note that $0 < \varepsilon \ll 1$ is a small parameter. Therefore we can use standard perturbation techniques. We employ these in Section 3.2 to find approximations of the eigenvalue curves at the bifurcation lines. Moreover, we also present approximations of the bifurcation lines themselves, which allows us to continue our analysis.

Then, in Section 3.3, we apply weakly non-linear stability analysis to the general model, using the relevant approximations made in the previous section.

This gives us information - as a Ginzburg-Landau Amplitude equation - about solutions of equation (3.1) of the form

$$\begin{pmatrix} m(x,t) \\ a(x,t) \end{pmatrix} = \begin{pmatrix} m_e \\ a_e \end{pmatrix} + A(\xi, \tau) e^{ik_c x + \omega t}.$$

where k_c is a wavelengths, ω is an imaginary eigenvalue, m_e and a_e characterize the uniform steady state and ξ and τ are a slow spatial and temporal variable, respectively. The meaning of these parameters and variables is explained in more depth later on in this chapter.

In Section 3.4 we return to the specific model for our mussel-algae system. In this section we apply the knowledge that we will have gained in the first sections of this chapter. This gives us an insight about the kind of solutions that are possible for system (3.1) when it is applied to the mussel-algae system. We also compare these results to the results found in the reaction-diffusion model as presented in section 1.2.

Finally in Section 3.5 we turn to numerical simulations once more to study our model in one spatial dimension. Here we simulate both choices for the density dependent movement speed. These simulations illustrate the analytical study of the sections before it and also give us clues about the other behaviour of solutions, for example on (very) long time scales or when solutions are not started at the uniform stationary point of the equation.

3.1 Linear Stability of the uniform steady states

Our first objective is to find the uniform stationary solutions of the model in system (3.1). We look for solutions of the form $(m(x,t), a(x,t)) \equiv (m_e, a_e)$ that satisfy this equation. Hence we simply need to find concentrations (m_e, a_e) such that

$$\begin{cases} 0 &= H(m_e, a_e); \\ 0 &= G(m_e, a_e). \end{cases} \quad (3.2)$$

Now, for the remainder of this Chapter, we assume that (m_e, a_e) is a specific uniform stationary solution (i.e. (m_e, a_e) solves system (3.2)). We want to study the stability of these stationary solutions. In order to do that, we need to figure out if stationary solutions persist under small perturbations of the form $(m(x,t), a(x,t)) = (m_e, a_e) + \delta(\tilde{m}(x,t), \tilde{a}(x,t))$ where $|\delta| \ll 1$.

The interaction terms H and G are relatively easy to compute in these points, as we can just approximate them with a Taylor polynomial as (note that we have $H(m_e, a_e) = 0 = G(m_e, a_e)$):

$$\begin{aligned} H(m_e + \delta\tilde{m}, a_e + \delta\tilde{a}) &= \delta \frac{\partial H}{\partial m}(m_e, a_e)\tilde{m} + \delta \frac{\partial H}{\partial a}(m_e, a_e) + \mathcal{O}(\delta^2) \\ G(m_e + \delta\tilde{m}, a_e + \delta\tilde{a}) &= \delta \frac{\partial G}{\partial m}(m_e, a_e)\tilde{m} + \delta \frac{\partial G}{\partial a}(m_e, a_e) + \mathcal{O}(\delta^2) \end{aligned}$$

It is also easy to see that $\Delta(m_e + \delta\tilde{m}) = \delta\Delta\tilde{m}$ and $\Delta(a_e + \delta\tilde{a}) = \delta\Delta\tilde{a}$ since (m_e, a_e) is a uniform stationary solution and hence its derivatives vanish.

Perhaps the most difficult term is the last remaining term, which we define by the functional

$$R(m, a) := \vec{\nabla} \cdot \left[v \left(v + m \frac{\partial v}{\partial m} \right) \vec{\nabla} m + v m \frac{\partial v}{\partial a} \vec{\nabla} a \right].$$

For notational convenience we define:

$$\begin{aligned} v_e &:= v(m_e, a_e) & \bar{v} &:= v(m_e + \delta \tilde{m}, a_e + \delta \tilde{a}) \\ \frac{\partial v_e}{\partial m} &:= \frac{\partial v}{\partial m}(m_e, a_e) & \frac{\partial \bar{v}}{\partial m} &:= \frac{\partial v}{\partial m}(m_e + \delta \tilde{m}, a_e + \delta \tilde{a}) \\ \frac{\partial \bar{v}}{\partial a} &:= \frac{\partial v}{\partial a}(m_e + \delta \tilde{m}, a_e + \delta \tilde{a}) & \frac{\partial v_e}{\partial a} &:= \frac{\partial v}{\partial a}(m_e, a_e) \end{aligned}$$

We want to linearize $R(m_e + \delta \tilde{m}, a_e + \delta \tilde{a})$. For this we find

$$\begin{aligned} R(m_e + \delta \tilde{m}, a_e + \delta \tilde{a}) &= \vec{\nabla} \cdot \left[\bar{v} \left(\bar{v} + m_e \frac{\partial \bar{v}}{\partial m} + \delta \tilde{m} \frac{\partial \bar{v}}{\partial m} \right) \vec{\nabla}(\delta \tilde{m}) + \bar{v}(m_e + \delta \tilde{m}) \frac{\partial \bar{v}}{\partial a} \vec{\nabla}(\delta \tilde{a}) \right] + \mathcal{O}(\delta^2) \\ &= \delta \vec{\nabla} \cdot \left[v_e \left(v_e + m_e \frac{\partial v_e}{\partial m} \right) \vec{\nabla} \tilde{m} + v_e m_e \frac{\partial v_e}{\partial a} \vec{\nabla} \tilde{a} \right] + \mathcal{O}(\delta^2). \end{aligned}$$

Here we have used the Taylor expansion as an approximation for \bar{v} , $\frac{\partial \bar{v}}{\partial m}$ and $\frac{\partial \bar{v}}{\partial a}$.

If we combine all observations we have made, we can find the following (linear) system for our small perturbation $\delta(\tilde{m}, \tilde{a})$ as:

$$\begin{cases} \frac{\partial \tilde{m}}{\partial t} = d_m [v_e(v_e + m_e \frac{\partial v_e}{\partial m}) \Delta \tilde{m} + v_e m_e \frac{\partial v_e}{\partial a} \Delta \tilde{a} - \kappa \Delta^2 \tilde{m}] + \varepsilon [\frac{\partial H_e}{\partial m} \tilde{m} + \frac{\partial H_e}{\partial a} \tilde{a}] \\ \frac{\partial \tilde{a}}{\partial t} = \varepsilon [d_a \Delta \tilde{a} + \frac{\partial G_e}{\partial m} \tilde{m} + \frac{\partial G_e}{\partial a} \tilde{a}] \end{cases} \quad (3.3)$$

where we have adapted the notation $\frac{\partial H_e}{\partial m} := \frac{\partial H}{\partial m}(m_e, a_e)$ and so on.

To study the linear stability of the uniform stationary point (m_e, a_e) we try to perturb it with waves, i.e. we take $(\tilde{m}, \tilde{a}) = \exp[i(\vec{k}, \vec{x}) + \omega t](\bar{m}, \bar{a})$. Here $\vec{k} = (k_x, k_y)$ is the wavelength of the wave and $(\bar{m}, \bar{a}) \in \mathbb{R}^2$.

Substituting this in the linear perturbed system of equation (3.3), gives the following set of coupled equations that need to be satisfied:

$$\begin{cases} \omega \bar{m} = -d_m |\vec{k}|^2 [v_e(v_e + m_e \frac{\partial v_e}{\partial m}) \bar{m} + v_e m_e \frac{\partial v_e}{\partial a} \bar{a} + \kappa |\vec{k}|^2 \bar{m}] + \varepsilon \frac{\partial H_e}{\partial m} \bar{m} + \frac{\partial H_e}{\partial a} \bar{a} \\ \omega \bar{a} = \varepsilon [-d_a |\vec{k}|^2 \bar{a} + \frac{\partial G_e}{\partial m} \bar{m} + \frac{\partial G_e}{\partial a} \bar{a}] \end{cases}$$

We can write this in matrix notation as

$$\omega \begin{pmatrix} \bar{m} \\ \bar{a} \end{pmatrix} = M(\vec{k}) \begin{pmatrix} \bar{m} \\ \bar{a} \end{pmatrix}.$$

Here $M(\vec{k})$ is a wavelength-dependent matrix, which is defined as

$$M(\vec{k}) := \begin{pmatrix} -d_m |\vec{k}|^2 [v_e(v_e + m_e \frac{\partial v_e}{\partial m}) + \kappa |\vec{k}|^2] + \varepsilon \frac{\partial H_e}{\partial m} & -d_m |\vec{k}|^2 v_e m_e \frac{\partial v_e}{\partial a} + \varepsilon \frac{\partial H_e}{\partial a} \\ \varepsilon \frac{\partial G_e}{\partial m} & \varepsilon [-d_a |\vec{k}|^2 + \frac{\partial G_e}{\partial a}] \end{pmatrix}. \quad (3.4)$$

In the matrix notation it is clear we are considering an eigenvalue problem. So to find the possible values of $\omega_{1,2} = \omega_{1,2}(\vec{k})$ we need to find the eigenvalues of the matrix $M(\vec{k})$. The sign of those eigenvalues then determines the stability of the uniform steady state under perturbations with wavelength \vec{k} ; if the real part of both eigenvalues is negative, the state is stable under these perturbations, whereas the state is unstable when the real part is positive.

In order for the uniform steady state to be stable under perturbations of all possible wavelengths \vec{k} , we need to have that all eigenvalues, of all possible wavelengths \vec{k} , are negative. That is, we need $\text{Re}(\omega_{1,2}(\vec{k})) < 0$ for all wavelengths \vec{k} .

However, it is also possible that there are a few specific wavelengths \vec{k}_c such that one or two of the eigenvalues $\omega_{1,2}(\vec{k}_c)$ has zero real part, while all the other eigenvalues, corresponding to the other possible wavelengths, still have negative real parts. In this case those specific wavelengths are called critical wavelengths, as the corresponding eigenvalues will be the first to become positive, and hence are the most critical.

3.1.1 On using the trace and the determinant to determine eigenvalues

In order to study the linear stability of the uniform steady state we thus need to study the behaviour of the eigenvalues $\omega_{1,2}(\vec{k})$. We do this by studying both the trace and the determinant of the matrix $M(\vec{k})$. As before we will denote the eigenvalues of $M(\vec{k})$ by $\omega_{1,2}(\vec{k})$. Without loss of generality we can assume $\text{Re}(\omega_1(\vec{k})) \geq \text{Re}(\omega_2(\vec{k}))$.

From linear algebra it is well known that the trace of a matrix corresponds to the sum of the eigenvalues and the determinant corresponds to the product of the eigenvalues. This means, for our matrix $M(\vec{k})$ that:

$$\begin{aligned}\text{Tr}(M(\vec{k})) &= \omega_1(\vec{k}) + \omega_2(\vec{k}); \\ \det(M(\vec{k})) &= \omega_1(\vec{k})\omega_2(\vec{k}).\end{aligned}$$

With this information, we can use the trace and the determinant of the matrix $M(\vec{k})$ to determine the signs of the eigenvalues $\omega_{1,2}(\vec{k})$. We know that the determinant determines the relation between the sign of both eigenvalues:

$$\begin{aligned}\text{if } \det M(\vec{k}) > 0 \text{ then } \text{sgn Re } \omega_1(\vec{k}) &= \text{sgn Re } \omega_2(\vec{k}); \\ \text{if } \det M(\vec{k}) = 0 \text{ then } \omega_1(\vec{k}) &= 0 \text{ or } \omega_2(\vec{k}) = 0; \\ \text{if } \det M(\vec{k}) < 0 \text{ then } \text{sgn Re } \omega_1(\vec{k}) &= -\text{sgn Re } \omega_2(\vec{k}).\end{aligned}$$

On the other hand the trace gives a clue on the sign of one of the eigenvalues:

$$\begin{aligned}\text{if } \text{Tr } M(\vec{k}) > 0 \text{ then } \text{Re } \omega_1 &> 0; \\ \text{if } \text{Tr } M(\vec{k}) = 0 \text{ then } \text{Re } \omega_1 &= -\text{Re } \omega_2; \\ \text{if } \text{Tr } M(\vec{k}) < 0 \text{ then } \text{Re } \omega_2 &< 0.\end{aligned}$$

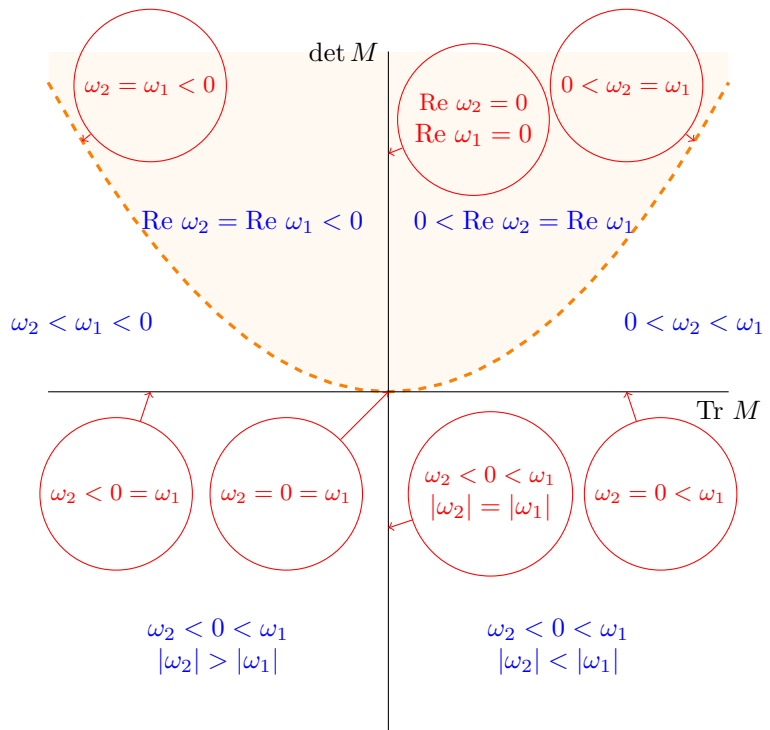


Figure 3.1 – Graphical illustration of the possible signs of the eigenvalues ω_1 and ω_2 depending on the trace and the determinant of the 2×2 matrix M , as discussed in the text. The dotted, orange line $\det M = (\text{Tr } M)^2/4$ is the crossing line between purely real and imaginary eigenvalues; the orange region denotes the region in which imaginary eigenvalues exist. From the figure it is clear that the real part of both eigenvalues is negative only in the north-western region of this plane, when $\det M > 0$ and $\text{Tr } M < 0$.

There is, however, also another relation between the eigenvalues of the matrix $M(\vec{k})$ and its trace and determinant. It is possible to write the dispersion relation in terms of the trace and determinant of $M(\vec{k})$ as

$$0 = \omega^2 - \text{Tr } M(\vec{k})\omega + \det M(\vec{k}).$$

So this means that the eigenvalues $\omega_{1,2}(\vec{k})$ can be expressed as

$$\omega_{1,2}(\vec{k}) = \frac{\text{Tr } M(\vec{k})}{2} \pm \frac{1}{2}\sqrt{\left(\text{Tr } M(\vec{k})\right)^2 - 4\det M(\vec{k})}.$$

So this means that complex eigenvalues only exist when $\det M(\vec{k}) > \frac{(\text{Tr } M(\vec{k}))^2}{4}$ and that $\text{Re}\omega_1(\vec{k}) = \text{Re}\omega_2(\vec{k})$ in this region. A graphical summary of our findings in this section is given in Figure 3.1.

From this analysis it is clear that we have two non-positive eigenvalues $\omega_1(\vec{k})$ and $\omega_2(\vec{k})$ only when both $\det M(\vec{k}) \geq 0$ and $\text{Tr } M(\vec{k}) \geq 0$. Moreover, we know that precisely one eigenvalue is zero when $\det M(\vec{k}) = 0$ and $\text{Tr } M(\vec{k}) > 0$ and that precisely two eigenvalues are purely complex if $\text{Tr } M(\vec{k}) = 0$ and $\det M(\vec{k}) > 0$. When $\text{Tr } M(\vec{k}) = 0$ and $\det M(\vec{k}) = 0$ hold simultaneously we know that both eigenvalues are zero.

3.1.2 The determinant and the trace of our matrix $M(\vec{k})$

Our analysis so far only inspected one particular value for the wavelength k . For our uniform steady state to be stable under perturbations of all wavelengths, we need $\text{Re } \omega_{1,2}(\vec{k}) < 0$ for all wavelengths \vec{k} . That is, we need $\det M(\vec{k}) > 0$ and $\text{Tr } M(\vec{k}) < 0$ for all wavelengths \vec{k} in order for the state to be stable under all of these perturbations.

So if our combination of parameters is such that these conditions are obeyed we know that our system is stable. However, our combination of parameters could also be such that either $\det M(\vec{k}) < 0$ or $\text{Tr } M(\vec{k}) > 0$ for some wavelength \vec{k} . In that case we know that at least one of the corresponding eigenvalues is positive and hence the uniform steady state is unstable under perturbations of this wavelength.

But, there is still a particular interesting situation left, that we have not yet discussed. We could have chosen our parameters in a way that there are a few wavelengths \vec{k} such that either $\det M(\vec{k}) = 0$ and $\text{Tr } M(\vec{k}) \leq 0$ or $\text{Tr } M(\vec{k}) = 0$ and $\det M(\vec{k}) \geq 0$, while the determinant is positive and the trace negative for all other wavelengths. This choice of parameters is called critical and the particular wavelengths that have this property are called critical wavelengths (for the given set of parameters).

These critical circumstances are particularly interesting since the state is nearly stable in this case and we can apply our weakly non-linear stability analysis to obtain amplitude equations to further investigate the stability of nearly uniform steady states. So this section is devoted to finding the form of the function $\vec{k} \mapsto \det M(\vec{k})$ and $\vec{k} \mapsto \text{Tr } M(\vec{k})$ for various parameter combinations.

To start with this we return to our matrix $M(\vec{k})$, that we defined in equation (3.4). For notational convenience we introduce the following new parameters:

$$\mu_{10} = \frac{\partial H_e}{\partial m} \quad \mu_{20} = \frac{\partial H_e}{\partial a} \quad (3.5a)$$

$$\mu_{11} = d_m v_e \left(v_e + m_e \frac{\partial v_e}{\partial m} \right) \quad \mu_{21} = d_m v_e m_e \frac{\partial v_e}{\partial a} \quad (3.5b)$$

$$\mu_{12} = d_m \kappa \quad \mu_{40} = \frac{\partial G_e}{\partial a} \quad (3.5c)$$

$$\mu_{30} = \frac{\partial G_e}{\partial m} \quad \mu_{41} = d_a \quad (3.5d)$$

From the conditions on our original parameters, we know that $\mu_{12} > 0$ and $\mu_{41} > 0$ since $d_a, d_m, \kappa > 0$. The sign of the other parameters is unknown and does depend on the specific form of v and the interaction terms G and H .

With this notation our matrix $M(\vec{k})$ reads:

$$M(\vec{k}) = \begin{pmatrix} -\mu_{12}|\vec{k}|^4 - \mu_{11}|\vec{k}|^2 + \varepsilon\mu_{10} & -\mu_{21}|\vec{k}|^2 + \varepsilon\mu_{20} \\ \varepsilon\mu_{30} & -\varepsilon\mu_{41}|\vec{k}|^2 + \varepsilon\mu_{40} \end{pmatrix} \quad (3.6)$$

The trace and the determinant can be computed and they turn out to be:

$$\begin{aligned} \text{Tr } M(\vec{k}) &= -\mu_{12}|\vec{k}|^4 - (\mu_{11} + \varepsilon\mu_{41})|\vec{k}|^2 + \varepsilon(\mu_{10} + \mu_{40}) \\ \det M(\vec{k}) &= \varepsilon \left(\mu_{12}\mu_{41}|\vec{k}|^6 + (\mu_{11}\mu_{41} - \mu_{12}\mu_{40})|\vec{k}|^4 \right. \\ &\quad \left. + (\mu_{21}\mu_{30} - \mu_{11}\mu_{40} - \varepsilon\mu_{10}\mu_{41})|\vec{k}|^2 + \varepsilon[\mu_{10}\mu_{40} - \mu_{20}\mu_{30}] \right) \end{aligned}$$

In the following paragraphs we study the possible forms of these polynomials in $|\vec{k}|$. For that it is easy to introduce another set of parameters:

$$\alpha = \mu_{12}\mu_{41} \quad \zeta = \mu_{12} \quad (3.7a)$$

$$\beta = \mu_{11}\mu_{41} - \mu_{12}\mu_{40} \quad \eta = \mu_{11} + \varepsilon\mu_{41} \quad (3.7b)$$

$$\gamma = \mu_{21}\mu_{30} - \mu_{11}\mu_{40} - \varepsilon\mu_{10}\mu_{41} \quad \theta = -\varepsilon(\mu_{10} + \mu_{40}) \quad (3.7c)$$

$$\delta = \varepsilon[\mu_{10}\mu_{40} - \mu_{20}\mu_{30}] \quad (3.7d)$$

where $\alpha > 0$ and $\zeta > 0$ since $\mu_{12}, \mu_{41} > 0$ as we have seen before.

We can now write the trace and the determinant as

$$\text{Tr } M(\vec{k}) = -\zeta|\vec{k}|^4 - \eta|\vec{k}|^2 - \theta \quad (3.8)$$

$$\det M(\vec{k}) = \varepsilon \left(\alpha|\vec{k}|^6 + \beta|\vec{k}|^4 + \gamma|\vec{k}|^2 + \delta \right) \quad (3.9)$$

Since $\zeta > 0$ and $\alpha > 0$ the form of these trace and determinant functions is completely determined by the chosen parameters η and θ (for the trace) and β, γ and δ (for the determinant). In the next sections we inspect the possible forms of the trace and determinant, for various values of the parameters.

3.1.3 On the form of $\det M(\vec{k})$

We start by characterizing the determinant. In our analysis we want to determine what choice of parameters leads to $\det M(\vec{k}) \geq 0$ for all possible wavelengths \vec{k} , as we want to identify the critical parameters and wavelengths.

Since $\varepsilon > 0$ the sign of the determinant is determined by the sign of the polynomial $B(\vec{k}) := \alpha|\vec{k}|^6 + \beta|\vec{k}|^4 + \gamma|\vec{k}|^2 + \delta$. We have seen that $\alpha > 0$. Hence we know that $B(\vec{k}) \rightarrow \infty$ as $|\vec{k}| \rightarrow \infty$. So to check when $B(\vec{k}) \geq 0$ for all wavelengths, we need to identify the minimum of the function B . Also note that the wavelength that leads to this minimum is our critical wavelength \vec{k}_c .

Setting the derivative of B with respect to $|\vec{k}|$ equal to zero gives us candidates for the minimum value. That is, we must solve

$$0 = 2\vec{k} \left(3\alpha|\vec{k}|^4 + 2\beta|\vec{k}|^2 + \gamma \right).$$

This is solved by $\vec{k} = 0$ or $|\vec{k}|^2 = \frac{1}{3\alpha}(-\beta \pm \sqrt{\beta^2 - 3\alpha\gamma})$. First we observe that $\vec{k} = 0$ is a solution regardless of the values of the parameters. The other possibility $|\vec{k}|^2 = \frac{1}{3\alpha}(-\beta \pm \sqrt{\beta^2 - 3\alpha\gamma})$ is only a solution when the right-hand side is real and positive. For $|\vec{k}|^2 = \frac{1}{3\alpha}(-\beta + \sqrt{\beta^2 - 3\alpha\gamma})$ this leads to the condition

$$(\beta, \gamma) \in \{(\beta, \gamma) \in \mathbb{R}^2 : \beta \geq 0, \gamma \leq 0\} \cup \{(\beta, \gamma) \in \mathbb{R}^2 : \beta \leq 0, \gamma \leq \beta^2/(3\alpha)\}$$

and for $|\vec{k}|^2 = \frac{1}{3\alpha}(-\beta - \sqrt{\beta^2 - 3\alpha\gamma})$ this leads to the condition

$$(\beta, \gamma) \in \{(\beta, \gamma) \in \mathbb{R}^2 : \beta \leq 0, 0 \leq \gamma \leq \beta^2/(3\alpha)\}$$

So we now have created three regions in the (β, γ) plane, with respectively one, two or three possible minimal points (see Figure 3.2). We still must determine when these candidates are actual (local) minimal points. To do that, we can use the second derivative test. We find for the possible candidates:

$$\text{for } \vec{k} = 0 : \operatorname{sgn} B''(k) = \operatorname{sgn} \gamma$$

$$\text{for } |\vec{k}|^2 = \frac{1}{3\alpha}(-\beta + \sqrt{\beta^2 - 3\alpha\gamma}) : \operatorname{sgn} B''(k) = \operatorname{sgn}(\beta^2 - 3\alpha\gamma - \beta\sqrt{\beta^2 - 3\alpha\gamma})$$

$$\text{for } |\vec{k}|^2 = \frac{1}{3\alpha}(-\beta - \sqrt{\beta^2 - 3\alpha\gamma}) : \operatorname{sgn} B''(k) = \operatorname{sgn}(\beta^2 - 3\alpha\gamma + \beta\sqrt{\beta^2 - 3\alpha\gamma})$$

So the second derivative test gives that $\vec{k} = 0$ is a (local) minimum if $\gamma > 0$ and $|\vec{k}|^2 = \frac{1}{3\alpha}(-\beta + \sqrt{\beta^2 - 3\alpha\gamma})$ if $\beta \leq 0$ and $\gamma \leq \frac{\beta^2}{3\alpha}$ or $\beta > 0$ and $\gamma < 0$. $|\vec{k}|^2 = \frac{1}{3\alpha}(-\beta - \sqrt{\beta^2 - 3\alpha\gamma})$ is never a local minimum, since $\operatorname{sgn} B''(k)$ is always negative in the region in which this possible candidate is an extreme value of B .

From this analysis it is clear that $\vec{k} = 0$ is the global minimum in region (I) and $|\vec{k}|^2 = \frac{1}{3\alpha}(-\beta + \sqrt{\beta^2 - 3\alpha\gamma})$ in region (II) (see Figure 3.2). In region (III) it is not yet clear which of those two values is the global minimum.

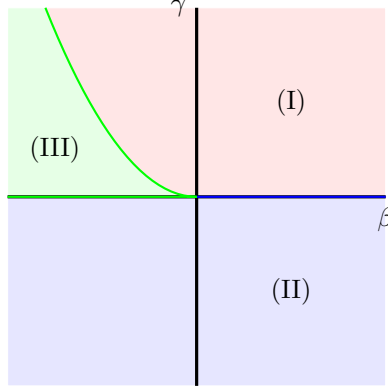


Figure 3.2 – Sketch of the (β, γ) plane, divided into three regions, with different possible *candidates* for the critical wavelength. In region I (red), we only have $\vec{k} = 0$, in region II (blue) we have $\vec{k} = 0$ or $|\vec{k}|^2 = \frac{1}{3\alpha}[-\beta + \sqrt{\beta^2 - 3\alpha\gamma}]$ and in region III (green) we have $k = 0$, $|\vec{k}|^2 = \frac{1}{3\alpha}[-\beta + \sqrt{\beta^2 - 3\alpha\gamma}]$ or we have $|\vec{k}|^2 = \frac{1}{3\alpha}[-\beta - \sqrt{\beta^2 - 3\alpha\gamma}]$ for the possible minimal values. Note that in going from region III to region I four possible wavelengths become imaginary (i.e. on the line $\{(\beta, \beta^2/(3\alpha)) : \beta < 0\}$ we have $\vec{k} = 0$ or $|\vec{k}|^2 = \frac{-\beta}{3\alpha}$. On the other line $\{(\beta, 0) : \beta < 0\}$ we have $\vec{k} = 0$ or $|\vec{k}|^2 = \frac{2|\beta|}{3\alpha}$ and on the line $\{(\beta, 0) : \beta \geq 0\}$ we have $\vec{k} = 0$.

To determine which of these wavelengths is the global minimum we must compare the different values of $B(k)$ for these wavelengths. Substituting these values in the function B gives

$$B(\vec{k} = 0) = \delta \quad (3.10a)$$

$$B(\vec{k}^*) = \delta + \frac{-\beta + \sqrt{\beta^2 - 3\alpha\gamma}}{27\alpha^2}(-\beta^2 + 6\alpha\gamma + \beta\sqrt{\beta^2 - 3\alpha\gamma}) \quad (3.10b)$$

where \vec{k}^* is a wavelength such that $|\vec{k}^*|^2 = \frac{1}{3\alpha}(-\beta + \sqrt{\beta^2 - 3\alpha\gamma})$.

Since $-\beta + \sqrt{\beta^2 - 3\alpha\gamma} > 0$ in region (III), we can determine the real global minimum by looking at the sign of the $L(\beta, \gamma; \alpha) := -\beta^2 + 6\alpha\gamma + \beta\sqrt{\beta^2 - 3\alpha\gamma}$. If $L(\beta, \gamma; \alpha) > 0$ then the minimum is attained at $\vec{k} = 0$. If $L(\beta, \gamma; \alpha) < 0$ then the minimum is attained in \vec{k}^* . If $L(\beta, \gamma; \alpha) = 0$ then both \vec{k} and \vec{k}^* are the global minima, since the value for B is the same for all these wavelengths.

With a fairly easy computation we find that $L(\beta, \gamma; \alpha) = 0$ when

$$(\beta, \gamma) \in \mathcal{A} := \left\{ (\beta, \gamma) : \beta < 0, \gamma = \frac{\beta^2}{4\alpha} \right\} \cup \{(\beta, \gamma) : \beta > 0, \gamma = 0\} \quad (3.11)$$

If (β, γ) lies above this set, then $L(\beta, \gamma; \alpha) > 0$ and when (β, γ) lies below this set then $L(\beta, \gamma; \alpha) < 0$.

So at this point it is clear that the minimal value for B is attained in $\vec{k} = 0$ when (β, γ) lies above the set \mathcal{A} and in $|\vec{k}|^2 = \frac{1}{3\alpha}(-\beta + \sqrt{\beta^2 - 3\alpha\gamma})$ when

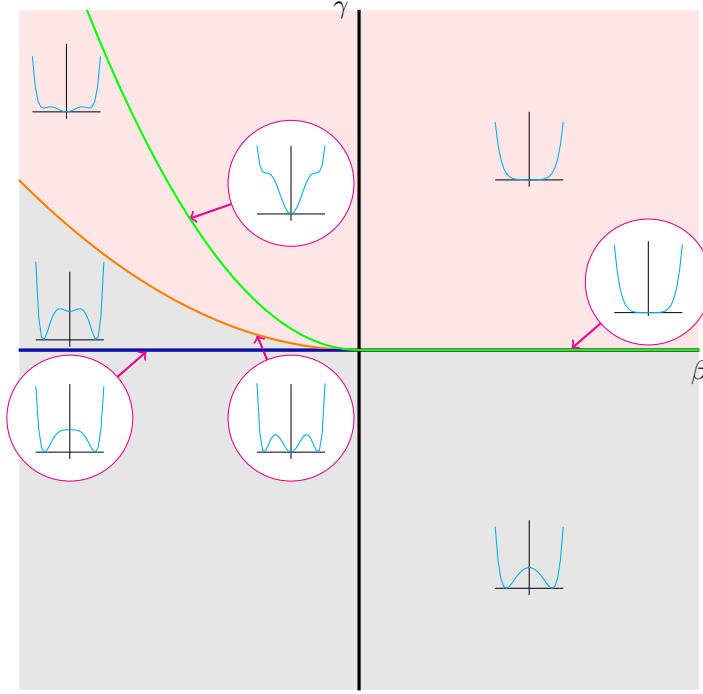


Figure 3.3 – Graphical illustration of the possible form of the function B as a function of the wavelength k , for various combination of the parameters β and γ , where we have chosen $\delta = \delta_c$. In the red regions the critical wavelength is $k_c = 0$ and $\delta_c = 0$, while in the grey region the critical wavelengths need to satisfy the condition $|\vec{k}_c|^2 = \frac{1}{3\alpha}[-\beta + \sqrt{\beta^2 - 3\alpha\gamma}]$ and here we find that the critical value is $\delta_c = \frac{-\beta + \sqrt{\beta^2 - 3\alpha\gamma}}{27\alpha^2}(\beta^2 - 6\alpha\gamma - \beta\sqrt{\beta^2 - 3\alpha\gamma})$. Only at the line $\{(\beta, \beta^2/(4\alpha)) : \beta < 0\}$ there are three critical wavelengths.

(β, γ) lies below the set \mathcal{A} . When $(\beta, \gamma) \in \mathcal{A}$ then we have both $\vec{k} = 0$ and $|\vec{k}|^2 = \frac{1}{3\alpha}(-\beta + \sqrt{\beta^2 - 3\alpha\gamma})$ as minimal values.

Now that we have identified the wavelength in which the minimum for B is attained, we can determine what condition need to be satisfied in order for the determinant to be non-negative for all wavelengths. For this we denote this minimal wavelength by \bar{k} . Then we need to have $B(\bar{k}) \geq 0$. From equation (3.10) it is clear that we need to have

$$\delta \geq 0$$

when $\bar{k} = 0$ and

$$\delta \geq \frac{-\beta + \sqrt{\beta^2 - 3\alpha\gamma}}{27\alpha^2}(\beta^2 - 6\alpha\gamma - \beta\sqrt{\beta^2 - 3\alpha\gamma})$$

when $\bar{k} \neq 0$.

Since the right-hand sides of these expressions coincide when $(\beta, \gamma) \in \mathcal{A}$ this requirement is in a well defined form. We also note that the critical parameter

combination is the combination such that the relevant equality holds. Thus we can define the critical value for δ as

$$\delta_c := \max \left\{ 0, \frac{-\beta + \sqrt{\beta^2 - 3\alpha\gamma}}{27\alpha^2} (\beta^2 - 6\alpha\gamma - \beta\sqrt{\beta^2 - 3\alpha\gamma}) \right\}.$$

The findings on $\det M(\vec{k})$ is also graphically shown in Figure 3.3 for a critical combination of parameters α , β , γ and δ .

3.1.4 On the form of $\text{Tr } M(\vec{k})$

To study the behaviour of the trace, we must recall the form of the trace of equation (3.8):

$$\text{Tr } M(\vec{k}) = -\zeta|\vec{k}|^4 - \eta|\vec{k}|^2 - \theta$$

This time, we want to find out under what parameter choices $\text{Tr } M(\vec{k}) \leq 0$ for all possible wavelengths \vec{k} . The parameter choices that lead to $\text{Tr } M(\vec{k}) = 0$ for a few wavelengths and $\text{Tr } M(\vec{k}) < 0$ for all other wavelengths, are called critical

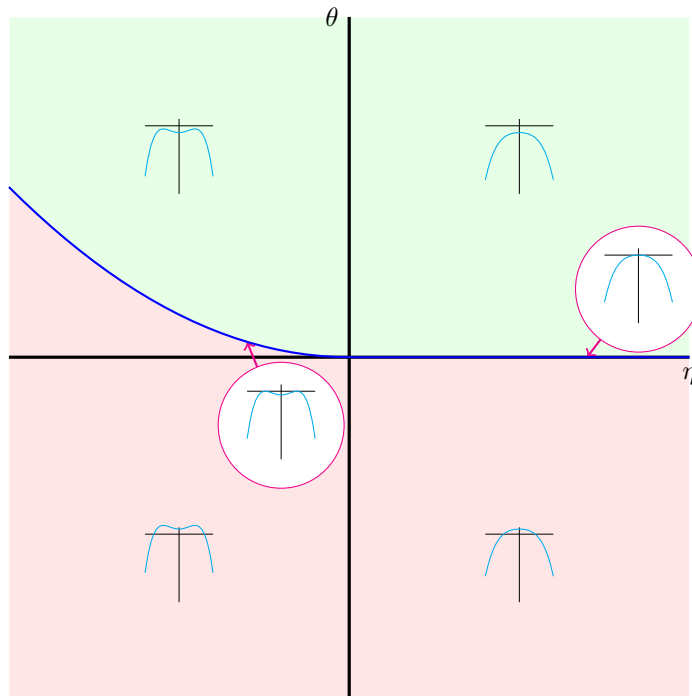


Figure 3.4 – Graphical illustration of the possible forms of the trace $\text{Tr } M(\vec{k})$ as a function of the wavelength \vec{k} , for various combinations of the parameters η and θ . In the green region we have $\text{Tr } M(\vec{k}) < 0$ for all wavelengths, while in the red region we have $\text{Tr } M(\vec{k}) > 0$ for a range of wavelengths. The blue line denotes where $\text{Tr } M(\vec{k}_c) = 0$ for a specific choice of the wavelength. That is, $\vec{k}_c = 0$ when $\eta > 0$ and $|\vec{k}_c|^2 = \frac{-\eta}{2\zeta}$ when $\eta < 0$.

and the corresponding wavelength \vec{k} corresponding to $\text{Tr } M(\vec{k}) = 0$ is called critical and denoted by \vec{k}_c .

Since $\zeta > 0$ as we have seen before, we know that $\text{Tr } M(\vec{k}) \rightarrow -\infty$ as $|\vec{k}| \rightarrow \infty$. So to check that the trace is everywhere non-negative it suffices to check if the trace is non-negative in its maximal value. We also note that the wavelength that realizes this maximum is the critical wavelength \vec{k}_c .

By differentiation we find the possible extreme wavelengths as $\vec{k} = 0$ and as $|\vec{k}|^2 = -\frac{\eta}{2\zeta}$. The latter wavelengths only exist when $\eta < 0$. By the second derivative test we find that $\vec{k} = 0$ is a maximum when $\eta > 0$ and that $|\vec{k}|^2$ corresponds to a maximum when $\eta < 0$. When $\eta = 0$ both possible candidates coincide and the maximum is then attained in $\vec{k} = 0$.

Let's denote the wavelength that attains the global minimum (for a given parameter combination ζ and η) by k^* . Then we know that the trace is non-positive for all wavelengths if $\text{Tr } M(k^*) \leq 0$. If the equality holds we know that we are in the critical situation and the wavelength k^* is called critical.

Substituting the candidates in $\text{Tr } M(\vec{k})$ gives the condition $\theta \geq 0$ when $\eta \geq 0$ and the condition $\theta \geq \frac{\eta^2}{4\zeta}$ when $\eta \leq 0$. So we can define $\theta_c = \max\left\{0, -\frac{\eta|\eta|}{4\zeta}\right\}$ and conclude that the trace is always negative when $\theta > \theta_c$ and that there is a critical wavelength only when $\theta = \theta_c$.

In Figure 3.4 the results of our analysis in this section is illustrated. The blue line denotes the critical line in the (η, θ) -plane, where we have a critical wavelength k_c and a critical parameter combination such that $\theta = \theta_c$. The green area shows the region of the (η, θ) plane where the trace is negative for all wavelengths.

3.1.5 Stability Analysis of the uniform stationary point

From the previous sections we have learned that $\text{Tr } M(\vec{k}) < 0$ for all wavelengths when $\theta > \theta_c$ and $\det M(\vec{k}) > 0$ for all wavelengths when $\delta > \delta_c$. Thus, when these two conditions (i.e. $\theta > \theta_c$ and $\delta > \delta_c$) hold, the uniform stationary point (m_e, a_e) is stable.

We are, however, especially interested in the case that the uniform stationary point is stable under perturbations of almost all wavelengths. This is the case when either the trace is zero (and the determinant non-negative) or the determinant is zero (and the trace non-positive), as we have discussed in section 3.1.1. If we denote the critical wavelength by \vec{k}_c we thus know now that

- if $\theta = \theta_c$ and $\delta > \delta_c$ then $\omega_{1,2} = \pm i\sqrt{\det M(\vec{k}_c)}$;
- if $\theta > \theta_c$ and $\delta = \delta_c$ then $\omega_2 = \text{Tr } M(\vec{k}_c) < 0 = \omega_1$;
- if $\theta = \theta_c$ and $\delta = \delta_c$ then $\omega_1 = \omega_2 = 0$.

In the previous sections we have seen that there are two possible critical wavelengths when $\theta = \theta_c$:

- (1) if $\eta \geq 0$ then $\theta_c = 0$ and $\vec{k}_c = 0$;

(2) if $\eta < 0$ then $\theta_c = \frac{\eta^2}{4\zeta}$ and $|\vec{k}_c|^2 = \frac{-\eta}{2\zeta}$.

We also saw that there are three possibilities when $\delta = \delta_c$:

(3) if (β, γ) lies above \mathcal{A} then $\delta_c = 0$ and $\vec{k}_c = 0$;

(4) if (β, γ) lies above \mathcal{A} then $\delta_c = \frac{-\beta + \sqrt{\beta^2 - 3\alpha\gamma}}{27\alpha^2} (-\beta^2 + 6\alpha\gamma + \beta\sqrt{\beta^2 - 3\alpha\gamma})$
and $|\vec{k}_c|^2 = \frac{1}{3\alpha} (-\beta + \sqrt{\beta^2 - 3\alpha\gamma})$;

(5) if $(\beta, \gamma) \in \mathcal{A}$ then $\delta_c = 0$ and we have both critical wavelengths $\vec{k}_c = 0$
and $|\vec{k}_c|^2 = \frac{1}{3\alpha} (-\beta + \sqrt{\beta^2 - 3\alpha\gamma})$.

3.2 Approximations, assuming $\delta, \theta > 0$ and $\mathcal{O}(\varepsilon)$

In the previous section, Section 3.1, we have introduced the parameters $\alpha, \beta, \gamma, \delta, \zeta, \eta$ and θ to describe the form of the determinant and the trace of $M(\vec{k})$ respectively. That is, we have defined these parameters such that

$$\begin{aligned}\det M(\vec{k}) &= \alpha|\vec{k}|^6 + \beta|\vec{k}|^4 + \gamma|\vec{k}|^2 + \delta; \\ \text{Tr}M(\vec{k}) &= -\zeta|\vec{k}|^4 - \eta|\vec{k}|^2 - \theta.\end{aligned}$$

With these definitions the dispersion relation corresponding to the matrix $M(\vec{k})$ became

$$0 = \omega^2 - \text{Tr}M(\vec{k})\omega + \det M(\vec{k}). \quad (3.12)$$

We also found a way to characterize the (linear) stability of the related uniform steady state: we need the determinant to be positive and the trace to be negative for all wavelengths. For the determinant this leads to the condition $\delta > \delta_c$ and for the trace to $\theta > \theta_c$, where

$$\delta_c = \max \left\{ 0, \frac{-\beta + \sqrt{\beta^2 - 3\alpha\gamma}}{27\alpha^2} (\beta^2 - 6\alpha\gamma - \beta\sqrt{\beta^2 - 3\alpha\gamma}) \right\}; \quad (3.13)$$

$$\theta_c = \max \left\{ 0, -\eta \frac{|\eta|}{4\zeta} \right\}. \quad (3.14)$$

In Figures 3.4 and Figure 3.3 we have illustrated the different possible cases for the trace and determinant respectively, for various combinations of parameters.

In this chapter we will assume that α and ζ are positive and of order $\mathcal{O}(1)$. This is a logical assumption, since $\alpha = d_a d_m \kappa$ and $\zeta = d_m \kappa$ and these parameters are all positive and typically of order $\mathcal{O}(1)$.

Because α and ζ are positive, it is possible to rescale the wavelength \vec{k} and the eigenvalue ω in the dispersion relation (see equation (3.12)). If we define $w =: \frac{\alpha^2}{\zeta^3} v$ and $\vec{k} =: \sqrt{\frac{\alpha}{\zeta^2}} \vec{m}$ we obtain the related dispersion relation

$$0 = v^2 - T(\vec{m})v + D(\vec{m}),$$

where T and D are the rescaled trace and determinant, which are defined as

$$T(\vec{m}) = -|\vec{m}|^4 - \frac{\zeta}{\alpha}\eta|\vec{m}|^2 - \frac{\zeta^3}{\alpha^2}\theta;$$

$$D(\vec{m}) = |\vec{m}|^6 + \frac{\zeta^2}{\alpha^2}\beta|\vec{m}|^4 + \frac{\zeta^4}{\alpha^3}\gamma|\vec{m}|^2 + \frac{\zeta^6}{\alpha^4}\delta.$$

Now, since ζ and α are both positive and of order $\mathcal{O}(1)$, this rescaling does not change the signs of the parameters, nor the order of them. Hence in our analysis in this chapter it is sufficient to investigate only the parameter combinations with $\alpha = 1$ and $\zeta = 1$.

Moreover, in this section we also assume that the parameters δ and θ are known and of order $\mathcal{O}(\varepsilon)$. The definition of these parameters in equation (3.7) makes this assumption reasonable. This assumption also implies that $\delta > 0$ and $\theta > 0$. This means that we can only have critical wavelengths, when either $\delta_c > 0$ or $\theta_c > 0$ (or both) and it also implies that $\vec{k} = 0$ won't be a critical wavelength. This ensures that we can apply the weakly non linear analysis in the next section, as this method tends to fail when the critical wavelength is $k_c = 0$, because the most critical perturbations are uniform in this case, whereas our method relies on a non-uniform critical wave.

Now that we have discussed these additional assumption, we have the starting point for the analysis in this section. We can formulate an approximation of the bifurcation lines and the eigenvalue curves, using $\alpha, \beta, \gamma, \delta$ and ζ, η, θ as our parameters. Because of the cumbersome computations, that use a lot of approximations and Taylor expansions we have put this analysis in Appendix B.

In this appendix it is shown that linear stability is guaranteed when $\eta \geq \eta_c$ and $\gamma \geq \gamma_c$, up to leading order. Here $\eta_c := -2\sqrt{\theta}$. The definition of γ_c is more difficult, as it depends on the order and sign of β . As this is very cumbersome to work with, we just assume that β is ‘large enough’¹. Then γ_c is defined as

$$\gamma_c := \begin{cases} \frac{\beta^2}{4} & \text{if } \beta < 0; \\ -2\sqrt{\delta\beta} & \text{if } \beta > 0. \end{cases}$$

This is the starting point for the analysis in this section. We start by reformulating these stability conditions, but now in terms of the μ -parameters, using μ_{11} and μ_{21} as our bifurcation parameters. Since these parameters contain the effect of adding the density dependent movement speed to the system, this gives us the best information of its added contribution to the dynamics of the system.

In Section 3.2.1 we determine the bifurcation lines in the (μ_{11}, μ_{21}) -parameter plane. Subsequently in Section 3.2.2 we present some possible eigenvalue curves on those critical bifurcation lines to illustrate the behaviour of the system near its critical arrangements.

3.2.1 Approximations of bifurcation plane

We first inspect the case when $\eta \geq \eta_c$ (i.e. when the trace becomes positive). In section B.1.1 we found that $\eta_c = -2\sqrt{\theta}$. Thus $\mathcal{O}(\eta_c) = \mathcal{O}(\sqrt{\varepsilon})$. From our

¹A precise statement can be found in Table B.3 in Appendix B

definition we also have $\eta = \mu_{11} + \varepsilon$. Since $\varepsilon \ll \sqrt{\varepsilon}$ we know that near the critical value we have $\eta = \mu_{11} = \eta_c$ up to leading order. Thus we know that $\eta \geq \eta_c$ is obeyed when $\mu_{11} \geq -2\sqrt{\theta}$. We can again define a critical value $\mu_{11,c} := -2\sqrt{\theta}$ and thus we have the condition $\mu_{11} \geq \mu_{11,c}$ that is needed for stability. On the critical line $\mu_{11} = \mu_{11,c}$ we also know that the critical wavelengths must satisfy $|\vec{k}_c|^2 = \sqrt{\theta}$. Note that it is also perfectly fine to define $\mu_{11,c} := -2\sqrt{\theta} - \varepsilon$, which also includes the higher order term.

In section B.1.2 we also found that the sign and order of the critical γ_c depends on the sign of β . Depending on the sign of β there is a different critical value γ_c and therefore a different condition that needs to be satisfied. From our definition of $\beta = \mu_{11} - \mu_{40}$ it is clear that $\beta > 0$ if and only if $\mu_{11} > \mu_{40}$ and $\beta < 0$ if and only if $\mu_{11} < \mu_{40}$. In the following we inspect the condition $\gamma \geq \gamma_c$ for both of these cases separately. For technical reasons we'll also assume that $\mathcal{O}(\mu_{10}) = \mathcal{O}(\varepsilon^\lambda)$ with $\lambda > -\frac{1}{3}$, such that we can neglect the term $\varepsilon\mu_{10}$ in the expression for γ .

Situation with $\mu_{11} < \mu_{40}$ ($\beta < 0$)

In this case we have $\gamma_c = \frac{\beta^2}{4}$ to leading order. Since $\beta = \mu_{11} - \mu_{40}$ we have $\gamma_c = \left(\frac{\mu_{11} - \mu_{40}}{2}\right)^2$. Now the condition $\gamma \geq \gamma_c$ becomes

$$\mu_{21}\mu_{30} \geq \left(\frac{\mu_{11} + \mu_{40}}{2}\right)^2.$$

If $\mu_{30} < 0$ the inequality that needs to be satisfied becomes

$$\mu_{21} \leq \left(\frac{\mu_{11} + \mu_{40}}{2}\right)^2 \frac{1}{\mu_{30}}.$$

and when $\mu_{30} > 0$ it becomes

$$\mu_{21} \geq \left(\frac{\mu_{11} + \mu_{40}}{2}\right)^2 \frac{1}{\mu_{30}}.$$

In both cases (i.e. regardless of the sign of μ_{30}) we also know that the critical wavelengths in this case are characterized by $|\vec{k}_c|^2 = -\frac{\beta}{2}$ up to leading order.

Situation with $\mu_{11} > \mu_{40}$ ($\beta > 0$)

Now $\beta < 0$ holds, we have $\gamma_c = -2\sqrt{\beta\delta}$. Thus the condition $\gamma \geq \gamma_c$ now becomes

$$\mu_{21}\mu_{30} \geq \mu_{11}\mu_{40} - 2\sqrt{(\mu_{11} - \mu_{40})\delta}.$$

If μ_{30} is negative the condition $\gamma \geq \gamma_c$ is equivalent to

$$\mu_{21} \leq \frac{\mu_{11}\mu_{40}}{\mu_{30}} - \frac{2}{\mu_{30}}\sqrt{(\mu_{11} - \mu_{40})\delta}.$$

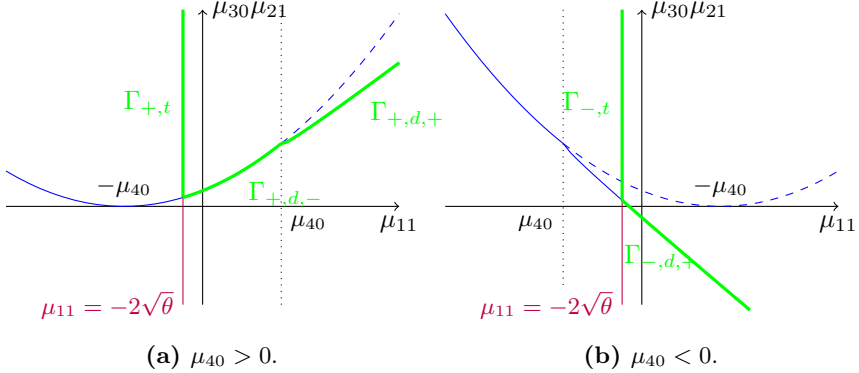


Figure 3.5 – The $(\mu_{11}, \mu_{30}\mu_{21})$ plane for $\mu_{40} > 0$ (a) and $\mu_{40} < 0$ (b). The bifurcation lines $\Gamma_{\pm,t/d}$ are the thicker lines. The uniform steady state (m_e, a_e) is stable when the parameters are such that they lie above and to the right of the bifurcation curves. Note that on $\Gamma_{\pm,t}$ the trace is zero and on $\Gamma_{\pm,d}$ the determinant is zero for some specific wavelengths \vec{k}_c . The blue lines in these sketches corresponds to the lines on which $\gamma = \gamma_c$ and the purple line corresponds to $\eta = \eta_c$. Note that $\beta > 0$ when $\mu_{11} > \mu_{40}$, explaining the subscript + in the naming of the bifurcation line.

and when $\mu_{30} > 0$ is

$$\mu_{21} \geq \frac{\mu_{11}\mu_{40}}{\mu_{30}} - \frac{2}{\mu_{30}}\sqrt{(\mu_{11} - \mu_{40})\delta}.$$

In this case the critical wavelengths are $|\vec{k}_c|^2 = \sqrt{\frac{\delta}{\beta}}$ up to leading order.

Bifurcation diagram in the (μ_{11}, μ_{21}) -plane

In the previous paragraphs we have found that $\eta \geq \eta_c$ when $\mu_{11} \geq -2\sqrt{\theta}$ and that $\gamma \geq \gamma_c$ when $\mu_{30}\mu_{21} \geq \mu_c$ where

$$\mu_c := \begin{cases} \left(\frac{\mu_{11} + \mu_{40}}{2}\right)^2 & \text{when } \mu_{11} < \mu_{40}; \\ \mu_{11}\mu_{40} - 2\sqrt{(\mu_{11} - \mu_{40})\delta} & \text{when } \mu_{11} > \mu_{40}. \end{cases}$$

We can now make a bifurcation diagram where we use $\mu_{30}\mu_{21}$ and μ_{11} as parameters. There are two different diagrams possible² depending on the sign of μ_{40} . Both of these possibilities are drawn in Figure 3.5.

As we have seen before, we can also put conditions on the parameter μ_{21} itself. Though, to do this, we need to know the sign of μ_{30} . Moreover, we know that

²One could argue that there is another possibility, when we choose $\mu_{40} < 0$ such that $-2\sqrt{\theta} < \mu_{40} < 0$. We have excluded this situation per our assumption that β is big enough, which is why we distinguish between μ_{40} positive or negative. We could refine this condition by looking at the sign of $\mu_{40} + \mu_{11,c} = \mu_{40} - 2\sqrt{\theta}$. Our conclusions will hold in this case, but will only make the bookkeeping more bothersome, which is why we haven't considered this in our analysis.

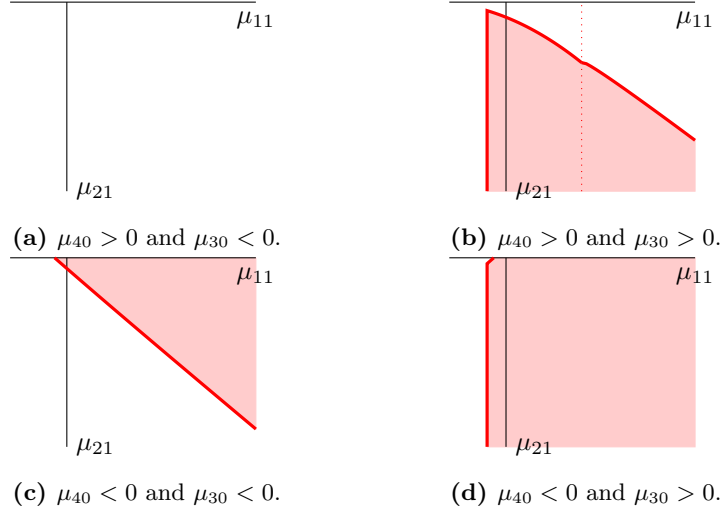


Figure 3.6 – The (μ_{11}, μ_{21}) plane for various possible values for μ_{40} and μ_{30} . The red regions denote the parameter region that corresponds to a stable uniform steady state (m_e, a_e) . See also Figure 3.5.

$\mu_{21} \geq 0$ (because $\frac{\partial m}{\partial a} < 0$, since adding additional algae to the system leads to a lower movement speed of the mussels). Hence, the region of parameter combinations (μ_{11}, μ_{21}) that leads to a stable uniform steady state, depends on the sign of μ_{40} and μ_{30} . The four possible forms of the stable regions are sketched in Figure 3.6.

In this section we have only considered the cases in which $\mathcal{O}(\beta) = \mathcal{O}(\varepsilon^\mu)$ with $\mu < 1/3$ (i.e. when β is big enough). We could also inspect the situations in which β is small. However, this only describes the behaviour very close to the line $\mu_{11} = \mu_{40}$ and is just a minor alteration of the line we already have found. Since we are mainly interested in the general behaviour and not specifically at the behaviour near $\mu_{11} = \mu_{40}$ we don't investigate this particular situation for now.

Moreover, the previous analysis is done under the assumption that $\delta > 0$ and $\theta > 0$. It is however possible to extend this analysis to $\delta = 0$ and/or $\theta = 0$ in a very natural way: in fact the bifurcation diagrams does not change drastically. The critical wavelengths and the eigenvalue curves on some of the bifurcation lines change significantly though, as we see later on³.

3.2.2 Approximations of eigenvaluecurves

Now that we have identified the bifurcation lines in the $(\mu_{11}, \mu_{30}\mu_{21})$ -plane, we want to determine the form of the eigenvalue curves on these lines. Here we are especially interested in the value of the critical wavelengths.

³The situations in which $\delta < 0$ or $\theta < 0$ are less interesting, since they correspond to situations for which the uniform steady state is unstable for a region of wavelengths.

In Section 3.1 we have already determined what values the critical wavelengths can take, depending on the parameter combinations. That is, for parameter combinations on Γ_t or Γ_d (see Figure B.2 and equation (B.4)) we have found the following conditions for the critical wavelengths:

$$|\vec{k}_c|^2 = \begin{cases} \sqrt{\theta}, & \text{on } \Gamma_t; \\ -\frac{1}{2}\beta, & \text{on } \Gamma_d \text{ when } \beta < 0; \\ \sqrt{\frac{\delta}{\beta}}, & \text{on } \Gamma_d \text{ when } \beta > 0. \end{cases}$$

In our bifurcation analysis of the $(\mu_{11}, \mu_{30}\mu_{21})$ -plane we came across all of these possibilities. The lines $\Gamma_{\pm,t}$ correspond to Γ_t , while $\Gamma_{\pm,d,+}$ correspond to Γ_d with $\beta > 0$ and finally $\Gamma_{+,d,-}$ corresponds to Γ_d with $\beta < 0$. So we have

$$|\vec{k}_c|^2 = \begin{cases} \sqrt{\theta}, & \text{on } \Gamma_{\pm,t}; \\ -\frac{1}{2}\beta, & \text{on } \Gamma_{+,d,-}; \\ \sqrt{\frac{\delta}{\beta}}, & \text{on } \Gamma_{\pm,d,+}. \end{cases}$$

The critical eigenvalues on a bifurcation line for which $\text{Tr } M(\vec{k}_c) = 0$ will be called $\vec{k}_{c,t}$ in the following, while we will denote the other critical eigenvalues, for which $\det M(\vec{k}_c) = 0$, by $\vec{k}_{c,d}$.

In section B.3.4 we have various possible scenarios for the bifurcation of eigenvalue curves, depending on the parameters β, γ and η and on which bifurcation line they lie. We observed that the eigenvalue curves change differently depending on whether $|\vec{k}_{c,t}| < |\vec{k}_{c,d}|$ or the other way around. The main difference between the two cases can be observed near $\Gamma_t \cap \Gamma_d$ where both sets of critical wavelengths can be observed simultaneously and the form of the curve depends on which wavelength is bigger.

The results in section B.3.4 were obtained under the assumption of a fixed β . In our current situation β does however depend on μ_{11} . This could lead to problems in our analysis in case β is small on Γ_t . One of our assumptions (i.e. $|\beta| \gg \sqrt{\varepsilon}$ near $\Gamma_{\pm,t}$) prevents this from happening. So near Γ_t the sign and order of β does not change and our observation from the last paragraph also applies to our current problem setting.

The sign of the parameter μ_{40} determines the form of the bifurcation line in the $(\mu_{11}, \mu_{30}\mu_{21})$ -plane as can be seen in Figure 3.5. When $\mu_{40} > 0$ we see that the lines $\Gamma_{+,t}$ and $\Gamma_{+,d,-}$ intersect. At the intersection point $\Gamma_{+,t} \cap \Gamma_{+,d,-}$ we therefore have $|\vec{k}_{c,t}| = \sqrt{\theta}$ and $|\vec{k}_{c,d}|^2 = -\frac{\beta}{2}$. Since we assumed that $|\beta| \gg \sqrt{\varepsilon}$ near $\Gamma_{+,t}$ we conclude that $|\vec{k}_{c,t}| < |\vec{k}_{c,d}|$ in this situation⁴.

The other possible bifurcation diagram arises when $\mu_{40} < 0$. Now we see that $\Gamma_{-,t}$ intersects with the curve $\Gamma_{-,d,+}$. Thus at $\Gamma_{-,t} \cap \Gamma_{-,d,+}$ we now have $|\vec{k}_{c,t}|^2 = \sqrt{\theta}$ and $|\vec{k}_{c,d}|^2 = \sqrt{\frac{\delta}{\beta}}$. Thus when $\delta > \theta\beta$ we again have $|\vec{k}_{c,t}| > |\vec{k}_{c,d}|$ and when $\delta < \theta\beta$ the critical wavelength $\vec{k}_{c,d}$ is smaller.

⁴Note that the conditions $\theta, \delta, \mu_{40} > 0$ are indeed compatible: we can choose the parameters $\mu_{10}, \mu_{20}, \mu_{30}$ and μ_{40} such that $\mu_{40} > 0$, $\mu_{10} < -\mu_{40}$ and $\mu_{20}\mu_{30} < \mu_{10}\mu_{40}$, e.g. $(\mu_{10}, \mu_{20}, \mu_{30}, \mu_{40}) = (-2, -3, 1, 1)$.

Table 3.1 – Summary of the possible critical wavelengths at the different bifurcation curves at which $\det M(\vec{k}_c) = 0$. Also, the ordering of the wavelengths $\vec{k}_{c,d}$ and $\vec{k}_{c,t}$ near $\Gamma_{\pm,t}$ is given. Note that $\vec{k}_{c,t} = \sqrt{\theta}$ for all cases. The results in this table hold under the assumption $\theta > 0$ and $\delta > 0$.

Position	additional condition	$ \vec{k}_{c,d} ^2$	Ordering near $\Gamma_{\pm,t}$
$\Gamma_{+,d,+}$		$ \vec{k}_{c,d} ^2 = \sqrt{\frac{\delta}{\beta}}$	(N/A)
$\Gamma_{+,d,-}$		$ \vec{k}_{c,d} ^2 = -\frac{\beta}{2}$	$ \vec{k}_{c,d} \gg \vec{k}_{c,t} $
$\Gamma_{-,d,+}$	$\mu_{20}\mu_{30} < -\mu_{40}^2$	$ \vec{k}_{c,d} ^2 = \sqrt{\frac{\delta}{\beta}}$	$ \vec{k}_{c,d} > \vec{k}_{c,t} $
$\Gamma_{-,d,+}$	$\mu_{20}\mu_{30} > -\mu_{40}^2$	$ \vec{k}_{c,d} ^2 = \sqrt{\frac{\delta}{\beta}}$	$ \vec{k}_{c,d} < \vec{k}_{c,t} $

It is not immediately clear whether both orderings of $|\vec{k}_{c,t}|$ and $|\vec{k}_{c,d}|$ are actually possible in our system, because the various conditions need not be compatible with each other. Since we have assumed from the start that $\theta > 0$ and $\delta > 0$ we already need $\mu_{10} < -\mu_{40}$ and $\mu_{10}\mu_{40} > \mu_{20}\mu_{30}$. Furthermore we inspected the case with $\mu_{40} < 0$. Now we need to determine the sign of $\delta - \theta\beta$ for parameter combinations under the aforementioned conditions. Since we are interested at the behaviour near $\Gamma_{-,t}$ we know that $|\beta| \gg \sqrt{\varepsilon}$. Therefore $\beta \approx -\mu_{40}$ to leading order, since μ_{11} is of order $\sqrt{\varepsilon}$ near $\Gamma_{-,t}$. Hence we can instead look at the sign of $\delta + \mu_{40}\theta$. Recalling the definitions of δ and θ from equation (3.7), we can even simplify this to

$$\operatorname{sgn}(\delta + \mu_{40}\theta) = \operatorname{sgn}(\mu_{10}\mu_{40} - \mu_{20}\mu_{30} - \mu_{40}(\mu_{10} + \mu_{40})) = \operatorname{sgn}(-\mu_{20}\mu_{30} - \mu_{40}^2)$$

Would the sign be negative then we obtain the condition $\mu_{20}\mu_{30} > -\mu_{40}^2$, while the additional condition becomes $\mu_{20}\mu_{30} < -\mu_{40}^2$ when the sign is positive. Since $\mu_{10} < -\mu_{40}$ from one of the assumption we now see that both signs are therefore possible.

A summary of the possible critical wavelengths on $\Gamma_{\pm,d,\pm}$ is given in Table 3.1. We now want to give all possible eigenvalue curves on the bifurcation lines. However, in our analysis in Section 3.1 we needed to distinguish between the possibilities $\theta^2 - 4\delta > 0$ and $\theta^2 - 4\delta < 0$ (i.e. pure real or complex eigenvalues near $\vec{k} = 0$). So we now need to determine to what conditions this correspond in our μ -parameters. Therefore we observe that

$$\begin{aligned} \theta^2 - 4\delta &= \varepsilon^2 \left[(\mu_{10} + \mu_{40})^2 - 4\mu_{10}\mu_{40} + 4\mu_{20}\mu_{30} \right] \\ &= \varepsilon^2 \left[(\mu_{10} - \mu_{40})^2 + 4\mu_{20}\mu_{30} \right]. \end{aligned}$$

Thus there are only complex eigenvalues around $\vec{k} = 0$ when we have $\mu_{20}\mu_{30} < -\left(\frac{\mu_{10} - \mu_{40}}{2}\right)^2$ and pure real eigenvalues when the inequality is reversed⁵.

Although it may seem now that there is a wide variety of eigenvalue curve deformations possible, this is not true. There are only four essential different scenarios we can encounter. Given a set of parameters $\mu_{10}, \mu_{20}, \mu_{30}, \mu_{40}$ we need to look at the following two things to determine which scenario is relevant:

⁵Note that the sign of $4\mu_{20}\mu_{30} + (\mu_{10} - \mu_{40})^2$ is not already fixed by the other conditions on these parameters and therefore we actually need to distinguish between cases with and without complex eigenvalues near $\vec{k} = 0$.

1. The ordering of $\vec{k}_{c,t}$ and $\vec{k}_{c,d}$ at $\mu_{11} = \mu_{11,c}$;
2. Whether or not the eigenvalues are complex at $\vec{k} = 0$ (i.e. the sign of $\theta^2 - 4\delta$).

In Figures 3.7-3.10 we have plotted the eigenvalue curves on the bifurcation lines for the four possibilities. First, in Figure 3.7 we have inspected the situation in which $|\vec{k}_{c,d}| > |\vec{k}_{c,t}|$ and the eigenvalues are complex at $\vec{k} = 0$. In Figure 3.8 we again have $|\vec{k}_{c,d}| > |\vec{k}_{c,t}|$, but now the eigenvalues are real at $\vec{k} = 0$. Then, in Figure 3.9 the eigenvalues are again complex at $\vec{k} = 0$, but now $|\vec{k}_{c,d}| < |\vec{k}_{c,t}|$. Finally we inspected the case where the eigenvalues are real at $\vec{k} = 0$ and $|\vec{k}_{c,d}| < |\vec{k}_{c,t}|$ in Figure 3.10.

Special cases $\theta = 0$ and $\delta = 0$

Up till now we have assumed that $\theta > 0$ and $\delta > 0$ are of order ε . In this section we relax this assumption and try to determine what happens when $\theta = 0$ or $\delta = 0$.

First, we consider what happens when $\theta = 0$. In this case we find that, regardless of the choice of parameters, we find that the eigenvalues at $\vec{k} = 0$ have zero real part. On $\Gamma_{\pm,t}$ the only critical wavelength now is $\vec{k}_{c,t} = 0$. Moreover, on the lines $\Gamma_{\pm,d,\pm}$ we have the same critical wavelengths as before plus $\vec{k}_{c,t} = 0$.

Moreover, it is clear that $|\vec{k}_{c,t}| < |\vec{k}_{c,d}|$ and $\theta^2 - 4\delta \leq 0$ for all possible parameters. Therefore there is only one possible scenario that can describe this case. This is illustrated in Figure 3.7. However, we must note that $\vec{k} = 0$ corresponds to a eigenvalue with zero real part in all of the pictured frames now that $\theta = 0$.

The other interesting special case occurs when we choose our parameters such that $\delta = 0$. Again $\vec{k} = 0$ is a critical wavelength for all possible parameter combinations. Therefore we find an additional critical wavelength on $\Gamma_{\pm,t}$. Moreover, on $\Gamma_{\pm,d,-}$ we also find this additional critical wavelength. Finally on $\Gamma_{\pm,d,+}$ there is now only one critical wavelength: $\vec{k}_{c,d} = 0$.

It is clear that at $\vec{k} = 0$ we always have real eigenvalues. However, this time there are still two scenarios possible: we have $|\vec{k}_{c,d}| > |\vec{k}_{c,t}|$ when $\mu_{40} > 0$ and $|\vec{k}_{c,d}| = 0 < |\vec{k}_{c,t}|$ when $\mu_{40} < 0$. The former case corresponds to the frames in Figure 3.8, while the latter corresponds to Figure 3.10.

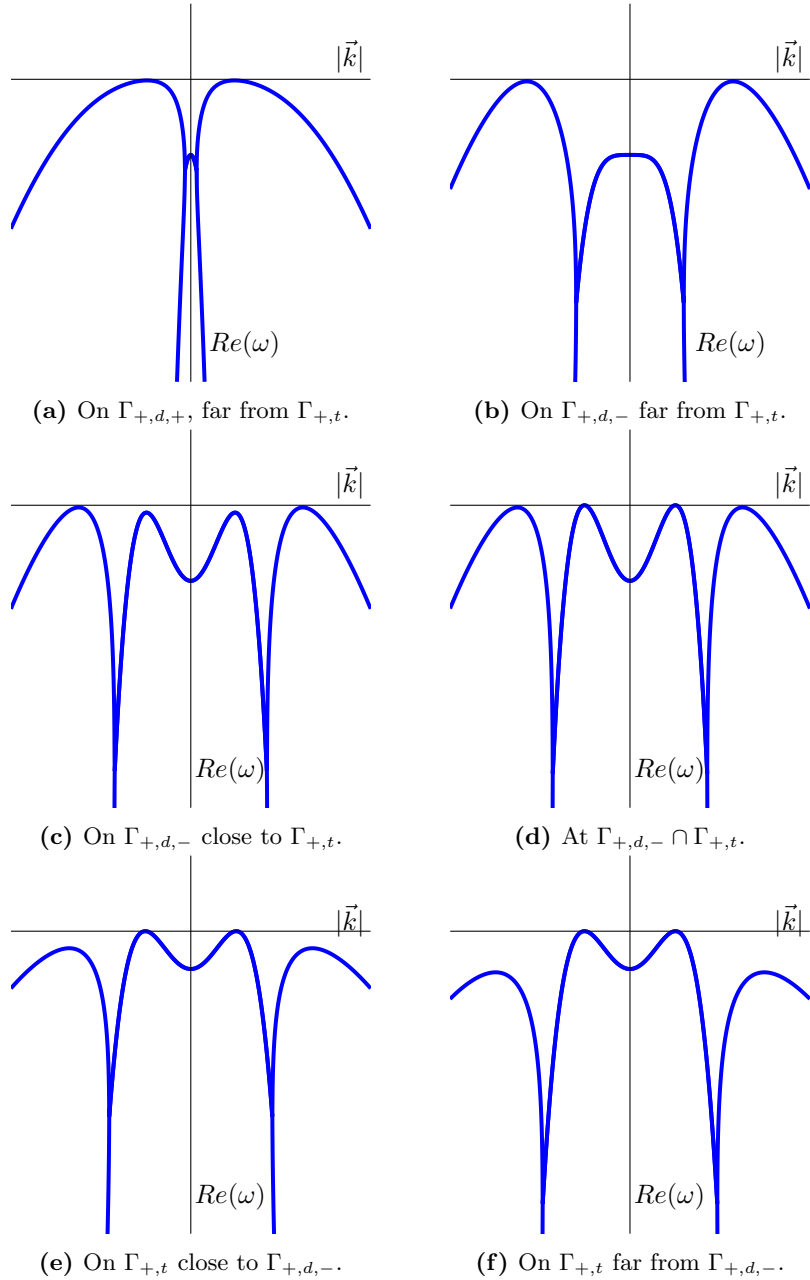


Figure 3.7 – The eigenvalue curves on the bifurcation lines when $|\vec{k}_{c,d}| > |\vec{k}_{c,t}|$ and $\mu_{20}\mu_{30} < -\left(\frac{\mu_{10}-\mu_{40}}{2}\right)^2$. These plots are made with Matlab and the parameter values we have used are: $\mu_{10} = -2, \mu_{20} = -19/8, \mu_{30} = 1, \mu_{40} = 1$ and we used $\varepsilon = \frac{1}{100}$. Furthermore we have taken $\mu_{11} = 1.25$ (a), $\mu_{11} = 0$ (b) $\mu_{11} = -2\sqrt{\theta} + \varepsilon$ (c), $\mu_{11} = -2\sqrt{\theta}$ (d), $\mu_{21} = \mu_{21,c} + \varepsilon$ (e) and $\mu_{21} = 0.45$ (f) and the other parameter such that we effectively are on the right bifurcation line. Here $\mu_{21,c}$ is the value for μ_{21} at $\Gamma_{+,d,-} \cap \Gamma_{+,t}$.

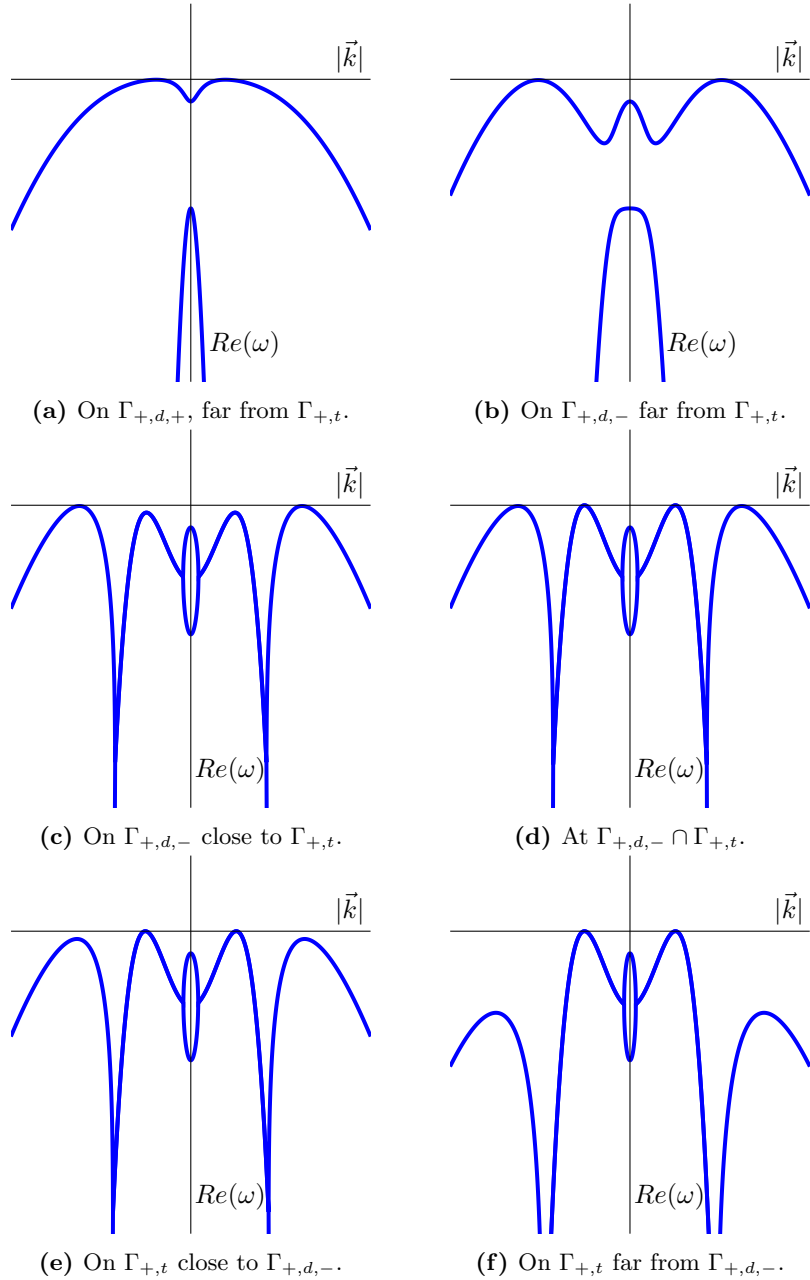


Figure 3.8 – The eigenvalue curves on the bifurcation lines when $|\vec{k}_{c,d}| > |\vec{k}_{c,t}|$ and $\mu_{20}\mu_{30} > -\left(\frac{\mu_{10}-\mu_{40}}{2}\right)^2$. These plots are made with Matlab and the parameter values we have used are: $\mu_{10} = -2$, $\mu_{20} = -17/8$, $\mu_{30} = 1$, $\mu_{40} = 1$ and we used $\varepsilon = \frac{1}{100}$. Furthermore we have taken $\mu_{11} = 1.25$ (a), $\mu_{11} = 0.2$ (b) $\mu_{11} = -2\sqrt{\theta} + \varepsilon$ (c), $\mu_{11} = -2\sqrt{\theta}$ (d), $\mu_{21} = \mu_{21,c} + 2\varepsilon$ (e) and $\mu_{21} = 0.45$ (f) and the other parameter such that we effectively are on the right bifurcation line. Here $\mu_{21,c}$ is the value for μ_{21} at $\Gamma_{+,d,-} \cap \Gamma_{+,t}$.

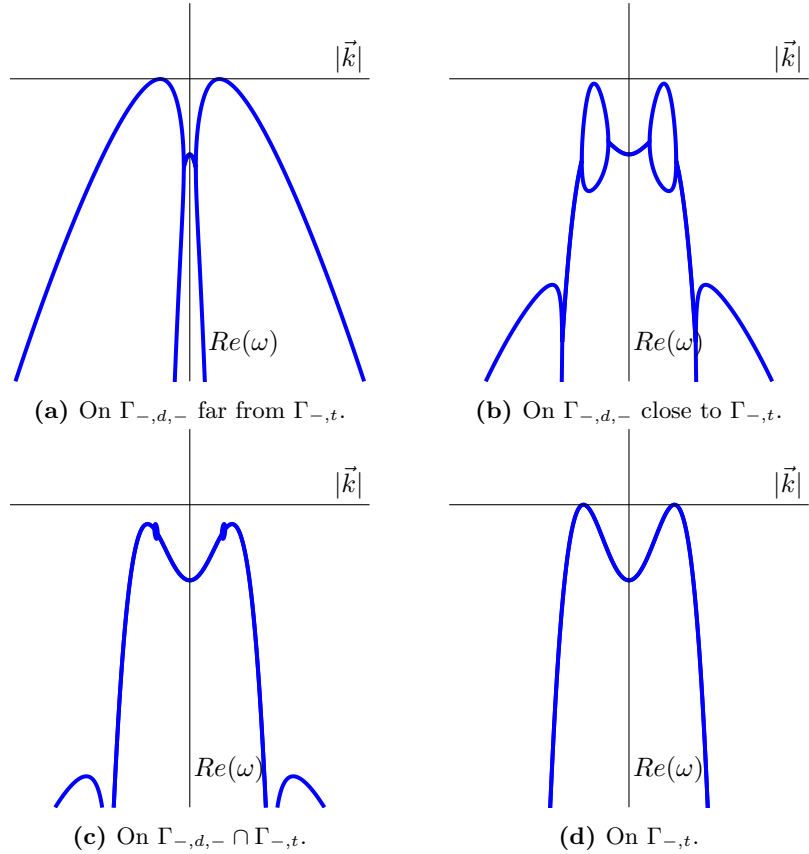


Figure 3.9 – The eigenvalue curves on the bifurcation lines when $|\vec{k}_{c,d}| < |\vec{k}_{c,t}|$ and $\mu_{20}\mu_{30} < -\left(\frac{\mu_{10}-\mu_{40}}{2}\right)^2$. These plots are made with Matlab and the parameter values we have used are: $\mu_{10} = 0, \mu_{20} = -3/8, \mu_{30} = 1, \mu_{40} = -1$ and we used $\varepsilon = \frac{1}{100}$. Furthermore we have taken $\mu_{11} = 1$ (a), $\mu_{11} = -0.10$ (b) $\mu_{11} = -2\sqrt{\theta}$ (c) and $\mu_{21} = 0.5$ (d) and the other parameter such that we effectively are on the right bifurcation line. Note that the plots clearly show that the real part of the eigenvalues are non-zero everywhere, whereas we reasoned there should be a few specific wavelengths with zero real part, because we have used many leading order approximations in our analysis. Would we have chosen a far smaller numerical value for ε , these plots would look better. Also note that in (c) we did not choose the correct value $\mu_{11,c}$ but a bigger one for the same reason.

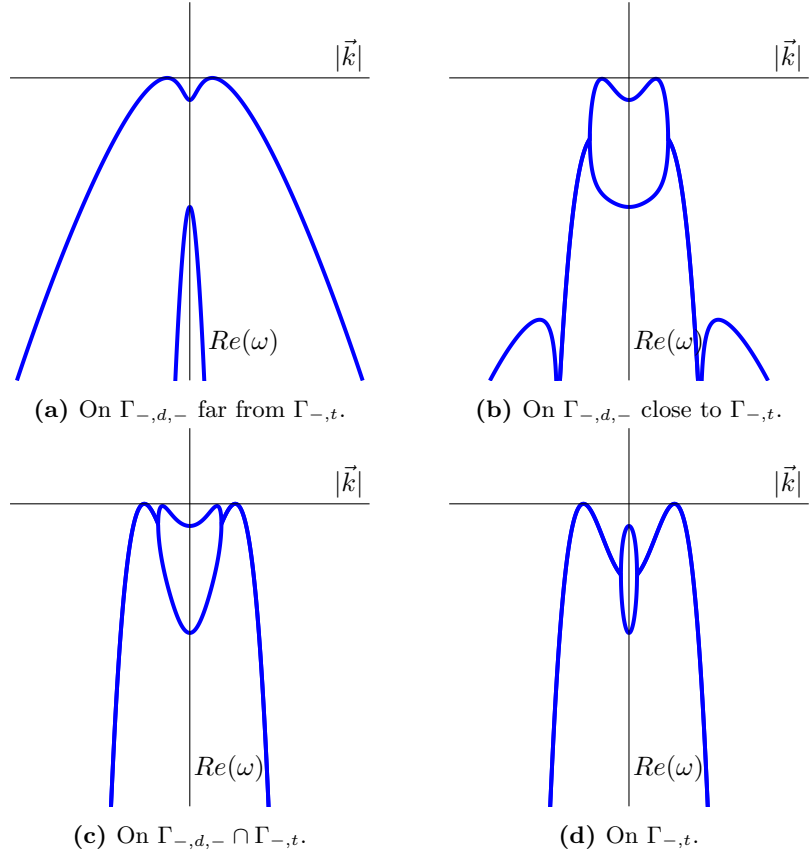


Figure 3.10 – The eigenvalue curves on the bifurcation lines when $|\vec{k}_{c,d}| < |\vec{k}_{c,t}|$ and $\mu_{20}\mu_{30} > -\left(\frac{\mu_{10}-\mu_{40}}{2}\right)^2$. These plots are made with Matlab and the parameter values we have used are: $\mu_{10} = 0, \mu_{20} = -1/8, \mu_{30} = 1, \mu_{40} = -1$ and we used $\varepsilon = \frac{1}{100}$. Furthermore we have taken $\mu_{11} = 1$ (a), $\mu_{11} = -0.10$ (b) $\mu_{11} = -2\sqrt{\theta}$ (c) and $\mu_{21} = 0.5$ (d) and the other parameter such that we effectively are on the right bifurcation line.

3.3 Modulation Equation when $\{\det \mathcal{M} = 0\}$ is crossed.

Up till now we have only inspected the linear stability of the uniform steady states of equation (3.1). It could however happen that patterns arise in this system, when the uniform steady state becomes unstable. To determine if this happens we turn to a weakly non linear analysis in this section. The final goal here is to find an amplitude equation that describes small perturbations of the original uniform stationary state near a critical situation on the bifurcation line $\Gamma_{\pm,d,\pm}$ (i.e. when the determinant changes sign).

More precisely we inspect deviations from this stationary state of the form $e^{ik_c x} \phi \vec{v}_1 A(\xi, \tau)$, where $0 < \phi \ll \varepsilon \ll 1$, \vec{v}_1 is the most unstable ‘direction’ and where ξ and τ are respectively the rescaled (slowly varying) spatial and temporal variables. For this analysis we abandon the two-dimensional setting and we’ll only inspect the one-dimensional situations (i.e. when we only have one spatial variable).

We inspect only the behaviour on the bifurcation lines $\Gamma_{\pm,d,\pm}$ as we see that this is the only relevant bifurcation line for our mussel system. For these lines we know that the determinant is zero at the critical wavelengths. Hence $\det M(k_c) = 0$ and $\omega_{1,2}(k_c) \leq 0$ are real. We need to choose our bifurcation parameters. Since both μ_{11} and μ_{21} depend on our choice for the function v for the speed of the mussels, we vary both of these parameters.

Conform the normal derivation of the amplitude equations we thus inspect what happens when $\mu_{11} = \mu_{11,c}(\mu_{21,c}) + \phi^2 r$ and $\mu_{21} = \mu_{21,c} + \phi^2 s$. Here r and s are constants of order $\mathcal{O}(1)$ that need to be chosen such that the combination (μ_{11}, μ_{21}) corresponds to linear instability of the uniform steady state (m_e, a_e) . See also Figure 3.11.

The constant $\mu_{11,c}(\mu_{21})$ is such that $(\mu_{11,c}(\mu_{21}), \mu_{30}\mu_{21}) \in \Gamma_{\pm,d,\pm}$. That is, this specific combination must be chosen in such a way that it corresponds to a critical situation in which the determinant of the Jacobian vanishes. We must also make sure that we have chosen $\mu_{21,c}$ such that it is far enough away from the transitions in the bifurcation curve (i.e. far away from $\Gamma_{\pm,t}$ and from $\Gamma_{\pm,d,\mp}$).

The matrix M (see equation (3.6)) in this situation is (note that we have chosen the parameters $\mu_{12} = 1$ and $\mu_{41} = 1$ as before for simplicity):

$$M = \begin{pmatrix} -k^4 - \mu_{11,c}(\mu_{21})k^2 + \varepsilon\mu_{10} - \phi^2 rk^2 & -\mu_{21}k^2 + \varepsilon\mu_{20} - \phi^2 sk^2 \\ \varepsilon\mu_{30} & -\varepsilon k^2 + \varepsilon\mu_{40} \end{pmatrix} \quad (3.15)$$

In this chapter we first investigate the ‘critical’ matrix \mathcal{M}_c and find the eigenvalues and eigenvectors. Then we turn to the rescaled spatial and temporal variables ξ and τ and use these to postulate a good expansion for the perturbation of the uniform stationary state. Finally we employ the full machinery of the weakly non linear stability analysis and derive an amplitude equation for this situation.

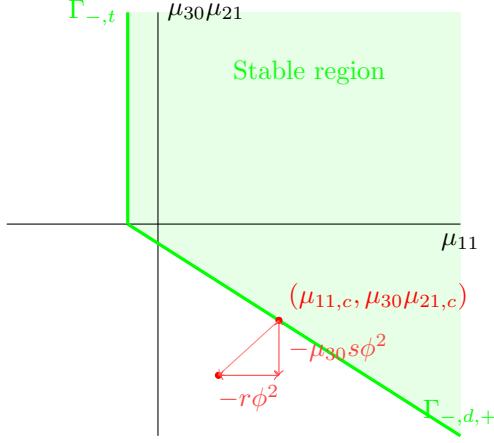


Figure 3.11 – Sketch of the bifurcation plane $(\mu_{11}, \mu_{30}\mu_{21})$ when $\mu_{40} < 0$ (see also Figure 3.5). For the non-linear analysis we want to choose $\mu_{21,c}$ and $\mu_{11,c}$ such that $(\mu_{11,c}, \mu_{30}\mu_{21,c}) \in \Gamma_{-,d,+}$ as sketched in this figure. Then we want to vary the parameters μ_{11} and μ_{21} a bit such that we are in the linear unstable region, as depicted in the figure.

3.3.1 The matrix \mathcal{M}_c

We have chosen $\mu_{11,c}$ and $\mu_{21,c}$ such that $(\mu_{11,c}, \mu_{30}\mu_{21}) \in \Gamma_{+,d,+}$. The matrix \mathcal{M}_c that corresponds to this specific choice of parameters is given by

$$\mathcal{M}_c = \begin{pmatrix} -k_c^4 - \mu_{11,c}(\mu_{21})k_c^2 + \varepsilon\mu_{10} & -\mu_{21}k_c^2 + \varepsilon\mu_{20} \\ \varepsilon\mu_{30} & -\varepsilon k_c^2 + \varepsilon\mu_{40} \end{pmatrix}.$$

The choice of parameters ensures that $\det \mathcal{M}_c = 0$. Therefore, we know that the eigenvalues are given by

$$\omega_1 = 0,$$

$$\omega_2 = \text{Tr } \mathcal{M}_c = -k_c^4 - (\mu_{11,c}(\mu_{21}) + \varepsilon)k_c^2 + \varepsilon(\mu_{10} + \mu_{40}).$$

We also need to find the corresponding eigenvectors. The first eigenvector $\vec{v}_1 = (x_1, y_1)$ must satisfy the following condition⁶:

$$\varepsilon\mu_{30}x_1 + (-\varepsilon k_c^2 + \varepsilon\mu_{40})y_1 = 0 \quad (3.16)$$

The second eigenvector $\vec{v}_2 = (x_2, y_2)$ must satisfy an other condition:

$$(\varepsilon\mu_{30})x_2 + (k_c^4 + \mu_{11,c}k_c^2 - \varepsilon\mu_{10})y_2 = 0 \quad (3.17)$$

Since the equation $\mathcal{M}_c x = b$ can only be solved when $b = (b_1, b_2) \in \text{Sp}(\vec{v}_2)$, we obtain a solvability condition. This solvability condition will be the final ingredient that ultimately will give us the desired amplitude equation. Hence a vector $b = (b_1, b_2)$ obeys the solvability conditions if and only if

$$\varepsilon\mu_{30}b_1 + (k_c^4 + \mu_{11,c}k_c^2 - \varepsilon\mu_{10})b_2 = 0.$$

⁶Note that we could also put these condition in an other form by reading of the other row of the matrix. This won't change the results, though it can make the formulas more (or sometimes less) cumbersome.

3.3.2 Perturbations

As stated before we are interested to see what happens when we perturb the uniform steady state (m_e, a_e) a little bit. We apply the standard way to model this perturbation in our non linear stability analysis. That is, we model this perturbation as a slow modulation of the most critical wave. That is a wave with wavenumber $k = k_c$. Thus we are interested in the following perturbation of our uniform steady state:

$$\begin{pmatrix} \bar{m} \\ \bar{a} \end{pmatrix} = \phi \vec{v}_1 A(\xi, \tau) e^{ik_c x} + c.c. + h.o.t. \quad (3.18)$$

Here *c.c.* means we also have the complex conjugates and *h.o.t.* means we also have higher order terms, both in ϕ and in the fourier expansion. Recall that we have $0 < \phi \ll 1$ here⁷. The vector \vec{v}_1 is the most unstable direction (i.e. its the eigenvector corresponding to the eigenvalue $\omega = 0$ in the matrix \mathcal{M}_c). Finally ξ and τ are the rescaled, slow spatial and temporal variables. The precise scaling of these two variables, as determined by the characteristics of the eigenvalue curves, is computed in the following sections.

Scaling of ξ

We first inspect the scaling of the spatial variables ξ . The scaling of ξ corresponds to the interval of wavelengths k for which the uniform steady state (m_e, a_e) is unstable when the bifurcation parameters are chosen such that $(\mu_{11}, \mu_{21}) = (\mu_{11,c}(\mu_{21,c}) + \phi^2 r, \mu_{21,c} + \phi^2 s)$. To determine this width, we can turn to the dispersion relation again and try to find for which wavelengths $\omega = 0$ is a solution. Thus we need to solve⁸

$$0 = \det M(k).$$

In this case, the matrix $M(k)$ is as in Equation (3.15). We can rewrite this matrix as follows

$$M(k) = \mathcal{M}_c(k) - \phi^2 k^2 \begin{pmatrix} r & s \\ 0 & 0 \end{pmatrix},$$

where the matrix $\mathcal{M}_c(k)$ is the matrix with the parameters such that they lie precisely on the bifurcation line $\Gamma_{\pm,d,\pm}$.

Working out the determinant of $M(k)$ we can express it with the determinant of $\mathcal{M}_c(k)$ as follows:

$$\det M(k) = \det \mathcal{M}_c(k) + \varepsilon \phi^2 k^2 (rk^2 - r\mu_{40} + s\mu_{30})$$

As we have chosen $0 < \phi \ll 1$ very small we know that k is very close to the critical wavelength k_c . Therefore we can define $z := k - k_c$ and we know that this is a very small variable. Thus we can assume that $|z| \ll 1$ and $|z| \ll |k_c|$.

⁷We use the symbol ϕ here instead of the perhaps more common used ε , because this symbol is already used in the description of our system (see Equation (3.1))

⁸Note that in this reasoning we implicitly use that ϕ is as small and $\mu_{21,c}$ is chosen well enough to ensure that the sign of the trace remains unchanged for our small perturbations of our parameters.

The condition $0 = \det M(k)$ can thus be approximated with a Taylor expansion. Thus we have the condition

$$0 = \det \mathcal{M}_c(k_c) + \frac{d \det \mathcal{M}_c(k_c)}{dk} z + \frac{d^2 \det \mathcal{M}_c(k_c)}{dk^2} \frac{z^2}{2} + \varepsilon \phi^2 [(k_c^2 + 2k_c z + z^2)(s\mu_{30} - r\mu_{40}) + r(k_c^4 + 4k_c^3 z + 6k_c^2 z^2)] + \mathcal{O}(z^3) \quad (3.19)$$

By construction we know that $\det \mathcal{M}_c(k_c) = 0$ and we also know that for the derivative we have $\frac{d \det \mathcal{M}_c(k_c)}{dk} = 0$ (as otherwise k_c won't be the argument of a maximum of this determinant⁹). An explicit computation of $\frac{d^2 \det \mathcal{M}_c(k_c)}{dk^2}$ gives its form as

$$\frac{d^2 \det \mathcal{M}_c(k_c)}{dk^2} = \varepsilon \frac{8}{3} (\beta^2 - \beta \sqrt{\beta^2 - 3\gamma} - 3\gamma).$$

This can only be zero when $\gamma = \beta^2/3$ or when $\beta \geq 0$ and $\gamma < 0$. Both of these cases cannot happen, since $\delta > 0$ and therefore the bifurcation line $\Gamma_{\pm,d,\pm}$ is such that (β, γ) always lies below these possibilities in the plane.

Turning back to the expanded dispersion relation of equation (3.19) we can now set $\det \mathcal{M}_c(k_c)$ and $\frac{d \det \mathcal{M}_c(k_c)}{dk}$ to zero. Moreover, we can only keep the highest orders to obtain the relation

$$0 = \frac{d^2 \det \mathcal{M}_c(k_c)}{dk^2} \frac{z^2}{2} + \varepsilon \phi^2 [k_c^2(s\mu_{30} - r\mu_{40}) + rk_c^4] + \mathcal{O}(\phi^2 z) + \mathcal{O}(z^3).$$

Note that this approximation is only valid when $|z^2| \gg |\phi^2 z|$. So after we have solved this equation for z we still need to check that this condition for the approximation holds. When $(s\mu_{30} - r\mu_{40}) + rk_c^4 \neq 0$ we then find that $\mathcal{O}(z^2) = \mathcal{O}(\phi^2)$. Thus the scaling of z is now clear, since $z = \mathcal{O}(\phi)$.

Note that when $(s\mu_{30} - r\mu_{40}) + rk_c^4 = 0$ we need to take the higher order terms into account. This amounts to $\mathcal{O}(z) = \mathcal{O}(\phi^2)$ and thus $\xi = \phi^2 x$. However, we do not focus on this situation as this is a very specific, which is not likely to occur. Also note that we can neglect the order of ε as the determinant $\det \mathcal{M}_c$ carries an ε in it as well, so they balance each other.

Scaling of τ

In the previous section we have found that $z = \mathcal{O}(\phi)$ is a reasonable scaling. Moreover we found that the wavelengths for which $\omega(k) = 0$ are $\mathcal{O}(\phi)$ close to the original critical wavelength k_c . So the unstable wavelengths (i.e. those for which $\omega(k) \geq 0$) can be written as $k = k_c + \phi K$ where K of order $\mathcal{O}(1)$ is chosen such that k lies in the interval with unstable wavelengths.

The eigenvalues corresponding to those wavelengths k will be written as $\omega(k)$. Since k lies close to k_c , we can approximate this eigenvalue with a Taylor expansion. As before we need to evaluate these eigenvalues for the new set of

⁹A simple computation with the explicit expression $|k_c|^2 = \frac{-\beta + \sqrt{\beta^2 - 3\gamma}}{3}$ will also quickly verify that the derivative of the determinant in k_c is zero.

parameters. The determinant and trace of the matrix $M(k)$ can now be expressed as

$$\begin{aligned}\det M(k) &= \det \mathcal{M}_c(k) + \varepsilon\phi^2k^2(rk^2 - r\mu_{40} + s\mu_{30}); \\ \text{Tr } M(k) &= \text{Tr } \mathcal{M}_c(k) - \phi^2rk^2.\end{aligned}$$

To compute the eigenvalue $\omega(k)$ we use the trace and the determinant. Thus we now have

$$\begin{aligned}\omega(k) &= \frac{\text{Tr } M(k)}{2} + \frac{1}{2}\sqrt{(\text{Tr } M(k))^2 - 4\det M(k)} \\ &= \frac{\text{Tr } \mathcal{M}_c(k)}{2} - \frac{\phi^2r}{2} \\ &\quad + \frac{1}{2}\sqrt{(\text{Tr } \mathcal{M}_c(k) - \phi^2r)^2 - 4\det \mathcal{M}_c(k) - 4\varepsilon\phi^2k^2(rk^2 - r\mu_{40} + s\mu_{30})}\end{aligned}\tag{3.20}$$

We now apply a Taylor expansion to the square root to obtain

$$\omega(k) = \omega_c(k) + N(k)\phi^2 + \mathcal{O}(\phi^4)\tag{3.21}$$

Here $\omega_c(k)$ is the eigenvalue curve with the original parameters (i.e. such that they lie on $\Gamma_{\pm,d,\pm}$) and $N(k)$ is some tedious and complicated term, which only vanishes for very specific choices of parameters. Finally we apply another Taylor expansion, this time around the wavenumber $k = k_c$. Since we have defined $k = k_c + \phi K$ we thus obtain the following:

$$\omega(k) = \omega_c(k_c) + \frac{d\omega_c(k_c)}{dk}\phi K + \frac{d^2\omega_c(k)}{dk^2}\phi^2 K^2 + N(k_c)\phi^2 + \mathcal{O}(\phi^3)\tag{3.22}$$

Since $\frac{d\omega_c(k_c)}{dk} = 0$ and $\omega_c(k_c) = 0$ we finally find that $\mathcal{O}(\omega(k)) = \mathcal{O}(\phi^2)$.

Now that we have established that $\mathcal{O}(\omega(k)) = \mathcal{O}(\phi^2)$ and $\mathcal{O}(k - k_c) = \mathcal{O}(\phi)$ we can introduce K and $W > 0$ both of order $\mathcal{O}(1)$ such that $\omega(k) = \phi^2 W$ and $k = k_c + \phi K$. Now we write the family of linearly unstable, spatially periodic perturbations of the uniform stationary state (m_e, a_e) as

$$e^{ikx+\omega(k)t} = e^{i(k_c+\phi K)x+\phi^2 W t} = e^{ik_c x + iK\phi x + W\phi^2 t} = A_{lin}(\phi x, \phi^2 t)e^{ik_c x}.$$

So from this observation we have justified the scaling $\xi = \phi x$ and $\tau = \phi^2 t$ as these are the arguments of the amplitude term A .

3.3.3 The full perturbation

In equation (3.18) we have made an assumption on the perturbation that we want to study. However this is not the full perturbation. Since our model is non linear the higher order terms of both the Fourier Series and the Taylor Series play a fundamental role. Therefore we must also incorporate these higher orders in our analysis. For notational simplicity we write $E := e^{ik_c x}$. Thus in order to ultimately derive the modulation equations for this system we use the following

Ansatz for the perturbations around our steady state:

$$\begin{aligned} E^0 \left[\phi^2 \begin{pmatrix} X_{02} \\ Y_{02} \end{pmatrix} + \dots \right] \\ \begin{pmatrix} \bar{m} \\ \bar{a} \end{pmatrix} = E \left[\phi \begin{pmatrix} v_{11} \\ v_{12} \end{pmatrix} A(\xi, \tau) + \phi^2 \begin{pmatrix} X_{12} \\ Y_{12} \end{pmatrix} + \phi^3 \begin{pmatrix} X_{13} \\ Y_{13} \end{pmatrix} + \dots \right] \\ E^2 \left[\phi^2 \begin{pmatrix} X_{22} \\ Y_{22} \end{pmatrix} + \dots \right] + c.c. \end{aligned}$$

Here $\vec{v}_1 = (v_{11}, v_{22})^T$ is the most unstable direction and $A(\xi, \tau)$ the amplitude as before. Moreover X_{ij} and Y_{ij} for $i, j \in \mathbb{N}_0$ are functions of ξ and τ .

In order to obtain the desired amplitude equations we need to substitute this whole perturbation into our original system. This results in a gigantic expression which has several different powers of E and ϕ . We can study this system at each independent level. That is, we can gather all terms of the form $\phi^a E^b$ for $a, b \in \mathbb{N}_0$. Because of the chosen expansion we know that the system must still hold for all these different possible levels. Ultimately the expression at the $a = 3, b = 1$ level yields the amplitude equation when we apply the solvability condition for $(X_{13}, Y_{13})^T$.

Before we are ready to exploit this machinery of the modulation equation we first need to modify our original system. Earlier we have already linearized this model in order to find the linear stability. Since we now want to find the amplitude equation at the $a = 3, b = 1$ level we need the Taylor expansion of all terms in the original model up to cubic order. That is, we must keep all constant, linear, quadratic and cubic interactions (and we can forget about the others as they have little effect).

3.3.4 Rewriting the equations

In the analysis thus far we have observed that we can set $\mu_{12} = 1$ and $\mu_{41} = 1$ without loss of generality. Since $\mu_{12} = d_m \kappa$ and $\mu_{41} = d_a$ (see equations (3.5)) we can forget about two parameters in our governing equations, simplifying them a little bit.

Moreover we are analysing the amplitude equation when there is only one spatial dimension involved. Therefore we denote derivatives with subscripts. The governing partial differential equation then reads

$$\begin{cases} m_t &= [d_m v(v + mv_m)m_x + d_m v m v_a a_x]_x - m_{xxxx} + \varepsilon H(m, a) \\ a_t &= \varepsilon a_{xx} + \varepsilon G(m, a) \end{cases} \quad (3.23)$$

Our next goal is now to rewrite this system so that we only have terms with up to cubic interactions (and ignoring all higher order interactions). It is clear that m_t, m_{xxxx}, a_t and a_{xx} are already in a good format, since they act linearly. Thus we need to expand the other three terms. This can be done easily by a Taylor expansion. This Taylor expansion must be done around the uniform steady state (m_e, a_e) .

As before we define $\bar{m} := m - m_e$ and $\bar{a} := a - a_e$ for the perturbations around the uniform steady state. The expansions of the (general) interactions terms $H(m, a)$ and $G(m, a)$ is clearly just the definition of the Taylor Series with two variables. Hence we obtain

$$\begin{aligned} H(m, a) &= H^e \\ &+ (H_m^e \bar{m} + H_a^e \bar{a}) \\ &+ \frac{1}{2} (H_{mm}^e \bar{m}^2 + 2H_{ma}^e \bar{m} \bar{a} + H_{aa}^e \bar{a}^2) \\ &+ \frac{1}{6} (H_{mmm}^e \bar{m}^3 + 3H_{mma}^e \bar{m}^2 \bar{a} + 3H_{maa}^e \bar{m} \bar{a}^2 + H_{aaa}^e \bar{a}^3) + h.o.t. \end{aligned}$$

where the subscript denotes to what variable we need to differentiate and the superscript reminds us that we need to take the value at the uniform steady state (m_e, a_e) . Again *h.o.t.* means that there are additional higher order interactions (but we will ignore them). Also note that for the other interaction term, $G(m, a)$, we find a similar expression but with the H 's replaced by G 's.

So now we only need to find a similar expansion for the last remaining term, $[d_m v(v + mv_m)m_x + d_m v m v_a a_x]_x$. As taking the derivative does not alter the order of the interactions, it suffices to only find the expansion for the expression inside the brackets. For notational simplicity we split this in two terms, $d_m v(v + mv_m)m_x$ and $d_m v m v_a a_x$. The expansion for the latter term is

$$\begin{aligned} &v(m, a) m v_a(m, a) a_x \\ &= (v^e + (v_m^e \bar{m} + v_a^e \bar{a}) + (v_{mm}^e \bar{m}^2 + 2v_{ma}^e \bar{m} \bar{a} + v_{aa}^e \bar{a}^2)/2) \cdot (m_e + \bar{m}) \\ &\quad \cdot (v_a^e + (v_{ma}^e \bar{m} + v_{aa}^e \bar{a}) + (v_{mma}^e \bar{m}^2 + 2v_{maa}^e \bar{m} \bar{a} + v_{aaa}^e \bar{a}^2)/2) \cdot \bar{a}_x + h.o.t. \\ &= v^e m_e v_a^e \bar{a}_x + v^e m_e (v_{ma}^e \bar{m} + v_{aa}^e \bar{a}) \bar{a}_x + v^e \bar{m} v_a^e \bar{a}_x + (v_m^e \bar{m} + v_a^e \bar{a}) m_e v_a^e \bar{a}_x \\ &\quad + v^e m_e (v_{mma}^e \bar{m}^2 + 2v_{maa}^e \bar{m} \bar{a} + v_{aaa}^e \bar{a}^2)/2 \bar{a}_x \\ &\quad + (v_{mm}^e \bar{m}^2 + 2v_{ma}^e \bar{m} \bar{a} + v_{aa}^e \bar{a}^2)/2 m_e v_a^e \bar{a}_x \\ &\quad + v^e \bar{m} (v_{ma}^e \bar{m} + v_{aa}^e \bar{a}) \bar{a}_x + (v_m^e \bar{m} + v_a^e \bar{a}) m_e (v_{ma}^e \bar{m} + v_{aa}^e \bar{a}) \bar{a}_x + (v_m^e \bar{m} + v_a^e \bar{a}) \bar{m} v_a^e \bar{a}_x \\ &\quad + h.o.t. \end{aligned}$$

The terms in this expression with the same interactions can be taken together. Doing this we can rewrite the Taylor expansion as

$$\begin{aligned} &d_m v(m, a) m v_a(m, a) a_x \\ &= \rho_a \bar{a}_x + \rho_{ma} \bar{m} \bar{a}_x + \rho_{aa} \bar{a} \bar{a}_x + \rho_{mma} \bar{m}^2 \bar{a}_x + \rho_{maa} \bar{m} \bar{a} \bar{a}_x + \rho_{aaa} \bar{a}^2 \bar{a}_x. \quad (3.24) \end{aligned}$$

Here the constants ρ denote the coefficient before the relevant interacting terms. More precisely these constants are defined as

$$\begin{aligned} \rho_a/d_m &:= v^e m_e v_a^e \\ \rho_{ma}/d_m &:= v^e m_e v_{ma}^e + v^e v_a^e + v_m^e m_e v_a^e \\ \rho_{aa}/d_m &:= v^e m_e v_{aa}^e + v_a^e m_e v_a^e \\ \rho_{mma}/d_m &:= v^e m_e v_{mma}^e / 2 + v_{mm}^e m_e v_a^e / 2 + v^e v_{ma}^e + v_m^e m_e v_{ma}^e + v_m^e v_a^e \\ \rho_{maa}/d_m &:= v^e m_e v_{maa}^e + v_{ma}^e m_e v_a^e + v^e v_{aa}^e + v_m^e m_e v_{aa}^e + v_a^e m_e v_{ma}^e + v_a^e v_a^e \\ \rho_{aaa}/d_m &:= v^e m_e v_{aaa}^e / 2 + v_{aa}^e m_e v_a^e / 2 + v_a^e m_e v_{aa}^e \end{aligned}$$

Now we turn our attention to the other term, $d_m v(v + mv_m) m_x$. With the same approach with which we have tackled the last term, we can also approximate this one:

$$\begin{aligned}
& v(v + mv_m) m_x \\
= & \left[v^e + (v_m^e \bar{m} + v_a^e \bar{a}) + \frac{1}{2}(v_{mm}^e \bar{m}^2 + 2v_{ma}^e \bar{m} \bar{a} + v_{aa}^e \bar{a}^2) \right] \\
& \left\{ \left[v^e + (v_m^e \bar{m} + v_a^e \bar{a}) + \frac{1}{2}(v_{mm}^e \bar{m}^2 + 2v_{ma}^e \bar{m} \bar{a} + v_{aa}^e \bar{a}^2) \right] \right. \\
& \left. + [m_e + \bar{m}] \left[v_m^e + (v_{mm}^e \bar{m} + v_{ma}^e \bar{a}) + \frac{1}{2}(v_{mmm}^e \bar{m}^2 + 2v_{mma}^e \bar{m} \bar{a} + v_{maa}^e \bar{a}^2) \right] \right\} \bar{m}_x
\end{aligned}$$

From this we find the following approximate expression:

$$\begin{aligned}
& d_m v(v + mv_m) m_x \\
= & \sigma_m \bar{m}_x + \sigma_{mm} \bar{m} \bar{m}_x + \sigma_{am} \bar{a} \bar{m}_x + \sigma_{mmm} \bar{m}^2 \bar{m}_x + \sigma_{mam} \bar{m} \bar{a} \bar{m}_x + \sigma_{aam} \bar{a}^2 \bar{m}_x
\end{aligned}$$

This time these constants are defined as

$$\begin{aligned}
\sigma_m/d_m &:= v^e(v^e + m_e v_m^e) \\
\sigma_{mm}/d_m &:= v_m^e(v^e + m_e v_m^e) + v^e v_m^e + v^e m_e v_{mm}^e + v^e v_m^e \\
\sigma_{am}/d_m &:= v_a^e(v^e + m_e v_m^e) + v^e v_a^e + v^e m_e v_{ma}^e \\
\sigma_{mmm}/d_m &:= \frac{1}{2} v_{mm}^e(v^e + m_e v_m^e) + \frac{1}{2} v^e v_{mm}^e + \frac{1}{2} v^e m_e v_{mmm}^e + v^e v_{mm}^e \\
&+ v_m^e(2v_m^e + m_e v_{mm}^e) \\
\sigma_{mam}/d_m &:= v_{ma}^e(v^e + m_e v_m^e) + v^e v_{ma}^e + v^e m_e v_{mma}^e + v^e v_{ma}^e \\
&+ v_m^e(v_a^e + m_e v_{ma}^e) + v_a^e(2v_m^e + m_e v_{mm}^e) \\
\sigma_{aam}/d_m &:= \frac{1}{2} v_{aa}^e(v_e + m_e v_m^e) + \frac{1}{2} v^e v_{aa}^e + \frac{1}{2} v^e m_e v_{maa}^e + v_a^e(v_a^e + m_e v_{ma}^e)
\end{aligned}$$

With this information about the expansions of the relevant terms in our original partial differential equation described in equation (3.23) we know what interactions act up to cubic interactions. We use the notation as defined in the previous paragraphs. Note that in our derivation of the expansions we have forgotten about the differential operator. In the complete system this differential operator is crucial though - so we must not forget about it. The system, with only interactions up to cubic order, is (where we have written m and a again, instead of \bar{m} and \bar{a} for notational simplicity)

$$\left\{ \begin{array}{l} m_t = \sigma_m m_{xx} + \sigma_{mm} m_{mm} m_{xx} + \sigma_{am} a m_{xx} + \sigma_{mmm} m^2 m_{xx} + \sigma_{mam} a m_{xx} \\ + \sigma_{aam} a^2 m_{xx} + \sigma_{mm} m_x^2 + 2\sigma_{mmm} m m_x^2 + \sigma_{mam} a m_x^2 \\ + \rho_a a_{xx} + \rho_m m a_{xx} + \rho_{aa} a a_{xx} + \rho_{mma} m^2 a_{xx} + \rho_{maa} m a a_{xx} + \rho_{aaa} a^2 a_{xx} \\ + \rho_{aa} a_x^2 + \rho_{maa} m a_x^2 + 2\rho_{aaa} a a_x^2 \\ + (\sigma_{am} + \rho_{ma}) a x m_x + (\sigma_{mam} + 2\rho_{mma}) m m_x a_x + (2\sigma_{aam} + \rho_{maa}) a m_x a_x \\ - m_{xxxx} \\ + \varepsilon H_m^e m + \varepsilon H_a^e a + \varepsilon H_{mm}^e / 2m^2 + \varepsilon H_{ma}^e m a + \varepsilon H_{aa}^e / 2a^2 \\ + \varepsilon H_{mmm}^e / 6m^3 + \varepsilon H_{mma}^e / 2m^2 a + \varepsilon H_{maa}^e / 2ma^2 + \varepsilon H_{aaa}^e / 6a^3; \\ a_t = \varepsilon a_{xx} + \varepsilon G_m^e m + \varepsilon G_a^e a + \varepsilon G_{mm}^e / 2m^2 + \varepsilon G_{am}^e m a + \varepsilon G_{aa}^e / 2a^2 \\ + \varepsilon G_{mmm}^e / 6m^3 + \varepsilon G_{mma}^e / 2m^2 a + \varepsilon G_{maa}^e / 2ma^2 + \varepsilon G_{aaa}^e / 6a^3. \end{array} \right.$$

As this is a large expansion it is easier for the eye if we introduce another few parameters, so that we do need to write as few coefficients as possible. We write $h_m := \varepsilon H_m^e$, $h_{mm} := \varepsilon H_{mm}^e/2$ and so on (and in a similar way g for the coefficients with G). In addition to that we also write

$$\begin{aligned}\tau_{ma} &:= \sigma_{am} + \rho_{ma}; \\ \tau_{mma} &:= \sigma_{mam} + 2\rho_{mma}; \\ \tau_{ama} &:= 2\sigma_{aam} + \rho_{maa}.\end{aligned}$$

With these coefficients defined we can write the governing system in the most easily readable form. In addition we have also chosen to color-code the equation: all m 's in the equation are blue, while all a 's are in red. We must also recall that we have perturbed our system a little bit, since we have chosen $\mu_{11} = \mu_{11,c} + \phi^2 r$ and $\mu_{21} = \mu_{21,c} + \phi^2 s$. Therefore the system also includes two terms involving ϕ^2 . We must note that due to this perturbation we should also get terms of the form $\phi^2 mm_{xx}$. These terms however only start to play a role at higher orders and therefore we can forget about them in this analysis. Hence the system becomes (note that the bold terms correspond to the bifurcated parameters) up to cubic order (and therefore up to the $\mathcal{O}(\phi^3)$ -level):

$$\left\{ \begin{array}{l} \mathbf{m}_t = \sigma_m \mathbf{m}_{xx} + \sigma_{mm} \mathbf{m} \mathbf{m}_{xx} + \sigma_{am} \mathbf{a} \mathbf{m}_{xx} + \sigma_{mmm} \mathbf{m}^2 \mathbf{m}_{xx} + \sigma_{mam} \mathbf{m} \mathbf{a} \mathbf{m}_{xx} \\ \quad + \sigma_{aam} \mathbf{a}^2 \mathbf{m}_{xx} + \sigma_{mm} \mathbf{m}_x^2 + 2\sigma_{mmm} \mathbf{m} \mathbf{m}_x^2 + \sigma_{mam} \mathbf{a} \mathbf{m}_x^2 \\ \quad + \rho_a \mathbf{a}_{xx} + \rho_{ma} \mathbf{m} \mathbf{a}_{xx} + \rho_{aa} \mathbf{a} \mathbf{a}_{xx} + \rho_{mma} \mathbf{m}^2 \mathbf{a}_{xx} + \rho_{maa} \mathbf{m} \mathbf{a} \mathbf{a}_{xx} \\ \quad + \rho_{aaa} \mathbf{a}^2 \mathbf{a}_{xx} + \rho_{aa} \mathbf{a}_x^2 + \rho_{maa} \mathbf{m} \mathbf{a}_x^2 + 2\rho_{aaa} \mathbf{a} \mathbf{a}_x^2 \\ \quad + \tau_{ma} \mathbf{m}_x \mathbf{a}_x + \tau_{mma} \mathbf{m} \mathbf{m}_x \mathbf{a}_x + \tau_{ama} \mathbf{a} \mathbf{m}_x \mathbf{a}_x \\ \quad - \mathbf{m}_{xxxx} + \mathbf{r} \phi^2 \mathbf{m}_{xx} + \mathbf{s} \phi^2 \mathbf{a}_{xx} \\ \quad + h_m \mathbf{m} + h_a \mathbf{a} + h_{mm} \mathbf{m}^2 + h_{ma} \mathbf{m} \mathbf{a} + h_{aa} \mathbf{a}^2 \\ \quad + h_{mmm} \mathbf{m}^3 + h_{mma} \mathbf{m}^2 \mathbf{a} + h_{maa} \mathbf{m} \mathbf{a}^2 + h_{aaa} \mathbf{a}^3 \\ \mathbf{a}_t = \varepsilon \mathbf{a}_{xx} + g_m \mathbf{m} + g_a \mathbf{a} + g_{mm} \mathbf{m}^2 + g_{ma} \mathbf{m} \mathbf{a} + g_{aa} \mathbf{a}^2 \\ \quad + g_{mmm} \mathbf{m}^3 + g_{mma} \mathbf{m}^2 \mathbf{a} + g_{maa} \mathbf{m} \mathbf{a}^2 + g_{aaa} \mathbf{a}^3 \end{array} \right. \quad (3.27)$$

In the next section we use this system, with only interactions up to cubic ones, to perform the weakly non linear analysis of the system. This gives us an equation that describes the dynamics of the amplitude $A(\xi, \tau)$, which in turn gives us the desired description of the patterns that arise in our system.

3.3.5 Weakly non linear stability analysis

We now do the tedious calculation that gives the modulation equations. We derive the equations at various $\phi^a E^b$ -levels. Note that we skip the $E^1 \phi$ level here, as this is just the linearized equation, which we have already studied extensively in the previous sections.

The $E^0 \phi^2$ -level

First we find at the $E^0 \phi^2$ -level the following system:

$$\begin{cases} 0 &= h_m X_{02} + h_a Y_{02} + 2\alpha |A|^2 \\ 0 &= g_m X_{02} + g_a Y_{02} + 2\beta |A|^2 \end{cases}$$

where

$$\begin{aligned}\alpha &:= h_{mm}v_{11}^2 + h_{ma}v_{11}v_{12} + h_{aa}v_{12}^2 \\ \beta &:= g_{mm}v_{11}^2 + g_{ma}v_{11}v_{12} + g_{aa}v_{12}^2\end{aligned}$$

Note that in these expressions we don't have any interactions of the form mm_{xx} or m_x^2 contributing. This can be explained by looking at $mm_{xx} + m_x^2 = (mm_x)_x$. Since we need mm_x to be a wave E^0 we find that the derivative vanishes at this $\mathcal{O}(\phi^2)$ level. Therefore we won't need to worry about these ugly terms at this level, yet.

When $h_m g_a - h_a g_m \neq 0$ (Note that an equality can never occur, since this would imply that the linear stability analysis already would have found that the wavelength $k = 0$ is unstable. So we can safely assume that $h_m g_a - h_a g_m \neq 0$.), we have the following solution:

$$\begin{pmatrix} X_{02} \\ Y_{02} \end{pmatrix} = \frac{2|A|^2}{h_m g_a - h_a g_m} \begin{pmatrix} h_a \beta - g_a \alpha \\ g_m \alpha - h_m \beta \end{pmatrix}$$

The $E^2\phi^2$ -level

At the $E^2\phi^2$ -level we obtain the system

$$\begin{cases} 0 &= h_m X_{22} + h_a Y_{22} - 4k_c^2 \sigma_m X_{22} - 4k_c^2 \rho_a Y_{22} - 16k_c^4 X_{22} + (\alpha + \hat{\alpha}) A^2 \\ 0 &= g_m X_{22} + g_a Y_{22} - 4k_c^2 \varepsilon Y_{22} + \beta A^2 \end{cases}$$

where

$$\hat{\alpha} := -2k_c^2 (\sigma_{mm} v_{11}^2 + \rho_{aa} v_{12}^2 + (\sigma_{am} + \rho_{ma}) v_{11} v_{12}).$$

The solution to this system is

$$\begin{pmatrix} X_{22} \\ Y_{22} \end{pmatrix} = \frac{A^2}{D_{22}} \begin{pmatrix} (h_a - 4k_c^2 \rho_a) \beta - (g_a - 4k_c^2 \varepsilon) (\alpha + \hat{\alpha}) \\ g_m (\alpha + \hat{\alpha}) - (h_m - 4k_c^2 \sigma_m - 16k_c^4) \beta \end{pmatrix}$$

where

$$D_{22} := (h_m - 4k_c^2 \sigma_m - 16k_c^4) (g_a - 4k_c^2 \varepsilon) - (h_a - 4k_c^2 \rho_a) g_m$$

For this to make sense we need to have that the denominator D_{22} is not equal to zero, which it is not, because the determinant of the critical matrix only vanishes at the wavelength $k = k_c$ and therefore not at the wavelength $k = 2k_c$, which is essentially what the denominator is in this expression.

The $E^1\phi^2$ -level

At the $E^1\phi^2$ level we see that all the higher order interaction terms vanish and we are only left with the linear terms. Because we are now working on the $\mathcal{O}(\phi^2)$ -level we also must take the derivative of the amplitude A into account. Therefore at the $E^1\phi^2$ -level we obtain the following set of equations:

$$\begin{cases} 0 &= (h_m - \sigma_m k_c^2 - k_c^4) X_{12} + (h_a - \rho_a k_c^2) Y_{12} + 2ik_c A_\xi (\sigma_m v_{11} + \rho_a v_{12} + 2k_c^2 v_{11}) \\ 0 &= g_m X_{12} + (g_a - \varepsilon k_c^2) Y_{12} + 2ik_c A_\xi v_{12} \varepsilon \end{cases}$$

Now, since $h_m = \varepsilon\mu_{10}$, $h_a = \varepsilon\mu_{20}$, $g_m = \varepsilon\mu_{30}$, $g_a = \varepsilon\mu_{40}$, $\sigma_m = \mu_{11}$ and $\rho_a = \mu_{21}$ we can rewrite this in terms of the critical matrix \mathcal{M}_c as follows:

$$\mathcal{M}_c \begin{pmatrix} X_{12} \\ Y_{12} \end{pmatrix} = -2ik_c A_\xi \begin{pmatrix} \mu_{11}v_{11} + \mu_{21}v_{12} + 2k_c^2 v_{11} \\ \varepsilon v_{12} \end{pmatrix}$$

As we have seen before, we can only solve this for (X_{12}, Y_{12}) whenever the vector $(\mu_{11}v_{11} + \mu_{21}v_{12} + 2k_c^2 v_{11}, \varepsilon v_{12})$ is in the span of the eigenvector corresponding to the non-zero eigenvalue. We can check that this is indeed the case, by substitution of this vector in the solvability condition of equation (3.17). We obtain by using the relation for the eigenvector $\vec{v}_1 = (v_{11}, v_{12})$ of equation (3.16)

$$\begin{aligned} & \mu_{30}((\mu_{11} + 2k_c^2)v_{11} + \mu_{21}v_{12}) + (k_c^4 + \mu_{11}k_c^2 - \varepsilon\mu_{10})v_{12} \\ &= v_{12}((\mu_{11} + 2k_c^2)(k_c^2 - \mu_{40}) + \mu_{21}\mu_{30} + k_c^4 + \mu_{11}k_c^2 - \varepsilon\mu_{10}) \\ &= 3k_c^4 + 2k_c^2(\mu_{11} - \mu_{40}) + (\mu_{21}\mu_{30} - \mu_{11}\mu_{40} - \varepsilon\mu_{10}) \\ &= 0 \end{aligned}$$

In this last step we use the fact that the derivative of the determinant of \mathcal{M} has a minimum in the wavelength k_c . This is more apparent when we change back to the greek symbols we introduced in equation (3.7). Then we see that $\beta = \mu_{11} - \mu_{40}$, $\gamma = \mu_{21}\mu_{30} - \mu_{11}\mu_{40} - \varepsilon\mu_{10}$ and that the determinant of \mathcal{M} is $k^6 + \beta k^4 + \gamma k^2 + \delta$. Thus clearly $3k_c^4 + 2k_c^2\beta + \gamma = 0$ in the critical wavelength $k = k_c$.

Now since the system at the $E^1\phi^2$ level satisfies the solvability condition we can introduce a higher order amplitude A_2 , which again depends on the slow spatial and time variables χ and τ . The expression for (X_{12}, Y_{12}) then can be expressed as

$$\begin{pmatrix} X_{12} \\ Y_{12} \end{pmatrix} = -2ik_c \zeta v_{12} A_\xi \begin{pmatrix} 1 \\ 0 \end{pmatrix} + \begin{pmatrix} v_{11} \\ v_{12} \end{pmatrix} A_2(\chi, \tau) \quad (3.28)$$

where

$$\begin{aligned} \zeta v_{12} &:= \frac{((\mu_{11} + 2k_c^2 - \varepsilon)v_{11} + \mu_{21}v_{12})}{\text{Tr}\mathcal{M}_c} \\ &= \frac{(\mu_{11} + 2k_c^2 - \varepsilon)(k_c^2 - \mu_{40}) + \mu_{21}\mu_{30}}{\mu_{30} \text{Tr}\mathcal{M}_c} v_{12}. \end{aligned}$$

The $E^1\phi^3$ -level

The final step in the derivation of the modulation equation is to find the system at the $E^1\phi^3$ -level and then apply the solvability condition to the resulting system. At this level we find that the system becomes

$$\begin{aligned} \mathcal{M}_c \begin{pmatrix} X_{13} \\ Y_{13} \end{pmatrix} &= A_\tau \begin{pmatrix} v_{11} \\ v_{12} \end{pmatrix} - \begin{pmatrix} [2\sigma_m ik_c + 4ik_c^3]X_{12,\xi} + 2\rho_a ik_c Y_{12,\xi} \\ 2\varepsilon ik_c Y_{12,\xi} \end{pmatrix} \\ &- \begin{pmatrix} v_{11}\sigma_m + 6k_c^2 v_{11} + \rho_a v_{12} \\ \varepsilon v_{12} \end{pmatrix} A_{\xi\xi} - \begin{pmatrix} Z_m \\ Z_a \end{pmatrix} |A|^2 A - \begin{pmatrix} -(rv_{11} + sv_{12})k_c^2 \\ 0 \end{pmatrix} A \end{aligned} \quad (3.29)$$

where Z_m and Z_a are parameters that are defined as

$$\begin{aligned}
Z_m = & v_{11}^3 [-3k_c^2 \sigma_{mmm} + 2k_c^2 \sigma_{mmm} + 3h_{mmm}] \\
& + v_{11}^2 v_{12} [-3k_c^2 \sigma_{mam} - 3k_c^2 \rho_{mma} + k_c^2 \sigma_{mam} + k_c^2 \tau_{mma} + 3h_{mma}] \\
& + v_{11} v_{12}^2 [-3k_c^2 \sigma_{aam} - 3k_c^2 \rho_{maa} + k_c^2 \rho_{maa} + k_c^2 \tau_{ama} + 3h_{maa}] \\
& + v_{12}^3 [-3k_c^2 \rho_{aaa} + 2k_c^2 \rho_{aaa} + 3h_{aaa}] \\
& + v_{11} x_{02} [-k_c^2 \sigma_{mm} + 2h_{mm}] \\
& + v_{11} y_{02} [-k_c^2 \sigma_{am} + h_{ma}] \\
& + v_{12} x_{02} [-k_c^2 \rho_{ma} + h_{ma}] \\
& + v_{12} y_{02} [-k_c^2 \rho_{aa} + 2h_{aa}] \\
& + v_{11} x_{22} [-k_c^2 \sigma_{mm} + 2h_{mm}] \\
& + v_{11} y_{22} [\sigma_{am} k_c^2 - 2\rho_{ma} k_c^2 + h_{ma}] \\
& + v_{12} x_{22} [-2\sigma_{am} k_c^2 + \rho_{ma} k_c^2 + h_{ma}] \\
& + v_{12} y_{22} [-k_c^2 \rho_{aa} + 2h_{aa}] \\
Z_a = & 3v_{11}^3 h_{mmm} + 3v_{11}^2 v_{12} h_{mma} + 3v_{11} v_{12}^2 h_{maa} + 3v_{12}^3 h_{aaa} \\
& + 2g_{mm} v_{11} x_{02} + g_{ma} v_{11} y_{02} + g_{ma} v_{12} x_{02} + 2g_{aa} v_{12} y_{02} \\
& + 2g_{mm} v_{11} x_{22} + g_{ma} v_{11} y_{22} + g_{ma} v_{12} x_{22} + 2g_{aa} v_{12} y_{22}
\end{aligned}$$

Here the parameters x_{02}, y_{02}, x_{22} and y_{22} are defined by the following relations:

$$\begin{pmatrix} X_{02} \\ Y_{02} \end{pmatrix} = \begin{pmatrix} x_{02} \\ y_{02} \end{pmatrix} |A|^2 \text{ and } \begin{pmatrix} X_{22} \\ Y_{22} \end{pmatrix} = \begin{pmatrix} x_{22} \\ y_{22} \end{pmatrix} A^2.$$

Now we can use the expression for (X_{12}, Y_{12}) that we found before in equation (3.28). From this expression we can see that the derivative with respect to ξ satisfies:

$$\begin{pmatrix} X_{12,\xi} \\ Y_{12,\xi} \end{pmatrix} = \begin{pmatrix} -2ik_c \zeta v_{12} A_{\xi\xi} \\ 0 \end{pmatrix} + \begin{pmatrix} v_{11} \\ v_{12} \end{pmatrix} A_{2,\xi}$$

We can incorporate this in the expression that we found at this $E^1 \phi^3$ -level. We thus find the following system

$$\begin{aligned}
\mathcal{M}_c \begin{pmatrix} X_{13} \\ Y_{13} \end{pmatrix} = & \begin{pmatrix} (rv_{11} + sv_{12})k_c^2 \\ 0 \end{pmatrix} A + A_\tau \begin{pmatrix} v_{11} \\ v_{12} \end{pmatrix} \\
& - 2ik_c \begin{pmatrix} [\sigma_m + 2k_c^2]v_{11} + \rho_a v_{12} \\ \varepsilon v_{12} \end{pmatrix} A_{2,\xi} - \begin{pmatrix} Z_m \\ Z_a \end{pmatrix} |A|^2 A \\
& - \begin{pmatrix} v_{11}\sigma_m + 6k_c^2 v_{11} + \rho_a v_{12} + 4\zeta k_c^2 [\sigma_m + 2k_c^2] v_{12} \\ \varepsilon v_{12} \end{pmatrix} A_{\xi\xi}.
\end{aligned} \tag{3.30}$$

This last equation is again of the form $\mathcal{M}_c x = b$. Thus we know it can only be solved when b satisfies the solvability condition of equation (3.17). Since there are various terms in the system that we obtained at this $E^1 \phi^3$ -level (i.e. terms with $A_{2,\xi}, A, |A|^2 A$ and A_τ) we can just apply the solvability condition on these various terms and later add them to obtain the amplitude equation.

$A_{2,\xi}$: For this term we need to apply the solvability condition on the vector $([\sigma_m + 2k_c^2]v_{11} + \rho_a v_{12}, \varepsilon v_{12})^T$. By noting that $\sigma_m = \mu_{11}$ and $\rho_a = \mu_{21}$ we

find the following expression after applying the solvability condition:

$$\begin{aligned}
& (\mu_{11} + 2k_c^2)\varepsilon\mu_{30}v_{11} + \varepsilon\mu_{30}\mu_{21}v_{12} + (k_c^4 + \mu_{11}k_c^2 - \varepsilon\mu_{10})\varepsilon v_{12} \\
&= \varepsilon v_{12}((\mu_{11} + 2k_c^2)(k_c^2 - \mu_{40}) + \mu_{30}\mu_{21} + k_c^4 + \mu_{11}k_c^2 - \varepsilon\mu_{10}) \\
&= \varepsilon v_{12}(3k_c^4 + 2(\mu_{11} - \mu_{40})k_c^2 + \mu_{30}\mu_{21} - \mu_{11}\mu_{40} - \varepsilon\mu_{10}) \\
&= 0
\end{aligned}$$

In the last step we once more have identified the expression as the condition that the determinant of \mathcal{M} has a minimum in the wavelength $k = k_c$. That is, in our greek parameters we can rewrite it to $\varepsilon v_{12}(3\alpha k_c^4 + 2\beta k_c^2 + \gamma)$, which is the expression for the derivative of the determinant, which needs to vanish at the critical wavelength k_c .

A_τ : Now the relevant vector is simply (v_{11}, v_{12}) . Thus the coefficient before A_τ in the amplitude equation is

$$\begin{aligned}
& \varepsilon\mu_{30}v_{11} + (k_c^4 + \mu_{11}k_c^2 - \varepsilon\mu_{10})v_{12} \\
&= v_{12}(k_c^4 + k_c^2(\mu_{11} + \varepsilon) - \varepsilon(\mu_{10} + \mu_{40})) \\
&= -v_{12}\text{Tr}\mathcal{M}_c
\end{aligned}$$

This last step can be seen most easily when we convert the parameters to the greek parameters ζ, η and θ . Then it is immediately clear that it really is the trace.

$A_{\xi\xi}$: For the coefficient corresponding to $A_{\xi\xi}$ the following vector is relevant

$$\left(\begin{array}{c} v_{11}\mu_{11} + 6k_c^2v_{11} + \mu_{21}v_{12} + 4\zeta k_c^2(\mu_{11} + 2k_c^2)v_{12} \\ \varepsilon v_{12} \end{array} \right)$$

To make life more easy we can recall that at the $E^1\phi^2$ -level we have verified that the vector $(\mu_{11}v_{11} + \mu_{21}v_{12} + 2k_c^2v_{11}, \varepsilon v_{12})$ is contained in the span of the eigenvector corresponding to the eigenvalue $\text{Tr}\mathcal{M}_c$. Therefore we can subtract this vector without modifying the solvability equation. Thus we can just apply this condition on the following vector instead:

$$\left(\begin{array}{c} 4k_c^2v_{11} + 4\zeta k_c^2(\mu_{11} + 2k_c^2)v_{12} \\ 0 \end{array} \right)$$

That results in the following coefficient for the term:

$$\begin{aligned}
& \varepsilon\mu_{30}(4k_c^2v_{11} + 4\zeta k_c^2(\mu_{11} + 2k_c^2)v_{12}) \\
&= \varepsilon v_{12}(4k_c^2(k_c^2 - \mu_{40}) + 4\mu_{30}\zeta k_c^2(\mu_{11} + 2k_c^2))
\end{aligned}$$

$|A|^2 A$: For this term the vector is (Z_m, Z_a) and the solvability condition then gives the coefficient

$$\varepsilon\mu_{30}Z_m + (k_c^4 + \mu_{11}k_c^2 - \varepsilon\mu_{10})Z_a$$

A : For this last term the vector is $([rv_{11} + sv_{12}]k_c^2, 0)^T$. Applied to the solvability condition this results to the coefficient

$$\varepsilon\mu_{30}k_c^2[-rv_{11} - sv_{12}] = \varepsilon v_{12}k_c^2[-r\mu_{40} + rk_c^2 + s\mu_{30}]$$

In the previous paragraphs we have determined the coefficients of the various terms in the amplitude equation (by applying the solvability condition). We can now, finally, combine all the terms and find an expression for our amplitude equation. We find then the amplitude equation as

$$\frac{\text{Tr } M_c}{\varepsilon} A_\tau = B_A A + B_{xx} A_{\xi\xi} + B_{AAA} |A|^2 A,$$

where

$$\begin{aligned} B_A &= k_c^2(rk_c^2 - r\mu_{40} + s\mu_{30}); \\ B_{xx} &= -4k_c^2((k_c^2 - \mu_{40}) + \mu_{30}\zeta(\mu_{11} + 2k_c^2)); \\ B_{AAA} &= \frac{-1}{\varepsilon v_{12}} (\varepsilon\mu_{30}Z_m + (k_c^4 + \mu_{11}k_c^2 - \varepsilon\mu_{10})Z_a). \end{aligned}$$

With standard rescaling we can easily rewrite this partial differential equation to the following one:

$$A_\tau = RA + bA_{\xi\xi} + h|A|^2 A \quad (3.31)$$

where

$$R = \frac{\varepsilon B_A}{\text{Tr } M_c} = \frac{\varepsilon k_c^2(rk_c^2 - r\mu_{40} + s\mu_{30})}{\text{Tr } M_c}; \quad (3.32)$$

$$b = \frac{\varepsilon B_{xx}}{\text{Tr } M_c} = \frac{-4\varepsilon k_c^2}{\text{Tr } M_c} [k_c^2 - \mu_{40} + \mu_{30}\zeta(\mu_{11} + 2k_c^2)]; \quad (3.33)$$

$$h = \frac{\varepsilon B_{AAA}}{\text{Tr } M_c} = \frac{\varepsilon\mu_{30}Z_m + (k_c^4 + \mu_{11}k_c^2 - \varepsilon\mu_{10})Z_a}{-v_{12} \text{Tr } M_c}. \quad (3.34)$$

We thus have established now that the dynamics near the critical bifurcation line $\Gamma_{\pm,d,\pm}$ can be described with the Ginzburg-Landau equation as modulation equation for the amplitude of the most critical wave $e^{ik_c x}$.

With this amplitude equation we can find solutions of the original, full, system of equation (3.1) of the form

$$(m(x, t), a(x, t)) = (m_e, a_e) + A(\varepsilon x, \varepsilon^2 t) e^{ik_c x} \quad (3.35)$$

where the amplitude A is a solution to the found real Ginzburg-Landau equation. What kind of solutions this amplitude equation gives is determined by the signs of the parameters R , b and h . A more in-depth study of this real Ginzburg-Landau equation can be found in Appendix C.

3.4 Analytic study of the Mussel's system

In the previous sections of this Chapter 3 we studied the model of equation (3.1) as a general model, that is applicable to a vast variety of population models. In this section we give an example of such an application, as we use it to model a mussel-algae system.

The general model, in equation (3.1) is however not directly applicable, as we still need to fill in the forms for the interactions terms H and G . In Section 1.1.3 we have seen that we need to choose these as

$$H(m, a) = ecam - \hat{d}_m \frac{k_m}{k_m + m} m;$$

$$G(m, a) = (A_{up} - a)\rho - \frac{c}{H} am,$$

where all parameters are positive for ecological reasons.

We can substitute these terms in our general model. However, we would end up with very many parameters in this model. Therefore we scale the parameters to reduce this number. In Section 1.2 we used a scaling for the reaction-diffusion type of description. We cannot use the exact same scaling now, since we have to deal with the movement dependent speed, which carries additional parameters. We can however use a scaling that is very similar.

When we use the ‘quadratic fit’ movement speed $v = c_1 m^2 + c_2 m + c_3 - da$ (see Section 1.1.4) it turns out we can use the following scalings: $M = \sqrt{\frac{c_1}{c_3}} m$, $A = \frac{a}{A_{up}}$, $\tau = \hat{d}_m t$, $(x, y) = \sqrt{\frac{d_m}{\hat{d}_m}} c_3(x', y')$. We must also define the following parameters as well:

$$\begin{aligned} \tilde{\beta} &:= \frac{c_2}{\sqrt{c_1 c_3}} & \nu &:= \frac{1}{k_m} \sqrt{\frac{c_3}{c_1}} \\ \tilde{d} &:= \frac{d_1 A_{up}}{c_3} & D &:= \frac{d_a}{d_m c_3^2} \\ \hat{\kappa} &:= \kappa \frac{\hat{d}_m}{d_m} \frac{1}{c_3^4} & \hat{\alpha} &:= \frac{\rho}{\hat{d}_m} \\ r &:= \frac{ec A_{up}}{\hat{d}_m} & \hat{\gamma} &:= \frac{c}{H} \frac{1}{\hat{d}_m} \sqrt{\frac{c_3}{c_1}} \end{aligned}$$

With this scaling the model for our specific case, for the description of a mussel-algae system that incorporates the density dependent movement speed of the mussels, becomes

$$\begin{cases} \frac{\partial M}{\partial \tau} &= \nabla' [V(V + M \frac{\partial V}{\partial M}) \nabla' M - VM \frac{\partial V}{\partial A} \nabla' A - \hat{\kappa} \nabla' \Delta' M] + \varepsilon \left[rAM - \frac{M}{1+\nu M} \right] \\ \frac{\partial A}{\partial \tau} &= \varepsilon D \Delta' A + \varepsilon [(1-A)\hat{\alpha} - \hat{\gamma} AM] \end{cases} \quad (3.36)$$

Here V is the redefined speed (i.e. $V = M^2 + \tilde{\beta}M + 1 - \tilde{d}A$). A similar approach is also possible for the ‘piecewise’ description of the density dependent movement speed, which results in a redefined speed as defined in equation (1.5). In the rest of this section we just write v for the redefined speed for notational convenience.

In the remainder of this section we analyse this model of equation (3.36). To do so we use the general results that we have developed in Section 3.1, Section 3.2 and Section 3.3. We start by finding the steady states in Section 3.4.1 and subsequently determine the bifurcation lines in the $(\tilde{\beta}, \tilde{d})$ -plane in Section 3.4.2. Finally we discuss the Ginzburg-Landau (amplitude) equation for this model in Section 3.4.3

Table 3.2 – In this table we have put the conditions under which the important terms are either positive or negative. In order for our candidate uniform steady state to be realistically possible, we need that all terms are either positive or negative.

term	positive	negative
$r - 1$	$r > 1$	$r < 1$
$\hat{\gamma} - \hat{\alpha}\nu r$	$r < \frac{\hat{\gamma}}{\hat{\alpha}\nu}$	$r > \frac{\hat{\gamma}}{\hat{\alpha}\nu}$
$\hat{\gamma} - \hat{\alpha}\nu$	$\hat{\alpha} < \frac{\hat{\gamma}}{\nu}$	$\hat{\alpha} > \frac{\hat{\gamma}}{\nu}$
all together	$1 < r < \frac{\hat{\gamma}}{\hat{\alpha}\nu}, \hat{\alpha} < \frac{\hat{\gamma}}{\nu}$	$\frac{\hat{\gamma}}{\hat{\alpha}\nu} < r < 1, \hat{\alpha} > \frac{\hat{\gamma}}{\nu}$

3.4.1 Uniform Steady States and their stability

Following the general procedure of Section 3.1 we must first determine all possible uniform steady states. To do this we must solve the coupled equations

$$\begin{cases} 0 = H(M, A) = M\left(rA - \frac{1}{1+\nu M}\right); \\ 0 = G(M, A) = (1-A)\hat{\alpha} - \hat{\gamma}AM. \end{cases}$$

There are two possible solutions to this problem. The first is easily identified as $(M_e, A_e) = (0, 1)$. With a bit more effort we can also see that another solution is $(M_e, A_e) = \left(\hat{\alpha}\frac{r-1}{\hat{\gamma}-\hat{\alpha}\nu r}, \frac{1}{r}\frac{\hat{\gamma}-\hat{\alpha}\nu r}{\hat{\gamma}-\hat{\alpha}\nu}\right)$.

So we have two possible candidates for uniform steady states of our mussel-algae interaction partial differential equation. However these solutions are not necessarily possible in reality. To ensure this, we must have that $M_e \geq 0$ and $A_e \geq 0$. Moreover, since A is bounded by the concentration of algae in higher sections of the water, we also must have that $A_e \leq 1$.

Clearly the solution $(M_e, A_e) = (0, 1)$ obeys all of these conditions. For the other possible uniform steady state this is not true in general. The non-negativity condition implies that we need $\text{sgn}(r-1) = \text{sgn}(\hat{\gamma} - \hat{\alpha}\nu r) = \text{sgn}(\hat{\gamma} - \hat{\alpha}\nu)$, since the parameters $\hat{\alpha}$ and r are positive. In Table 3.2 we have identified under what circumstances these terms have which sign. The other condition, $A_e \leq 1$, is coincidentally automatically obeyed when all terms have the same sign.

Proceeding with our general approach we now must find the linearized system. We can use the general form that we have found in equation (3.3). For this we however need to compute the derivatives of our interaction terms. These interaction terms turn out to be given by

$$\begin{aligned} \frac{\partial H}{\partial M}(M, A) &= rA - \frac{1}{(1+\nu M)^2} & \frac{\partial H}{\partial A}(M, A) &= rM \\ \frac{\partial G}{\partial M}(M, A) &= -\hat{\gamma}A & \frac{\partial G}{\partial A}(M, A) &= -\hat{\alpha} - \hat{\gamma}M \end{aligned}$$

Thus the linearized system for our specific mussel-algae system is then easily

verified to be

$$\begin{cases} \frac{\partial M}{\partial t} = & \vec{\nabla} \cdot \left[v_e (v_e + M_e \frac{\partial v_e}{\partial M}) \right] \vec{\nabla} M + v_e M_e \frac{\partial v_e}{\partial A} \vec{\nabla} A - \hat{\kappa} \vec{\nabla} \Delta M \\ & + \varepsilon \left[(r A_e - \frac{1}{(1+\nu M_e)^2}) M + r M_e A \right]; \\ \frac{\partial A}{\partial t} = & \varepsilon D \Delta A + \varepsilon [-\hat{\gamma} A_e M + (-\hat{\alpha} - \hat{\gamma} M_e) A]. \end{cases}$$

Applying the standard perturbation $(M, A) = (\bar{m}, \bar{a}) \exp[i(\vec{k}, \vec{x}) + \omega t]$ gives us the eigenvalue problem

$$\omega \begin{pmatrix} \bar{m} \\ \bar{a} \end{pmatrix} = M(\vec{k}) \begin{pmatrix} \bar{m} \\ \bar{a} \end{pmatrix}$$

where the matrix $M(\vec{k})$ is now given by

$$M(\vec{k}) = \begin{pmatrix} -\hat{\kappa} |\vec{k}|^4 - \mu_{11} |\vec{k}|^2 + \varepsilon \left[r A_e - \frac{1}{(1+\nu M_e)^2} \right] & -\mu_{21} |\vec{k}|^2 + \varepsilon r M_e \\ -\varepsilon \hat{\gamma} A_e & -\varepsilon D |\vec{k}|^2 + \varepsilon [-\hat{\alpha} - \hat{\gamma} M_e] \end{pmatrix} \quad (3.37)$$

And thus the μ -parameters as introduced in equation (3.5) can now be found by comparing the form of the matrix $M(\vec{k})$ in equation (3.37) and in equation (3.6). We thus obtain the following values

$$\begin{aligned} \mu_{10} &= r A_e - \frac{1}{(1+\nu M_e)^2} & \mu_{20} &= r M_e \\ \mu_{11} &= v_e \left(v_e + M_e \frac{\partial v_e}{\partial M} \right) & \mu_{21} &= v_e M_e \frac{\partial v_e}{\partial A} \\ \mu_{12} &= \hat{\kappa} & \mu_{40} &= -\hat{\alpha} - \hat{\gamma} M_e \\ \mu_{30} &= -\hat{\gamma} A_e & \mu_{41} &= D \end{aligned}$$

In the next subsections we first inspect the uniform steady state given by $(M_e, A_e) = (0, 1)$ and determine its stability. Then we turn to the non-trivial uniform steady state and try to determine the linear stability of this state as well.

Linear Stability of $(M_e, A_e) = (0, 1)$

To study the linear stability of the steady state $(M_e, A_e) = (0, 1)$, we first determine the form of the matrix $M(\vec{k})$ using equation (3.37). To do so, we first observe that $\mu_{21} = 0$ and $\mu_{11} = v_e^2$. Hence the matrix $M(\vec{k})$ turns out to be

$$M(\vec{k}) = \begin{pmatrix} -\hat{\kappa} |\vec{k}|^4 - v_e^2 |\vec{k}|^2 + \varepsilon(r-1) & 0 \\ -\varepsilon \hat{\gamma} & -\varepsilon D |\vec{k}|^2 - \varepsilon \hat{\alpha} \end{pmatrix}.$$

From this matrix it is clear that the eigenvalues are $\omega_1 = -\hat{\kappa} |\vec{k}|^4 - v_e^2 |\vec{k}|^2 + \varepsilon(r-1)$ and $\omega_2 = -\varepsilon D |\vec{k}|^2 - \varepsilon \hat{\alpha}$. Obviously $\omega_2 < 0$ for all possible wavelengths \vec{k} . The maximal value for ω_1 is obtained when $\vec{k} = 0$. In this case $\omega_1 = \varepsilon(r-1)$. Hence we know that $\omega_1 < 0$ when $r < 1$. Since the parameter r must be positive,

this means that the steady state $(M_e, A_e) = (0, 1)$ is linearly stable only when $0 < r < 1$.

The reasoning above already gives us a classification of the the (linear) stability of the steady state. The general approach of section 3.1 was not needed though. It is however good to check if we could obtain the same conclusion by using it.

Our first step in this is calculating the concrete values of the various μ -parameters in correspondence with equation (3.38). We find (where we also immediately indicate the signs if we are able to):

$$\begin{aligned}\mu_{10} &= (r - 1) & \mu_{20} &= 0 \\ \mu_{11} &= v_e^2 > 0 & \mu_{21} &= 0 \\ \mu_{12} &= \hat{\kappa} > 0 & \mu_{40} &= -\hat{\alpha} < 0 \\ \mu_{30} &= -\hat{\gamma} < 0 & \mu_{41} &= D > 0\end{aligned}$$

And subsequently we need to find the parameters α through δ and ζ through θ . The definitions of these parameters in equation (3.7) help us find them quickly:

$$\begin{aligned}\alpha &= \hat{\kappa}D > 0 & \zeta &= \hat{\kappa} > 0 \\ \beta &= v_e^2D + \hat{\alpha}\hat{\kappa} > 0 & \eta &= (1 - d)^2 + \varepsilon D > 0 \\ \gamma &= \hat{\alpha}v_e^2 - \varepsilon D(r - 1) & \theta &= -\varepsilon[(r - 1) - \alpha] \\ \delta &= -\varepsilon\hat{\alpha}(r - 1)\end{aligned}$$

Since we know that the critical value δ_c is either zero or positive, we know that it is necessary for δ to be positive in order for the state to be linearly stable. Since $\hat{\alpha}$ is positive, this means that we need $r < 1$.

From this necessary condition we obtain that $\gamma > 0$. Now, since β and γ are positive, we can look at Figure 3.3 to see that $\delta_c = 0$ (and not something larger than zero). Moreover, since $\eta > 0$ we know by looking at Figure 3.4 that $\theta_c = 0$. When $r > 1$ we know that $\theta > \varepsilon\hat{\alpha} > 0$ and thus this confirms that the condition $r > 1$ is also sufficient.

Hence our general approach gives us the same conclusion: when $r \in (0, 1)$ the uniform steady state $(M_e, A_e) = (0, 1)$ is linearly stable.

Linear Stability of the non-trivial uniform steady state

We now turn our attention to the more complex non-trivial uniform steady state given by $(M_e, A_e) = \left(\hat{\alpha}\frac{r-1}{\hat{\gamma}-\hat{\alpha}\nu r}, \frac{1}{r}\frac{\hat{\gamma}-\hat{\alpha}\nu r}{\hat{\gamma}-\hat{\alpha}\nu}\right)$. We skip the computation of the matrix $M(\vec{k})$ for now and immediately give the μ -parameters. We obtain

$$\mu_{10} = \frac{\nu M_e}{(1 + \nu M_e)^2} \quad \mu_{20} = r M_e \tag{3.41a}$$

$$\mu_{11} = v_e \left(v_e + M_e \frac{\partial v_e}{\partial M} \right) \quad \mu_{21} = v_e M_e \frac{\partial v_e}{\partial A} \tag{3.41b}$$

$$\mu_{12} = \hat{\kappa} \quad \mu_{40} = -\frac{\hat{\alpha}}{A_e} \tag{3.41c}$$

$$\mu_{30} = -\hat{\gamma} A_e \quad \mu_{41} = D \tag{3.41d}$$

where we have used that $rA_e - \frac{1}{(1+\nu M_e)^2} = \frac{\nu M_e}{(1+\nu M_e)^2}$ and that $-\hat{\alpha} - \hat{\gamma}M_e = -\frac{\hat{\alpha}}{A_e}$ (analogous as what is used in [17] and section 1.2).

We can then also determine the parameters $\alpha, \beta, \gamma, \delta, \zeta, \eta$ and θ again. For these we find

$$\begin{aligned}\alpha &= D\hat{\kappa} & \zeta &= \hat{\kappa} \\ \beta &= \mu_{11}D + \hat{\kappa}\frac{\hat{\alpha}}{A_e} & \eta &= \mu_{11} + \varepsilon D \\ \gamma &= \mu_{11}\frac{\hat{\alpha}}{A_e} - \mu_{21}\hat{\gamma}A_e - \varepsilon\frac{\nu M_e}{(1+\nu M_e)^2} & \theta &= \varepsilon\left[\frac{\hat{\alpha}}{A_e} - \frac{\nu M_e}{(1+\nu M_e)^2}\right] \\ \delta &= \varepsilon\frac{\hat{\alpha}(r-1)(\hat{\gamma} - \hat{\alpha}\nu r)}{\hat{\gamma} - \hat{\alpha}\nu}\end{aligned}$$

where we now have used that $\hat{\gamma}rA_eM_e - \frac{\nu M_e}{(1+\nu M_e)^2}\frac{\hat{\alpha}}{A_e} = \frac{\hat{\alpha}(r-1)(\hat{\gamma} - \hat{\alpha}\nu r)}{\hat{\gamma} - \hat{\alpha}\nu}$.

At this point it is good to recall that this uniform steady state only exists when $\text{sgn}(r-1) = \text{sgn}(\hat{\gamma} - \hat{\alpha}\nu r) = \text{sgn}(\hat{\gamma} - \hat{\alpha}\nu)$. Now, if these all where negative then we find that $\delta < 0$. However, as we found in our general analysis, we know that the critical $\delta_c \geq 0$. Hence in the case all these three terms are negative, the steady state is linear unstable.

So from this point onwards we assume that all these terms are positive. Looking back at Table 3.2 we see that this already puts the following constraints on our parameter space: we need $1 < r < \frac{\hat{\gamma}}{\hat{\alpha}\nu}$ and $\frac{\hat{\gamma}}{\hat{\alpha}\nu} > 1$.

3.4.2 Bifurcation Lines

The bifurcation diagrams that we have constructed in Section 3.2.1 are general diagrams that hold for general forms of the density dependent movement speed v . However, we want to apply it to our specific mussel-algae system. As we have seen before, in the previous section, in this specific model there is a trivial uniform steady state $(M_e, A_e) = (0, 1)$ and a non-trivial uniform stationary state $(M_e, A_e) = \left(\hat{\alpha}\frac{r-1}{\hat{\gamma}-\hat{\alpha}\nu r}, \frac{1}{r}\frac{\hat{\gamma}-\hat{\alpha}\nu r}{\hat{\gamma}-\hat{\alpha}\nu}\right)$.

We expect patterns to arise at the moment this latter, non-trivial, steady state becomes unstable. Therefore it is useful to find the bifurcation lines in this situation. In the previous sections we have seen the various possible bifurcation curves, in the general system (see Section 3.2.1 and Figure 3.5b). For this specific mussel-algae system we have already found the values of the μ -parameters for the non-trivial stationary state in equation (3.41).

We can just take these μ -values and the bifurcation lines in the $(\mu_{11}, \mu_{30}\mu_{21})$ -plane. However the real parameters of the mussel system are not given by these parameters, but rather by the parameters that are included in the system of equation (3.36). From this we know that the parameters that determine μ_{11} constitute of β and \tilde{d} in case of the ‘quadratic fit’ speed $v = v_q$ and $\tilde{\beta}, \tilde{d}$ and γ_0 in case of the ‘piecewise’ speed $v = v_p$. In this section we determine the bifurcation planes expressed in terms of these parameters.

In order to make these bifurcation curves in this case, we want to apply the analysis we already have done in Section 3.2.1. In this analysis we have however assumed that $\mu_{12} = \hat{\kappa} = 1$ and $\mu_{41} = D = 1$. Therefore we must do so here. As noted before, this is just a result of (additional) scaling and does not influence the generality of this approach.

Since $\mu_{40} = -\frac{\hat{\alpha}}{A_e} < 0$ is negative, we immediately know that only the bifurcation diagram of Figure 3.5b can correspond to our mussel-algae system. Thus we know that the trace is negative only when $\mu_{11} > -2\sqrt{\theta}$ and that the determinant is positive when $\mu_{30}\mu_{21} > \mu_{11}\mu_{40} - 2\sqrt{(\mu_{11} - \mu_{40})\delta}$.

We first look at the condition for the determinant (which is only valid and relevant when the trace is negative, so that the root is well-defined). As we have seen we have $\mu_{30} < 0$ and $\mu_{40} < 0$. Moreover, we also know that $\mu_{21} \leq 0$, since adding algae never increases the movement speed per assumption. Hence we find that the left-hand side is positive. When $\mu_{11} > 0$ the right-hand side is negative. Thus when $\mu_{11} > 0$ the inequality always holds. Thus this condition can only be violated when $\mu_{11} < 0$.

The condition on the trace however tells us that $\mu_{11} > -2\sqrt{\theta} = \mathcal{O}(\sqrt{\varepsilon})$. Thus the critical line for μ_{11} , that describes when the trace becomes positive is given by $\mu_{11,C} = -2\sqrt{\theta}$ and as a consequence, the critical value for μ_{21} , that tells us when the determinant becomes negative, is also of order $\mathcal{O}(\sqrt{\varepsilon})$. This essentially is already captured in Section 3.2.1, in Figure 3.6d.

So we know that the uniform steady state is linear stable when $\mu_{11} > 0$ and unstable when $\mu_{11} < -2\sqrt{\theta}$. When μ_{11} is in between those two values the state is unstable when μ_{21} is small enough and stable otherwise.

Bifurcation diagram for the ‘quadratic’ speed $v = v_q$

When we take the ‘quadratic approach’ for the density dependent movement speed $v = v_q$, we can determine that the condition $\mu_{11} > 0$ translates to the condition $3M_e^2 + 2\tilde{\beta}M_e + 1 - \tilde{d}A_e > 0$ and the condition $\mu_{11} < -2\sqrt{\theta}$ translates to $(M_e^2 + \tilde{\beta}M_e + 1 - \tilde{d}A_e)(3M_e^2 + 2\tilde{\beta}M_e + 1 - \tilde{d}A_e) < -2\sqrt{\theta}$. A straightforward computation then tells us that the uniform steady state is linearly stable when

$$\tilde{\beta} > \beta_0 := -\frac{3M_e^2 + 1}{2M_e} + \tilde{d}\frac{A_e^2}{2M_e}$$

and unstable when

$$\tilde{\beta} < \beta_1 := -\frac{5M_e^2 + 3 - 3dA_e}{4M_e - e} + \frac{\sqrt{(M_e^2 - 1 + dA_e)^2 - 16\sqrt{\theta}}}{4M_e}.$$

If the root does not exist, then the trace is always negative, for all wavelengths, regardless of the value of $\tilde{\beta}$.

When $\beta \in (\beta_1, \beta_0)$ then the stability is not clear. In this region it depends on size of μ_{21} . When this value is small enough the system is unstable, otherwise it is stable. This generally corresponds to situations with d close to zero (i.e. $v_a \approx 0$) or close to the curve $\tilde{\beta}^2 = 4(1 - \tilde{d})$ (i.e. $v \approx 0$). It is possible to

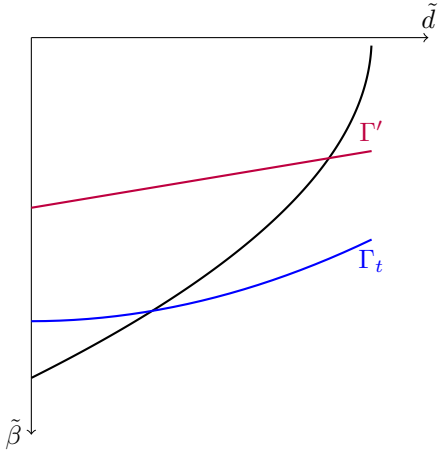


Figure 3.12 – Schematic illustration of (half of the) parameter plane $(\tilde{\beta}, \tilde{d})$. Here the black line denotes the curve $\tilde{\beta}^2 = 4(1 - \tilde{d})$ (i.e. $v > 0$). The blue line denotes the bifurcation line Γ_t . The red line, denoted as Γ' , denotes the line at which $\mu_{11} = 0$. Below the blue line the uniform steady state is unstable; above the red line it is stable. Between Γ' and Γ_t the stability is determined by the size of μ_{21} . Note that this is an illustration of one of the possible situation. These lines not necessarily need to lie in the admissible region, dictated by $v > 0$.

determine a precise condition on the value of μ_{21} but this is very cumbersome and does not give us more insight in the system. A sketch of the bifurcation diagram (for $v = v_q$) is given in Figure 3.12.

Bifurcation diagram for the piecewise speed $v = v_p$

We can also inspect the bifurcations that occur in the system when we use the piecewise formulation for the density dependent movement speed. In this situation we have

$$v(M, A) = \begin{cases} v_1(M, A) = 1 - \tilde{\beta}M & \text{when } M < \tilde{\beta}/2 \\ v_2(M, A) = \frac{1-\tilde{\beta}^2}{2} + \gamma_0 e^{-\tilde{d}A}(M - \tilde{\beta}/2) & \text{when } M > \tilde{\beta}/2 \end{cases}$$

Since $\frac{\partial v_2}{\partial M} > 0$ we know that $\mu_{11} > 0$ when $M > \frac{\tilde{\beta}}{2}$. Hence in this situation we always find a negative trace and a positive determinant, and thus a stable uniform stationary point.

On the other hand, when $M < \tilde{\beta}/2$ we have $\frac{\partial v_1}{\partial A} = 0$ and therefore $\mu_{21} = 0$. A simple manipulation of the condition on the determinant then tells us that the determinant becomes negative as soon as $\mu_{11} = (1 - \tilde{\beta}M_e)(1 - 2\tilde{\beta}M_e) < 0$. This is a stricter condition than the one on the trace (i.e. $\mu_{11} < -2\sqrt{\theta}$).

Therefore we see that in this situation the state is stable when $\tilde{\beta} < \frac{1}{2M_e}$ and unstable otherwise. So it is clear that, with the piecewise description $v = v_p$ for the density dependent movement speed, we have one bifurcation point and the determinant (corresponding to the critical wavelength) changes sign.

Note that in Section 2.1 we have studied the stability of uniform stationary points of the (general) Cahn-Hilliard equation. Here we found a condition for linear stability that can be translated to the condition $\mu_{11} > 0$. This is more or less the same conditions as we have found now, for the full system.

3.4.3 Modulation Equation

In Section 3.3 we have derived a general amplitude equation that can be used to describe the behaviour of the system of equation (3.1) near critical circumstances. We studied the situation in which both μ_{11} and μ_{21} were perturbed a little bit into the (linear) unstable region. In this section we apply this result to the specific mussel system. This time we use $\tilde{\beta}$ as our (only) bifurcation parameter, as this parameter influences the density dependent movement speed the most. We use this to study small variation from the non-trivial steady state of the mussel system as given in equation (3.36).

In Section 3.4.2 we showed that, when the determinant of $\mathcal{M}(k_c)$ changes signs, we must have $\mu_{11} < 0$ and $\mu_{21} \leq 0$ and both must be of order $\mathcal{O}(\sqrt{\varepsilon})$ or smaller. Moreover, we have seen in equation (3.4.2) that $\mu_{40} < 0$ and $\mu_{30} < 0$. Therefore we know that we are dealing with the bifurcation line $\Gamma_{-,d,-}$ and that $k_c^2 \approx \sqrt{\delta/\tilde{\beta}}$ (See Section 3.2.1). Upon noting that $\beta = \mu_{11} - \mu_{40} \approx -\mu_{40}$ and $\delta = \mathcal{O}(\varepsilon)$ we find that $k_c^2 = \mathcal{O}(\sqrt{\varepsilon})$. These approximations are necessary to simplify the parameters found in the amplitude equation (3.31).

The parameter R

We first want to inspect the parameter R (see equation (3.32)). However, to do so, we need to determine the signs of r and s first. Recall that $r = \frac{\mu_{11} - \mu_{11,c}}{\phi^2}$ and $s = \frac{\mu_{21} - \mu_{21,c}}{\phi^2}$. What we do now is change the parameter $\tilde{\beta}$ - our bifurcation parameter - from its critical value β_c , as determined in Section 3.4.2. We set $\beta = \beta_c - \phi^2 z$, where $z > 0$ when we use the quadratic movement speed.

It is not hard to determine how much the movement speed changes, and we can see that $v = v^c - \phi^2 z M_e$, $v_m = v_m^c - \phi^2 z$ and $v_a = v_a^c$ where v^c , v_m^c and v_a^c are the original (critical) values of these parameters. Working out the expression for μ_{11} and μ_{21} (with this new parameter $\tilde{\beta} = \tilde{\beta}_c - \phi^2 z$) we obtain

$$\begin{aligned}\mu_{11} &= \mu_{11,c} - \phi^2 z (M_e(v_c + mv_m^c) + 2v_c M_e) \\ \mu_{21} &= \mu_{21,c} - \phi^2 z v_a^c\end{aligned}$$

Since $v_c + mv_m^c = 0$ and $v_a^c \leq 0$ we thus know that $r < 0$ and $s \geq 0$. Now we can turn to the value for R and first observe that we can simplify the expression since $k_c^2 = \mathcal{O}(\sqrt{\varepsilon})$, while μ_{40} and μ_{30} are assumed to be $\mathcal{O}(1)$. Hence we find

$$R = \frac{\varepsilon k_c^2 (r k_c^2 - r \mu_{40} + s \mu_{30})}{\text{Tr} \mathcal{M}_c} \approx \varepsilon k_c^2 \frac{s \mu_{30} - r \mu_{40}}{\text{Tr} \mathcal{M}_c} \quad (3.43)$$

Because $r > 0$, $s < 0$, $\mu_{30} < 0$, $\mu_{40} < 0$, $k_c^2 > 0$ and $\text{Tr} \mathcal{M}_c < 0$ (because we are assuming that we first cross the line $\Gamma_{-,d,-}$ and thus we assume that the trace is still negative), we thus know that $R > 0$ for our mussel model.

A similar approach can also be applied to the other description of the movement speed, the ‘piecewise’ description $v = v_p$. Here we must use $\tilde{\beta} = \tilde{\beta}_c + \phi^2 z$. The computations are similar and the end result is the same: $R > 0$, always.

The parameters b and h

Although we could manage to simplify the parameter R using approximations and determine the sign, we are not able to do this for the parameters b and h (see equation (3.33) and (3.34)). It is possible to reduce the number of terms in these expression, but there are still way too many parameters to determine what can happen. Therefore we should just take these as they are and compute the values and signs each time we want to use the amplitude equations for a new set-up, with different system parameters.

Because of all the approximations we have used in our analysis, these parameters are also very sensitive to changes in the original parameter. A very small difference in the original parameters or the critical value of $\tilde{\beta}_c$ can already change the signs of b and h - and we have no way to determine these exactly via the means we have studied in this study. Therefore we don’t think we can present accurate values or even signs for the constants b and h for the simulations that we have done in Section 3.5.

If we were able to accurately find (at least) the signs of these parameters b and h , we would be able to find the possible forms of the amplitude A . This in turn gives us information about solutions of the original partial differential equation (equation (3.1)) as these solutions have the form

$$(M(x, t), A(x, t)) = (M_e, A_e) + A(\varepsilon x, \varepsilon^2 t) e^{ik_c x} \quad (3.44)$$

More information about the solutions of the Real Ginzburg-Landau equation can be found in Appendix C, which contains an in-depth study of all possible (stationary) solutions to the Real Ginzburg-Landau for various possible signs of the parameters R , b and h .

3.5 Simulations

In the previous sections of this Chapter we have studied the full model of equation (3.1) analytically. In this section we supplement the thus gained knowledge via simulations of the specific mussel-algae system that we studied analytically in Section 3.4. As we did with our simulation of the Cahn-Hilliard equation (i.e. $\varepsilon = 0$) in Section 2.3 we again only present the results of simulations of the system with one spatial dimension.

In the previous sections we have not cared about the boundary conditions of the system for our analysis. For simulations these boundary conditions are however necessary. We just use an extension of the natural boundary conditions, as we

have used them throughout Chapter 2, that is

$$\begin{aligned} m_x(0) &= m_x(L) = 0; \\ m_{xxx}(0) &= m_{xxx}(L) = 0; \\ a_x(0) &= a_x(L) = 0. \end{aligned}$$

These conditions, the so-called no-flux boundary conditions, make sure that there is no mass flowing through the boundary of our domain.

As before, in Chapter 2, all simulations are started from an uniform state $(m, a)(x, 0) = (m_0, a_0)$, where a small perturbation of this state makes sure that we won't stay in an unstable stationary state. The Fortran code used to make these simulations is kindly provided by Paul Zegeling and uses finite-difference numerical methods on a moving grid.

Throughout this section we use these simulations to get an insight in the behaviour of the full population model as presented in equation (3.1). We study both descriptions of the density dependent movement speed (see Section 1.1.4).

3.5.1 Short time behaviour

As we did in Chapter 2 we start by looking at the short time behaviour of the system. We have seen, in the previous section of this chapter, that patterns can arise out of the uniform steady states of the system, when the parameters are chosen well enough. Specifically, we again obtained similar conditions as in Chapter 2, as there is again a spinodal region in which we expect patterns to arise.

In Figure 3.13 and Figure 3.14 we give the results of simulations of the system where we use the ‘quadratic’ description of the density dependent movement speed $v = v_q$. In Figure 3.13 we tested the model when the concentration of algae has no influence at the movement speed at all (i.e. $\tilde{d} = 0$), whereas the model of Figure 3.14 incorporates the effect of the algae on this speed. These simulations show the existence of patterns in both cases. In fact, there is no clear difference to be seen in these simulation between the patterns that arise in both cases, or even between these patterns and the patterns for the model without interaction, as seen in Section 2.3.

We also come to this conclusion when we study simulations of the ‘piecewise’ description for the density dependent movement speed $v = v_p$. Results of these simulations are shown in Figure 3.15 and Figure 3.16, for the model without and with the effect of the algae concentration on the movement speed, respectively. Again, both situations lead to similar patterns.

3.5.2 Long time behaviour

Now that we have established, via simulations, that the full system really possess patterns that are similar to the patterns seen in the standard Cahn-Hilliard equation, it is logical to investigate the similarities even further. We have seen

in Chapter 2 that the Cahn-Hilliard equation has a very specific long-time behaviour called Ostwald Ripening.

In the simulation in Section 2.3 we observed this ripening. There we found out that the system chooses a pattern, then sticks to this patterns for a very long time to eventually change the patterns to a new one with a smaller wavelength. This process continues until all mass is located at one side of the domain.

So is this property also present in the full mussel model? To investigate this, we have done several long-time simulations with our model. In Figure 3.17 and Figure 3.18 we show the results of a simulations with respectively the ‘quadratic’ and the ‘piecewise’ density dependent movement speed. Although the switching between patterns still happens in both of these, the ripening effect seems somewhat different than before: the mass transformation - that was clearly visible in the Cahn-Hilliard simulations of Section 2.3 - is now less profound. We were also not able to find a set of parameters that led to a realization of the global minimizer. This all suggests that the long-time behaviour of the system is even more subtle than before.

3.5.3 Other initial conditions

All previous simulations were executed with the steady state as starting point. Though our analysis in the rest of this chapter has only focussed on those situations, it is still interesting to see what happens when we start with other initial conditions. We have seen that the simulations, starting from the steady state, led to patterns when this steady state was located in the spinodal region. So two natural questions come to mind: what happens when we start outside this region, still keeping the steady state in it? And what happens if we do start in the spinodal region, but the steady state is located outside of it?

We start with the first question. In Figure 3.19 we show the results from a simulation in which the steady state is still located in the spinodal region, but we start outside of it. What we see here is that the system first follows the (slow) interaction terms until the system is (nearly) in the steady state. Subsequently the familiar patterns start to appear coming from this steady state. Note that the colours in these plots are relative. This explains why the patterns in these plots may falsely seem less striking, while they are as prominent as before.

Then on to the next question. To answer this one, we simulate a system that has a steady state that is not located in the spinodal region and set the initial conditions such that we in fact do start in this region. In Figure 3.20 we have plotted the results of such a simulation. We can see that this set-up does not lead to patterns. Despite the system starting in the spinodal region, it still follows the slow interaction terms. Therefore the system ultimately arrives at its steady state (which is now stable, as it is not located in the spinodal region).

These simulations illustrate the behaviour of our full system. Initially the system follows the (slow) interaction terms until it is close to the non-trivial steady state. If this steady state is located in the spinodal region, then the behaviour of the Cahn-Hilliard equation takes over and patterns arise. From the simulations in this section it is not completely clear what happens to these patterns over

very long time periods: not all patterns persist in the long run - as in the standard Cahn-Hilliard equation - though the ripening effect seems different to the standard Cahn-Hilliard (Ostwald) ripening.

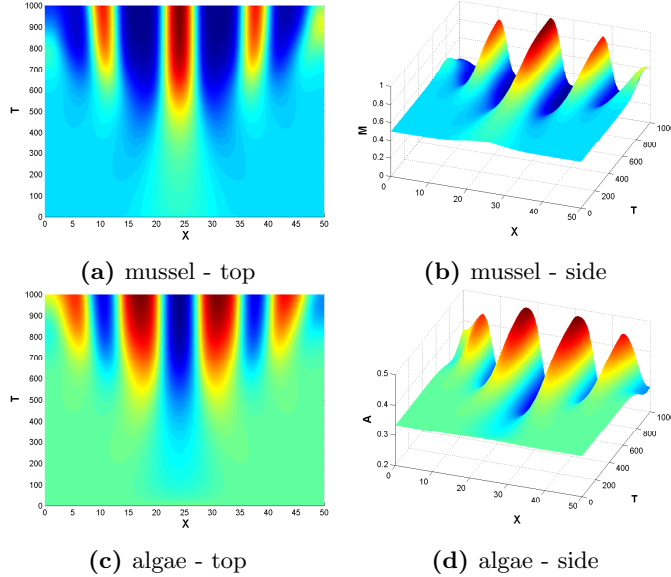


Figure 3.13 – Patternplot of a simulation of the initial behaviour of equation 3.1 with ‘quadratic’ speed $v = v_q$ on a one-dimensional domain $[0, L]$ *without* algae having an effect on the movement speed. In (a) the mussel density from the top and in (b) from the side; (c) the algae density from top and in (d) from the side. The colours denote the density, on a scale from low (blue) to high (red) densities. Parameter values: $L = 50$, $T = 1000$, $\tilde{\beta} = -1.9$, $\tilde{d} = 0$, $\varepsilon = 0.0005$, $\kappa = 0.05$, $d_m = 1$, $d_a = 1$, $\tilde{\alpha} = 1$, $\tilde{\gamma} = 4$, $\nu = 1$, $r = 2$, $m_0 = 0.5$, $a_0 = 0.333$.

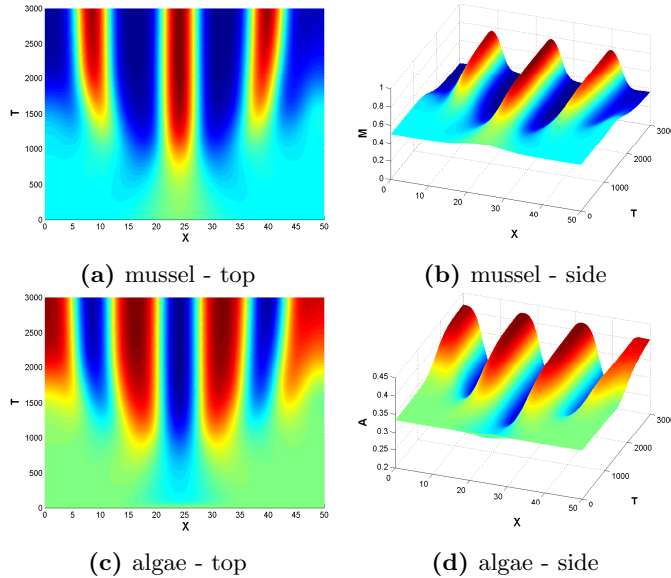


Figure 3.14 – Patternplot of a simulation of the initial behaviour of equation 3.1 with ‘quadratic’ speed $v = v_q$ on a one-dimensional domain $[0, L]$ *with* algae having an effect on the movement speed. In (a) the mussel density from the top and in (b) from the side; (c) the algae density from top and in (d) from the side. The colours denote the density, on a scale from low (blue) to high (red) densities. Parameter values: $L = 50$, $T = 1000$, $\tilde{\beta} = -1.85$, $\tilde{d} = 0.05$, $\varepsilon = 0.0005$, $\kappa = 0.05$, $d_m = 1$, $d_a = 1$, $\tilde{\alpha} = 1$, $\tilde{\gamma} = 4$, $\nu = 1$, $r = 2$, $m_0 = 0.5$, $a_0 = 0.333$.

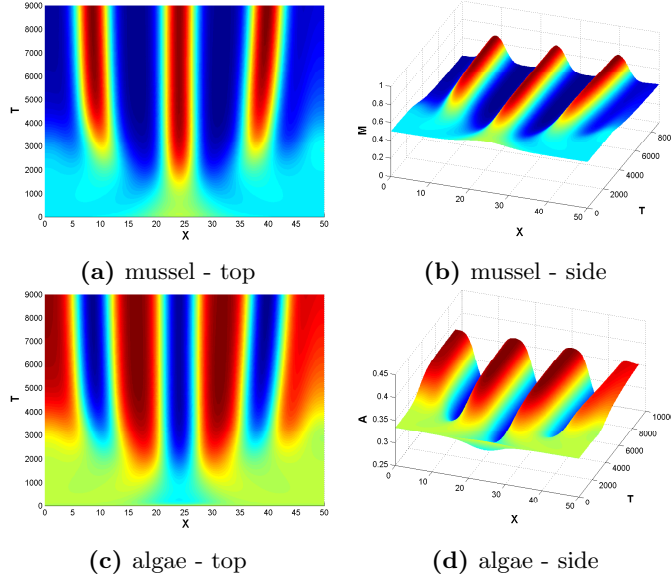


Figure 3.15 – Patternplot of a simulation of the initial behaviour of equation 3.1 with ‘piecewise’ speed $v = v_p$ on a one-dimensional domain $[0, L]$ *without* the algae concentration having an effect on the movement speed. In (a) the mussel density from top and in (b) from the side; (c) the algae density from top and in (d) from the side. The colours denote the density, on a scale from low (blue) to high (red) densities. Parameter values: $L = 50$, $T = 3000$, $\tilde{\beta} = 1.35$, $\tilde{d} = 0$, $\gamma_0 = 1$, $K = 1$, $\varepsilon = 0.0005$, $\kappa = 0.01$, $d_m = 3$, $d_a = 1$, $\tilde{\alpha} = 1$, $\tilde{\gamma} = 4$, $\nu = 1$, $r = 2$, $m_0 = 0.5$, $a_0 = 0.333$

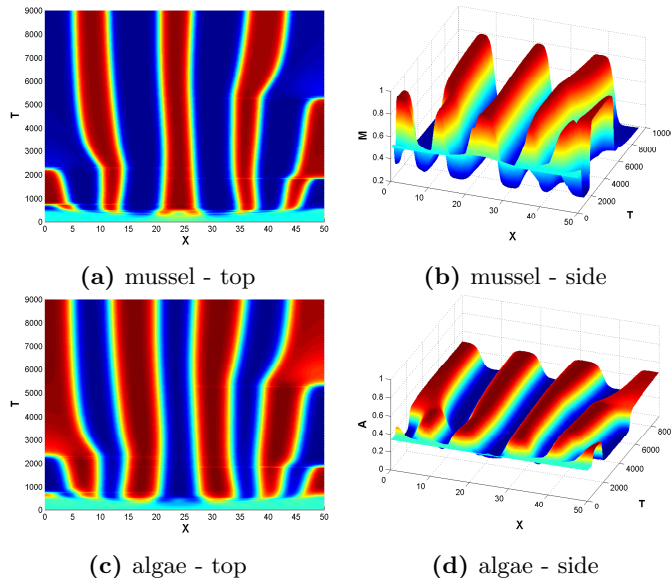


Figure 3.16 – Patternplot of a simulation of the initial behaviour of equation 3.1 with ‘piecewise’ speed $v = v_p$ on a one-dimensional domain $[0, L]$ *with* the algae concentration having an effect on the movement speed. In (a) the mussel density from top and in (b) from the side; (c) the algae density from top and in (d) from the side. The colours denote the density, on a scale from low (blue) to high (red) densities. Parameter values: $L = 50$, $T = 9000$, $\tilde{\beta} = 1.35$, $\tilde{d} = 1$, $\gamma_0 = 1$, $K = 1$, $\varepsilon = 0.0005$, $\kappa = 0.01$, $d_m = 3$, $d_a = 1$, $\tilde{\alpha} = 1$, $\tilde{\gamma} = 4$, $\nu = 1$, $r = 2$, $m_0 = 0.5$, $a_0 = 0.333$

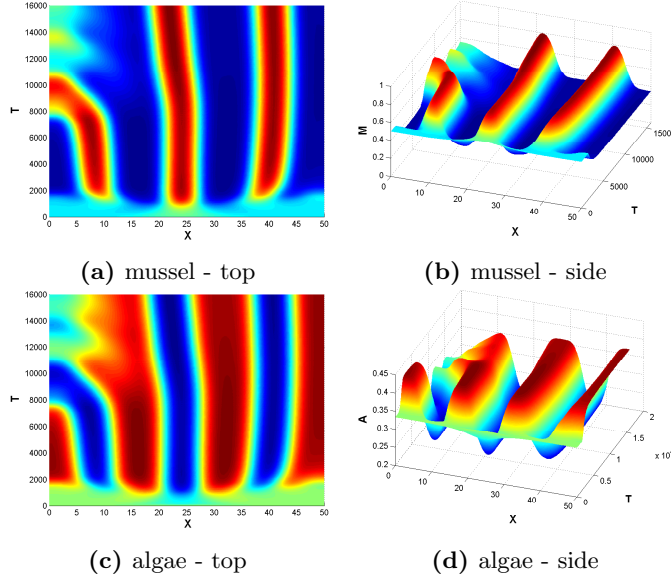


Figure 3.17 – Patternplot of a simulation of the long-time behaviour of equation (3.1) with ‘quadratic’ movement speed $v = v_q$ on a one-dimensional domain $[0, L]$ with algae having an effect on the movement speed. In (a) the mussel density from top and in (b) from the side; (c) the algae density from top and in (d) from the side. The colours denote the density, on a scale from low (blue) to high (red) density. Parameter values: $L = 50$, $T = 16000$, $\tilde{\beta} = -1.85$, $\tilde{d} = 0.05$, $\varepsilon = 0.0005$, $\kappa = 0.05$, $d_m = 1$, $d_1 = 1$, $\tilde{\alpha} = 1$, $\tilde{\gamma} = 4$, $\nu = 1$, $r = 2$, $m_0 = 0.5$, $a_0 = 0.3333$.

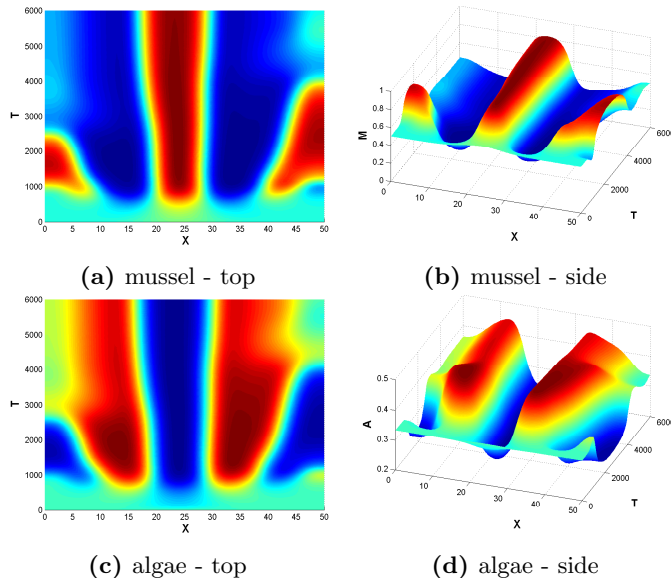


Figure 3.18 – Patternplot of a simulation of the long-time behaviour of equation (3.1) with ‘quadratic’ movement speed $v = v_p$ on a one-dimensional domain $[0, L]$ with algae having an effect on the movement speed. In (a) the mussel density from top and in (b) from the side; (c) the algae density from top and in (d) from the side. The colours denote the density, on a scale from low (blue) to high (red) density. Parameter values: $L = 50$, $T = 16000$, $\tilde{\beta} = 1.35$, $\tilde{d} = 1$, $\gamma_0 = 1$, $K = 1$, $\varepsilon = 0.0005$, $\kappa = 0.05$, $d_m = 3$, $d_1 = 1$, $\tilde{\alpha} = 1$, $\tilde{\gamma} = 4$, $\nu = 1$, $r = 2$, $m_0 = 0.5$, $a_0 = 0.3333$.

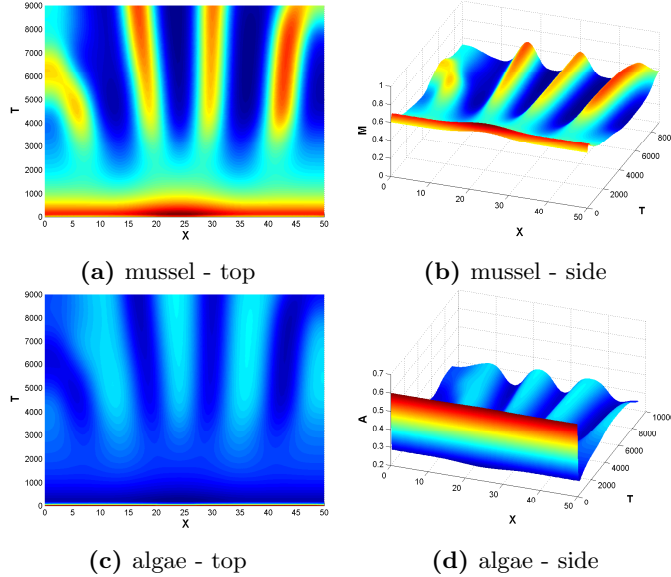


Figure 3.19 – Patternplot of a simulation of equation (3.1) with ‘piecewise’ speed $v = v_p$ on a one-dimensional spatial domain $[0, L]$ *without* algae having an effect on the density dependent movement speed, started from outside the spinodal region. In (a) the mussel density from top and in (b) from the side; (c) the algae density from top and in (d) from the side. The colours denote the density, on a scale from low (blue) to high (red) densities. Parameter values: $L = 50$, $T = 9000$, $\tilde{\beta} = 1.35$, $\tilde{d} = 0$, $\gamma_0 = 1$, $K = 1$, $\varepsilon = 0.0005$, $\kappa = 0.01$, $d_m = 3$, $d_a = 1$, $\tilde{\alpha} = 1$, $\tilde{\gamma} = 4$, $\nu = 1$, $r = 2$, $m_0 = 0.6$, $a_0 = 0.6$, $m_e = 0.5$, $a_e = 0.3333$.

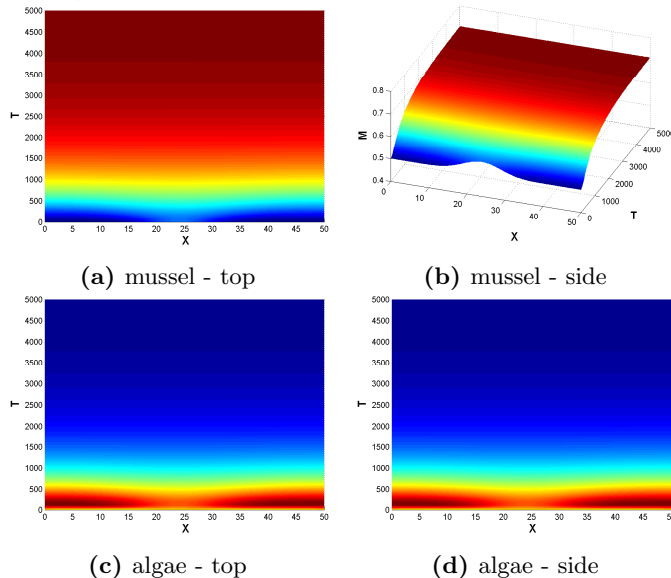


Figure 3.20 – Patternplot of a simulation of equation (3.1) with ‘piecewise’ speed $v = v_p$ on a one-dimensional spatial domain $[0, L]$ *without* algae having an effect on the density dependent movement speed, started from inside the spinodal region to a steady state located outside the spinodal region. In (a) the mussel density from top and in (b) from the side; (c) the algae density from top and in (d) from the side. The colours denote the density, on a scale from low (blue) to high (red) densities. Parameter values: $L = 50$, $T = 5000$, $\tilde{\beta} = 1.35$, $\tilde{d} = 0$, $\gamma_0 = 1$, $K = 1$, $\varepsilon = 0.0005$, $\kappa = 0.01$, $d_m = 3$, $d_a = 1$, $\tilde{\alpha} = 1$, $\tilde{\gamma} = 3.4$, $\nu = 1$, $r = 2$, $m_0 = 0.5$, $a_0 = 0.333$, $m_e = 5/7 \approx 0.7$, $a_e = 7/24 \approx 0.3$.

Conclusion & Outlook

In this master thesis we have studied a modified predator-prey model, where the normal, diffusive movement of one of the involved species is replaced with a density-dependent fast movement speed. We have seen in Chapter 1 that this leads to a Cahn-Hilliard equation for the movement of this specie. Combined with the normal interaction terms, that work on a much slower time scale this led to the following system describing a new sort of predator-prey model that was our main object of study:

$$\frac{\partial m}{\partial t} = d_m \nabla \left[v \left(v + m \frac{\partial v}{\partial m} \right) \nabla m + v m \frac{\partial v}{\partial a} \nabla a - \kappa \nabla \Delta m \right] + \varepsilon H(m, a) \quad (3.45a)$$

$$\frac{\partial a}{\partial t} = \varepsilon d_a \Delta a + \varepsilon G(m, a) \quad (3.45b)$$

where v is the density dependent movement speed and H and G are the interaction terms.

We have seen that this description indeed leads to patterns in the animal population. In Chapter 2 we have seen that the Cahn-Hilliard like movement (i.e. setting $\varepsilon = 0$ in the system) already can explain the existence of patterns. We have inspected the dynamics of solutions of the Cahn-Hilliard equation starting from an uniform steady state. We found that these uniform states were decomposed to form patterns only if they were located in the spinodal region, i.e. when they obeyed the condition $v(m_e) \left(v(m_e) + m_e \frac{\partial v(m_e)}{\partial m} \right) < 0$. We found no qualitative difference between the two proposed descriptions for the speed of Section 1.1.4 - only the amount of roots seems relevant.

When this condition is obeyed, we can expect patterns (when the domain is large enough). These patterns however are not stable. When we wait long enough, we see that the solution suddenly and rapidly changes to another pattern, with a smaller typical wavelength. We also studied this process, called Ostwald Ripening, and found that infinitesimal mass transportation was the key process that is responsible for this ripening effect.

Real-life animal populations have no such thing; only whole, complete animals can move and not fractions of animals. Therefore the found Ostwald Ripening can come to a hold in real-life environments, whereas the equations tell us that it should continue. This is a possible explanation for the wavelength selection that was observed in experiments with mussels (see Figure 3.21).

It not easy to test this hypothesis. Mathematically it translates to a violation

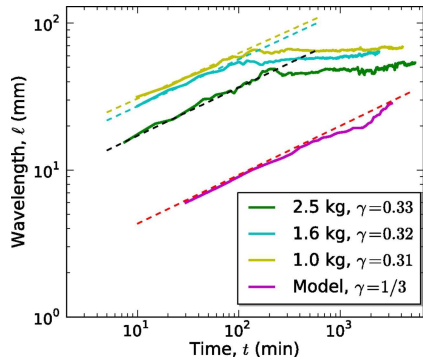


Figure 3.21 – Correlation between the typical wavelength of patterns for mussels, in experimental set-up (blue and green lines) and in a numerical simulation (purple). The dashed lines are linear fits over the initial behaviour (i.e. before a wavelength is ‘selected’). For the numerical simulation the theorized power law is used instead. In these plots we can clearly see that there is some sort of wavelength selection in the experiments after some hours.

of the continuity assumption, as we essentially are saying that not all values are possible for the density of mussels. Therefore one should really come up with another, discrete model to really overcome this shortcoming. An other, more pragmatic, solution would be to only allow mass transportation in the model when enough mass is transported. This is however very difficult to incorporate and gives a model that cannot be studied easily with the standard analytical mathematical methods.

It is also possible to test this hypothesis via experiments. As argued before, it seems that the Ostwald Ripening only stops because too little mass needs to be transported. If this is the case, then the system would still favour an other configuration - with a smaller wavelength - but it just can’t possible get to that configuration. With an experiment one could try to find a way to help the system get to this other, favourable, state. If this is possible - and the system indeed can maintain this new, better configuration, then this suggests that this infinitesimal mass transportation is indeed the cause to the observed wavelength selection. This experimental approach is however also very difficult, as it requires advanced knowledge about the preferred configurations and the ability to set-up the animals in exactly that way.

In Chapter 3 we studied the full-system (i.e. $\varepsilon \neq 0$). Via simulations we observed that the system first evolves (uniformly) to its uniform steady state. Subsequently the system can possibly form patterns, but roughly only if the steady state is located in the spinodal region - similarly to the single Cahn-Hilliard equation. The patterns here also looked similar to the patterns created by a Cahn-Hilliard equation.

We were however not able to understand the long time behaviour of these patterns. It is yet unclear if the ripening effect is still present in this full system, though simulations suggest it is. In the literature there are numerous studies of the long time behaviour of the Cahn-Hilliard equation, using interactions between pulse solutions. Possibly these approaches can also be used on this full

system to understand what happens in the long run to the patterns.

Moreover we have also only studied what happens to solutions that start from uniform steady states. There are however also predator-prey models for which this assumption is not valid at all. If we for example want to study the dynamics of an elk herd and their prey, vegetation, it is more natural to model the vegetation as a non-uniform concentration profile: vegetation is not distributed equally, but there are places with lots of vegetation and places without any vegetation at all. This already gives problems for the system with $\varepsilon = 0$, as it leads to a modified Cahn-Hilliard equation of the form

$$\frac{\partial m}{\partial t} = d_m \nabla \left(v(m, x) \left(v(m, x) + m \frac{\partial v(m, x)}{\partial m} \right) \nabla m + v(m, x) m \frac{\partial v(m, x)}{\partial x} - \kappa \nabla \Delta m \right).$$

A study of this equation can give new insights in the patterns that occur in elk herd populations, but can also indicate what happens when we use non-uniform starting configurations in other population models, for example in the mussel-algae model that we have heavily studied in this thesis.

It is also interesting to recall that the standard reaction-diffusion predator-prey population model already leads to patterns, as we have seen in Chapter 1. The patterns that we have found in this model however have typically (much) larger wavelengths than the patterns that arise due to the density dependent movement speed, as we have seen in Chapter 2 and Chapter 3. In mussel beds that are found in nature, people have found several, layered patterns. For instance, there are patterns with large wavelengths (in the order of metres) and patterns with much smaller wavelengths (in the order of centimetres). Therefore one is tempted to think that the reaction-diffusion system is a good description for these large patterns, while the Cahn-Hilliard movement is good to capture the smaller patterns that appear in a significant faster time frame.

However this must mean that there is a transition between the two models. We have not been able to precisely formulate this transition: when you look at the full model of equation (3.45) you can try to scale the temporal and spatial variables and ignore the smallest terms, but this does not lead to a reaction-diffusion model, because of the terms $v(v + m \frac{\partial v}{\partial m})$ and $vm \frac{\partial v}{\partial a}$ that give non-linearities that are not present in the normal reaction-diffusion equation. Possibly there is another way to connect both models, or similar models, which seems an interesting study for a follow-up research.

Finally we must acknowledge that most of this thesis covered the situation in only one spatial dimension. In reality this is of course not realistic at all, and the addition of a second spatial dimension is absolutely necessary to be able to get good comparisons between the mathematical results and real-life experiments - as for example the ripening effect is described differently in the one-dimensional Cahn-Hilliard equation, compared to the two-dimensional equation. The analytical approach would however become even more tedious and frankly should only be done when we have a better understanding of the dynamics of the model with one spatial dimensions - for instance if we have a better understanding of what the modulation equations tell us in this case.

Acknowledgments

First and foremost I'd like to thank my thesis supervisor *Vivi Rottschäfer* for her help and guidance during my year working on this research and for introducing me to this topic. Moreover, I also want to thank *Johan van de Koppel* from the Royal Netherlands Institute for Sea Research (NIOZ) for the discussion on the ecological aspect and the tour in his labs. I also need to thank *Paul Zegeling* from the Utrecht University as he kindly provided me with a good, practical and fast numerical simulation of the model which allowed me to quickly run several simulations on the model - something I couldn't have done otherwise. Finally my thanks to *Christian Hamster* - who is currently working on a similar project for his master thesis - for several discussions and brainstorms about patterns and mussels.

Appendix A

Modulation Equation for Reaction-Diffusion system

In Section 1.2 we studied a reaction-diffusion system that describes the interaction between mussels and algae. We used a linear stability analysis to determine the stability of the uniform stationary states of this system. We also want to study the possibility of patterns arising from these uniform states, when the parameters are just ‘a little unstable’. For this we apply weakly non-linear stability analysis and we need to find the relevant modulation equations, as we discussed in Section 1.2. This computation is very technical and cumbersome and therefore it is included in this appendix for those who are interested in the details.

In the rest of this section we first determine the relevant scalings for the slow space and time variables, ξ and τ . Then we want to substitute the Ansatz of equation (1.16) into the our scaled system (equation (1.6)), where we should be carefull about the ‘higher order terms’ that start to play a role. Finally this gives us a partial differential equation for the amplitude A in our Ansatz that in turn then gives us an approximation of the solutions of our original reaction-diffusion equation.

Slow spatial variable ξ and slow time variable τ

In our linear stability analysis we have found an expression for the critical $\tilde{\mu}_c(k)$ in equation (1.13). We know that $\frac{\partial \tilde{\mu}_c}{\partial k}(k_c) = 0$ per construction. In general $\frac{\partial^2 \tilde{\mu}_c}{\partial k^2}(k_c) \neq 0$. For k close to k_c we have $\tilde{\mu}_c(k) = \tilde{\mu}_c(k_c) + \frac{\partial^2 \tilde{\mu}_c}{\partial k^2}(k_c)[k - k_c]^2$. We can define $K := k - k_c$ and hence find $\tilde{\mu}_c(k_c + K) = \tilde{\mu}_c + \frac{\partial^2 \tilde{\mu}_c}{\partial k^2}(k_c)K^2$. We are interested in the situation where $\tilde{\mu} = \tilde{\mu}_C - \varepsilon^2 s$. This means that when $\tilde{\mu}$ lies on the curve $\{(k, \tilde{\mu}_c(k))\}$ we find that K is of order $\mathcal{O}(\varepsilon)$. Therefore there is a region of unstable wavelengths around k_c of size proportional to ε .

We also want to know how much the eigenvalues change when $\tilde{\mu}$ is changed a little (and therefore when k is changed a little). For this we turn back to the dispersion relation in equation (1.10). We want to compute $\omega(k)$ now for the

band of unstable wavelengths. Hence we must find $\omega(k)$ in the situation with $\tilde{\mu} = \tilde{\mu}_C - \varepsilon^2 s$ and $k^2 = k_c^2 + \varepsilon^2 L$ (with L some order $\mathcal{O}(1)$ constant). Solving this dispersion relation gives us the following form for $\omega_{1,2}$:

$$\omega_{1,2} = \frac{\bar{B} + \varepsilon^2 \hat{B}}{2\tilde{\gamma}} \pm \frac{1}{2\tilde{\gamma}} \sqrt{\bar{B} - 4\tilde{\gamma}\bar{C} + \varepsilon^2 (2\bar{B}\hat{B} - 4\tilde{\gamma}\hat{C})},$$

where

$$\begin{aligned}\bar{B} &= -\left((1 + \tilde{\gamma}\tilde{\mu}_C)|k_c|^2 + \tilde{\alpha}/A_e - \tilde{\gamma}\frac{M_e}{(1 + M_e)^2} \right) \\ \hat{B} &= -(-s|k_c|^2 + (1 + \tilde{\gamma}\tilde{\mu}_C)L) + \mathcal{O}(\varepsilon^2) \\ \bar{C} &= \tilde{\mu}_C|k_c|^4 + |k_c|^2\left(\tilde{\mu}_C\tilde{\alpha}/A_e - \frac{M_e}{(1 + M_e)^2}\right) + \frac{\tilde{\alpha}(r-1)(1-\tilde{\alpha}r)}{1-\tilde{\alpha}} \\ \hat{C} &= 2\tilde{\mu}_C|k_c|^2L - s|k_c|^4 + L\left(\tilde{\mu}_C\tilde{\alpha}/A_e - \frac{M_e}{(1 + M_e)^2}\right) - |k_c|^2s\tilde{\alpha}/A_e + \mathcal{O}(\varepsilon^2)\end{aligned}$$

Using a Taylor expansion of the root and noting that $\frac{\bar{B}}{2\tilde{\gamma}} + \frac{1}{2\tilde{\gamma}}\sqrt{\bar{B}^2 - 4\tilde{\gamma}\bar{C}} = 0$, because per construction of the critical parameter $\tilde{\mu}_C$ and the critical wavelength k_c we need to have $\omega_c = 0$ as well. Hence we must conclude that $\omega \propto \varepsilon^2$ as the found expression at the $\mathcal{O}(\varepsilon^2)$ -level does not vanish in general and there is no $\mathcal{O}(\varepsilon)$ -level.

Now this means that in this specific situation (i.e. $k = k_c + \varepsilon\bar{k}$, $\tilde{\mu} = \tilde{\mu}_C - \varepsilon^2 s$ and $\omega = \omega_c + \varepsilon^2 \bar{\omega}$ with \bar{k} and $\bar{\omega}$ of order $\mathcal{O}(1)$) the waves is proportional to

$$\exp[i[k_c + \varepsilon\bar{K}]x + \varepsilon^2 \tilde{\omega}t] = \exp[ik_c x] \exp[i\varepsilon\bar{K}x] + \tilde{\omega}\varepsilon^2 t = A_{lin}(\varepsilon x, \varepsilon^2 t)e^{ik_c x}.$$

So we can express these deviations in terms of an amplitude A and the wave with wavelength k_c . The parameters of the function A_{lin} are hence suited as our slow spatial and time variables. Thus we should define $\xi = \varepsilon x$ and $\tau = \varepsilon^2 t$.

Preparations for the Weakly Non-Linear Analysis

We want to use the assumed form of the perturbation of equation (1.16). To do this, we first must rewrite the rescaled reaction-diffusion equation using Taylor approximations of the non-linear terms (around the uniform stationary state). We must make sure that we only have interactions up to cubic order (this depends on the specific scalings we have found for $\tilde{\mu}$, ξ and τ). So our first task is to compute the various derivatives of $H(M, A) = rMA - \frac{M}{1+M}$ and $G(M, A) = \tilde{\alpha}(1-A) - MA$ and evaluate them at (M_e, A_e) .

$$\begin{aligned}
\frac{\partial H}{\partial m}(M_e, A_e) &= \frac{M_e}{(1+M_e)^2}, & \frac{\partial G}{\partial m}(m_e, a_e) &= -A_e, \\
\frac{\partial H}{\partial a}(M_e, A_e) &= rM_e, & \frac{\partial G}{\partial a}(m_e, a_e) &= -\tilde{\alpha} - M_e = -\tilde{\alpha}/A_e \\
\frac{\partial^2 H}{\partial m^2}(M_e, A_e) &= \frac{2}{(1+M_e)^3}, & \frac{\partial^2 G}{\partial m^2}(m_e, a_e) &= 0, \\
\frac{\partial^2 H}{\partial m \partial a}(M_e, A_e) &= r, & \frac{\partial^2 G}{\partial m \partial a}(M_e, A_e) &= -1, \\
\frac{\partial^2 H}{\partial a^2}(M_e, A_e) &= 0, & \frac{\partial^2 G}{\partial a^2}(m_e, a_e) &= 0, \\
\frac{\partial^3 H}{\partial m^3}(M_e, A_e) &= \frac{-6}{(1+M_e)^4}, & \frac{\partial^3 G}{\partial m^3}(m_e, a_e) &= 0, \\
\frac{\partial^3 H}{\partial m^2 \partial a}(M_e, A_e) &= 0, & \frac{\partial^3 G}{\partial m^2 \partial a}(M_e, A_e) &= 0, \\
\frac{\partial^3 H}{\partial m \partial a^2}(M_e, A_e) &= 0, & \frac{\partial^3 G}{\partial m \partial a^2}(M_e, A_e) &= 0, \\
\frac{\partial^3 H}{\partial a^3}(M_e, A_e) &= 0, & \frac{\partial^3 G}{\partial a^3}(M_e, A_e) &= 0.
\end{aligned}$$

So the reaction-diffusion system can now be rewritten to a form that only involves up to cubic interactions. This formulation is valid for all small perturbations of the form $(M, A) = (M_e, A_e) + (\bar{M}, \bar{A})$ and for the parameter value $\tilde{\mu} = \tilde{\mu}_C - \varepsilon^2 s$. The system is in this situation given by

$$\begin{aligned}
\frac{\partial \bar{M}}{\partial t} &= \tilde{\mu}_C \Delta \bar{M} + \frac{M_e}{(1+M_e)^2} \bar{M} + r M_e \bar{A} + r \bar{M} \bar{A} + \frac{1}{(1+M_e)^3} \bar{M}^2 \\
&\quad - \frac{1}{(1+M_e)^4} \bar{M}^3 - \varepsilon^2 s \Delta \bar{M} \tag{A.1a}
\end{aligned}$$

$$\tilde{\gamma} \frac{\partial \bar{A}}{\partial t} = \Delta \bar{A} - A_e \bar{M} - \tilde{\alpha}/A_e \bar{A} - \bar{A} \bar{M} \tag{A.1b}$$

If we use the Ansatz of equation (1.16), we see that the interaction terms generate terms with other wavelengths - for example $e^{ik_c x} e^{ik_c x} = e^{i2k_c x}$. For notational convenience we write $E := e^{ik_c x}$. These other waves play a role in the system and we therefore must consider them when we try to find the partial differential equation for the amplitude A . So we must expand our Ansatz and consider perturbations of the form

$$\begin{aligned}
(\bar{M}, \bar{A}) &= E^0 \quad [\quad \varepsilon^2 \vec{A}_{20}(\chi, \tau) \quad + \dots \quad] \\
&\quad + E^1 \quad [\varepsilon \vec{v}_{11} A(\chi, \tau) \quad + \varepsilon^2 \vec{A}_{21}(\chi, \tau) \quad + \varepsilon^3 \vec{A}_{31}(\chi, \tau) + \dots \quad] \\
&\quad + E^2 \quad [\quad \varepsilon^2 \vec{A}_{22}(\chi, \tau) \quad + \dots \quad] \\
&\quad + c.c. \quad + h.o.t.
\end{aligned}$$

The functions \vec{A}_{20} , \vec{A}_{31} , \vec{A}_{21} and \vec{A}_{31} are all functions of the slow time and spatial variables τ and ξ . We denote $\vec{A}_{ij} = (m_{ij}, a_{ij})$ for all $i, j \in \mathbb{N}$.

The following step in the weakly non-linear stability analysis involves using this complete Ansatz on the system of equation (A.1). Then we inspect the resulting system at each $\varepsilon^i E^{j'}$ level. Doing so gives us information about all functions \tilde{A}_{ij} and finally at the $\mathcal{O}(\varepsilon^3 E^1)$ -level we obtain a partial differential equation for the amplitude A . In the next sections we inspect the system at the various levels, working our way up to the system at the $\mathcal{O}(\varepsilon^3 E^1)$ -level.

The $\mathcal{O}(\varepsilon^1 E^1)$ -level

At the $\mathcal{O}(\varepsilon^1 E^1)$ -level we just find the linearised system again. That is, we just have the eigenvalue problem $\mathcal{M}_C \vec{v}_{11} = \lambda_1 \vec{v}_{11}$ where $\lambda_1 = 0$ and

$$\mathcal{M}_C := \begin{pmatrix} \frac{M_e}{(1+M_e)^2} - \tilde{\mu}_C k_c^2 & r M_e \\ -A_e & -\frac{\tilde{\alpha}}{A_e} - k_c^2 \end{pmatrix}$$

After a fairly long computation one can check that an eigenvector is given by

$$\vec{v}_{11} = (m_{11}, a_{11}) = \left(-r(1 - \tilde{\alpha})^2(1 + \sqrt{1 - \tilde{\alpha}r}), (1 - \tilde{\alpha}r)^2 \right).$$

It can also be checked that the other eigenvector is $\vec{w} = (\tilde{\mu}_C m_{11}, a_{11})$, with the corresponding eigenvalue $\omega_1 = (\tilde{\mu}_C - 1)(k_c^2 + \tilde{\alpha}/A_e)$. In the end we see that the amplitude equation appears as a consequence of the solvability condition that $\mathcal{M}_c x = \vec{b} = (b_1, b_2)$ can only be solved for x if $\vec{b} \in Sp(\vec{w})$, because the other eigenvalue is zero. Thus we find the solvability condition for this system as

$$a_{11}b_1 - \tilde{\mu}_C m_{11}b_2 = 0. \quad (\text{A.2})$$

The $\mathcal{O}(\varepsilon^2 E^0)$ -level

At the $\mathcal{O}(\varepsilon^2 E^0)$ -level the resulting system is

$$\begin{aligned} 0 &= \frac{M_e}{(1+M_e)^2} m_{20} + r M_e a_{20} + 2\phi|A|^2 \\ 0 &= -A_e m_{20} - \frac{\tilde{\alpha}}{A_e} a_{20} + 2\theta|A|^2 \end{aligned}$$

where ϕ and θ are defined as

$$\begin{aligned} \phi &:= r m_{11} a_{11} + \frac{m_{11}^2}{(1+M_e)^3} \\ \theta &:= -m_{11} a_{11} \end{aligned}$$

Using standard linear algebra, we can solve this system and find the solution

$$\vec{A}_{20} = \begin{pmatrix} m_{20} \\ a_{20} \end{pmatrix} = \frac{2|A|^2}{r M_e A_e - \frac{M_e}{(1+M_e)^2} \frac{\tilde{\alpha}}{A_e}} \begin{pmatrix} r M_e \theta + \frac{\tilde{\alpha}}{A_e} \phi \\ -A_e \phi - \frac{M_e}{(1+M_e)^2} \theta \end{pmatrix}.$$

The $\mathcal{O}(\varepsilon^2 E^2)$ -level

At this level we obtain the system

$$\begin{aligned} 0 &= \left(\frac{M_e}{(1+M_e)^2} - 4\tilde{\mu}_C k_c^2 \right) m_{22} + r M_e a_{22} + \phi A^2 \\ 0 &= -A_e m_{22} + \left(-\frac{\tilde{\alpha}}{A_e} - 4k_c^2 \right) m_{20} + \theta A^2 \end{aligned}$$

This system has the following solution

$$\vec{A}_{22} = \begin{pmatrix} m_{22} \\ a_{22} \end{pmatrix} = \frac{A^2}{D} \begin{pmatrix} r M_e \theta + (\tilde{\alpha}/A_e + 4k_c^2)\phi \\ -A_e \phi + (4\tilde{\mu}_C k_c^2 - \frac{M_e}{(1+M_e)^2})\theta \end{pmatrix},$$

where

$$D = r M_e A_e - \frac{M_e}{(1+M_e)^2} \frac{\tilde{\alpha}}{A_e} - 4k_c^2 \left(\frac{M_e}{(1+M_e)^2} - \tilde{\mu}_C \frac{\tilde{\alpha}}{A_e} \right) + 16\tilde{\mu}_C k_c^4.$$

The $\mathcal{O}(\varepsilon^2 E^1)$ -level

Working out the system on the $\mathcal{O}(\varepsilon^2 E^1)$ -level we find the following system

$$\mathcal{M}_c \vec{A}_{21} = -2ik_c A_\xi \begin{pmatrix} \tilde{\mu}_C m_{11} \\ a_{11} \end{pmatrix}.$$

Clearly the right-hand side obeys the solvability condition. Hence the general solution of this system is

$$\vec{A}_2 = \frac{-2ik_c A_\xi}{\omega_1} \vec{w} + A_2(\xi, \tau) \vec{v}_{11}.$$

where ω_1 is the eigenvalue corresponding to the eigenvector \vec{w} and A_2 is a second, higher order amplitude, which again depends on the slow space variable ξ and the slow time variable τ . With standard linear algebra we can also write this solution as

$$\vec{A}_2 = \frac{-2ik_c A_\xi}{\omega_1} (\tilde{\mu}_C - 1) \begin{pmatrix} m_{11} \\ 0 \end{pmatrix} + A_2(\xi, \tau) \vec{v}_{11} \quad (\text{A.3})$$

where A_2 now denotes another amplitude.

The $\mathcal{O}(\varepsilon^3 E^1)$ -level

Finally we can look at the $\varepsilon^3 E^1$ -level. Here we must note that we now also need to take the expansion in $\tilde{\mu}$ into account (i.e. $\tilde{\mu} = \tilde{\mu}_C - \varepsilon^2 s$). The resulting system at this level is

$$\begin{aligned} M_c \vec{A}_{31} &= \begin{pmatrix} m_{11} \\ \tilde{\gamma} a_{11} \end{pmatrix} A_\tau + s |k_c|^2 \begin{pmatrix} m_{11} \\ 0 \end{pmatrix} A - \begin{pmatrix} \tilde{\mu}_C m_{11} \\ a_{11} \end{pmatrix} A_{xx} \\ &\quad - \begin{pmatrix} r[m_{11}(y_{20} + y_{22}) + a_{11}(x_{20} + x_{22})] + 2m_{11}(x_{20} + x_{22})(1+m_e)^{-3} \\ -[m_{11}(y_{20} + y_{22}) + a_{11}(x_{20} + x_{22})] \end{pmatrix} |A|^2 A \\ &\quad + 3 \frac{m_{11}^3}{(1+m_e)^4} \begin{pmatrix} 1 \\ 0 \end{pmatrix} |A|^2 A - 2ik_c \begin{pmatrix} \tilde{\mu}_C m_{21,x} \\ a_{21,x} \end{pmatrix} \end{aligned} \quad (\text{A.4})$$

Here we have denoted

$$\vec{A}_{20} = \begin{pmatrix} m_{20} \\ a_{20} \end{pmatrix} = \begin{pmatrix} x_{20} \\ y_{20} \end{pmatrix} |A|^2$$

and

$$\vec{A}_{22} = \begin{pmatrix} m_{22} \\ a_{22} \end{pmatrix} = \begin{pmatrix} x_{22} \\ y_{22} \end{pmatrix} A^2$$

For notational convenience we write $X := x_{20} + x_{22}$ and $Y := y_{20} + y_{22}$. Now, we need to apply the solvability condition of equation (A.2) to the expression on the right hand side of equation (A.4). This gives us

$$\begin{aligned} 0 &= a_{11}m_{11}(1 - \tilde{\gamma}\tilde{\mu}_C)A_\tau + s|k_c|^2a_{11}m_{11}A \\ &\quad - 2i\tilde{\mu}_C(a_{11}[k_c m_{12,\chi}] - m_{11}[k_c a_{12,\chi}]) \\ &\quad - [(\tilde{\mu}_C m_{11}a_{11} + ra_{11}^2 + m_{11}a_{11}(1 + m_e)^{-3})X + (\tilde{\mu}_C m_{11}^2 + rm_{11}a_{11})Y \\ &\quad - m_{11}^3a_{11}(1 + m_e)^{-4}]|A|^2A \end{aligned} \quad (\text{A.5})$$

If we recall the solution for \vec{A}_{21} in equation (A.3) we can eliminate the second amplitude A_2 and we obtain the following equation

$$\begin{aligned} 0 &= a_{11}m_{11}(1 - \tilde{\gamma}\tilde{\mu}_C)A_\tau + s|k_c|^2a_{11}m_{11}A \\ &\quad - 4a_{11}m_{11}\tilde{\mu}_C(\tilde{\mu}_C - 1)/\omega_1 k_c^2 A_{\chi\chi} \\ &\quad - [(\tilde{\mu}_C m_{11}a_{11} + ra_{11}^2 + m_{11}a_{11}(1 + m_e)^{-3})X + (\mu_c m_{11}^2 + rm_{11}a_{11})Y \\ &\quad - m_{11}^3a_{11}(1 + m_e)^{-4}]|A|^2A \end{aligned} \quad (\text{A.6})$$

This equation can be rewritten as

$$A_\tau = \frac{s|k_c|^2}{\tilde{\gamma}\tilde{\mu}_C - 1}A + \frac{4\tilde{\mu}_C}{\omega_1} \frac{\tilde{\mu}_C - 1}{1 - \tilde{\gamma}\tilde{\mu}_C} k_c^2 A_{\chi\chi} + \frac{h}{a_{11}m_{11}(1 - \tilde{\gamma}\tilde{\mu}_C)}|A|^2A,$$

where

$$\begin{aligned} h &= (\tilde{\mu}_C m_{11}a_{11} + ra_{11}^2 + m_{11}a_{11}(1 + M_e)^{-3})X + (\tilde{\mu}_C m_{11}^2 + rm_{11}a_{11})Y \\ &\quad - m_{11}^3a_{11}(1 + M_e)^{-4}. \end{aligned}$$

Now, we introduce another triplet of quantities for notational convenience:

$$\begin{aligned} \rho_1 &:= -\frac{s|k_c|^2}{\tilde{\gamma}\tilde{\mu}_C - 1}; \\ \rho_2 &:= -\frac{4\tilde{\mu}_C}{\omega_1} \frac{\tilde{\mu}_C - 1}{\tilde{\gamma}\tilde{\mu}_C - 1} = -\frac{4\tilde{\mu}_C}{\tilde{\gamma}\tilde{\mu}_C - 1} \frac{1}{|k_c|^2 + \tilde{\alpha}/A_e}; \\ \rho_3 &:= -\frac{1}{a_{11}m_{11}} \frac{1}{(\tilde{\gamma}\tilde{\mu}_C - 1)}. \end{aligned}$$

where we have used the value of the eigenvalue ω_1 . That is

$$\omega_1 = (\tilde{\mu}_C - 1) \left(|\vec{k}_c|^2 + \tilde{\alpha}/A_e \right)$$

In section 1.2.2 we have found two condition (i.e. equation (1.11) and (1.12)) on the system's parameters, which were necessary to possible have stable uniform steady state solution (m_e, a_e) . As we discussed, these two conditions are satisfied for the specific parameters of the mussel-algae system. From the first inequality, equation (1.11), we can obtain the inequality

$$\tilde{\mu}_C \tilde{\gamma} = \tilde{\gamma} \frac{M_e}{(1 + M_e)^2} \frac{1}{2|k_c|^2 + \tilde{\alpha}/A_e} < \frac{\tilde{\alpha}/A_e}{2|k_c|^2 + \tilde{\alpha}/A_e} < 1.$$

Hence we find that $\tilde{\mu}\tilde{\gamma} - 1$ must be negative. Since $s, |k_c|^2, \tilde{\mu}_C$ and a_{11} are positive and m_{11} is negative, the above presented definitions of ρ_1, ρ_2 and ρ_3 ensure that these are all positive.

With use of these constants, the modulation equation becomes

$$A_\tau = -\rho_1 A + \rho_2 k_c^2 A_{\chi\chi} - \rho_3 h |A|^2 A.$$

At this point we can write this equation in a more standardized Ginzburg-Landau form by rescaling χ, τ and A . To do this, we introduce $\bar{\tau} = C_1 \tau$, $\bar{\chi} = C_2 \chi$ and $\bar{A} = C_3 A$. By choosing $C_1 = \rho_1$, $C_3 = \sqrt{\rho_3/\rho_1}$ and $C_2 = \sqrt{\rho_2/\rho_1} \frac{1}{k_c^2}$. Hence the modulation equation for this one-dimensional perturbation becomes (suppressing the bars):

$$A_\tau = -A + A_{\chi\chi} - h |A|^2 A$$

The sign of h depends on the specific values for all parameters. In Appendix C we inspect the Ginzburg-Landau in detail.

Appendix B

Approximations for bifurcation planes

In Section 3.2 we give approximations of the bifurcation lines and eigenvalue curves, when we work with the μ -parameters (i.e. we use μ_{11} and μ_{21} as our bifurcation parameters). The results in that section are not self-contained and refer to a similar analysis, using η and γ as bifurcation parameters. In this appendix we give the details of this study to which we refer in Section 3.2.

B.1 Approximation of bifurcation lines

Our first goal is to find approximations of the bifurcation lines. These lines, in the parameter space, indicate when either the trace or the determinant changes signs. In turn this tells us for what values of our parameters the uniform steady state is linearly stable and when it is unstable. We first inspect when the trace changes sign and then find out when the determinant changes sign.

B.1.1 On the trace

To have linear stability we need to have $\theta > \theta_c$. As we have seen before we have $\theta_c = \max\{0, -\eta \frac{|\eta|}{4}\}$. This means that $\theta_c = 0$ when $\eta \geq 0$ and $\theta_c = \frac{\eta^2}{4}$ when $\eta < 0$.

We have assumed that θ is positive and of order $\mathcal{O}(\varepsilon)$. This means that when we always have $\theta > 0$. So, when $\eta \geq 0$ the trace of $M(\vec{k})$ is negative for all wavelengths.

When $\eta < 0$, however, the critical value θ_c increases to $\theta_c = \frac{\eta^2}{4}$. Now, in order to still have linear stability we need $\theta > \theta_c = \frac{\eta^2}{4}$, and we have a critical situation when $\theta = \theta_c = \frac{\eta^2}{4}$. Since θ is of order $\mathcal{O}(\varepsilon)$ it is clear that this inequality can

only be satisfied when θ_c is of order $\mathcal{O}(\varepsilon)$ as well. From this it is clear that η need to be of order $\mathcal{O}(\sqrt{\varepsilon})$.

More precisely, we can write $\theta = \varepsilon t$, where $t > 0$ and of order $\mathcal{O}(1)$. Then the critical situation $\theta = \theta_c$ is attained when $\eta = -2\sqrt{\varepsilon}\sqrt{t}$. So this means that the trace is negative for all possible wavelengths when $\eta > -2\sqrt{\varepsilon}\sqrt{t}$ and the trace is positive for some range of wavelengths when $\eta < -2\sqrt{\varepsilon}\sqrt{t}$. When $\eta = -2\sqrt{\varepsilon}\sqrt{t}$ the trace is zero for the set of wavelengths with $|\vec{k}|^2 = \frac{-\eta}{2}$ (and negative for all others). This is the critical situation and therefore we define $\eta_c := -2\sqrt{\varepsilon}\sqrt{t}$.

B.1.2 On the determinant

For linear stability we need the determinant to be positive for all wavelengths \vec{k} . This means that we need to have $\delta > \delta_c$. Per assumption we know that $\delta > 0$. Thus if $\delta_c = 0$ this condition is trivially obeyed. Thus when (β, γ) lies above (or on) the line \mathcal{A} (see equation (3.11) and the red region in Figure 3.3) the determinant is positive for all possible wavelengths.

The characterization in the other regions is not as clear. In this region the critical value δ_c is positive and thus it is not immediately clear when the condition $\delta > \delta_c$ is obeyed. Since δ is of order $\mathcal{O}(\varepsilon)$ it is only possible for this condition to hold, when δ_c is of order $\mathcal{O}(\varepsilon)$ as well. Recalling the value of δ_c in this region, as stated in equation (3.13), we have

$$27\delta_c = \left(-\beta + \sqrt{\beta^2 - 3\gamma} \right) \left(\beta^2 - 6\gamma - \beta\sqrt{\beta^2 - 3\gamma} \right). \quad (\text{B.1})$$

We have already seen that this expression is zero when $(\beta, \gamma) \in \mathcal{A}$. So when $\beta \geq 0$ and $\gamma = 0$ or when $\beta \leq 0$ and $\gamma = \frac{\beta^2}{4}$ the critical value $\delta_c = 0$. In the neighbourhood of this line (but below it!), we find parameter combinations such that δ_c is positive and of order $\mathcal{O}(\varepsilon)$.

So we essentially have two different situations we need to deal with. First, we have the case when $\beta < 0$ and $\gamma \approx \beta^2/4$. Secondly there is the case when $\beta > 0$ and $\gamma \approx 0$. For both of these cases we assume that β is of order $\mathcal{O}(\varepsilon^\mu)$, where $\mu \in \mathbb{R}$. We then investigate what this imposes on the order of $\gamma - \max\left\{0, -\beta\frac{|\beta|}{4}\right\}$.

Case $\beta < 0$

As stated before, when $\beta < 0$ we know that $\delta_c = 0$ when $\gamma = \frac{\beta^2}{4}$. Now we assume that $\beta = \varepsilon^\mu b$ and that $\gamma = \frac{\beta^2}{4} + \varepsilon^\nu g = \varepsilon^{2\mu} \frac{b^2}{4} + \varepsilon^\nu g$, where $b, g < 0$ are of order $\mathcal{O}(1)$. This corresponds to a parameter combination such that (β, γ) lies close to \mathcal{A} but still below it. The exponents μ and ν are at this point unknown and must be chosen such that δ_c is of order ε . In this section we determine what conditions this implies on the exponents μ and ν .

To do this we evaluate the expression for δ_c at the point (β, γ) and determine the leading order of this expression. The leading order must be of order ε . To be more precise we assume that $\delta_c = \varepsilon z$ where $z > 0$ is of order

$\mathcal{O}(1)$. Now, the most difficult part in the expression for δ_c is the square root $\sqrt{\beta^2 - 3\gamma} = \sqrt{\varepsilon^{2\mu} \frac{b^2}{4} - 3\varepsilon^\nu g}$. With a Taylor approximation we can get rid of this root. However, there are now three essentially different possibilities: (1) $2\mu < \nu$, (2) $2\mu > \nu$ and (3) $2\mu = \nu$. We inspect them one by one.

- (1) In this case the leading order in the root is $\varepsilon^{2\mu}$. Hence we can approximate the root with $\sqrt{\varepsilon^{2\mu} \frac{b^2}{4} - 3\varepsilon^\nu g} = \varepsilon^\mu \frac{|b|}{2} + 3\varepsilon^{\nu-\mu} \frac{g}{b}$. Thus by substituting this into equation (B.1) we obtain up to leading order

$$\begin{aligned} 27\delta_c = 27\varepsilon z &= \left(-\varepsilon^\mu b - \varepsilon^\mu \frac{b}{2} + 3\varepsilon^{\nu-\mu} \frac{g}{b} \right) \\ &\quad \left(\varepsilon^{2\mu} b^2 - \frac{3}{2} \varepsilon^{2\mu} b^2 - 6\varepsilon^\nu g - \varepsilon^\mu b \left(\varepsilon^\mu \frac{-b}{2} + \varepsilon^{\nu-\mu} 3 \frac{g}{b} \right) \right) \\ &= \left(\frac{-3}{2} \varepsilon^\mu b + 3\varepsilon^{\nu-\mu} \frac{g}{b} \right) (-9\varepsilon^\nu g) \\ &= \frac{27}{2} \varepsilon^{\mu+\nu} g b - 27\varepsilon^{2\nu-\mu} \frac{g^2}{b} \end{aligned}$$

In this situation we have $2\mu < \nu$ and therefore $\mu < \nu - \mu$. The leading order of the right-hand side is thus $\varepsilon^{\mu+\nu}$. So our final equality becomes

$$\varepsilon z = \varepsilon^{\mu+\nu} \frac{gb}{2}.$$

In order for this to hold, we must have $\mu + \nu = 1$ and $g = \frac{2z}{b}$. From the first condition we also learn that this case - with $2\mu < \nu$ - can only happen when $\mu < \frac{1}{3}$ and that $\nu = 1 - \mu$ in this case.

- (2) When $2\mu > \nu$ the leading order of the root's argument is $\mathcal{O}(\varepsilon^\nu)$. Hence the root now must be approximated as

$$\sqrt{\varepsilon^{2\mu} \frac{b^2}{4} - 3\varepsilon^\nu g} = \sqrt{-3g} \varepsilon^{\nu/2} + \varepsilon^{2\mu-\nu/2} \frac{b^2}{4\sqrt{-3g}}$$

Therefore the leading order of our expression for δ_c changes. We now have up to leading order

$$\begin{aligned} 27\delta_c = 27\varepsilon z &= \left(-\varepsilon^\mu b + \varepsilon^{\nu/2} \sqrt{-3g} + \varepsilon^{2\mu-\nu/2} \frac{b^2}{8\sqrt{-3g}} \right) \\ &\quad \left(-\varepsilon^{2\mu} \frac{b^2}{2} - 6\varepsilon^\nu g - \varepsilon^{\mu+\nu/2} b \sqrt{-3g} - \varepsilon^{3\mu-\nu/2} \frac{b^2}{8\sqrt{-3g}} \right) \end{aligned}$$

Because we are inspecting the case in which $2\mu > \nu$, we know that we have $\mu, 2\mu - \nu/2 > \nu/2$ and that $\mu + \nu/2, 3\mu - \nu/2 > \nu$. Therefore up to leading order the equation becomes

$$27\varepsilon z = -\varepsilon^{3\nu/2} 6g \sqrt{-3g} \tag{B.2}$$

And this equality only holds when $\nu = \frac{2}{3}$ and $g = -3(z/2)^{2/3}$. Because $2\mu > \nu$ this means that μ must satisfy $\mu > \frac{1}{3}$.

Table B.1 – Summary of the results in section B.1.2. We have inspected the case when $\beta = \varepsilon^\mu b$ and $\gamma = \frac{\beta^2}{4} + \varepsilon^\nu g$, where $b, g < 0$ and of order $\mathcal{O}(1)$ and determined when the expression for δ_c can be written as $\delta_c = \varepsilon z$ with $z > 0$ of order $\mathcal{O}(1)$.

exponent μ	exponent ν	explicit solution
$\mu < \frac{1}{3}$	$\nu = 1 - \mu$	$g = \frac{2z}{b}$
$\mu = \frac{1}{3}$	$\nu = \frac{2}{3}$	existence is guaranteed
$\mu > \frac{1}{3}$	$\nu = \frac{2}{3}$	$g = -3(z/2)^{\frac{2}{3}}$

- (3) Finally we inspect the case $2\mu = \nu$. In this case the root cannot be expanded and we must use $\sqrt{\varepsilon^{2\mu} \frac{b^2}{4} - 3\varepsilon^\nu g} = \varepsilon^\mu \sqrt{\frac{b^2}{4} - 3g}$. Therefore equation (B.1) becomes up to leading order

$$27\delta_c = 27\varepsilon z = \varepsilon^{3\mu} \left(-b + \sqrt{\frac{b^2}{4} - 3g} \right) \left(-\frac{1}{2}b^2 - 6g - b\sqrt{b^2/4 - 3g} \right)$$

To ensure that the orders match up we need $\mu = \frac{1}{3}$ and therefore $\nu = \frac{2}{3}$ (note that the expression on the right-hand side never vanishes for $b, g < 0$). It is not easy to explicitly solve this equation. However, for given b it is clear that the right-hand side becomes zero when $g \uparrow 0$ and tends to infinity when $g \rightarrow -\infty$. Therefore the intermediate value theorem guarantees that a solution exists.

The results of this subsection are summarized in Table B.1. These results tell us about the condition that are imposed on the parameters β and γ to ensure that $\delta_c = \varepsilon z$ (with $z > 0$ of order $\mathcal{O}(1)$) in the case that $\beta < 0$.

Case $\beta > 0$

When $\beta > 0$ we know that the critical $\delta_c = 0$ when $\gamma = 0$. Therefore we now inspect the situation when $\beta = \varepsilon^\mu b$ and $\gamma = \varepsilon^\nu g$ with $b > 0$ and $g < 0$ and both of order $\mathcal{O}(1)$. Again we want to determine the conditions for various exponents ν that ensure that $\delta_c = \varepsilon z$ with $z > 0$ of order $\mathcal{O}(1)$. As before the three essentially different possibilities are (1) $2\mu < \nu$, (2) $2\mu > \nu$ and (3) $2\mu = \nu$. We inspect each of these.

- (1) As before the leading order of the root's argument is $\varepsilon^{2\mu}$. Therefore the root can be approximated as

$$\sqrt{\beta^2 - 3\gamma} = \sqrt{\varepsilon^{2\mu} b^2 - 3\varepsilon^\nu g} = \varepsilon^\mu b - \frac{3}{2}\varepsilon^{\nu-\mu} \frac{g}{b}$$

Therefore the expression for δ_c of equation (B.1) becomes up to leading order:

$$\begin{aligned} 27\delta_c = 27\varepsilon z &= \left(-\frac{3}{2}\varepsilon^{\nu-\mu} \frac{g}{b} \right) \left(\varepsilon^{2\mu} b^2 - 6\varepsilon^\nu g - \varepsilon^{2\mu} b^2 + \frac{3}{2}\varepsilon^\nu g \right) \\ &= \frac{27}{4}\varepsilon^{2\nu-\mu} \frac{g^2}{b} \end{aligned}$$

Table B.2 – Summary of the results in section B.1.2. We have inspected the case when $\beta = \varepsilon^\mu b$ and $\gamma = \varepsilon^\nu g$, where $b > 0, g < 0$ and of both parameters of order $\mathcal{O}(1)$ and determined when the expression for δ_c can be written as $\delta_c = \varepsilon z$ with $z > 0$ of order $\mathcal{O}(1)$.

exponent μ	exponent ν	explicit solution
$\mu < \frac{1}{3}$	$\nu = \frac{1}{2} + \frac{\mu}{2}$	$g = -2\sqrt{bz}$
$\mu = \frac{1}{3}$	$\nu = \frac{2}{3}$	existence is guaranteed
$\mu > \frac{1}{3}$	$\nu = \frac{2}{3}$	$g = -3(z/2)^{\frac{2}{3}}$

Clearly for this equality to hold we need $2\nu - \mu = 1$ and $g = -2\sqrt{bz}$ (since g needs to be negative). This leads to the condition that $\mu < \frac{1}{3}$ and $\nu = \frac{1}{2} + \frac{\mu}{2}$.

- (2) Here the root can be approximated as

$$\sqrt{\varepsilon^{2\mu} b^2 - 3\varepsilon^\nu g} = \varepsilon^{\nu/2} \sqrt{-3g} + \frac{b^2}{2\sqrt{-3g}} \varepsilon^{2\mu-\nu/2}$$

Therefore we now find the following expression for δ_c up to leading orders

$$\begin{aligned} 27\delta_c = 27\varepsilon z &= \left(-\varepsilon^\mu b + \sqrt{-3g}\varepsilon^{\nu/2} + \frac{b^2}{2\sqrt{-3g}}\varepsilon^{2\mu-\nu/2} \right) \\ &\quad \left(\varepsilon^{2\mu} b^2 - 6\varepsilon^\nu g - \varepsilon^{\mu+\nu/2} \sqrt{-3g}b + \frac{b^3}{2\sqrt{-3g}}\varepsilon^{3\mu-\nu/2} \right) \\ &= -6\sqrt{3g}\sqrt{-g}\varepsilon^{3\nu/2} \end{aligned}$$

So this leads to the conditions $\nu = \frac{2}{3}$, $\mu > \frac{1}{3}$ and $g = -3(z/2)^{\frac{2}{3}}$.

- (3) In this case the root cannot be expanded. So we find the following expression for δ_c up to leading order

$$27\delta_c = 27\varepsilon z = \varepsilon^{3\mu} \left(-b + \sqrt{b^2 - 3g} \right) \left(b^2 - 6g - b\sqrt{b^2 - 3g} \right)$$

So to have the same orders of ε on both sides we need $\mu = \frac{1}{3}$ and therefore $\nu = \frac{2}{3}$ (again note that the expression never vanishes, when $\gamma < 0$ and $b > 0$). As before finding the exact solution is a horrible task, but we can again see that there must be a solution, because - for a fixed $b > 0$ - we know that the right-hand side tends to zero as $g \uparrow 0$ and tends to infinity when $g \rightarrow -\infty$. So by the intermediate value theorem we know that a solution must exist.

The results of this subsection are summarized in Table B.2. These results tell us about the condition we need to impose on the parameters β and γ to ensure that $\delta_c = \varepsilon z$, where $z > 0$ of order $\mathcal{O}(1)$, in the case $\beta > 0$.

General β

In the previous two subsections we have inspected the cases $\beta < 0$ and $\beta > 0$. So at this moment we have the information for all possible orders of β , except

Table B.3 – Summary of the results on the determinant. We have inspected all possibilities for the sign and the order of $\beta = \varepsilon^\mu b$ and determined the corresponding order of the difference between the point (β, γ) and the point on the line \mathcal{A} with the same β , which we have defined as $\varepsilon^\nu g$ to ensure that $\delta_c = \varepsilon z$ is of order $\mathcal{O}(\varepsilon)$. Moreover, we have also tried to find the explicit solution. Also see Figure B.1 for a sketch of the situation.

sgn β	exponent μ	exponent ν	explicit solution
$\beta < 0$	$\mu < 1/3$	$\nu = 1 - \mu$	$g = \frac{2z}{b}$
$\beta < 0$	$\mu = 1/3$	$\nu = 2/3$	existence is guaranteed
$\beta < 0$	$\mu > 1/3$	$\nu = 2/3$	$g = -3(z/2)^{\frac{2}{3}}$
$\beta = 0$	-	$\nu = 2/3$	$g = -3(z/2)^{\frac{2}{3}}$
$\beta > 0$	$\mu > 1/3$	$\nu = 2/3$	$g = -3(z/2)^{\frac{2}{3}}$
$\beta > 0$	$\mu = 1/3$	$\nu = 2/3$	existence is guaranteed
$\beta > 0$	$\mu < 1/3$	$\nu = (1 + \mu)/2$	$g = -2\sqrt{bz}$

for $\beta = 0$. In this case, however, equation (B.1) reduces to

$$27\delta_c = 6\sqrt{3}(-\gamma)^{3/2}$$

Hence if we set $\delta_c = \varepsilon z$ with $z > 0$, we find the solution $\gamma = 3(z/2)^{2/3}\varepsilon^{2/3}$.

At this point we have inspected all the possible situations for β . We have summarized our findings in Table B.3. In Figure B.1 we have sketched the various possibilities in the (β, γ) plane.

As we have stated many times before, when $\delta > \delta_c$ the determinant of the matrix $M(\vec{k})$ is positive for all wavelengths \vec{k} and when $\delta < \delta_c$ this determinant is negative for some range of wavelengths \vec{k} . At the critical value $\delta = \delta_c$ the determinant is non-negative for all wavelengths and there are a few critical wavelengths.

Since we have assumed that $\delta = \varepsilon d$ where $d > 0$ is of order $\mathcal{O}(1)$. Hence only when the parameters β and γ are such that δ_c is of order $\mathcal{O}(\varepsilon)$ can it ever happen that we have a critical wavelength (due to the determinant). So this means that only when (β, γ) is contained in the red region of Figure B.1 we can possibly find that the determinant is non-negative for all wavelengths and identically zero for some critical wavelengths \vec{k}_c .

If we assume that $\delta = \varepsilon d$ is fixed, and that we know the order and sign of β , we can use Table B.3 to find what value for γ is critical (i.e. replace z with d in this table). We'll call this critical value γ_c . Now from the previous analysis it is clear that the uniform steady state is stable when $\gamma > \gamma_c$ and that there are critical wavelengths when $\gamma = \gamma_c$.

In this case the critical wavelengths are those with $|\vec{k}_c|^2 = \frac{1}{3}(-\beta + \sqrt{\beta^2 - 3\gamma})$. We can apply the same order analysis on this expression to find the leading order of $|\vec{k}_c|^2$. The results of this analysis are given in Table B.4.

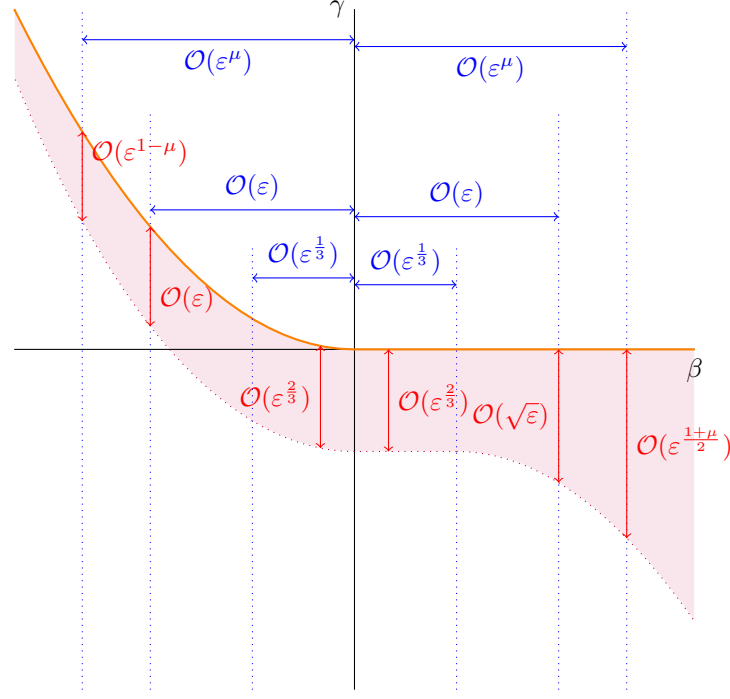


Figure B.1 – Schematic illustration of the region in the (β, γ) plane where the critical δ_c is of order $\mathcal{O}(\varepsilon)$. See also Table B.3. The blue lines denote orders of β , the red one the orders of γ . The orange line in this illustration is the line where $\delta_c = 0$. In the region above the orange line $\delta_c = 0$ and thus $\delta > \delta_c$ is always satisfied. Hence the determinant is positive for all wavelengths. In the region below the purple line δ_c is larger than order $\mathcal{O}(\varepsilon)$ and hence $\delta < \delta_c$. Thus in this region there is a range of wavelengths with positive eigenvalues and thus the system cannot be linearly stable in this region.

Table B.4 – In this table we summarize the various possible critical values γ_c and critical wavelengths \vec{k}_c , for given parameters $\delta = \varepsilon d$ and $\beta = \varepsilon^\mu b$. Here $\gamma_c = \max\{0, -\beta \frac{|\beta|}{4}\} + \varepsilon^\nu g_c$ (see Table B.3). This table only shows the leading order of these critical values.

sgn β	exponent μ	γ_c (or g_c)	$ \vec{k}_c ^2$
$\beta < 0$	$\mu < 1/3$	$\varepsilon^\nu g_c = \frac{2d}{b} \varepsilon^{1-\mu}$	$ \vec{k}_c ^2 = -\frac{1}{2} \varepsilon^\mu b$
$\beta < 0$	$\mu = 1/3$	existence guaranteed	$ \vec{k}_c ^2 = \frac{1}{3} \varepsilon^{1/3} (-b + \sqrt{b^2/4 - 3g})$
$\beta < 0$	$\mu > 1/3$	$\varepsilon^\nu g_c = -3(d/2)^{2/3} \varepsilon^{2/3}$	$ \vec{k}_c ^2 = \varepsilon^{1/3} \sqrt{-g/3}$
$\beta = 0$	-	$\gamma_c = -3(d/2)^{2/3} \varepsilon^{2/3}$	$ \vec{k}_c ^2 = \varepsilon^{1/3} \sqrt{-g/3}$
$\beta > 0$	$\mu > 1/3$	$\gamma_c = -3(d/2)^{2/3} \varepsilon^{2/3}$	$ \vec{k}_c ^2 = \varepsilon^{1/3} \sqrt{-g/3}$
$\beta > 0$	$\mu = 1/3$	existence guaranteed	$ \vec{k}_c ^2 = \varepsilon^{1/3} (-b + \sqrt{b^2 - 3g})$
$\beta > 0$	$\mu < 1/3$	$\gamma_c = -2\sqrt{bd\varepsilon} \frac{1+\mu}{2}$	$ \vec{k}_c ^2 = -\frac{1}{2} \varepsilon^{\frac{1-\mu}{2}} g/b$

B.2 Bifurcation lines in the (η, γ) -plane

In the previous sections we have determined that the trace of the matrix $M(\vec{k})$ is negative for all wavelengths \vec{k} when $\eta > \eta_c$ and that the determinant is positive for all wavelengths when $\gamma > \gamma_c$, for given values of the parameters β, δ and θ . We also saw that the order of γ_c depends on the order of β (see Table B.4). From this we learn that there are bifurcations when $\gamma = \gamma_c$ or when $\eta = \eta_c$. In this section we further investigate the parameter space (η, γ) .

Again, we assume that $\beta = \varepsilon^\mu b$, $\delta = \varepsilon d$ and $\theta = \varepsilon t$. Furthermore we denote $\gamma = \varepsilon^\nu g$ and $\eta = \varepsilon^\tau e$, where the parameters b, d, t, g and e are of order $\mathcal{O}(1)$. In section B.1.1 we have found that $\eta_c = -2\sqrt{\varepsilon}\sqrt{t}$ and in section B.1.2 we saw that the order and the sign of γ_c depends on the value of $\beta = \varepsilon^\mu b$. More precisely we found

$$\gamma_c = \begin{cases} g\varepsilon^{2\mu} & \text{with } g > 0, \text{ when } \mu < 1/3 \text{ and } b < 0; \\ g\varepsilon^{2/3} & \text{with } g < 0, \text{ when } \mu \geq 1/3; \\ g\varepsilon^{\frac{1+\mu}{2}} & \text{with } g < 0, \text{ when } \mu < 1/3 \text{ and } b > 0. \end{cases} \quad (\text{B.3})$$

We want to study the stability of the system, for varying parameters γ and η . With the previous insight it is now clear that there are essentially three different forms of the (η, γ) parameter plane, depending on the sign and order of the parameter β . We have sketched all three of these possibilities in Figure B.2.

So it is now clear that there are two bifurcation curves in the (η, γ) plane. The bifurcations we are here encountering are those that make the stationary state unstable. Thus the bifurcation occurs at the boundary of the green area (see Figure B.2). The boundary on which $\gamma = \gamma_c$ we'll denote by Γ_d and the other boundary, on which $\eta = \eta_c$, we'll define as Γ_t . Thus we have

$$\Gamma_d = \{(\eta, \gamma_c) : \eta = \eta_c\} \quad (\text{B.4a})$$

$$\Gamma_t = \{(\eta_c, \gamma) : \gamma = \gamma_c\} \quad (\text{B.4b})$$

From our analysis it is clear that on Γ_d there is a band of critical wavelengths with a specific absolute value (see Table B.4 for the precise conditions for these wavelengths). For these wavelengths \vec{k}_c we know that the determinant of $M(\vec{k})$ is zero, but the trace is negative (as long as $\eta > \eta_c$). Thus at these critical wavelengths one eigenvalue is zero, while the other is negative. So in the neighbourhood of these critical wavelengths, the corresponding eigenvalues are real as well.

On Γ_t , however, there is another band of critical wavelengths, with a (different) absolute value (i.e. $|\vec{k}_c|^2 = \sqrt{\varepsilon}\sqrt{t}$). For these the trace of $M(\vec{k})$ is zero, while the determinant is positive (as long as $\gamma > \gamma_c$). Hence at these critical values both eigenvalues are purely imaginary. Moreover, at a neighbourhood around this band the corresponding eigenvalues are complex as well.

Finally, on $\Gamma_t \cap \Gamma_d = \{(\eta_c, \gamma_c)\}$ we normally find two bands of critical wavelengths. One with purely imaginary eigenvalues, and one band with one eigenvalue identically zero (coming from being on the half-line Γ_t or Γ_d respectively). However, when the parameters β, θ and δ are chosen well, it could happen that

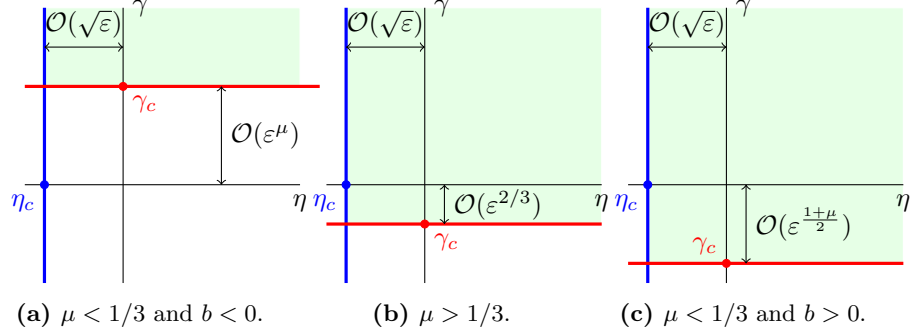


Figure B.2 – The possible forms of the (η, γ) -parameter plane, depending on the sign and order of $\beta = \varepsilon^\mu b$. The blue line denotes the critical line where $\eta = \eta_c$ and hence there are some wavelengths \vec{k} such that $\text{Tr } M(\vec{k}) = 0$. The red line denotes the other critical line, where $\gamma = \gamma_c$. On this line there are wavelengths \vec{k} such that $\det M(\vec{k}) = 0$. The green area is the region of the (η, γ) plane where the trace is negative and the determinant is positive for all wavelengths. Thus in this region the uniform stationary point is stable.

these band coincide. Then at these critical wavelengths we'll find that both eigenvalues are identically zero and it is not clear what happens in the neighbourhood of these wavelengths.

B.3 Approximation of Eigenvalue curves

We would like to present all possible eigenvalue curves on the bifurcation curve $\Gamma_t \cup \Gamma_d$. However, in order to make these, we need to know for what combination of parameters and wavelengths the eigenvalues become complex. We know that the eigenvalues of the matrix $M(\vec{k})$ are

$$\omega_{1,2} = \frac{\text{Tr } M(\vec{k})}{2} \pm \frac{1}{2} \sqrt{\left(\text{Tr } M(\vec{k}) \right)^2 - 4 \det M(\vec{k})}.$$

Thus we know that the eigenvalues are complex when $\Delta := \text{Tr } M(\vec{k})^2 - 4 \det M(\vec{k})$ is negative. In the next subsections we'll delve into this matter and produce eigenvalue curves for parameter combinations on the half-line Γ_d and Γ_t , by inspecting the sign of Δ .

B.3.1 Eigenvalue curves on Γ_t

We'll first inspect the possible eigenvaluecurves on Γ_t . On this half-line we have $\eta = \eta_c = -2\sqrt{\varepsilon}\sqrt{t}$ and the critical eigenvalues are $|\vec{k}_c|^2 = \sqrt{\varepsilon}\sqrt{t}$. Now, to study when the eigenvalues become complex, we need to determine when $\Delta < 0$. We'll first expand the previously given expression for Δ and we find that

$$\Delta = |\vec{k}|^8 + (2\eta - 4\varepsilon)|\vec{k}|^6 + (\eta^2 + 2\varepsilon t - 4\varepsilon\beta)|\vec{k}|^2 + (2\varepsilon\eta t - 4\varepsilon\gamma)|\vec{k}|^2 + \varepsilon^2(t^2 - 4d).$$

From this expression it is already clear that $\Delta > 0$ when $|\vec{k}| \rightarrow \infty$. Also when $|\vec{k}| \downarrow 0$ it is clear that the last term dominates. Hence $\Delta \approx \varepsilon^2(t^2 - 4d)$ when $|\vec{k}| \downarrow 0$. So when $t^2 - 4d < 0$ we find $\Delta < 0$ for wavelengths with absolute value close to zero. Thus the corresponding eigenvalues are complex when $t^2 - 4d < 0$ for these wavelengths. Also, in the previous section we already observed that there are wavelengths around the critical wavelength that correspond to complex eigenvalues.

However, there can be other bands of wavelengths that correspond to complex eigenvalues. To determine whether this happens, we must study the sign of Δ . For this we again are going to find the dominant ε -term in the expression for Δ . For this we introduce the notation $\eta = \varepsilon^\tau e$, $\beta = \varepsilon^\mu b$, $\gamma = \varepsilon^\nu g$ and $|\vec{k}|^2 = \varepsilon^\rho |\vec{m}|^2$ where e, b, g, m are of order $\mathcal{O}(1)$. Thus the expression for Δ becomes:

$$\begin{aligned} \Delta = & \varepsilon^{4\rho} |\vec{m}|^8 + (2\varepsilon^\tau e - 4\varepsilon) \varepsilon^{3\rho} |\vec{m}|^6 + (\varepsilon^{2\tau} e^2 + 2\varepsilon t - 4b\varepsilon^{\mu+1}) \varepsilon^{2\rho} |\vec{m}|^4 \\ & + (2\varepsilon^{\tau+1} et - 4\varepsilon^{\nu+1} g) \varepsilon^\rho |\vec{m}|^2 + \varepsilon^2 (t^2 - 4d) \end{aligned} \quad (\text{B.5})$$

Now, for values $(\eta, \gamma) \in \Gamma_t$ we know that $\eta = \eta_c$. Hence $\tau = 1/2$ and $e < 0$. Thus the expression simplifies to

$$\begin{aligned} \Delta = & \varepsilon^{4\rho} |\vec{m}|^8 + (2\varepsilon^{1/2} e - 4\varepsilon) \varepsilon^{3\rho} |\vec{m}|^6 + (\varepsilon e^2 + 2\varepsilon t - 4b\varepsilon^{\mu+1}) \varepsilon^{2\rho} |\vec{m}|^4 \\ & + (2\varepsilon^{3/2} et - 4\varepsilon^{\nu+1} g) \varepsilon^\rho |\vec{m}|^2 + \varepsilon^2 (t^2 - 4d). \end{aligned}$$

Since we are only interested in the leading orders, we can further simplify this to the following expression, which only has the possible highest order terms

$$\begin{aligned} \Delta = & \varepsilon^{4\rho} |\vec{m}|^8 + 2e\varepsilon^{3\rho+1/2} |\vec{m}|^6 + (\varepsilon(e^2 + 2t) - 4\varepsilon^{\mu+1} b) \varepsilon^{2\rho} |\vec{m}|^4 \\ & + (2\varepsilon^{3/2} et - 4\varepsilon^{\nu+1} g) \varepsilon^\rho |\vec{m}|^2 + \varepsilon^2 (t^2 - 4d). \end{aligned}$$

When the leading term of Δ is negative, we know that Δ is negative as well. Hence we must investigate which terms can be negative and see when they dominate. There are four terms that can be negative:

- (1) The first possibility is the term $2e\varepsilon^{3\rho+1/2} |\vec{m}|^6$. This one is always negative.
- (2) The second is the term $(\varepsilon(e^2 + 2t) - 4\varepsilon^{\mu+1} b) \varepsilon^{2\rho} |\vec{m}|^4$. This term is negative when $b > 0$ and $\mu < 0$.
- (3) The third term $(2\varepsilon^{3/2} et - 4\varepsilon^{\nu+1} g) \varepsilon^\rho |\vec{m}|^2$ is negative when $\nu > 1/2$ or when $g > 0$.
- (4) The last term, $\varepsilon^2 (t^2 - 4d)$ is negative when $t^2 - 4d < 0$.

(Note that there are special cases, when orders are equal. We have purposely neglected these as they only further complicate the notation. What happens in these cases should be clear from the analysis of the other cases.)

We already saw that the fourth possibilities leads to complex eigenvalues around wavelengths with $|\vec{k}| = 0$. For the other three possibilities we determine for what values of ρ these terms are dominant. This immediately tells us what the order is of the wavelengths that are complex due to this term. We inspect the possibilities one by one.

- (1) This term is dominant when $\varepsilon^{3\rho+1/2}$ is bigger than the other powers of ε . This means that the following inequalities need to be satisfied:

$$\begin{aligned} 3\rho + 1/2 &< 4\rho \\ 3\rho + 1/2 &< 2\rho + 1 \\ 3\rho + 1/2 &< 2\rho + 1 + \mu \\ 3\rho + 1/2 &< \rho + 3/2 \\ 3\rho + 1/2 &< \rho + 1 + \nu \\ 3\rho + 1/2 &< 2 \end{aligned}$$

The first condition leads to $\rho < 1/2$, while the second leads to $\rho > 1/2$. Hence we must conclude that this term never dominates.

- (2) The second term dominates when the following inequalities are obeyed

$$\begin{aligned} 2\rho + \mu + 1 &< 4\rho \\ 2\rho + \mu + 1 &< 3\rho + 1/2 \\ 2\rho + \mu + 1 &< \rho + 3/2 \\ 2\rho + \mu + 1 &< \rho + 1 + \nu \\ 2\rho + \mu + 1 &< 2 \end{aligned}$$

These conditions lead to the following condition on the exponent ρ :

$$\max\left\{\frac{\mu+1}{2}, \frac{2\mu+1}{2}\right\} < \rho < \min\left\{\frac{1-2\mu}{2}, \nu-\mu, \frac{1-\mu}{2}\right\}$$

Since the term is only negative when $b > 0$ and $\mu < 0$, we know that $\mu + 1 > 2\mu + 1$ for the possible exponents μ . Moreover, $1 - \mu < 1 - 2\mu$. Thus this condition simplifies to

$$\frac{\mu+1}{2} < \rho < \min\left\{\nu-\mu, \frac{1-\mu}{2}\right\}$$

We can easily verify that there are always exponents ρ that satisfy this inequality, when $\nu > \frac{3\mu-1}{2}$. So this term does indeed lead to complex eigenvalues.

- (3) The term $(2\varepsilon^{3/2}et - 4\varepsilon^{\nu+1}g)\varepsilon^\rho|\vec{m}|^2$ is dominant when the the exponents satisfy the following inequalities:

$$\begin{aligned} \rho + 1 + \min\{1/2, \nu\} &< 4\rho \\ \rho + 1 + \min\{1/2, \nu\} &< 3\rho + 1/2 \\ \rho + 1 + \min\{1/2, \nu\} &< 2\rho + 1 + \min\{0, \mu\} \\ \rho + 1 + \min\{1/2, \nu\} &< 2 \end{aligned}$$

Now, in determining what terms could be negative, we observed that this term is negative when $\nu > 1/2$ or when $\nu < 1/2$ and $g > 0$. In the case that $\nu > 1/2$ we know that $\min\{1/2, \nu\} = 1/2$. Hence we find the following condition on ρ :

$$\max\{1/2, 1/2 - \nu\} < \rho < 1/2$$

So it is clear that there are no exponents ρ that satisfy this.

On the other hand, when $\nu < 1/2$ we have $\min\{1/2, \nu\} = \nu$. Thus in this case we have the following condition for ρ :

$$\max\left\{\frac{1+\nu}{3}, \frac{1+2\nu}{4}, \nu, \nu - \mu\right\} < \rho < 1 - \nu$$

Solving this, we obtain that there are exponents ρ that satisfy this relation when $\nu < \min\{\frac{1+\mu}{2}, \frac{1}{2}\}$.

Therefore we can conclude that this term leads to complex eigenvalues when $\nu < \min\{\frac{1+\mu}{2}, \frac{1}{2}\}$ and $g > 0$. For these we find $\mathcal{O}(\vec{k}) = \mathcal{O}(\varepsilon^{\rho/2})$ with ρ such that

$$\max\left\{\frac{1+\nu}{3}, \nu - \mu\right\} < \rho < 1 - \nu$$

(4) The last term, $\varepsilon^2(t^2 - 4d)$, dominates when the following inequalities hold

$$\begin{aligned} 2 &< 4\rho \\ 2 &< 3\rho + \frac{1}{2} \\ 2 &< 2\rho + 1 \\ 2 &< 2\rho + 1 + \mu \\ 2\rho + \frac{3}{2} & \\ 2\rho + 1 + \nu & \end{aligned}$$

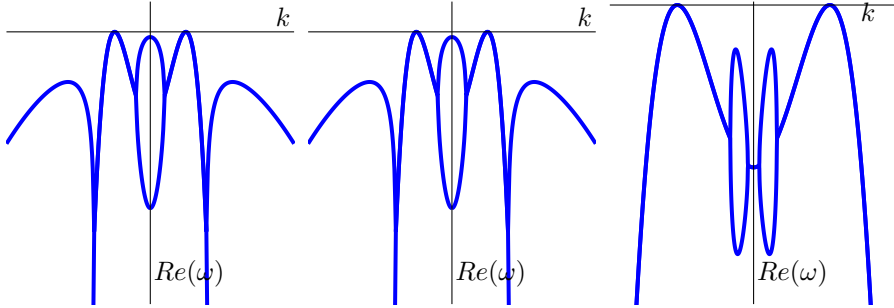
These inequalities are all obeyed when $\rho > \max\{\frac{1}{2}, \frac{1-\mu}{2}, 1 - \nu\}$.

Now, with this we have identified four possible regions of wavelengths for which the eigenvalues are complex:

- (i) Around $\rho = 1/2$, which is the order of the critical wavelengths $|\vec{k}_c|$;
- (ii) The region $\rho \in (\frac{\mu+1}{2} < \rho < \min\{\nu - \mu, \frac{1-\mu}{2}\})$ which only exists when $b > 0$, $\mu < 0$ and $\nu > \frac{3\mu-1}{2}$;
- (iii) The region $\rho \in (\max\{\frac{1+\nu}{3}, \nu - \mu\} < \rho < 1 - \nu)$, which only exists when $g > 0$ and $\nu < \max\{\frac{1}{2}, \frac{1+\mu}{2}\}$.
- (iv) The region $\rho \in (\max\{\frac{1}{2}, \frac{1-\mu}{2}, 1 - \nu\}, \infty)$, which exists when $t^2 - 4d < 0$.

With this regions identified it is possible to make plots of the possible eigenvalue curves. However, we first must acknowledge that it is possible for the regions to overlap. For instance the second region is always include $\rho = 1/2$ and therefore overlap with the first region. Also, clearly the fourth region overlaps the first region when $\mu > 0$ and $\nu > 0$.

For the second region, we can observe that it also contains $\rho = 1/2$ when $\nu \notin (\frac{2\mu+1}{2}, \frac{1+\mu}{2})$ with $\mu < 0$. Since $\mu < 0$ and $b > 0$ we however know that $\mathcal{O}(\gamma_c) = \mathcal{O}(\varepsilon^{\frac{1+\mu}{2}})$. As we are studying the behaviour on the line Γ_t we know that $\gamma \geq \gamma_c$. Hence when $\nu \in (\frac{2\mu+1}{2}, \frac{1+\mu}{2})$ with $\mu < 0$, we know that $g > 0$. This means that in this case also the third region is present. So if the second



(a) Eigenvalue curve for parameter choice such that $t^2 - 4d > 0$.

(b) Eigenvalue curve for parameter choice such that $t^2 - 4d < 0$.

(c) Eigenvalue curve for parameter choice such that $t^2 - 4d < 0$ and such that the regions containing \vec{k}_c and $\vec{k} = 0$ are separated by a region with real eigenvalues.

Figure B.3 – Sketch of the possible eigenvalue curves on Γ_t . These plots are made with Matlab, where we have used $b = -1$, $\mu = 0$, $g = 1$, $\nu = 0$, $d = 1$, $\eta = \eta_c = 2\sqrt{\varepsilon}\sqrt{t}$ and $t = 6$ (a) or $t = 1$ (b). For figure (c) we have used $b = 1$, $d = 1$, $t = 19/10$, $\mu = -1$, $g = -1$, $\nu = -1/10$ and $\eta = \eta_c$. For the plotting we have set $\varepsilon = \frac{1}{100}$. In both figures we can clearly see the critical wavelengths for which $|\vec{k}_c|^2 = \sqrt{\varepsilon}\sqrt{t}$. In Figure (a) it looks as though the wavelengths $\vec{k} = 0$ becomes critical when the parameters would be chosen slightly different. This does not happen though, as we have assumed $\mathcal{O}(\theta) = \mathcal{O}(\delta) = \mathcal{O}(\varepsilon)$ and thus the eigenvalue in $\vec{k} = 0$ is always negative (and of order $\mathcal{O}(\varepsilon)$).

region does not overlap with any other region, this means that the second region only contains big wavelengths (i.e. $\rho > \max\left\{\frac{1+\mu}{3}, \nu - \mu\right\}$).

Since we are mainly interested in the behaviour for which the eigenvalues are close to zero, we can focus only on the behaviour of the eigenvalue curve for small wavelengths. Hence by the above reasoning we always find that there's always a region of complex eigenvalues that contains $\rho = \frac{1}{2}$. This region may also include $\vec{k} = 0$, but it need not. It can also happen that there are two region with complex eigenvalues, one containing $\rho = \frac{1}{2}$ and one containing $\vec{k} = 0$, separated by a small region with real eigenvalues.¹. This can, however, only happen in very specific cases, when the fourth region does not coincide with any of the others.

The possibilities for the eigenvalue curves on Γ_t are plotted in Figure B.3.

B.3.2 Eigenvalue curves on Γ_d

To find the eigenvalue curves on the bifurcation line Γ_d we need to apply a similar analysis as before. This time we need to fix $\gamma = \gamma_c$. But, the sign and order of γ_c depends on the sign and order of β (see equation (B.3)). So we need to do

¹Note that we have neglected what happens when ρ is very small, since we are mainly interested in the behaviour for small wavelengths, with small eigenvalues.

the whole analysis for all these three possible scenarios. Luckily the analysis for most of the cases is similar and therefore we analyze them simultaneously. Again we determine the form of Δ . By substitution of $\gamma_c = \varepsilon^\nu g_c$ in equation (B.5), we now have

$$\begin{aligned}\Delta = & \varepsilon^{4\rho} |\vec{m}|^8 + (2\varepsilon^\tau e - 4\varepsilon) \varepsilon^{3\rho} |\vec{m}|^6 + (\varepsilon^{2\tau} e^2 + 2\varepsilon t - 4b\varepsilon^{\mu+1}) \varepsilon^{2\rho} |\vec{m}|^4 \\ & + (2\varepsilon^{\tau+1} et - 4\varepsilon^{\nu+1} g_c) \varepsilon^\rho |\vec{m}|^2 + \varepsilon^2 (t^2 - 4d).\end{aligned}$$

Again we must identify which terms can become negative and under what conditions this happens. We now find the following possibilities:

- (1) The term $2\varepsilon^\tau - 4\varepsilon < 0$ when $\tau > 1$ or when $\tau < 1$ and $e < 0$. Since $\eta \geq \eta_c = -2\sqrt{\varepsilon}\sqrt{t}$ on Γ_d the condition $e < 0$ implies that $\tau > 1/2$. Thus this term is negative when either of the following set of conditions is satisfied:
 - (a) $\tau > 1$;
 - (b) $e < 0$ and $\tau \in (1/2, 1)$.
- (2) The term $2\varepsilon^{2\tau} e^2 + 2\varepsilon t - 4b\varepsilon^{\mu+1} < 0$ when $b > 0$ and $\mu < \min\{2\tau - 1, 0\}$.
- (3) The term $2\varepsilon^{\tau+1} et - 4\varepsilon^{\nu+1} g < 0$ in either of the following two cases
 - (a) $e < 0$ and $\tau < \nu$;
 - (b) $g > 0$ and $\tau > \nu$.
- (4) The last term, $\varepsilon^2 (t^2 - 4d)$, is negative when $t^2 - 4d < 0$.

As before we need to determine when these terms are dominating the expression for Δ . For all of the previously mentioned cases we are going to inspect when they dominates.

- (1a) When $\tau > 1$, we know $\varepsilon^\tau < \varepsilon$. Hence for the term to dominate the following inequalities need to be satisfied

$$3\rho + 1 < 4\rho, 2\rho + 2\tau, 2\rho + 1, 2\rho + \mu + 1, \rho + 1 + \tau, \rho + 1 + \nu, 2$$

We can rewrite these condition to the following more straight-forward condition

$$1 < \rho < 2\tau, 1, 0, \mu, \tau/2, \nu/2, 1/3$$

Clearly there are no ρ that satisfy this, as $1 < 0$ is false. So this situation will not lead to complex eigenvalues.

- (1b) In this situation we assume that $e < 0$ and $\tau \in (1/2, 1)$. Now we have $\tau < 1$ and therefore $\min\{1, \tau\} = \tau$. Now the term is dominant when the following inequalities hold

$$3\rho + \tau < 4\rho, 3\rho + \min\{2\tau, 1, \mu + 1\}, \rho + 1 + \min\{\tau, \nu\}, 2$$

Since $\tau > 1/2$ we have $\min\{2\tau, 1\} = 1$. Thus this condition reduces to

$$3\rho + \tau < 4\rho, 2\rho + 1 + \min\{0, \mu\}, \rho + 1 + \min\{\tau, \nu\}, 2$$

And this condition can then again be written in the following way

$$\tau < \rho < 1 - \tau, 1 - \tau + \mu, 1/2, \frac{1 + \nu - \tau}{2}, \frac{2 - \tau}{3}$$

But this condition can not be satisfied as well, since $\tau > \frac{1}{2}$ in this particular case. Hence we see that the term (1) cannot be dominant and therefore won't lead to complex eigenvalues.

- (2) We now inspect term (2). For this, we assume that $b > 0$ and that $\mu < \min\{2\tau - 1, 0\}$. This term is dominating when

$$2\rho + \mu + 1 < 4\rho, 3\rho + 1, 3\rho + \tau, \rho + 1 + \tau, \rho + 1 + \nu, 2$$

This corresponds to the following condition on ρ :

$$\mu, \frac{\mu + 1}{2}, \mu + 1 - \tau < \rho < \nu - \mu, \tau - \mu, \frac{1 - \mu}{2}$$

Now we observe that $\frac{\mu+1}{2} > \mu, \mu + 1 - \tau$ when $\mu < 1, 2\tau - 1$. As we have assumed that $\mu < \min\{2\tau - 1, 0\}$ this is always the case. Also $\frac{1-\mu}{2} < \tau - \mu$ when $\mu < 2\tau - 1$. Moreover, since $b > 0$ and $\mu < 0$ we know that $\mathcal{O}(\gamma_c) = \mathcal{O}\left(\varepsilon^{\frac{1+\mu}{2}}\right)$ Hence $\nu = \frac{1+\mu}{2}$. Thus this condition finally reduces to

$$\frac{1 + \mu}{2} < \rho < \frac{1 - \mu}{2}$$

It is possible to find values for the exponent ρ that satisfy this condition when $\mu < 0$. Since per assumption we have $\mu < \min\{2\tau - 1, 0\}$ in this case, we find that there indeed is a region in which there are complex eigenvalues when these conditions are obeyed (i.e. $b > 0$ and $\mu < \min\{2\tau - 1, 0\}$).

- (3a) For this case we assume that $e < 0$ and $\tau < \nu$. Since $e < 0$ implies that $\tau > \frac{1}{2}$ we essentially have the condition $\nu > \tau > \frac{1}{2}$. Now, this term is dominant when the following inequalities are obeyed

$$\rho + \tau + 1 < 4\rho, 3\rho + \tau, 3\rho + 1, 2\rho + 1, 2\rho + 1 + \mu, 2$$

This corresponds to the following conditions on the exponent ρ :

$$\frac{\tau + 1}{3}, \frac{1}{2}, \frac{\tau}{2}, \tau, \tau - \mu < \rho < 1 - \tau$$

Since $\tau < 1 - \tau$ is only possible when $\tau < 1/2$ we see that there are no exponents ρ that can satisfy all these conditions, because we already have assumed that $\tau > 1/2$. So this term, with these conditions, does not lead to complex eigenvalues.

- (3b) For this case we assume that $g > 0$ and $\tau > \nu$. Since $g > 0$ implies that $\gamma_c > 0$ we know that $b < 0$, $\mu < 1/3$ and $\nu = 2\mu$. Now, this term is dominant when

$$\rho + \nu + 1 < 4\rho, 3\rho + \tau, 3\rho + 1, 2\rho + 2\tau, 2\rho + 1, 2\rho + 1 + \mu, 2$$

So this corresponds to exponents ρ that obey the following set of inequalities:

$$\frac{2\mu + 1}{3}, \frac{2\mu + 1 - \tau}{2}, \mu, 2\mu + 1 - 2\tau, 2\mu < \rho < 1 - 2\mu$$

We can easily verify that all these inequalities can be obeyed when we have $\mu < \frac{1}{4}, \frac{\tau}{2}, \frac{1+\tau}{6}$. Thus we see that this region contains complex eigenvalues when $\mu = \frac{\nu}{2} < \frac{1+\tau}{6}, \frac{\tau}{2}, \frac{1}{4}$ (and of course $g > 0, b < 0$).

(4) Finally, the last term dominates when

$$2 < 4\rho, 3\rho + \tau, 3\rho + 1, 2\rho + 2\tau, 2\rho + 1, 2\rho + 1 + \mu, \rho + \tau + 1, \rho + \nu + 1$$

Now these condition lead to the following set of inequalities for ρ :

$$\rho > \max\left\{\frac{1}{2}, \frac{2-\tau}{3}, \frac{1}{3}, 1-\tau, \frac{1-\mu}{2}, 1-\nu\right\}$$

We observe that $\frac{1}{2} > \frac{2-\tau}{3}$ when $\tau > \frac{1}{2}$ and $1-\tau > \frac{2-\tau}{3}$ when $\tau < \frac{1}{2}$. Thus we can simplify this set of inequalities to

$$\rho > \max\left\{\frac{1}{2}, 1-\tau, 1-\nu, \frac{1-\mu}{2}\right\}$$

So at this point we have identified the following possible regions for the exponent ρ in which the eigenvalues are complex under the right set of conditions.

- (I) The set $\rho \in (\frac{1+\mu}{2}, \frac{1-\mu}{2})$ under the conditions $b > 0$ and $\mu < \min\{2\tau-1, 0\}$;
- (II) The set

$$\rho \in \left(\max\left\{\frac{2\mu+1}{3}, \frac{2\mu+1-\tau}{2}, \mu, 2\mu+1-2\tau, 2\mu\right\}, 1-2\mu \right)$$

under the conditions $\mu = \frac{\nu}{2} < \frac{1+\tau}{6}, \frac{\tau}{2}, \frac{1}{4}, g > 0$ and $b < 0^2$;

- (III) The set

$$\rho \in \left(\max\left\{\frac{1}{2}, 1-\tau, 1-\nu, \frac{1-\mu}{2}\right\}, \infty \right)$$

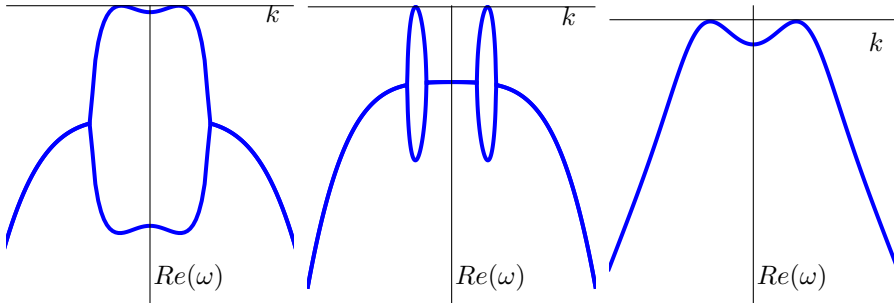
when $t^2 - 4d < 0$.

Clearly not all regions always exist simultaneously. Since region (I) requires $b > 0$ and the second $b < 0$ we see that these two never coexist. It could however happen that regions (I) and (II) exists simultaneously. In this case we need $t^2 - 4d < 0$, $b > 0$ and $\mu < \{2\tau-1, 0\}$. As $\mu < \frac{1}{3}$ and $b > 0$ this corresponds to the case in which $\mathcal{O}(|\vec{k}_c|^2) = \mathcal{O}(\varepsilon^{\frac{1-\mu}{2}})$. Since $\det M(\vec{k}) = 0$, we know that there are no complex eigenvalues in the neighbourhood of the critical wavelength. Moreover, we observe that in region (I) we have $\rho < \frac{1-\mu}{2}$ and in region (III) we have $\rho > \frac{1-\mu}{2}$. Thus when regions (I) and (III) both exist, they don't overlap and there is a region with real eigenvalues between them.

It is also possible for region (II) and (III) to exist simultaneously. Now we have $\mathcal{O}(|\vec{k}_c|^2) = \mathcal{O}(\varepsilon^\mu)$. Also we find that $\rho > \mu$ in region (II) and $\rho > \frac{1}{2} > \mu$ in region (III). Moreover we can see that $1-\mu \geq \frac{1}{2}, 1-\tau, 1-\nu, \frac{1-\mu}{2}$ in this situation. Therefore the regions (II) and (III) must overlap when they both exist.

So from this analysis, we know that there essentially are five different forms of eigenvalue curves that are possible to occur. We have plotted these in Figure B.4.

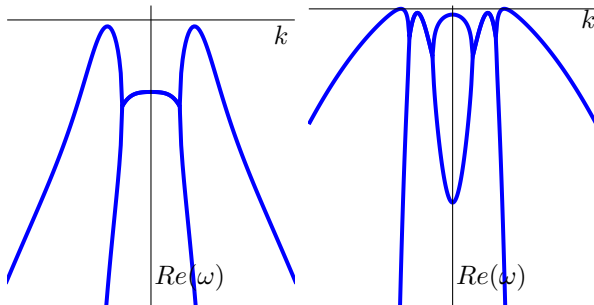
²Note that the condition $g > 0$ is already implied by the conditions $b < 0$ and $\mu < \frac{1}{3}$.



(a) Eigenvalue curve for parameter choice such that $t^2 - 4d > 0$, $b > 0$ and $\mu < \min\{2\tau - 1, 0\}$. Note that the eigenvalues become real again for very large wavelengths, but this isn't included in the plot.

(b) Eigenvalue curve for parameter choice such that $t^2 - 4d < 0$, $b > 0$ and $\mu < \min\{2\tau - 1, 0\}$. Note that the eigenvalues become real again for very large wavelengths, but this isn't included in the plot.

(c) Eigenvalue curve for parameter choice such that $t^2 - 4d > 0$ and not both $b > 0$ and $\mu < \min\{2\tau - 1, 0\}$ and such that region (II) does not exist. Only one eigenvalue is plotted here.



(d) Eigenvalue curve for parameter choice such that $t^2 - 4d < 0$ and not both $b > 0$ and $\mu < \min\{2\tau - 1, 0\}$.

(e) Eigenvalue curve for parameter choice such that $t^2 - 4d > 0$ and not both $b > 0$ and $\mu < \min\{2\tau - 1, 0\}$ and such that region (II) does exist.

Figure B.4 – Sketch of the possible eigenvalue curves on Γ_d . These plots are made with Matlab, where we have used $b = 1$, $d = 1$, $e = 1$, $\tau = 1$, $\gamma = \gamma_c$ and $\mu = 1$ and $t = 6$ (a), $\mu = 1$ and $t = 1$ (b), $\mu = 0$ and $t = 6$ (c) or $\mu = 0$ and $t = 1$ (d). For (e) we have used $b = -1$, $d = 1$, $e = -2\sqrt{6} + 1/10$, $\tau = 1/2$, $\gamma = \gamma_c$, $\mu = 0$ and $t = 6$. For the plotting we have set $\varepsilon = \frac{1}{100}$. In these figures we can clearly see the critical wavelengths. Note that the scaling is chosen to better show the behaviour for the wavelengths with small eigenvalues in each case and therefore the scaling isn't the same in all figures. Also note that due to the numerical estimate $\varepsilon = \frac{1}{100}$, the eigenvalue at the critical wavelengths seem to be non-negative. This is purely a numerical issue. Also note that in Figure (c) only one eigenvalue is plotted and that in Figures (a) en (b) the eigenvalues start to be real again for very large wavelengths, which are not included in these plots.

B.3.3 Eigenvalue curves on $\Gamma_t \cap \Gamma_d$

Finally we must still investigate what happens when we choose our parameters γ and η such that $\gamma = \gamma_c$ and $\eta = \eta_c$. As argued before, we typically see two bands of critical values, one coming from a zero trace and one from a zero determinant. We denote by \vec{k}_t the critical wavelength for which the trace is zero and we define \vec{k}_d as the critical wavelength for which the determinant is zero. We know that $\mathcal{O}(|\vec{k}_t|^2) = \mathcal{O}(\varepsilon^{1/2})$ and $\mathcal{O}(|\vec{k}_d|^2) = \mathcal{O}(\varepsilon^\sigma)$ where σ can be read from Table B.4:

$$\sigma = \begin{cases} \mu & \text{if } \mu < 1/3 \text{ and } b < 0; \\ \frac{1}{3} & \text{if } \mu \geq \frac{1}{3}; \\ \frac{1-\mu}{2} & \text{if } \mu < 1/3 \text{ and } b > 0. \end{cases}$$

We can then determine which critical wavelength lies closer to zero by inspecting the exponents. We see that $\sigma > \frac{1}{2}$ only when $\mu < 0$ and $b > 0$. In this case $|\vec{k}_d| < |\vec{k}_t|$. In the other case, when $\mu > 0$ or $b < 0$, we have $|\vec{k}_t| < |\vec{k}_d|$. We can also have $\mu = 0$ and then the wavelengths have the same order. When this happens and the parameters are chosen well enough it could happen that $\vec{k}_d = \vec{k}_t$ (i.e. this happens when $bt = d$).

To draw the possible eigenvalue curves we need to figure out which situations lead to complex eigenvalues once again. Luckily, we can use the analysis we did before. Since in our current case we have $\eta = \eta_c$ and $\gamma = \gamma_c$ we know that our analysis of Γ_t and Γ_d must both hold simultaneously.

On Γ_t we could have two distinct regions for the exponent ρ in which the eigenvalues are complex:

- (A) A region that includes $\rho = \frac{1}{2}$;
- (B) A region for which $\rho < \frac{1}{2}$ that only exists when $b > 0$, $\mu < 0$ and when $\nu \in (\frac{2\mu+1}{2}, \frac{1+\mu}{2})$.

Since we want to know what happens on $\Gamma_d \cap \Gamma_t$ we know that $\gamma = \gamma_c$. Therefore in region (B) we must have $\nu = \frac{1+\mu}{2}$. So the inequality for region (B) can never be satisfied and therefore region (B) cannot occur on $\Gamma_t \cap \Gamma_d$.

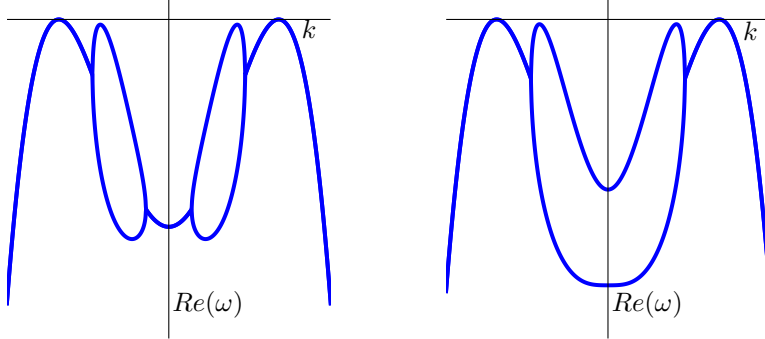
On the other bifurcation line, Γ_d , we have found the following regions with complex eigenvalues:

- (I) A region for which $\rho < \sigma$, which only exists when we have $b > 0$ and $\mu < \min\{2\tau - 1, 0\}$.
- (II) A region for which $\rho > \sigma$, which only exists when $b < 0$ and $\mu < \frac{1+\tau}{6}, \frac{\tau}{2}, \frac{1}{4}$;
- (III) A region that includes $\rho = 0$, which only exists when $t^2 - 4d < 0$;

Here region (II) and (III) overlap when they both exist. We also note that region (I) and (II) both should contain the exponent $\rho = 1/2$ when they exist³. Thus these regions overlap with region (A).

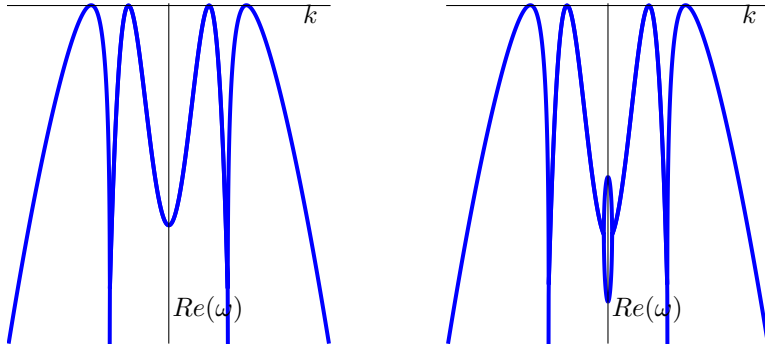
Hence we know that there can only be complex eigenvalues in the neighbourhood of \vec{k}_t and near $\vec{k} = 0$ (when $t^2 - 4d < 0$). So there are six different eigenvalue curves possible. We have plotted these in Figure B.5.

³To see this we must remember that on $\Gamma_t \cap \Gamma_d$ we have $\tau = \frac{1}{2}$



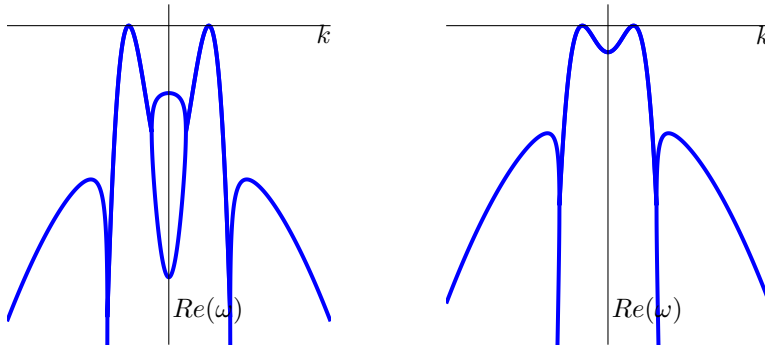
(a) Eigenvalue curve for parameter choice such that $|\vec{k}_d| < |\vec{k}_t|$ and $t^2 - 4d < 0$.

(b) Eigenvalue curve for parameter choice such that $|\vec{k}_d| < |\vec{k}_t|$ and $t^2 - 4d > 0$.



(c) Eigenvalue curve for parameter choice such that $|\vec{k}_d| > |\vec{k}_t|$ and $t^2 - 4d < 0$.

(d) Eigenvalue curve for parameter choice such that $|\vec{k}_d| > |\vec{k}_t|$ and $t^2 - 4d > 0$.



(e) Eigenvalue curve for parameter choice such that $|\vec{k}_d| = |\vec{k}_t|$ and $t^2 - 4d < 0$.

(f) Eigenvalue curve for parameter choice such that $|\vec{k}_d| = |\vec{k}_t|$ and $t^2 - 4d > 0$.

Figure B.5 – Plot of the possible eigenvalue curves on $\Gamma_t \cap \Gamma_d$. These plots are made with Matlab. We have used $b = 1, d = 1, \mu = 1/4, \gamma = \gamma_c, \eta = \eta_c$ for (a) and (b), where $t = 39/20$ (a) or $t = 41/20$ (b). For (c) and (d) we have used $b = -1, d = 1, \mu = 0, \gamma = \gamma_c, \eta = \eta_c$ and $t = 39/40$ (c) or $t = 83/40$ (d). Finally for (e) and (f) we have used $b = 1, \mu = 0, \gamma = \gamma_c, \eta = \eta_c, t = d/b$ and $d = 6$ (e) or $d = 1$ (f). We have used $\varepsilon = \frac{1}{100}$. Note that due to this numerical estimate, the eigenvalue at the critical wavelength may appear as non-zero in these plots.

B.3.4 Bifurcation of the eigenvalue curves

In the previous section we have investigated the possibilities of the eigenvalue curves on the bifurcation lines Γ_t and Γ_d for most of the possible parameter combinations⁴. In this section we use this characterization to visualize the change of the eigenvalue curves along the bifurcation lines Γ_t and Γ_d .

Because we ignored the special cases in the analysis in last section, the bifurcation of the eigenvalue curves is only clear when $\beta = \varepsilon^\mu b > 0$ and $\mu < 0$ or when $\beta = \varepsilon^\mu b < 0$ and $\mu < \frac{1}{4}$. The other possible parameter choices cannot be formally characterized with our current analysis, as we need to carefully inspect all neglected special cases for this. However, the behaviour for these choices is similar to the behaviour in the second case we are going to inspect.

The rest of this section is dedicated to the aforementioned specific parameter choices:

1. $\beta = \varepsilon^\mu b > 0$ with $\mu < 0$;
2. $\beta = \varepsilon^\mu b < 0$ with $\mu < \frac{1}{4}$.

For both of these cases we inspect what happens when $t^2 - 4d < 0$ and when $t^2 - 4d > 0$.

$\beta > 0$ and $\mu < 0$

For this choice of the parameter β we have $\gamma_c < 0$ and of order $\mathcal{O}(\varepsilon^{\frac{1+\mu}{2}})$. So we know that the (η, γ) parameter-plane is as in Figure B.2c. Now there are two different possible bifurcations of the eigenvalue curves, depending on the sign of $t^2 - 4d$.

The bifurcation of the eigenvalue curve in case $t^2 - 4d < 0$ is drawn in Figure B.6 and for $t^2 - 4d > 0$ in Figure B.7. These figures show how different wavelengths can be critical depending on the choice of the parameters η and γ .

$\beta < 0$ and $\mu < \frac{1}{4}$

For this choice $\gamma_c > 0$ and the (η, γ) parameter-plane is as in Figure B.2a. Again we need to distinguish between the cases $t^2 - 4d < 0$ and $t^2 - 4d > 0$. In Figure B.8 we have illustrated the possibility $t^2 - 4d < 0$, while in Figure B.9 we have plotted the eigenvalue curves when $t^2 - 4d > 0$.

⁴Note that we have deliberately ignored the special cases in our analysis.

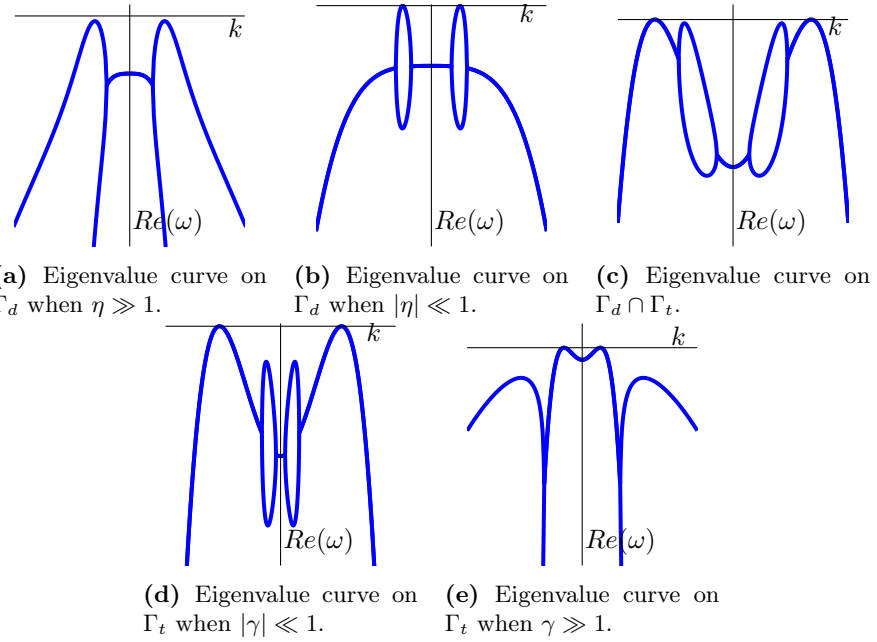


Figure B.6 – The various possible eigenvalue curves on the bifurcation lines Γ_t and Γ_d when $\beta > 0$ and $\mu < 0$ and $t^2 - 4d < 0$.

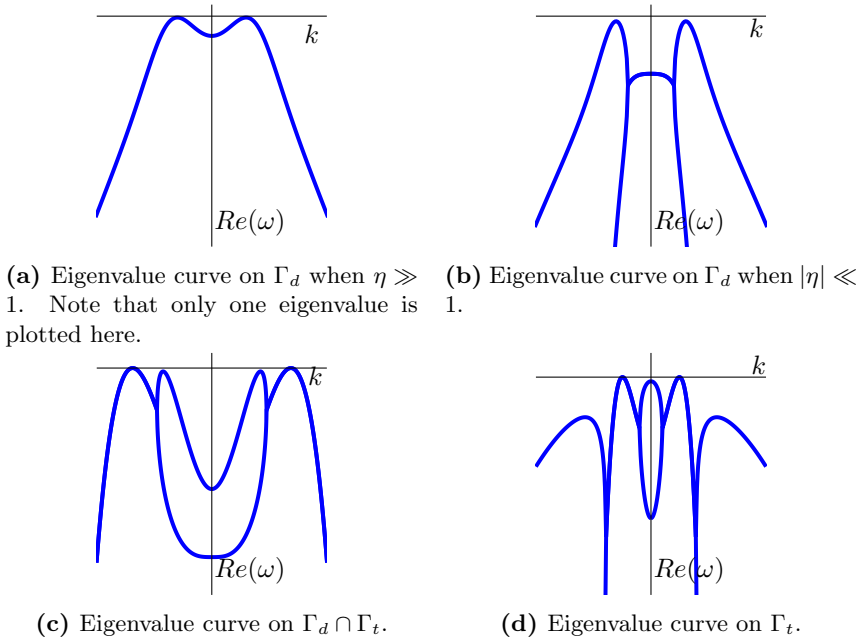
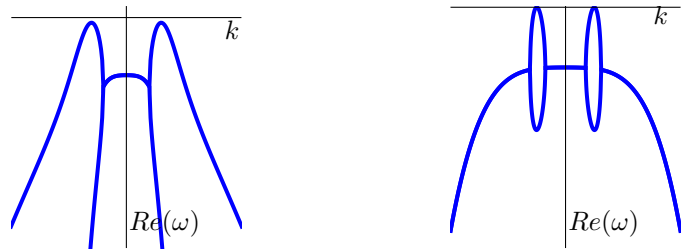
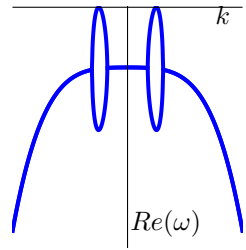


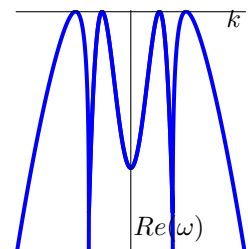
Figure B.7 – The various possible eigenvalue curves on the bifurcation lines Γ_t and Γ_d when $\beta > 0$ and $\mu < 0$ and $t^2 - 4d > 0$.



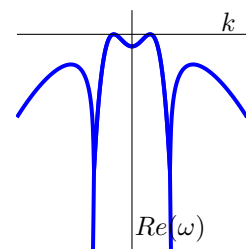
(a) Eigenvalue curve on Γ_d when $\eta \gg 1$.



(b) Eigenvalue curve on Γ_d when $|\eta| \ll 1$.

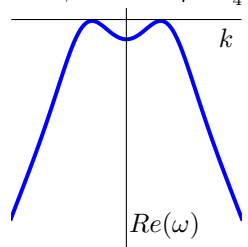


(c) Eigenvalue curve on $\Gamma_d \cap \Gamma_t$.

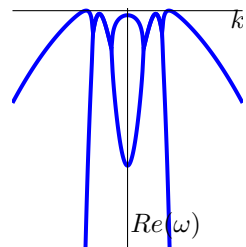


(d) Eigenvalue curve on Γ_t .

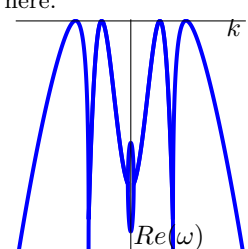
Figure B.8 – The various possible eigenvalue curves on the bifurcation lines Γ_t and Γ_d when $\beta < 0$ and $\mu < \frac{1}{4}$ and $t^2 - 4d < 0$.



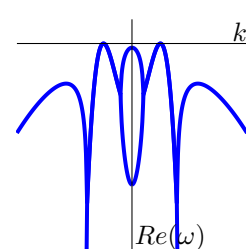
(a) Eigenvalue curve on Γ_d when $\eta \gg 1$. Note that only one eigenvalue is plotted here.



(b) Eigenvalue curve on Γ_d when $|\eta| \ll 1$.



(c) Eigenvalue curve on $\Gamma_d \cap \Gamma_t$.



(d) Eigenvalue curve on Γ_t .

Figure B.9 – The various possible eigenvalue curves on the bifurcation lines Γ_t and Γ_d when $\beta < 0$ and $\mu < \frac{1}{4}$ and $t^2 - 4d > 0$.

Appendix C

Study of the Real Ginzburg-Landau Equation

In many cases, including our model for the mussel-algae interaction, the standard weakly non-linear stability analysis results in the real Ginzburg-Landau equation to describe the dynamics of the amplitude A :

$$A_\tau = RA + bA_{\xi\xi} + h|A|^2A \quad (\text{C.1})$$

where τ and ξ are the slow time and spatial scales that were introduced in the non-linear analysis. The parameters R, b and h are determined by the parameters of the original problem. In the normal standard Real Ginzburg-Landau equation we have $R, b > 0$ and $h < 0$.

In the derivation of the Ginzburg-Landau equation we have made the following Ansatz for the solution of the original partial differential equation:

$$m(x, t) = m_e + A(\xi, \tau)e^{ik_c x}$$

Here the wavelength k_c is the critical wavelength (i.e. the wavelength such that one of the eigenvalues is zero and the other is non-positive) and m_e is the relevant uniform stationary state of the original problem. So when we know the (complex) function A , we also know the behaviour of the original partial differential equation for parameter combinations close to the critical combination (that led to the existence of a critical wavelength k_c).

Therefe in this section we study the real Ginzburg-Landau equation. We focus on the (possible) stationary solutions to this equation and with their stability. From this we can determine what kind of behaviour is possible for A when τ is large.

The description in equation (C.1) is not the usual formulation of the Ginzburg-Landau equation. To write it in its normal form we have to introduce the scaling $\tau' = |R|\tau, \xi = \sqrt{|R|/|b|}\xi', A = \sqrt{|R|/|h|}A'$, which preserves the flow of time. Then the expression can be rewritten as

$$A'_{\tau'} = \text{sgn}(R)A' + \text{sgn}(b)A'_{\xi'\xi'} + \text{sgn}(h)|A'|^2A'.$$

We can also use the scaling $\tau'' = \text{sgn}(R)\tau'$ now to find the expression

$$A'_{\tau''} = A' + \text{sgn}(Rb)A'_{\xi'\xi'} + \text{sgn}(Rh)|A'|^2A'.$$

When we do this last scaling we should note that we have reversed time when $R < 0$. That is, when $R < 0$ we have possibly changed the stability of the found stationary solutions.

During this chapter we work with the following equation, in which we have suppressed the apostrophes

$$A_\tau = A + bA_{\xi\xi} + h|A|^2A.$$

Here $b, h \in \{1, -1\}$ depending on the signs of the original b, h and R as argued before. When we speak of stability during this chapter we mean the stability for the system with $R > 0$.

C.1 Reformulation in polar coordinates

The amplitude A in the Ginzburg-Landau equation is complex. Moreover the partial differential equation is phase invariant: if A is a solution to the equation then so is $Ae^{i\theta}$ for some fixed $\theta \in [0, 2\pi)$. Therefore it is logical to write $A(\tau, \xi) = \rho(\tau, \xi)e^{i\psi(\tau, \xi)}$ where ρ and ψ are now real-valued functions. With this transformation we can rewrite the partial differential equation as the following system

$$\begin{cases} \rho_\tau &= \rho + b\rho_{\xi\xi} - b\rho\psi_\xi^2 + h\rho^3 \\ \rho\psi_\tau &= 2b\rho_\xi\psi_\xi + \rho\psi_{\xi\xi}. \end{cases}$$

Our first goal is to find the stationary solutions of this system. Therefore we seek $\rho(\xi, \tau) = \rho(\xi)$ and $\psi(\xi, \tau) = 0$ and we can set the time derivatives equal to zero. Hence stationary solutions must satisfy

$$\begin{cases} 0 &= \rho + b\rho_{\xi\xi} - b\rho\psi_\xi^2 + h\rho^3 \\ 0 &= 2b\rho_\xi\psi_\xi + b\rho\psi_{\xi\xi}. \end{cases} \quad (\text{C.2})$$

We can multiply the second equation with $\frac{\rho}{b}$ and integrate it once to obtain a conserved quantity. The first equation can also be integrated: this can be seen when we multiply it by $2\rho_\xi$ and note that we can use the second equation to rewrite it. Hence we can find the following conserved quantities:

$$\begin{aligned} \Omega &:= \rho^2\psi_\xi \\ K &:= \rho^2 + \frac{h}{4}\rho^4 + b\rho_\xi^2 + b\frac{\Omega^2}{\rho^2} \end{aligned}$$

Therefore we know that $\psi_\xi = \frac{\Omega}{\rho^2}$. Substitution in equation (C.2) then gives the following ordinary differential equation for ρ :

$$0 = \rho + h\rho^3 + b\rho_{\xi\xi} - b\frac{\Omega^2}{\rho^3}$$

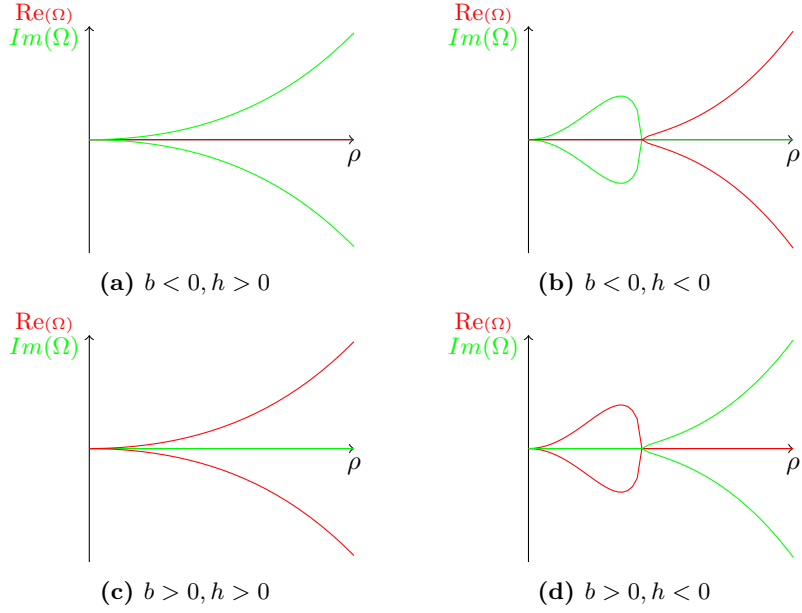


Figure C.1 – Sketches of the functions $\Omega = \pm\rho^2 \sqrt{\frac{1+h\rho^2}{b}}$ for the possible different signs of h and b . In all these figures the red line denotes the real part of Ω , while the green line denotes the imaginary part.

We want to write this as a system of first order ordinary differential equations. Therefore we introduce $v := \rho_\xi$. The resulting system then becomes

$$\begin{cases} \rho_\xi &= v \\ v_\xi &= \frac{\Omega^2}{\rho^3} - \frac{1}{b}\rho - \frac{h}{b}\rho^3 \end{cases} \quad (\text{C.3})$$

The fixed points of this system must satisfy $\rho_\xi = 0$ and $v_\xi = 0$. This means that we need to have $v = 0$ and $\frac{\Omega^2}{\rho^3} - \frac{1}{b}\rho - \frac{h}{b}\rho^3 = 0$. Hence we need to have

$$\Omega = \pm\rho^2 \sqrt{\frac{1+h\rho^2}{b}}.$$

The amount of solutions to this expression depends on the signs of h and b . For instance, if $h > 0$ and $b < 0$ we have only a solution when $\Omega = 0$ and $\rho = 0$. All these possibilities are sketched in Figure C.1. In the next sections we study these possibilities one by one.

All the expressions involving Ω are symmetric under the reflection $\Omega \rightarrow -\Omega$. Therefore it is sufficient to study only the behaviour for Ω positive. Now, we inspect what happens for $\Omega > 0$ fixed (the degenerate case when $\Omega = 0$ is considered with later on).

From the sketches in Figure C.1 we can see that we have 0, 1 or 2 fixed points with $\rho > 0$, depending on the value of Ω and the signs of h and b . When we have a fixed points, we want to study its character. To do so, we need to linearize

the system of equation (C.3). The linearized system (around the fixed point $(\rho_*, 0)$) can be computed to be

$$\frac{d}{d\xi} \begin{pmatrix} \rho \\ v \end{pmatrix} = \begin{pmatrix} 0 & 1 \\ -3\frac{\Omega^2}{\rho_*^4} - \frac{1}{b} - 3\frac{h}{b}\rho_*^2 & 0 \end{pmatrix} \begin{pmatrix} \rho \\ v \end{pmatrix}$$

From this we can easily compute the eigenvalues of the fixed point. When we recall that $\Omega = \pm\rho_*^2\sqrt{\frac{1+h\rho_*^2}{b}}$ for the fixed point we can reformulate it and obtain the eigenvalues as

$$\begin{aligned} \lambda_{\pm} &= \pm\sqrt{-3\frac{\Omega^2}{\rho_*^4} - \frac{1}{b} - 3\frac{h}{b}\rho_*^2} \\ &= \pm\sqrt{2}\sqrt{-\frac{2}{b} - \frac{3h}{b}\rho_*^2} \end{aligned} \quad (\text{C.4})$$

C.2 Phase planes

In the last section we have derived some generally usable equation that will characterize the system of equation (C.3). In this chapter we use these expressions in order to find the phase planes of this system, for all possible values of $\Omega > 0$, $b \in \{1, -1\}$ and $h \in \{1, -1\}$.

$$b < 0, h > 0$$

When $b < 0$ and $h > 0$ and we choose $\Omega > 0$ we can see in Figure C.1 that there are no fixed points in the system. Moreover, the system can now be written as

$$\begin{cases} \rho_\xi &= v \\ v_\xi &= \frac{\Omega^2}{\rho^3} + \rho + \rho^3 \end{cases}$$

Therefore we see that $\rho_\xi > 0$ when $v > 0$ and $\rho_\xi < 0$ when $v < 0$ and that $v_\xi > 0$ for all $\rho > 0$. The phase plane of this situation is given in Figure C.2a. We see that solutions for ρ are unbounded. This would mean that the amplitude A is unbounded, which violates the assumption that the perturbation is small. Hence when $b < 0$ and $h > 0$ the Ginzburg-Landau equation is not be the right modulation equation for the problem.

$$b < 0, h < 0$$

From Figure C.1 we see that there is always one fixed point when $\Omega > 0$. Moreover, we can determine that $\rho_* > 1$ for the fixed point. Now the eigenvalues of the fixed point can be computed with equation (C.4) and we obtain $\lambda_{\pm} = \pm\sqrt{2}\sqrt{2 - 3\rho_*^2}$. Since $\rho_* > 1$ we find that the eigenvalues are both purely imaginary and hence the fixed point is now a center.

The phase plane of this situation is given in Figure C.2b. Since the system is symmetric in $\{v = 0\}$ we thus find infinitely many periodic orbits for ρ around the fixed point. Note that all these solutions are bounded and hence do not violate the smallness assumption on the amplitude A .

$$b > 0, h > 0$$

When $b > 0$ and $h > 0$ we can see in Figure C.1 that there is always one fixed point when $\Omega > 0$. Computation of the eigenvalues gives that, again, the fixed point is a center. Hence the phase plane is similar to the previous case, where $b > 0, h < 0$ (see Figure C.2b). This time, however, the value of ρ_* can in fact be smaller than 1, as can be seen in Figure C.1.

$$b > 0, h < 0$$

In this last situation, we have $b = 1$ and $h = -1$. It is clear from Figure C.1 that there is a value Ω_* such that the system has two fixed points if $\Omega \in (0, \Omega_*)$ and no fixed points if $\Omega > \Omega_*$. The value for Ω_* can be found by finding the maximum of the function $\Omega = \rho^2 \sqrt{1 - \rho^2}$. By a simple computation we find that the maximum is attained when $\rho = \sqrt{\frac{2}{3}}$ and that $\Omega_* = \sqrt{\frac{4}{27}}$.

Now, when $\Omega > \Omega_*$ the system has no fixed points. We are now essentially in the same situation as we had when $b < 0$ and $h > 0$. That is, the phase plane of Figure C.2a again describes the behaviour of the system. Again the solutions are unbounded and therefore not good solutions.

On the other hand, when $\Omega \in (0, \Omega_*)$ we now find two fixed points $(\rho_1, 0)$ and $(\rho_2, 0)$ with $\rho_1 < \sqrt{\frac{2}{3}} < \rho_2$. The eigenvalues in this situation are

$$\lambda_{\pm} = \pm \sqrt{2} \sqrt{-2 + 3\rho_*^2}$$

Since $\rho_1 < \sqrt{\frac{2}{3}} < \rho_2$ we find that the fixed point $(\rho_1, 0)$ is a center and $(\rho_2, 0)$ is a saddle point. In this case we find - beside those unbounded solutions - two fixed points, a homoclinic orbit and periodic orbits (enclosed in the homoclinic orbit).

We haven't talked about what happens when $\Omega = \Omega_*$. Here a saddle-node bifurcation occurs and the phase plane looks very similar to the one in Figure C.2a with the addition that there is now one single fixed point at $(\sqrt{\frac{2}{3}}, 0)$ (which is unstable). So this situation gives us only one additional bounded solution: the fixed point itself.

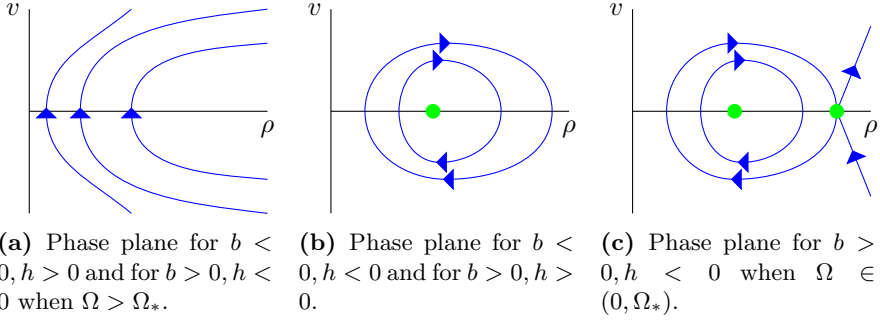


Figure C.2 – Sketches of the possible phase planes of equation (C.3) for different values for b, h and $\Omega > 0$. In all these figures the green dots denote the fixed points (if any) and the blue lines are sketches of a few orbits.

C.3 Stationary solutions of the Ginzburg-Landau equation

In the previous section we have determined the stationary solutions of the system of equation (C.3) for all possible situations. Here we have found several, different bounded solutions for ρ :

- *Saddle points:* when $b > 0, h < 0$ and $\Omega \in (0, \Omega_*]$;
- *Centers:* when $b > 0, h < 0, \Omega \in (0, \Omega_*)$ and when $\text{sgn}(b) = \text{sgn}(h)$;
- *Periodic solutions:* when $b > 0, h < 0, \Omega \in (0, \Omega_*)$ and when $\text{sgn}(b) = \text{sgn}(h)$;
- *Homoclinic connections:* when $b > 0, h < 0$ and $\Omega \in (0, \Omega_*)$.

In this section we determine how these kind of solutions for ρ gives us solutions for the amplitude A in the Ginzburg-Landau equation we started with. We inspect the different stationary solutions for ρ_* one by one.

C.3.1 Uniform solutions $\rho(\xi) = \rho_*$

When we have a uniform stationary solution $\rho(\xi) = \rho_*$ we can use the conserved quantity $\Omega = \rho^2 \psi_\xi$ to conclude that $\psi_\xi = \frac{\Omega}{\rho_*^2}$. Therefore $\psi(\xi) = \frac{\Omega}{\rho_*^2} \xi = \sqrt{\frac{1+h\rho_*^2}{b}} \xi$ (note that because of the phase-invariance of the Ginzburg-Landau equation we can forget about the integration constant).

So from this we find the following stationary solutions to the Ginzburg-Landau equation:

$$A(\xi) = \rho_* \exp\left(i \frac{\Omega}{\rho_*^2} \xi\right)$$

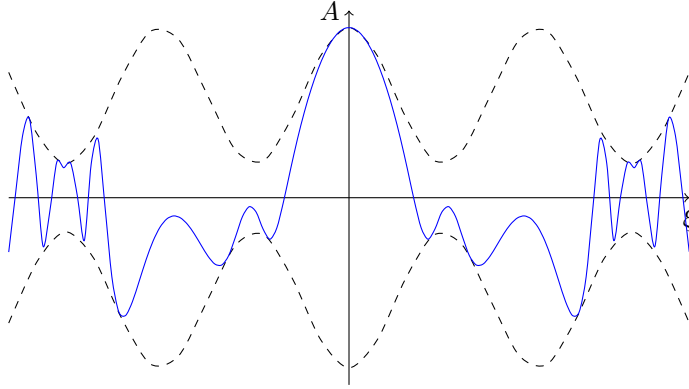


Figure C.3 – Sketch of a possible quasi-periodic solution of the Ginzburg-Landau equation. The blue line is the quasi-periodic solution, while the dotted, black lines give the values of $|A|$ and $-|A|$.

C.3.2 Periodic solutions

The second sort of stationary solutions are the period solutions $\rho(\xi)$ for which $\rho(\xi + T) = \rho(\xi)$ where T is the period of the solution. Since $\psi_\xi = \frac{\Omega}{\rho^2}$ we find that ψ_ξ is also a periodic solution, with the same period. Therefore we find $\psi(\xi) = \int_0^\xi \frac{\Omega}{\rho(\xi')^2} d\xi'$ where we have set $\psi(0) = 0$ because of the phase invariance of the Ginzburg-Landau equation. The solution for the amplitude A now is

$$A(\xi) = \rho(\xi) \exp\left(i \int_0^\xi \frac{\Omega}{\rho(\xi')^2} d\xi'\right).$$

It is not easy to find the exact form of this solution, since we need to determine the solution for ρ , and then integrate $\frac{1}{\rho^2}$. We can however say something qualitatively about this kind of solutions. It is clear that $A(\xi) \in [-\rho(\xi), \rho(\xi)]$ per construction. Moreover we know that ψ_ξ attains a maximum when ρ attains a minimum and vice versa. Hence ψ increases fastest/slowest when ρ is smallest/biggest. We should also note that $\psi_\xi > 0$ and therefore ψ is a monotonically increasing function. In Figure C.3 we have sketched a possible form of such quasi-periodic solutions of the Ginzburg-Landau equation.

C.3.3 Homoclinic connections

The last kind of solutions that we encountered were homoclinic connections $\rho(\xi)$ where $\rho(\xi) \rightarrow \rho_* > \sqrt{\frac{2}{3}}$ when $\xi \rightarrow \pm\infty$. Again, $\psi_\xi(\xi) = \frac{\Omega}{\rho(\xi)^2}$ and therefore $\psi_\xi(\xi) \rightarrow \frac{\Omega}{\rho_*^2}$ when $\xi \rightarrow \pm\infty$. Hence for very large $|\xi|$ the solution for the amplitude A is very similar to a periodic solution, as we found before.

When $|\xi|$ is not big, we find the solution to be similar to the quasi-periodic solution, again bounded between $-\rho(\xi)$ and $\rho(\xi)$. A possible form of this amplitude A is given in Figure C.4.

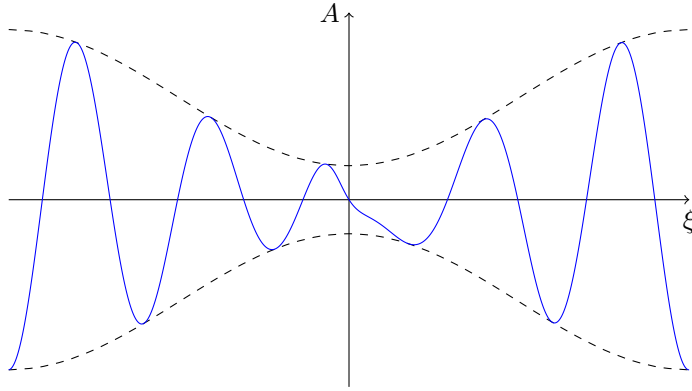


Figure C.4 – Sketch of a possible solution of the Ginzburg-Landau equation, coming from a homoclinic connection. The blue line is the solution, the dotted, black lines give the values $|A|$ and $-|A|$.

C.4 The situation when $\Omega = 0$

This far we have neglected the special case when $\Omega = 0$. When $\Omega = 0$ we know that $0 = \Omega = \rho^2 \psi_\xi$. Therefore we find either $\rho \equiv 0$ or $\psi_\xi \equiv 0$. When $\rho = 0$ we have just found the amplitude $A \equiv 0$, which isn't very useful. Thus we inspect the other situation, where we have $\psi_\xi = 0$ and hence ψ is constant.

In this situation the system of equation (C.3) reduces to the system

$$\begin{cases} \rho_\xi &= v \\ v_\xi &= -\frac{1}{b}\rho - \frac{h}{b}\rho^3 \end{cases} \quad (\text{C.5})$$

The fixed points of this system are $(0, 0)$ and $(\sqrt{-1/h}, 0)$. This last one of course only exists when $h < 0$.

Computation of the eigenvalues is straight-forward and we obtain that $(0, 0)$ is a saddle when $b < 0$ and a center when $b > 0$. The fixed point $(-\sqrt{-1/h}, 0)$ is a center when $b < 0$ and a saddle when $b > 0$.

The phase planes for the various signs for b and h are given in Figure C.5. We again see the possibility of periodic solution. Moreover we see the possibility of a homoclinic and a heteroclinic connection, either connection $\rho = 0$ with $\rho = 0$ (when $b < 0, h < 0$) or connecting $\rho = \pm\sqrt{-1/h}$ with $\rho = \mp\sqrt{-1/h}$ (when $b > 0, h < 0$). Sketches of these solutions are given in Figure C.6.

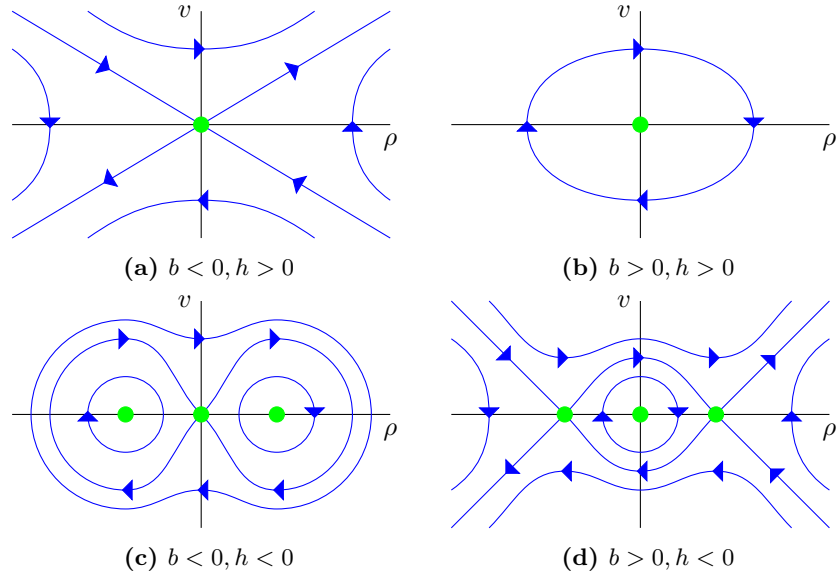


Figure C.5 – Sketches of the phase planes of the system in equation (C.5) for all possible signs of b and h . The green circles denote the fixed points and the blue lines are some of the orbits.

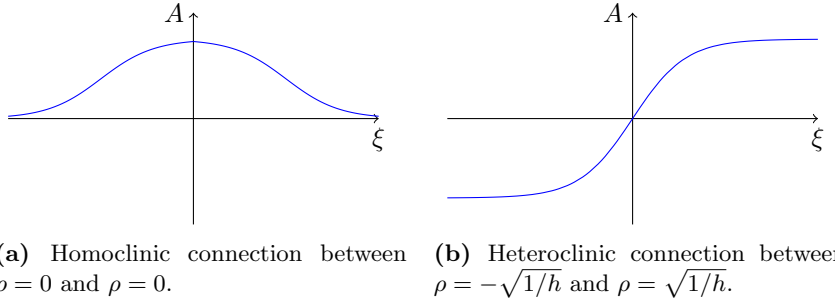


Figure C.6 – Sketches of possible homoclinic(a) and heteroclinic(b) orbits than can occur in the Ginzburg-Landau system when $\Omega = 0$, $h < 0$ and $b > 0$ (for the heteroclinic orbits) and $b < 0$ (for the homoclinic orbits).

C.5 Stability of the stationary solutions

In order to really determine what is happening with the Ginzburg-Landau equation it is necessary to determine the stability of the previously found stationary solutions. It's easiest to do this linear stability analysis in the system with polar coordinates. At this point we also write the complete equation again (i.e. we do not assume $R = 1$). The system in polar coordinates then becomes

$$\begin{cases} \rho_\tau &= R\rho + b\rho\xi_\xi - b\rho\psi_\xi^2 + h\rho^3 \\ \rho\psi_\tau &= 2b\rho_\xi\psi_\xi + b\rho\psi_{\xi\xi} \end{cases} \quad (\text{C.6})$$

To determine the stability of the stationary solutions we look into perturbations of the form $(\rho, \psi) = (\rho_0, \psi_0) + \delta(\hat{\rho}, \hat{\psi})$. At the $\mathcal{O}(\delta)$ -level the equation the linearized system then becomes

$$\begin{cases} \hat{\rho}_\tau &= \left(R + b\partial_\xi^2 - b\psi_{0,\xi}^2 + 3h\rho_0^2 \right) \hat{\rho} - 2b\rho_0\psi_{0,\xi}\partial_\xi\hat{\psi} \\ \rho_0\hat{\psi}_\tau &= (2b\psi_{0,\xi}\partial_\xi + b\psi_{0,\xi\xi})\hat{\rho} + \left(2b\rho_{0,\xi}\partial_\xi + b\rho_0\partial_\xi^2 \right) \hat{\psi} \end{cases} \quad (\text{C.7})$$

Then we want to derive a dispersion relation and therefore we set $(\hat{\rho}, \hat{\psi}) = e^{iq\xi + \omega(q)\tau}(r, s)$. Substitution then gives, after a little manipulation the following system

$$\omega \begin{pmatrix} r \\ s \end{pmatrix} = \begin{pmatrix} R - bq^2 - b\psi_{0,\xi}^2 + 3h\rho_0^2 & -2b\rho_0\psi_{0,\xi}iq \\ \frac{2b\psi_{0,\xi}}{\rho_0}iq + \frac{b\psi_{0,\xi\xi}}{\rho_0} & 2b\frac{\rho_{0,\xi}}{\rho_0}iq - bq^2 \end{pmatrix} \begin{pmatrix} r \\ s \end{pmatrix} \quad (\text{C.8})$$

In the following sections we try to find the linear stability of the previously found stationary states, for all possible cases, given by the signs of R, b and h .

C.5.1 Uniform states

The first stationary solutions that we want to investigate are those for which $A(\xi) \equiv A$. We have seen before that there are three of those uniform solutions: $A = 0$ and $A = \pm 1$ (which only exists when $h < 0$). In both of these cases the Jacobian matrix can be reduced because $\rho_{0,\xi} \equiv 0$ and $\psi_{0,\xi} \equiv 0$. We thus obtain

$$J = \begin{pmatrix} R - bq^2 + 3h\rho_0^2 & 0 \\ 0 & -q^2 \end{pmatrix} \quad (\text{C.9})$$

Hence one eigenvalue is $\lambda_1 = -q^2$, while the second is $\lambda_2 = R - bq^2 + 3h\rho_0^2$. For stability both eigenvalues need to be negative.

When we inspect the uniform state $A = 0$, we see that $\lambda_2 = R - bq^2$ and thus $\lambda_2 < 0$ for all q when $R < 0$. For the uniform states $A = \pm 1$ we find $\lambda_2 = R - \rho_0^2 - bq^2$ (because $h < 0$ for these fixed points to exist). Hence $\lambda_2 < 0$ for all wavelengths, regardless of the value of R .

We should note that $\lambda_1 = 0$ when $q = 0$. This comes from the fact that the Ginzburg-Landau equation is phase invariant. Hence in fact we find that there is a circle of stationary points $\{e^{i\pi}\}$ and this circle is an attracting set (note that for $A \equiv 0$ this set is just a single point).

C.5.2 Periodic solutions of the form $A(\xi) = a(\theta)e^{i\theta\xi}$

The second stationary solutions we have found were the periodic solutions of the form $A = \rho_* e^{i\frac{\Omega}{\rho_*^2}\xi}$, which can also be written as $A = a(\theta)e^{i\theta\xi}$ for some $\theta \in \mathbb{R}$, where $a(\theta) = \sqrt{\frac{b\theta^2 - R}{h}}$ (for values of b, R, h, θ for which this makes sense). This means that the Jacobian in this situation becomes

$$J = \begin{pmatrix} 2[b\theta^2 - R] - bq^2 & -2ib\theta\rho_0q \\ 2iq\frac{b\theta}{\rho_0} & -bq^2 \end{pmatrix}$$

The determinant and the trace of this matrix are easily verified to be

$$\begin{aligned} \text{Tr} J &= 2(-bq^2 + (b\theta^2 - R)) \\ \det J &= q^2(b^2q^2 + 2b(R - 3b\theta^2)) \end{aligned}$$

To find linear stability of these periodic orbits we need to have $\text{Tr} J < 0$ and $\det J > 0$ for all wavelengths q . So that means we need to have $b > 0$, $b\theta^2 - R < 0$ and $b(R - 3b\theta^2) > 0$ simultaneously. We also need to have $\frac{b\theta^2 - R}{h} > 0$ to ensure that $a(\theta) \in \mathbb{R}$. So from this it is clear that these kind of periodic solutions are only stable when $R, b > 0$, $h < 0$ and $\theta^2 < \frac{R}{3b}$. This result is called the Eckhaus stability. Whenever these solutions exist for other values of (R, b, h) they are unstable.

C.5.3 Periodic solutions of the form $A(\xi) = \rho(\xi)$.

We have also found a set of periodic solutions of the form $A(\xi) = \rho(\xi)$ for some periodic function $\rho(\xi)$. That means that we also implicitly have $\psi_\xi = 0$. Hence we can obtain the following linearized system, which can easily be derived from equation (C.7):

$$\begin{cases} \hat{\rho}_\tau &= \left(R + b\partial_\xi^2 + 3h\rho_0^2 \right) \hat{\rho} \\ \rho_0 \hat{\psi}_\tau &= \left(2b\rho_{0,\xi}\partial_\xi + b\rho_0\partial_\xi^2 \right) \hat{\psi} \end{cases}$$

Again we want to find the stability using our test functions $(\hat{\rho}, \hat{\psi}) = (r, s)e^{iq\xi + \omega\tau}$. However, since ρ_0 is not constant, our previous approach is not good. Instead we need to take a formal Fourier transform of this equation. Here we denote the Fourier transform of ρ_0^2 by $\hat{\rho}_0^2$. Then we can see that the new system becomes

$$\begin{cases} \omega r &= \left(-bq^2 + R + 3h\hat{\rho}_0^2(q) \right) r \\ \omega s &= (-3bq^2)s \end{cases}$$

It is immediately clear that the eigenvalues are $\omega_1(q) = -bq^2 + R + 3h\hat{\rho}_0^2(q)$ and $\omega_2(q) = -3bq^2$. To have stability we need again need to have $b > 0$ so that $\omega_2 < 0$ for all $q \neq 0$. To have $\omega_1(q) < 0$ we need to have $-bq^2 + R + 3h\hat{\rho}_0^2(q) < 0$ for all wavelengths q .

Since ρ_0 is a periodic function, $\hat{\rho}_0^2$ is a periodic function as well. Hence the Fourier transform of $\hat{\rho}_0^2$ is zero almost everywhere. Hence for almost all q $\omega_1 < 0$ is guaranteed when $R < 0$. However, for special values of q (that are linked to the period of the function ρ_0) the condition becomes $R + 3h < 0$ and hence we see we also need to have $h < 0$. Hence these kind of periodic functions are stable when $R < 0, b > 0$ and $h < 0$.

However, in our derivation from previous sections, we have found that these kind of periodic solution cannot exist when $Rb < 0$ and $Rh > 0$ (see Figure C.5). Therefore these kind of periodic solutions never occur as stable stationary solutions of the Ginzburg-Landau equation.

C.5.4 The other stationary solutions

So far we have not yet discussed the stability of the quasi-periodic functions and the homoclinic and heteroclinic connections (see Figure C.6). The computation of the stability of these solutions is not straight-forward and one needs to solve the linearized (inhomogenous) system completely. That is, we need to find all possible eigenvalues and determine the sign of their real parts. As this is non-trivial and is a complete study of its own, we have chosen to not pursue this at this moment.

Bibliography

- [1] A. M. Turing. The chemical basis of morphogenesis. *237(641):37–72*, 1952.
- [2] A. Koch and H. Meinhardt. Biological pattern formation: from basic mechanisms to complex structures. *Rev. Mod. Phys.*, 66:1481–1507, Oct 1994.
- [3] Koen Siteur, Eric Siero, Maarten B. Eppinga, Jens D.M. Rademacher, Arjen Doelman, and Max Rietkerk. Beyond turing: The response of patterned ecosystems to environmental change. *Ecological Complexity*, 20(0):81 – 96, 2014.
- [4] C.R. Nugent, W.M. Quarles, and T.H. Solomon. Experimental studies of pattern formation in a reaction-advection-diffusion system. *Physical review letters*, 93(21):218301, 2004.
- [5] Quan-Xing Liu, Arjen Doelman, Vivi Rottschäfer, Monique de Jager, Peter M.J. Herman, Max Rietkerk, and Johan van de Koppel. Phase separation explains a new class of self-organized spatial patterns in ecological systems. *Proceedings of the National Academy of Sciences*, 110(29):11905–11910, 2013.
- [6] Johan van de Koppel, Joanna C. Gascoigne, Guy Theraulaz, Max Rietkerk, Wolf M. Mooij, and Peter M.J. Herman. Experimental evidence for spatial self-organization and its emergent effects in mussel bed ecosystems. *Science*, 322(5902):739–742, 2008.
- [7] Daniel T. Haydon, Juan M. Morales, Adelle Yott, Deborah A. Jenkins, Rick Rosatte, and John M. Fryxell. Socially informed random walks: incorporating group dynamics into models of population spread and growth. *Proceedings of the Royal Society of London B: Biological Sciences*, 275(1638):1101–1109, 2008.
- [8] Brian R. Silliman, Johan van de Koppel, Mark D. Bertness, Lee E. Stanton, and Irving A. Mendelssohn. Drought, snails, and large-scale die-off of southern u.s. salt marshes. *Science*, 310(5755):1803–1806, 2005.
- [9] John W. Cahn and John E. Hilliard. Free energy of a nonuniform system. i. interfacial free energy. *The Journal of Chemical Physics*, 28(2), 1958.
- [10] John W. Cahn. Free energy of a nonuniform system. ii. thermodynamic basis. *The Journal of Chemical Physics*, 30(5), 1959.

- [11] John W. Cahn and John E. Hilliard. Free energy of a nonuniform system. iii. nucleation in a two-component incompressible fluid. *The Journal of Chemical Physics*, 31(3), 1959.
- [12] I.M. Lifshitz and V.V. Slyozov. The kinetics of precipitation from supersaturated solid solutions. *Journal of Physics and Chemistry of Solids*, 19(1–2):35 – 50, 1961.
- [13] E. van Groesen and J. Molenaar. *Continuum modeling in the physical sciences*. Monographs on mathematical modeling and computation. Society for Industrial and Applied Mathematics, 2007.
- [14] Mark J. Schnitzer. Theory of continuum random walks and application to chemotaxis. *Physical Review E*, 48(4):2553, 1993.
- [15] J.D. Murray. *Mathematical biology: I. An introduction*. Interdisciplinary Applied Mathematics. Springer, 2002.
- [16] Johan van de Koppel, Max Rietkerk, Norbert Dankers, and Peter M.J. Herman. Scale-dependent feedback and regular spatial patterns in young mussel beds. *The American Naturalist*, 165(3):E66–E77, 2005.
- [17] Richard A. Cangelosi, David J. Wollkind, Bonni J. Kealy-Dichone, and Inthira Chaiya. Nonlinear stability analyses of turing patterns for a mussel-algae model. *Journal of mathematical biology*, pages 1–46, 2014.
- [18] Rong-Hua Wang, Quan-Xing Liu, Gui-Quan Sun, Zhen Jin, and Johan van de Koppel. Nonlinear dynamic and pattern bifurcations in a model for spatial patterns in young mussel beds. *Journal of the Royal Society Interface*, 6(37):705–718, 2009.
- [19] Jack Carr, Morton E. Gurtin, and Marshall Slemrod. Structured phase transitions on a finite interval. *Archive for rational mechanics and analysis*, 86(4):317–351, 1984.
- [20] Amy Novick-Cohen and Lambertus A. Peletier. The steady states of the one-dimensional cahn-hilliard equation. *Applied mathematics letters*, 5(3):45–46, 1992.
- [21] Amy Novick-Cohen. The cahn-hilliard equation. *Handbook of differential equations: evolutionary equations*, 4:201–228, 2008.
- [22] Charles M. Elliott and Zheng Songmu. On the cahn-hilliard equation. *Archive for Rational Mechanics and Analysis*, 96(4):339–357, 1986.
- [23] Charles M. Elliott. The cahn-hilliard model for the kinetics of phase separation. In *Mathematical models for phase change problems*, pages 35–73. Springer, 1989.
- [24] Amy Novick-Cohen and Lee A. Segel. Nonlinear aspects of the cahn-hilliard equation. *Physica D: Nonlinear Phenomena*, 10(3):277 – 298, 1984.
- [25] Nicholas Alikakos, Peter W. Bates, and Giorgio Fusco. Slow motion for the cahn-hilliard equation in one space dimension. *Journal of Differential Equations*, 90(1):81 – 135, 1991.

- [26] C. Clarke. *The science of ice cream*. RSC paperbacks. Royal Society of Chemistry, 2004.
- [27] Charles Kittel, Paul McEuen, and Paul McEuen. *Introduction to solid state physics*, volume 8. Wiley New York, 1976.
- [28] Helmut Schiessel. Statistical physics ii: course notes, 2012.
- [29] P. Nelson. *Biological physics: energy, information, life*. W. H. Freeman, 2003.
- [30] Nicholas D. Alikakos and Giorgio Fusco. The equations of ostwald ripening for dilute systems. *Journal of statistical physics*, 95(5-6):851–866, 1999.
- [31] JochenW. Schmidt and Walter Heß. Positivity of cubic polynomials on intervals and positive spline interpolation. *BIT Numerical Mathematics*, 28(2):340–352, 1988.
- [32] Y. Nishiura. *Far-from-equilibrium dynamics*. Iwanami series in modern mathematics. American Mathematical Society, 2002.
- [33] Philip K. Chan and Alejandro D. Rey. A numerical method for the nonlinear cahn-hilliard equation with nonperiodic boundary conditions. *Computational Materials Science*, 3(3):377 – 392, 1995.
- [34] J.S. Langer. Theory of spinodal decomposition in alloys. *Annals of Physics*, 65(1):53 – 86, 1971.